




6-2015

Wind Oscillator for Power Generation

RS Vewen Ramasamy
Western Michigan University

Follow this and additional works at: https://scholarworks.wmich.edu/masters_theses

 Part of the Aerospace Engineering Commons, Natural Resources and Conservation Commons, and the Sustainability Commons

Recommended Citation

Ramasamy, RS Vewen, "Wind Oscillator for Power Generation" (2015). *Masters Theses*. 600.
https://scholarworks.wmich.edu/masters_theses/600

This Masters Thesis-Open Access is brought to you for free and open access by the Graduate College at ScholarWorks at WMU. It has been accepted for inclusion in Masters Theses by an authorized administrator of ScholarWorks at WMU. For more information, please contact wmu-scholarworks@wmich.edu.



WIND OSCILLATOR FOR POWER GENERATION

by

RS Vewen Ramasamy

A thesis submitted to the Graduate College
in partial fulfillment of the requirements
for the Degree of Master of Science in Engineering (Mechanical)
Department of Mechanical and Aerospace Engineering
Western Michigan University
June 2015

Thesis Committee:

Tianshu Liu, Ph.D., Chair
Parviz Merati, Ph.D.
Javier Montefort, Ph.D.

WIND OSCILLATOR FOR POWER GENERATION

RS Vewen Ramasamy, M.S.E.

Western Michigan University, 2015

This thesis describes in detail the design, mechanical, electrical and software considerations in developing a working model for the non-conventional wind power converter called Wind Oscillator. This was based on the concept developed and patented by Tianshu Liu in the paper “Wind Oscillator and Rotor for Power Generation”[1]. In order to verify the practicality of this idea, a working model of the Wind Oscillator was designed, built and tested in the Western Michigan University wind tunnel facility. LabVIEW data acquisition and photogrammetry was performed on the model so as to evaluate the power generated by the Wind Oscillator and to study the performance and ways to improve the device.

The study found that the root-mean-square (RMS) voltage output of the Wind Oscillator had a steady increase for increasing wind speed. The increase in the Angle of Attack (AoA) of the wing, AoA of the arm and the vertical position of the spring also increased the RMS voltage output of the device. The photogrammetric study of the arm and the wing reveals the difference in requested AoA for the arm and the wing by the user through the LabVIEW interface and the actual AoA of the arm and the wing. Finally, the pendulum photogrammetry helped to quantify the power output of the device.

Copyright by
RS Vewen Ramasamy
2015

ACKNOWLEDGMENTS

I would like to extend my heartfelt thanks to Dr. Tianshu Liu, my advisor, for giving me an opportunity to work on this project. Without his support and guidance, this thesis would not have been possible; it has been an honor to have him as advisor.

I would like to thank Dr. Javier Montefort for all of his patience in sharing the wind tunnel with me and help by showing me how to conduct photogrammetric studies. I would also like to thank Dr. Parviz Merati for all the guidance and the support he gave monetarily as it would be impossible for me to complete my project without it. I would also like to recognize Patrick Wewengkang for helping me in running the wind tunnel.

Many thanks to Mr. Peter Thannhauser for his help with setting up and running the experiment; he helped me with the LabVIEW establishment and supervised me when running the trials. Without his help, I would not have been able to run the experiment.

Last, but definitely not least, I would like to thank my friends, parents, and my family for their constant support; who was always there for me with love, support, encouragement, and motivation.

RS Vewen Ramasamy

TABLE OF CONTENTS

ACKNOWLEDGMENTS	ii
LIST OF TABLES	v
LIST OF FIGURES	vi
CHAPTER	
I. INTRODUCTION	1
II. OBJECTIVE OF THE STUDY	6
III. CONCEPTUAL DESIGN	7
IV. MECHANICAL DESIGN	10
Mechanical Dimension	14
Mechanical Dynamics	16
Spring	19
Torsional Spring	20
Leaf Spring	24
Bearing	41
Counter Weight	44
Gear and Belt	47
V. ELETRONIC DESIGN	48
Optical Encoder	48
Optical Encoder – Arm	49
Optical Encoder – Wing	52
Digital IO & Power Drivers	57
Power Supply	60
National Instruments (NI) Data Acquisition (DAQ) Modules	62
Stepper Motor	63
VI. GENERATOR DESIGN	67
Brushed dc Motor	67

Table of Contents – continued

CHAPTER	
	Pendulum 69
VII. SOFTWARE DESIGN.....	70
	LabVIEW (Laboratory Virtual Instrument Engineering Workbench) 70
	LabVIEW - Control..... 71
	LabVIEW – Data Acquisition..... 79
VIII. WIND TUNNEL TESTING.....	82
	Model Set Up and Wind Tunnel Calibration 82
	RMS Voltage Data Acquisition and Analysis 86
	Photogrammetry..... 112
IX. CONCLUSION AND FUTURE WORK.....	128
	CONCLUSION 128
	FUTURE WORK..... 130
BIBLIOGRAPHY	132
APPENDICES: Minitab Output.....	145
	A. Full factorial design 146
	B. DOE for all the factorials 148
	C. DOE for selected factorials 151
APPENDICES: Matlab Code.....	153
	A. Benchmark..... 154
	B. Wind tunnel speed calibration 156
	C. LabVIEW data acquisition analysis 1 (leaf spring height 7,8 and 9) 158
	D. LabVIEW data acquisition analysis 2 (leaf spring height 7in)..... 167
	E. LabVIEW data acquisition analysis 3 (leaf spring height 8in)..... 172
	F. LabVIEW data acquisition analysis 4 (leaf spring height 9in)..... 177
	G. Wing and arm photogrammetry target tracking..... 182
	H. Wing and arm photogrammetry data analysis 186
	I. Pendulum photogrammetry target tracking 193
	J. Pendulum photogrammetry data analysis 197

LIST OF TABLES

1. Number of oscillations the spring allows the system to make with the wind on...22	22
2. The number of oscillations spring number two allows the system to make with the wind turned on and off right after the fan on conditions.22	22
3. Experimental plan from Minitab.....29	29
4. Detailed experimental plan.....30	30
5. Data collected (12/6/2014 @ 3pm).....30	30
6. Parameters for the single ended electrical optical encoder [131].51	51
7. Parameters for E2 Optical Kit Encoder shown above [135].55	55
8. Specifications of different models for 150W power supply [140].61	61

LIST OF FIGURES

1. Power in respect to HAWT rotor diameter [12-125].	2
2. Annual average wind speed at 30m elevation [126].	3
3. Annual average wind speed at 80m elevation [127].	4
4. Conceptual design of the wind oscillator [1].	7
5. Basic schematic of the Wind Oscillator [1].	8
6. The Solidworks Isometric view of the whole system.	10
7. The isometric view of the actual setting of the device.	11
8. Mechanical and electrical components of the model wind oscillator in Solidworks design.	12
9. Dimensions of the model wind oscillator from the frontal view.	14
10. Dimensions of the model wind oscillator from the side view.	14
11. Dimensions of the model wind oscillator from the top view.	15
12. Cross section of NACA 0012 airfoil [128].	16
13. Characteristic graphs for NACA 0012 at different Reynolds Numbers [129].	17
14. The force distribution on the system at a particular position.	18
15. Side view of the right leg of the system.	20
16. Side view of the torsional spring in Solidworks drawing and in real system set up	20
17. Side view of the leaf spring in the system.	24

List of Figures – continued

18.	Isometric view of the leaf spring.	26
19.	Side view of the spring setting.....	28
20.	Normal probability plot.....	31
21.	Half normal probability plot.....	32
22.	Residual plots for deflection.....	34
23.	Residual versus A (Weight).....	35
24.	Residual versus B (Location of the weight)	35
25.	Residual versus C (Length of the spring).....	36
26.	Residual versus D (Thickness of the spring).....	36
27.	Main effect plot for deflection.....	37
28.	Interaction plot for deflection	38
29.	Box plot for deflection	39
30.	The top view of the system shows the locations on the bearings in Solidworks. ...	41
31.	The actual location of the bearings on the device from top view.	41
32.	The location of the flanged ball bearings in detail Solidworks drawing.....	43
33.	The actual location and setting of the bearings on the device.	43
34.	Isometric view of the model oscillator without counter balance.	44
35.	The attachment of counter weight to the wing in Solidworks.....	45
36.	The actual location of the counter balance and how it is attached to the wing.	46

List of Figures – continued

37. Gear and belt mechanisms on the device.	47
38. HB6M Hollow Bore Optical Encoder [130].	49
39. The optical encoder located at the end of the middle rod in Solidworks.	49
40. The location of the optical encoder which is located at the end of the middle rod.....	50
41. Dimensions of the HB6M Hollow Bore Optical Encoder [132].	51
42. E2 Optical Kit Encoder with and without cover respectively [133].....	52
43. Dimensions of the E2 Optical Kit Encoder [134].....	53
44. The optical encoder located at the quarter chord of the wing.	53
45. Optical encoders located at the quarter chord of the wings and a zoomed in view of the encoder.	54
46. Timing characteristics of the encoders [136].	56
47. Simplified schematic of the motor controller [137].....	57
48. Schematic Diagram of A4988 Stepper Motor Driver [138].....	59
49. 150W single output switching power supply [139].	60
50. Three different models of the NI DAQs.....	62
51. 14 oz-in hybrid stepper motor [141].	63
52. Schematics of the stepper motor [141].....	63
53. Pullout torque curve at 24VDC, 0.5A, half step [142].....	65
54. The location of the hybrid stepper motor with the covering.	65

List of Figures – continued

55.	The location of the stepper motors on the arm and a zoomed in image showing how it is connected to the wing.	66
56.	Brushed dc motor in Tamiya high power gearbox [143] set up on the motor stand.	67
57.	Typical voltage output from model wind oscillator trough DC motor.	68
58.	Pendulum setting of the device.	69
59.	Front panel of the LabVIEW program controlling the device.	72
60.	Simplified block diagram of the control system.	73
61.	The main VI controlling the system.	74
62.	The sequence of event for the main VI controlling the system.	75
63.	The sub VI that is responsible for initializing the system.	76
64.	The sub VI that is controlling the angle of attack of the wings.	77
65.	Detailed block diagram of the control system.	78
66.	Detailed block diagram of the control system.	78
67.	Front panel of the LabVIEW program used to collect data from the Wind Oscillator	79
68.	The VI that collects and records raw and calculated RMS voltage data.....	81
69.	Model wind oscillator set up in the Advanced Design Wind Tunnel at WMU.....	82
70.	Anemometer[144].	84
71.	Wind speed inside wind tunnel calibration based on wind tunnel fan speed.	84
72.	Extrapolated wind speed versus fan speed graph based on the calibration data ...	85

List of Figures – continued

73.	Typical voltage output from model wind oscillator through DC motor.	86
74.	RMS voltage output for different leaf spring heights when arm AoA is ± 5 degree and wing AoA is ± 15 degree.	89
75.	RMS voltage output for different leaf spring heights when arm AoA is ± 5 degree and wing AoA is ± 20 degree.	89
76.	RMS voltage output for different leaf spring heights when arm AoA is ± 5 degree and wing AoA is ± 30 degree.	90
77.	Comparison of all the RMS voltage output graphs when arm AoA is ± 5 degree.	90
78.	RMS voltage output for different leaf spring heights when arm AoA is ± 9 degree and wing AoA is ± 15 degree.	92
79.	RMS voltage output for different leaf spring heights when arm AoA is ± 9 degree and wing AoA is ± 20 degree.	92
80.	RMS voltage output for different leaf spring heights when arm AoA is ± 9 degree and wing AoA is ± 30 degree.	93
81.	Comparison of all the RMS voltage output graphs when arm AoA is ± 9 degree.	93
82.	RMS voltage output for different leaf spring heights when arm AoA is ± 13 degree and wing AoA is ± 15 degree.	94
83.	RMS voltage output for different leaf spring heights when arm AoA is ± 13 degree and wing AoA is ± 20 degree.	95
84.	RMS voltage output for different leaf spring heights when arm AoA is ± 13 degree and wing AoA is ± 30 degree.	95
85.	Comparison of all the RMS voltage output graphs when arm AoA is ± 13 degree.	96

List of Figures – continued

86. Comparison of all the RMS voltage output graphs when wing AoA is ± 15 degree.	97
87. Comparison of all the RMS voltage output graphs when wing AoA is ± 20 degree.	97
88. Comparison of all the RMS voltage output graphs when wing AoA is ± 30 degree.	98
89. RMS voltage output for different wing AoA when arm AoA is ± 5 degree and leaf spring height is 7 in.	99
90. RMS voltage output for different wing AoA when arm AoA is ± 9 degree and leaf spring height is 7 in.	99
91. RMS voltage output for different wing AoA when arm AoA is ± 13 degree and leaf spring height is 7 in.	100
92. RMS voltage output for different arm AoA when wing AoA is ± 15 degree and leaf spring height is 7 in.	100
93. RMS voltage output for different arm AoA when wing AoA is ± 20 degree and leaf spring height is 7 in.	101
94. RMS voltage output for different arm AoA when wing AoA is ± 30 degree and leaf spring height is 7 in.	101
95. Comparison of all the RMS voltage output graphs when leaf spring height is 7 in.	102
96. RMS voltage output for different wing AoA when arm AoA is ± 5 degree and leaf spring height is 8 in.	103
97. RMS voltage output for different wing AoA when arm AoA is ± 9 degree and leaf spring height is 8 in.	103
98. RMS voltage output for different wing AoA when arm AoA is ± 13 degree and leaf spring height is 8 in.	104

List of Figures – continued

99. RMS voltage output for different arm AoA when wing AoA is ± 15 degree and leaf spring height is 8 in.....	104
100. RMS voltage output for different arm AoA when wing AoA is ± 20 degree and leaf spring height is 8 in.....	105
101. RMS voltage output for different arm AoA when wing AoA is ± 30 degree and leaf spring height is 8 in.....	105
102. Comparison of all the RMS voltage output graphs when leaf spring height is 8 in.	106
103. RMS voltage output for different wing AoA when arm AoA is ± 5 degree and leaf spring height is 9 in.....	107
104. RMS voltage output for different wing AoA when arm AoA is ± 9 degree and leaf spring height is 9 in.....	108
105. RMS voltage output for different wing AoA when arm AoA is ± 13 degree and leaf spring height is 9 in.....	108
106. RMS voltage output for different arm AoA when wing AoA is ± 15 degree and leaf spring height is 9 in.....	109
107. RMS voltage output for different arm AoA when wing AoA is ± 20 degree and leaf spring height is 9 in.....	109
108. RMS voltage output for different arm AoA when wing AoA is ± 30 degree and leaf spring height is 9 in.....	110
109. Comparison of all the RMS voltage output graphs when leaf spring height is 9 in.	110
110. Leading wing and arm photogrammetry target point locations.....	112
111. Actual angle of the wing and arm when the incoming wind speed is 1.06m/s (34rpm).....	114

List of Figures – continued

112. Actual angle of the wing and arm when the incoming wind speed is 1.17m/s (36rpm).....	114
113. Actual angle of the wing and arm when the incoming wind speed is 1.38m/s (40rpm).....	115
114. Actual angle of the wing and arm when the incoming wind speed is 1.59m/s (44rpm).....	115
115. Actual angle of the wing and arm when incoming wind speed is 1.81m/s (48rpm).....	116
116. Actual angle of the wing and arm when the incoming wind speed is 2.02m/s (52rpm).....	116
117. Actual angle of the wing and arm when the incoming wind speed is 2.23m/s (56rpm).....	117
118. Actual angle of the wing and arm when the incoming wind speed is 2.45m/s (60rpm).....	117
119. Actual angle of the wing and arm when the incoming wind speed is 2.66m/s (64rpm).....	118
120. Actual angle of the wing and arm when the incoming wind speed is 2.87m/s (68rpm).....	118
121. Actual angle of the wing and arm when the incoming wind speed is 2.98m/s (70rpm).....	119
122. Comparison between set arm angle and actual arm angle	120
123. Comparison between set wing AoA and AoA respective to arm and incoming wind direction.	121
124. Pendulum photogrammetry target point setting for calculating mechanical power.....	122

List of Figures – continued

125. Mechanical power output of the system with a mass of 32.2g on each side on the pendulum for incoming wind speed of 1.6m/s (44rpm)	124
126. Mechanical power output of the system with a mass of 70.2g on each side on the pendulum for incoming wind speed of 1.6m/s (40rpm)	124
127. Mechanical power output of the system with a mass of 70.2g on each side on the pendulum for incoming wind speed of 1.6m/s (44rpm)	125
128. Mechanical power output of the system with a mass of 70.2g on each side on the pendulum for incoming wind speed of 1.6m/s (48rpm)	125
129. Mechanical power output trend in respective to wind speed for half of the system.....	126
130. Mechanical power output trend in respective to wind speed for the whole system.....	127

CHAPTER I

INTRODUCTION

Wind energy is one of the important alternative renewable energy resources that is seeing a steady growth throughout the world, especially in the United States of America for the past decade. Traditionally, Horizontal Axis Wind Turbines (HAWT) and Vertical Axis Wind Turbines (VAWT) are used to harvest electricity from wind. Comparing between HAWT and VAWT, HAWT has been and is still being used as the main platform for commercial wind energy harvesting [2-11]. Commercially available HAWT are limited by the aerodynamic loading on the blade of the turbine which increases from the hub to the tip. Therefore, in order to significantly increase the aerodynamic surface area of a HAWT, the size of the HAWTs is increased and this in return increases the gravitational and inertial loading on the blades. Figure 1 shows power rated of HAWT at 12 to 14m/s wind versus rotor diameter of HAWT collected from manufacturers. It can be seen from the collected data that in order to attain higher power output, HAWT manufacturers are increasing the size of their products.

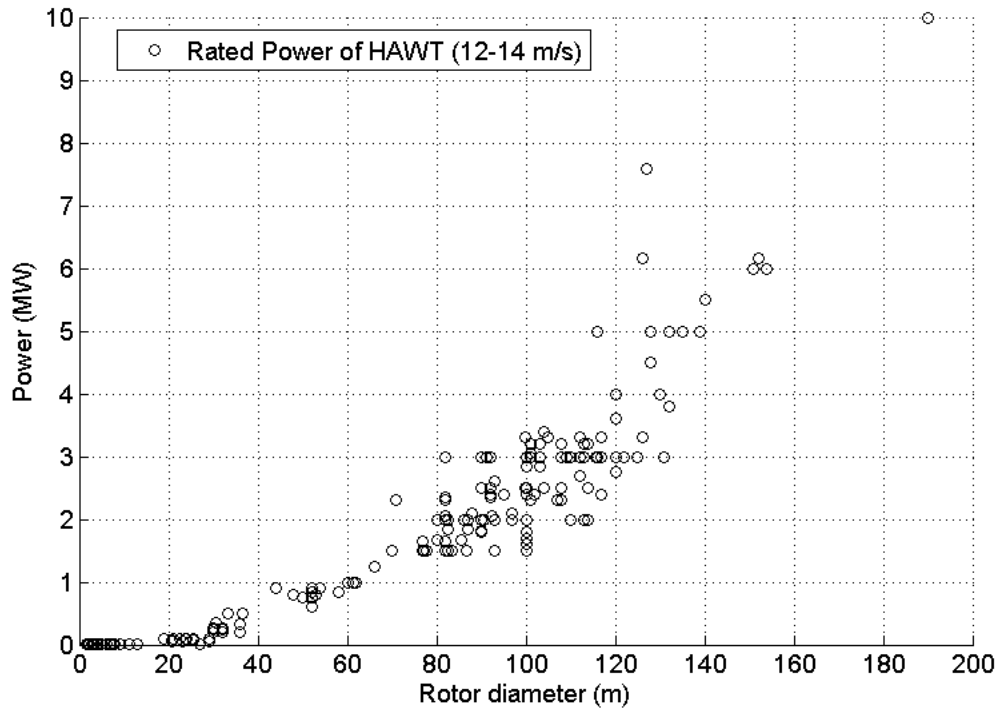


Figure 1: Power in respect to HAWT rotor diameter [12-125].

This limits the efficiency and performance of the HAWT at lower wind speed and a wind speed of around 5m/s is needed to get a commercial wind turbine to operate. Therefore these wind turbines can only be placed in regions where there is significantly strong wind throughout the year for maximum efficiency. However, most regions have wind speed that is less than 5m/s throughout the year and this can be seen clearly in the maps below by National Renewable Energy Laboratory (NREL).

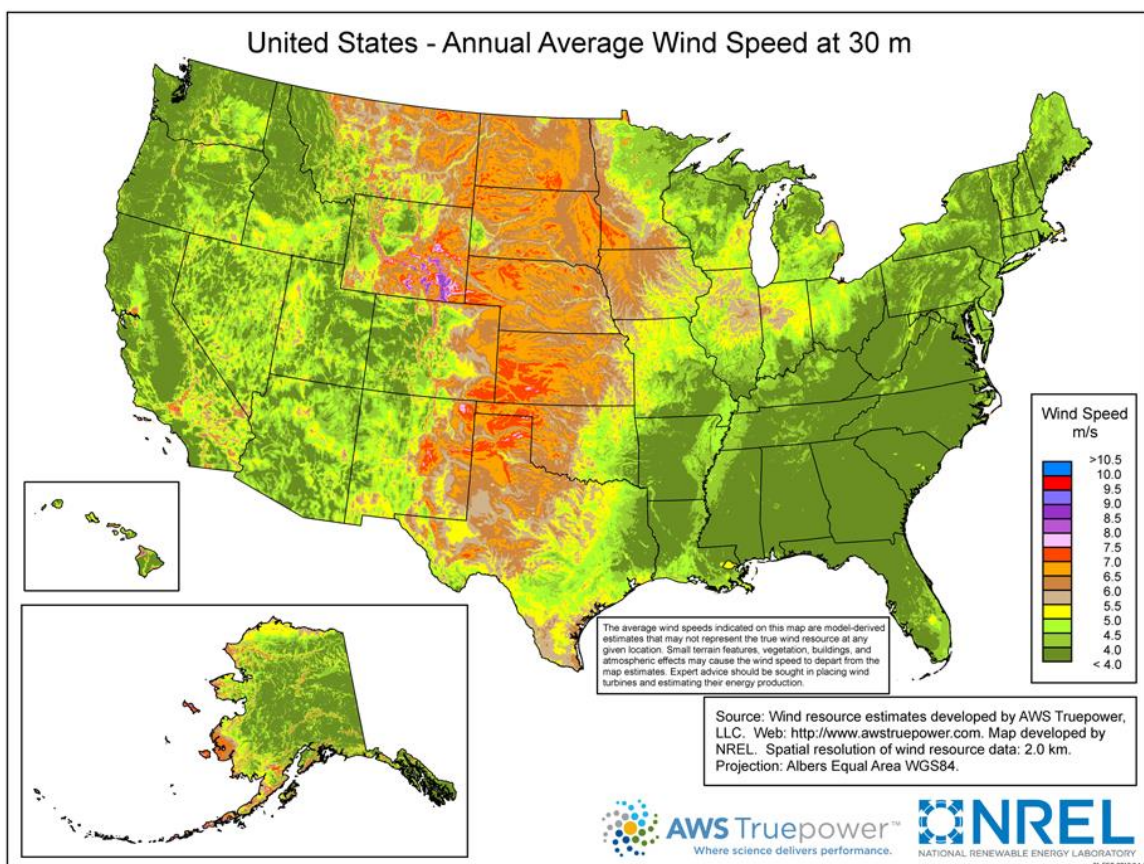


Figure 2: Annual average wind speed at 30m elevation [126].

The map in figure 2 shows the distribution of average wind speed at 30 meters elevation per year in the United States. As shown in figure 2, average wind speed of less than 5 m/s wind is much more prevalent throughout the region except for mountainous regions where the average wind speed is much higher. The average wind speed in the South-East coast region is less than 4m/s. The map in figure 3 shows the annual average wind distribution at 80 meters elevation which has average wind speeds of less than 6m/s in most regions.

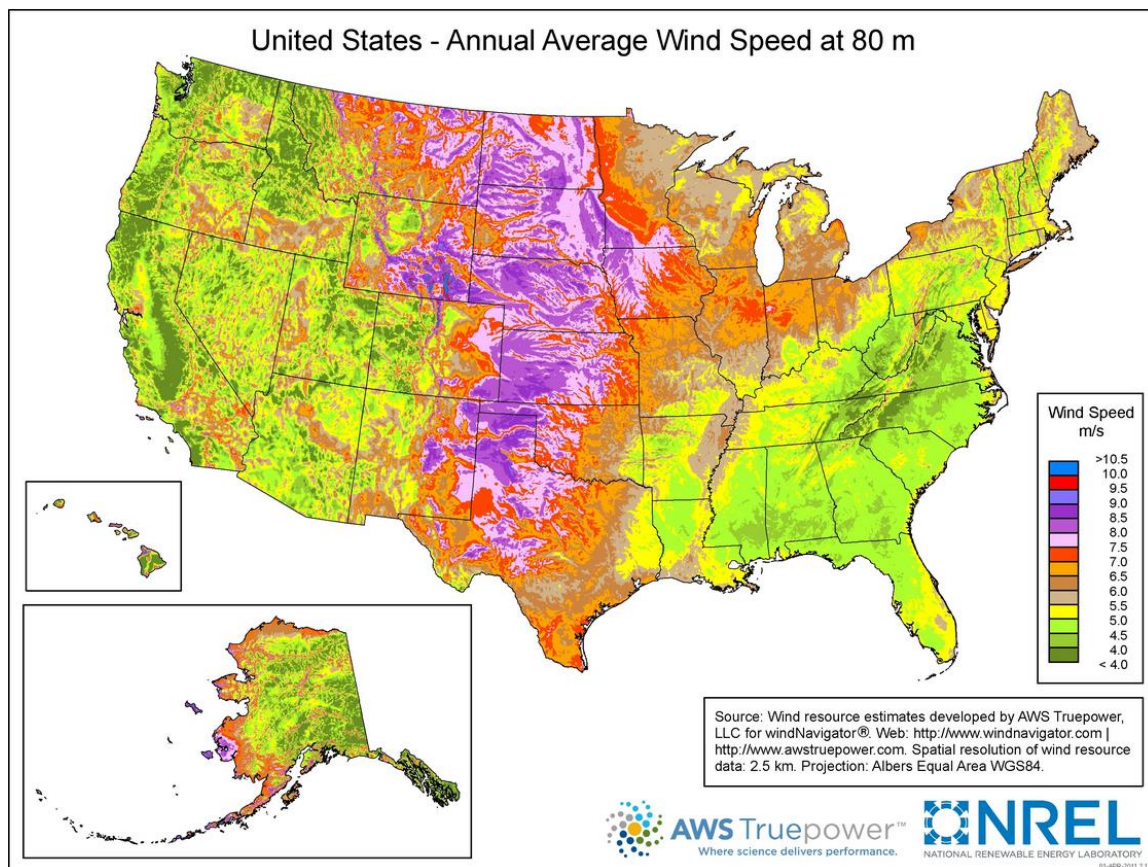


Figure 3: Annual average wind speed at 80m elevation [127].

The comparison between the two maps shows that the annual average wind speeds increases with higher altitude. This is the main reason as to why the commercially available wind turbines are getting bigger and taller - so as to reach the high wind speed regions. This reduces the down time of HAWT due to wind speeds that are lower than its cut in speed. However, it still would not be operating at its maximum capacity as the rated wind speed for large wind turbines are in the range of 12 to 14 m/s - as shown earlier in figure 1.

A non-conventional wind energy harvester that can operate in both high and low wind conditions is required. This can only be achieved by having a system that utilizes the entire aerodynamic surface with minimal inertial and gravitational loading.

CHAPTER II

OBJECTIVE OF THE STUDY

The goal of this experiment is to prove the concept wind energy harvester called Wind Oscillator by Tianshu Liu in “Wind Oscillator and Rotor for Power Generation”[1]. The oscillating wind turbine is analytically proven to operate efficiently at low wind speeds of below 5m/s as well as high wind speeds of higher than 15m/s. This removes the requirement for the wind turbine to be constructed at an elevation of 30 meters or above, which in turn reduces the construction cost of the wind turbine.

A model of the Wind Oscillator was designed, built and tested in the wind tunnel to evaluate the feasibility of the concept. Several experiments were conducted in the wind tunnel not only to evaluate the model but also to analyze the model under different configurations. Experiments conducted in the wind tunnel are

- LabVIEW data acquisition and analysis of RMS voltage output from dc motor generator.
- Photogrammetry study of the motion of arm and the wing to optimize the device.
- Photogrammetry study of the pendulum to calculate mechanical energy output of the model.

CHAPTER III

CONCEPTUAL DESIGN

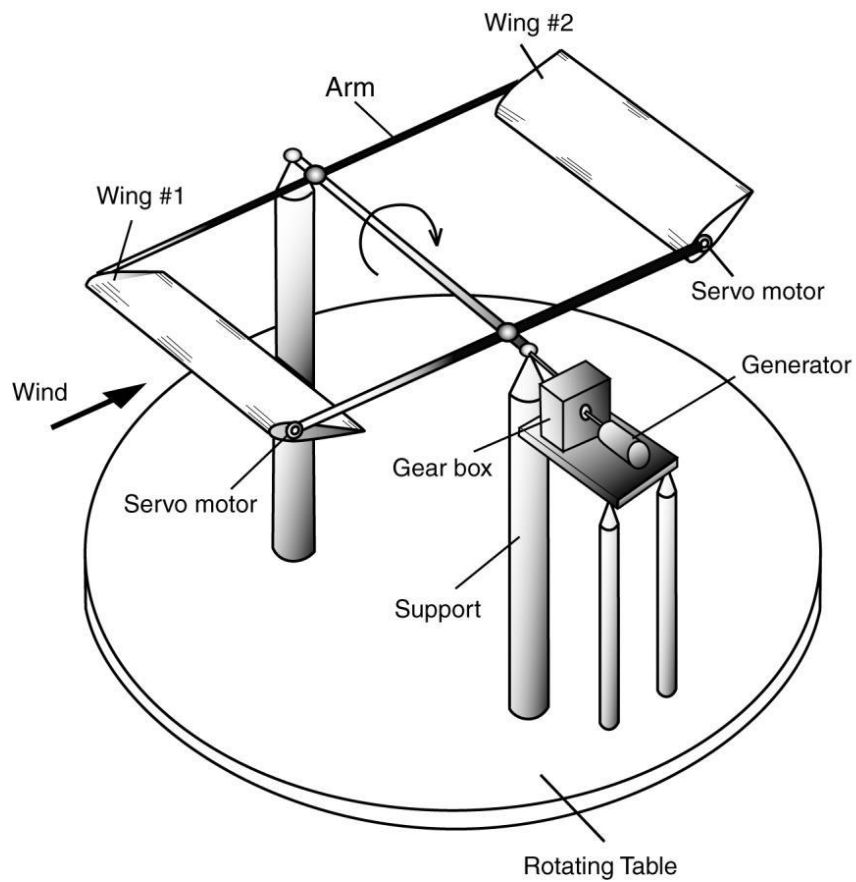


Figure 4: Conceptual design of the wind oscillator [1].

The basic design of the Wind Oscillator will be based on the Tianshu Liu's conceptual design shown in figure 4. The main components of the Wind Oscillator are rectangular wings with symmetrical airfoil profile which are mounted at the end of two

parallel bars in a tandem setting. Both wings are connected to the bar at their quarter chord and balanced around it and this makes the center of gravity (cg) and the aerodynamic center (ac) to be at the same location which allows the wings to pivot round their quarter chord. Since the weight for both wings are balanced out the weight does not play a significant role in the operation of the system.

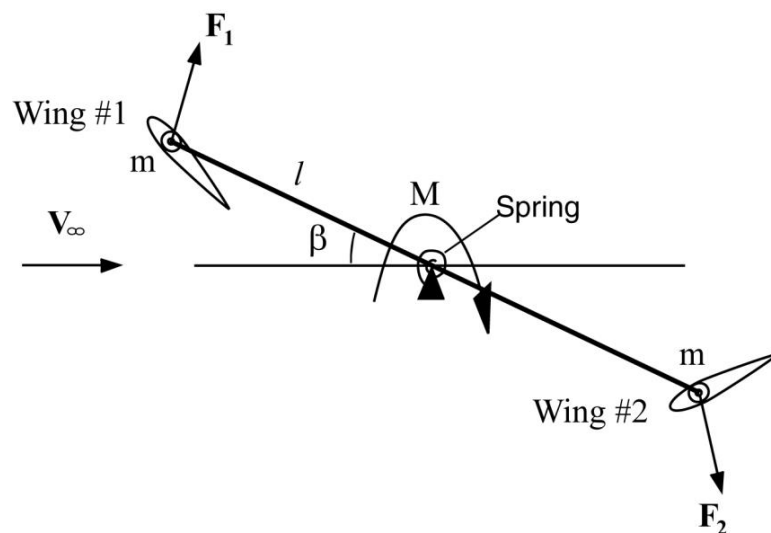


Figure 5: Basic schematic of the Wind Oscillator [1].

In the tandem setting the wing first to encounter the incoming wind is considered to be the leading wing or Wing #1, and the wing behind it to be the trailing wing or Wing #2 as shown in figure 5. The spring constrains the motion of the device from being rotational and retains the oscillating motion by either acting as a spring or a dampener depending on the wind condition. The AoA of the wings are controlled by motors at the quarter chord of the wings which allows for the oscillating motion of the device.

When the leading wing and trailing wing are set to be in the positive and negative angle of attack respectively, this creates a rotational motion at the center of the arms holding both the wings. Once the arm reaches a set angle, the polarities of the wings are switched and this makes the leading wing to have a negative AoA and the trailing wing to have a positive AoA. This switch allows the device to rotate in the counterclockwise motion. Both clockwise and counter clockwise motions generate torque which runs the generator and converts it to electrical energy. The movements of the device can be monitored and controlled by having a closed-loop feedback system.

Wing Oscillator addresses the negative points of HAWT by maximizing and utilizing the aerodynamics surface area by having two rectangular flapping wings. The inertia in the control of AoA can be reduced by using light composite materials. The gravitational loading of the device are balanced out in this system.

CHAPTER IV

MECHANICAL DESIGN

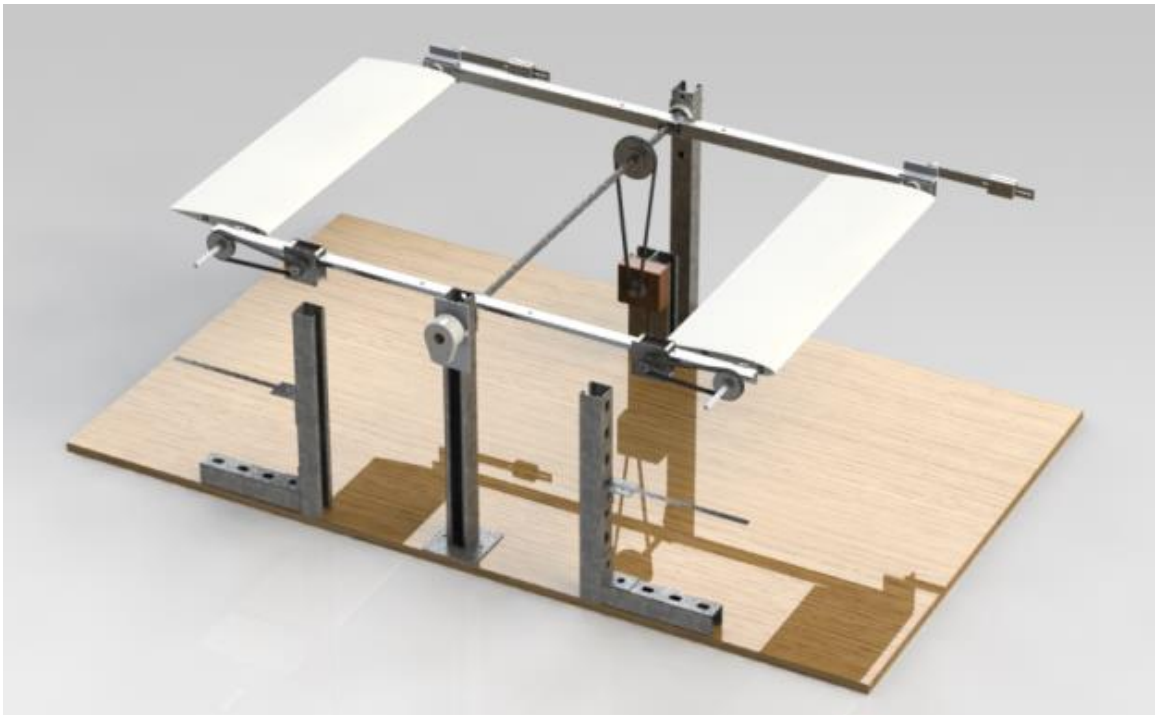


Figure 6: The Solidworks Isometric view of the whole system.

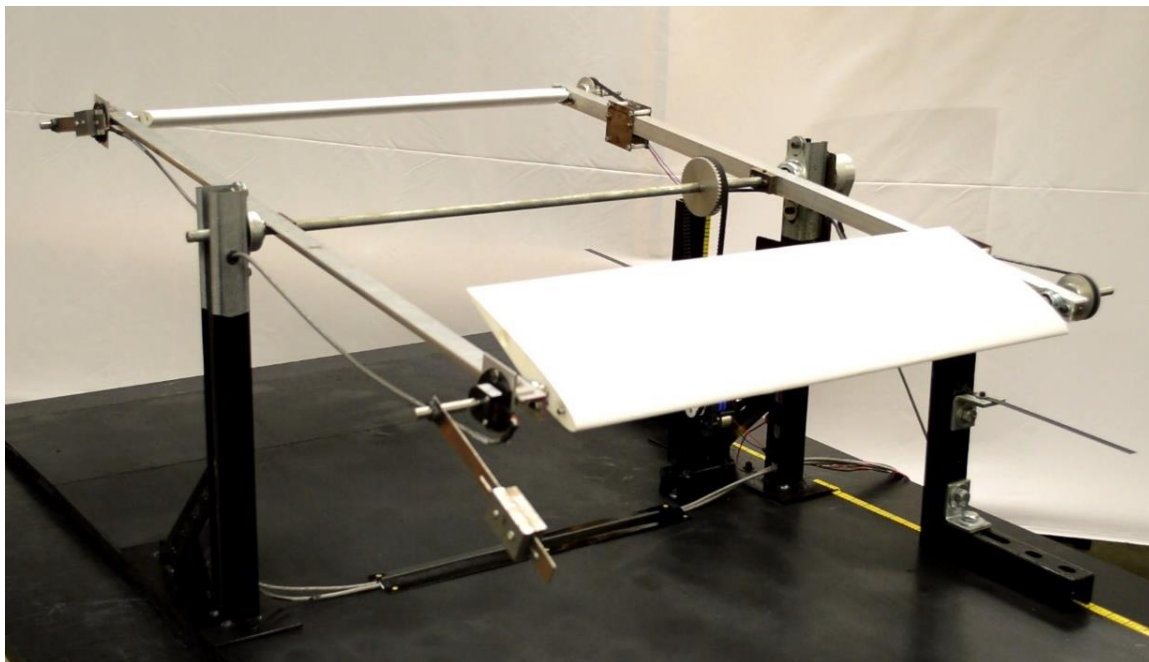


Figure 7: The isometric view of the actual setting of the device.

The Wind Oscillator model was designed, built and tested in the wind tunnel. The Solidworks design of the model is shown in figure 6 and the actual set up of the model is shown in figure 7. Figure 8 shows the different Mechanical and electrical components of the model wind oscillator in Solidworks design.

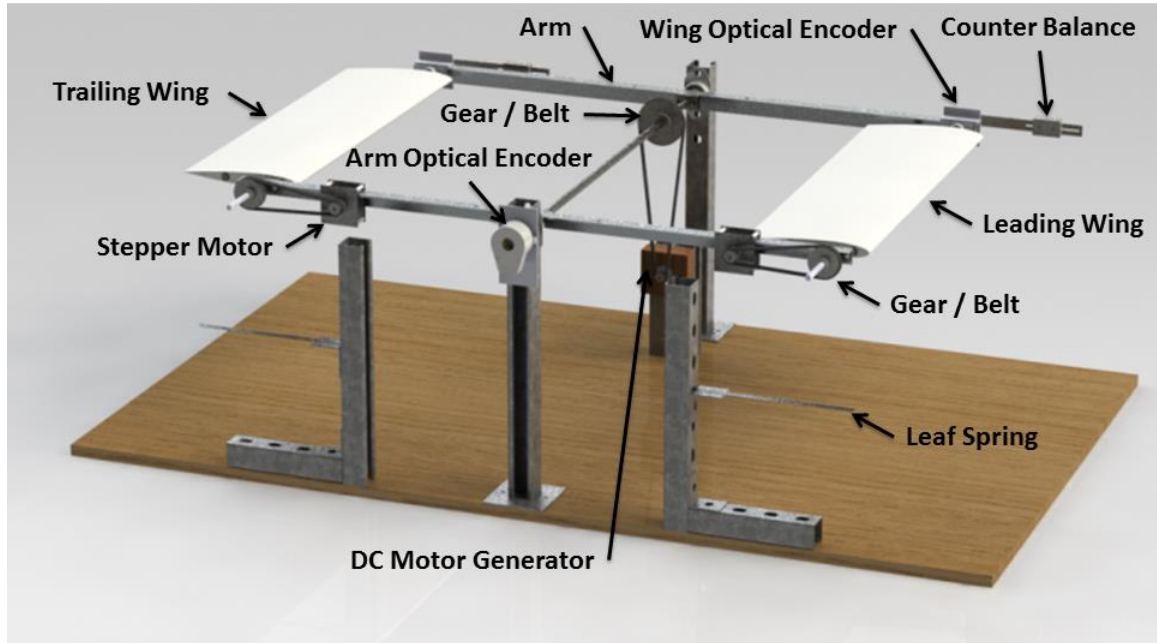


Figure 8: Mechanical and electrical components of the model wind oscillator in Solidworks design.

The front and rear wings of the model are made out of plastic with the cross section of NACA 0012 airfoil. The dimension of each wing is 8.454in (0.2m) in chord length and 25.59in (0.65m) in span. Both wings were placed in line with the two parallel bars in the middle which act as the arms of the system. This allows the model to be in a naturally balanced state with respect to its weight. Each wing is actuated by two separate motors located on one of the arms with equal amount of space between the middle of the arm to each motor in order to retain the weight balance of the system. The control of the wings by the motor are amplified using gear and belt system to increase the response time of the wings. The wings are controlled at the quarter chord which is the aerodynamic center of an airfoil but since the center of gravity also plays an important part in the

operation of this device, both the aerodynamic center and center of gravity need to be located at the same location on the airfoil.

Counter balance weights were introduced to the rod that runs through the quarter chord of the wing which moved the center of gravity to the location of aerodynamic center. Optical rotary encoders were placed at the quarter chord of each wing to monitor the angle of the wings with respect to the location of the arm. The arms were later connected by a rod that runs through the middle of the arm to ensure that each side of the arm was equally balanced. The rod is later connected to two parallel legs to hold the system up from the ground. More sensitive rotary encoder was placed at the middle rod to monitor the angle of the arm at a specific location. The middle rod is connected to a DC motor generator through a gear and belt system. A leaf spring system is placed below the arms and was set to interact with the rod sticking out of the quarter chord of the wings not only as a spring for lower wind scenarios but also as a dampener for high wind scenarios. In the earlier case, the spring helps to restore kinetic energy back into the system and sets the range of motion of the device in latter case. The dimensions of the model are shown in figures 8, 9 and 10 which were restrained by the dimensions of the wind tunnel test section.

Mechanical Dimension

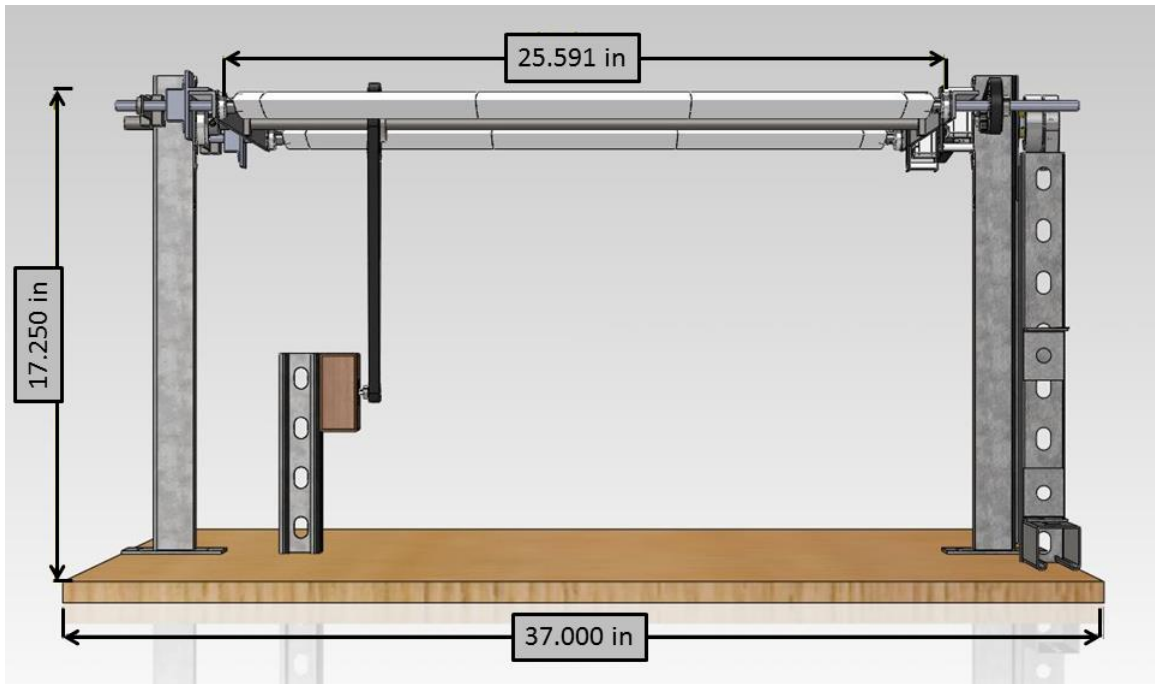


Figure 9: Dimensions of the model wind oscillator from the frontal view.

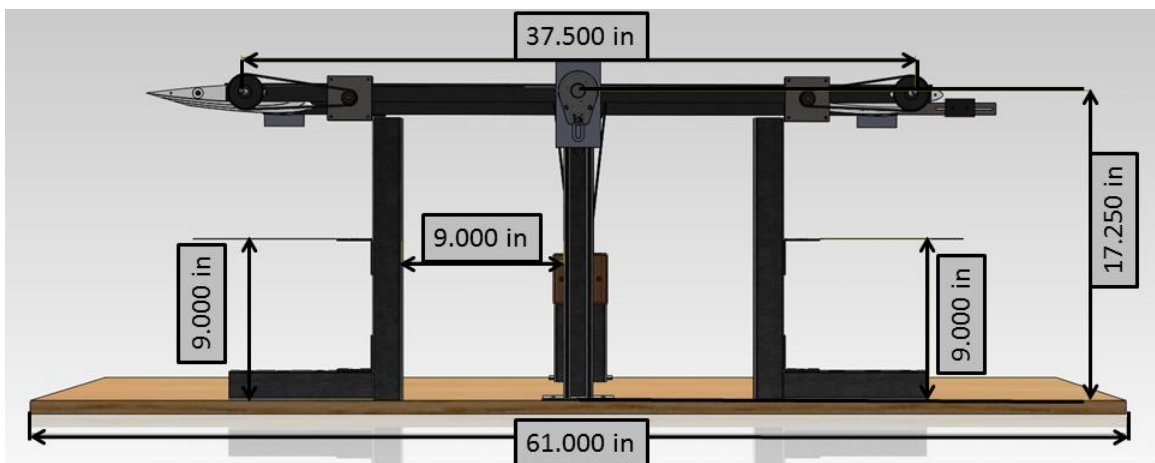


Figure 10: Dimensions of the model wind oscillator from the side view.

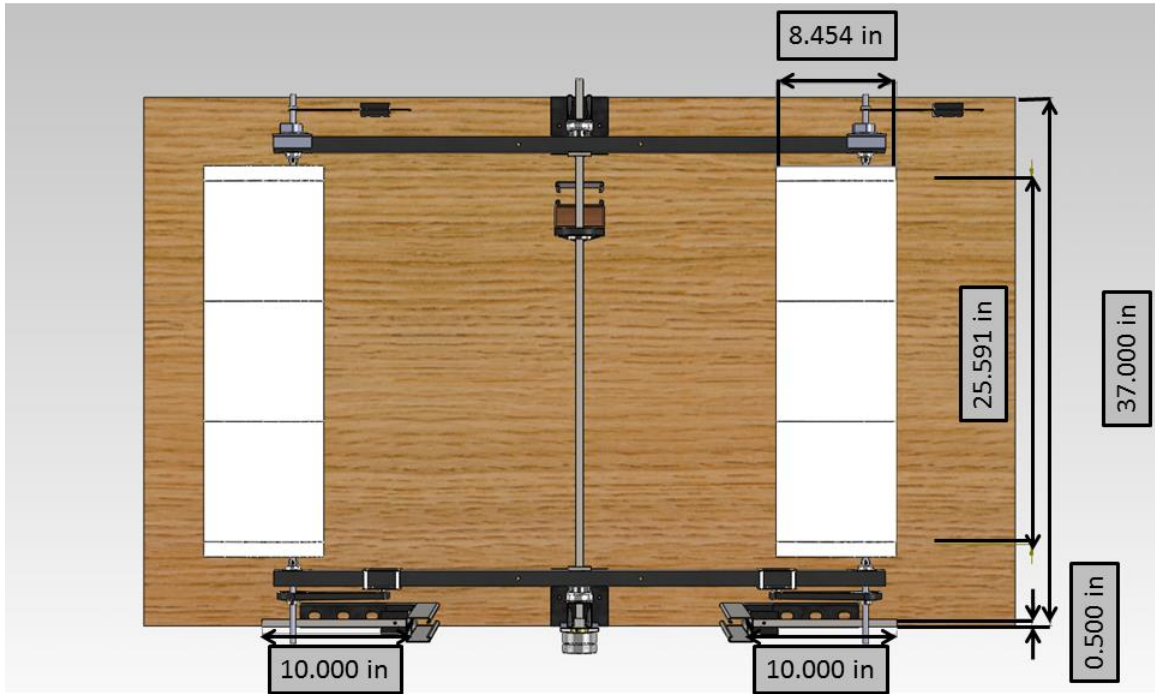


Figure 11: Dimensions of the model wind oscillator from the top view.

Mechanical Dynamics

The airfoil used in the system is a National Advisory Committee for Aeronautics (NACA) 0012 with a chord length of 0.2m and a span of 0.65m for each wing. NACA 0012 was chosen because the system required symmetrical airfoils to generate lift while the wing is moving up and down. Figure 12 shows the cross section of the NACA 0012.

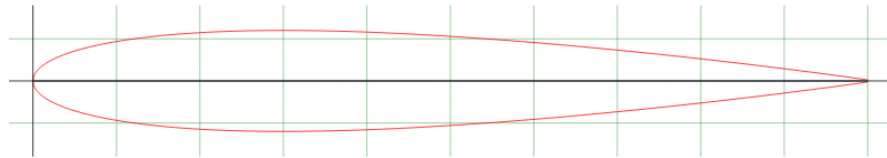


Figure 12: Cross section of NACA 0012 airfoil [128].

The graph in figure 13 shows the characteristic of a NACA 0012 at a Reynolds number of 50,000 (1), 100,000 (2) and 150,000 (3) respectively. Based on Reynolds number of 140000 for NACA 0012 and with sea level air characteristic, the maximum performance or lift created by of NACA 0012 in a 20m/s wind is calculated. Based on basic calculations, each wing can produce about 1.75 Newton of lift and 0.0955 Newton of drag. The gravity or the weight of the wings does not play an important role as they were counter balanced as shown in the figure 14.

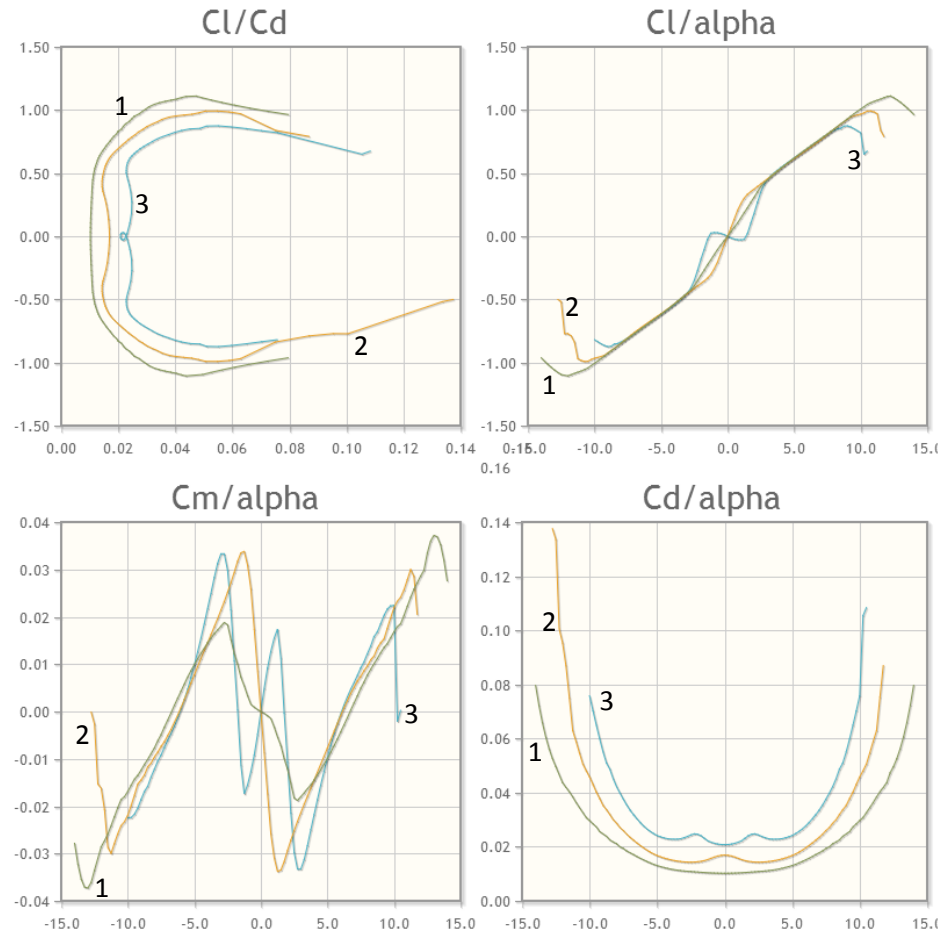


Figure 13: Characteristic graphs for NACA 0012 at different Reynolds Numbers [129].

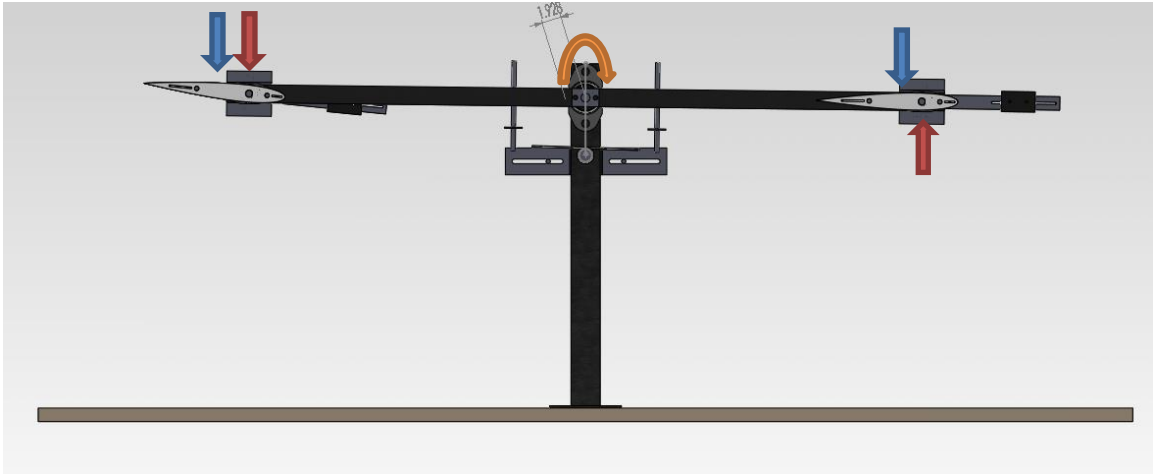


Figure 14: The force distribution on the system at a particular position.

Figure 14 shows the force distribution on the system where the blue arrow denotes the gravitational force and the red denotes the lift force generated by the wing. Since the system was balanced out, the system relied solely on the lift generated by the wings to operate. The total torque generated by the wings at the pivoting point theoretically is about 1.68 Newton meter. The total torque generated at the quarter chord of each individual wing is about 0.277 Newton meter. Therefore the motor that controls the wing would be able to withstand the torque produced by the wing.

Spring

The spring plays an important part in the operation of the device. In real life conditions, the spring would be subjected to a range of wind speeds which increases and decreases unpredictably. Thus, the device must be able to withstand these sudden changes. The spring in general will allow this to be accomplished without any electronic control or any major modification to the device. At higher wind speeds, the spring behaves as a dampener to protect the device from any major damage. At lower wind speeds, the spring allows for the transfer of kinetic energy back to the device and helps the arm to bounce back when the angle of the wings are reversed.

Different type of springs were considered for the device and two of them were tested to see which one would suit well in terms of quick and easy manipulation and the practicality of the spring on the device. The springs that were initially considered were compression spring, extension spring, torsional spring and leaf spring. Compression and extension springs were dropped from the consideration as it would not be practical when the Wind Oscillator is built to its actual size. Torsional and leaf springs were tested to see both their practicality and performance.

Torsional Spring

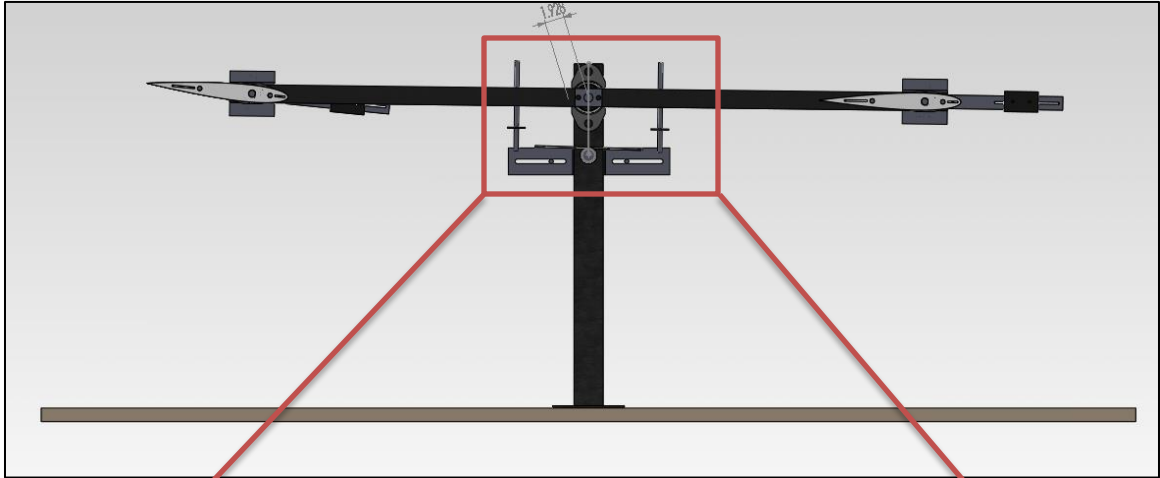


Figure 15: Side view of the right leg of the system.

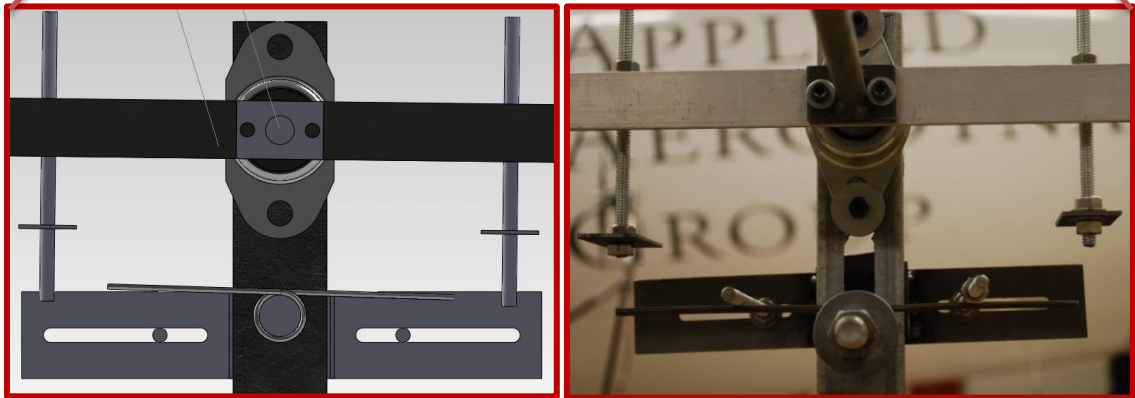


Figure 16: Side view of the torsional spring in Solidworks drawing and in real system set up

The torsional spring is one of the main components of the system. The side view of the location of the spring is shown in figure 15. The close up of the side view is shown in figure 16 both in Solidworks drawing and also in the actual system. This helped to conserve the energy generated by the wings as the wing pushes down on the torsional spring through the bar that is protruding from the main arm and helped the arm to bounce back up when the direction of the wing is reversed. This allows for the frequency of the system to be maintained at a certain range and the frequency can be increased or decreased based on the stiffness of the spring assuming the wind speed is constant. The torsional spring also behaves as a dampener. As the wind speed increases, the frequency or the speed that the arm moves from the top position to the bottom position increases. This also increased the force generated by the system. The spring helped to dampen the additional force and to reduce damage to the system. The spring also maintains the range of travel of the arms.

Three different commercially available springs with different spring constants were tested to observe their effect on the system. A commercially available industrial fan was used in testing the torsional spring. Each spring was tested at high and low wind speed of the fan. At each speed, the number of oscillations the spring allowed the system to make is measured at three different time intervals. The number of oscillations the system makes after the wind source is cut off is also measured to observe the sensitivity of the system. The springs were set to allow the system to oscillate a maximum of 18 degrees per direction.

	Time (mins)	Spring 1	Spring 2	Spring 3
Low	0	0	0	0
	1	5.75	7.25	6.5
	5	41	43	41.5
	10	85.5	87.75	86
High	0	0	0	0
	1	9.5	9	8
	5	46.5	48	47
	10	94.5	97	95.5

Table 1: Number of oscillations the spring allows the system to make with the wind on.

Spring 2	Time (mins)	Oscillations (Fan On)	Oscillations (Fan Off)
Low	0	0	0
	1	7.25	1.25
	5	43	1.25
	10	87.75	1.25
High	0	0	0
	1	9	1.25
	5	48	1.25
	10	97	1.5

Table 2: The number of oscillations spring number two allows the system to make with the wind turned on and off right after the fan on conditions.

Table 1 shows that spring number two allowed the system to make more oscillations compared to the other two springs at both high and low wind speed. The spring constant for spring number two is 30.22inch pounds per 360 degree. The oscillations for the fan off condition were measured right after the specified time period. Table 2 shows the number of oscillations spring number two allows the system to make with the wind turned on and off. It can be seen that the number of oscillation the number two springs made for the fan off condition for each setting is the same except for at high fan speed for duration of 10 minutes which produced 1.5 oscillations.

The implementation of torsion spring was also later dropped as it was not practical to change the spring for a range of wing speeds.

Leaf Spring

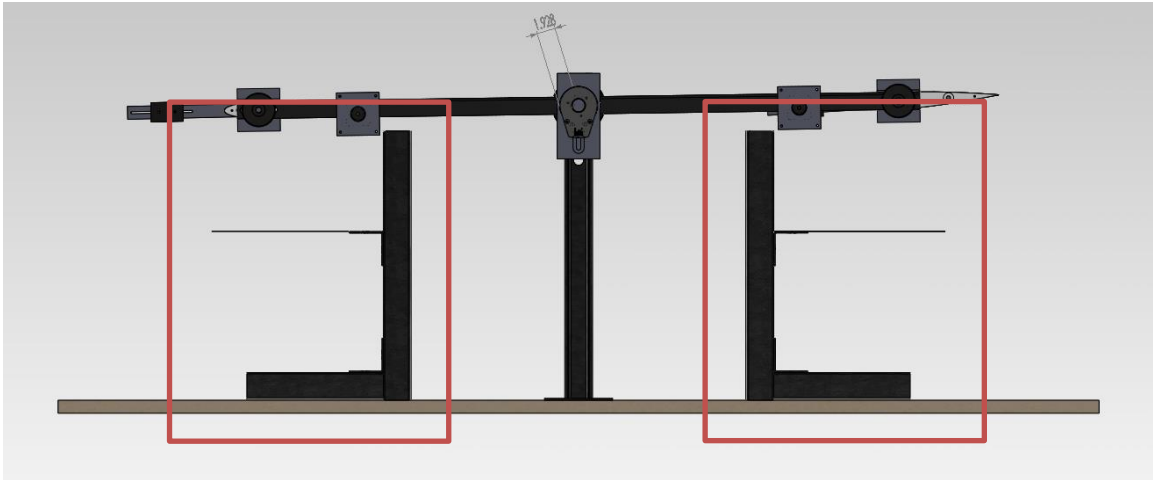


Figure 17: Side view of the leaf spring in the system.

The torsional springs were then replaced by leaf springs which allowed the user to fully manipulate its spring stiffness. The side view of the setup of the leaf spring is shown in figure 17. Isometric view of the spring is shown in figure 18. The leaf spring behaved exactly like the torsion spring but it also allows the user to control the height and the length of the spring which directly affects the stiffness of the spring and the frequency that the system oscillates. The leaf spring also behaves as a dampener based on the setting of the device. Therefore, it was very important to fully understand the characteristic of the leaf spring as it will greatly affect the performance of the device. Basic experiments were conducted to test the practicality as well as the performance of the leaf spring. The experiment would include four different variables with two levels each. The factors chosen were weight, location of the weight, spring length and spring thickness. The width

of the spring and the location on the spring where the deflection is observed was held constant for this experiment.

The response variable selected for this experiment is the height of the spring deflection from the level position to the deflected position of the spring at a particular fixed position for all the spring settings. The deflection will be always measured at the location where the weight will be hung furthest from the fixed point which is 7 inches. The location where the reading of the deflection was taken from was fixed because the aim of the experiment is to analyze the deflection of the spring at that point. That location was also chosen because when a beam bends it would not bend in a linear pattern. The deflection increases from the fixed point, all the way to the tip of the beam; therefore it is logical to choose the furthest point away from the fixed position. Greater deflection also allows for more sensitive reading to be taken.

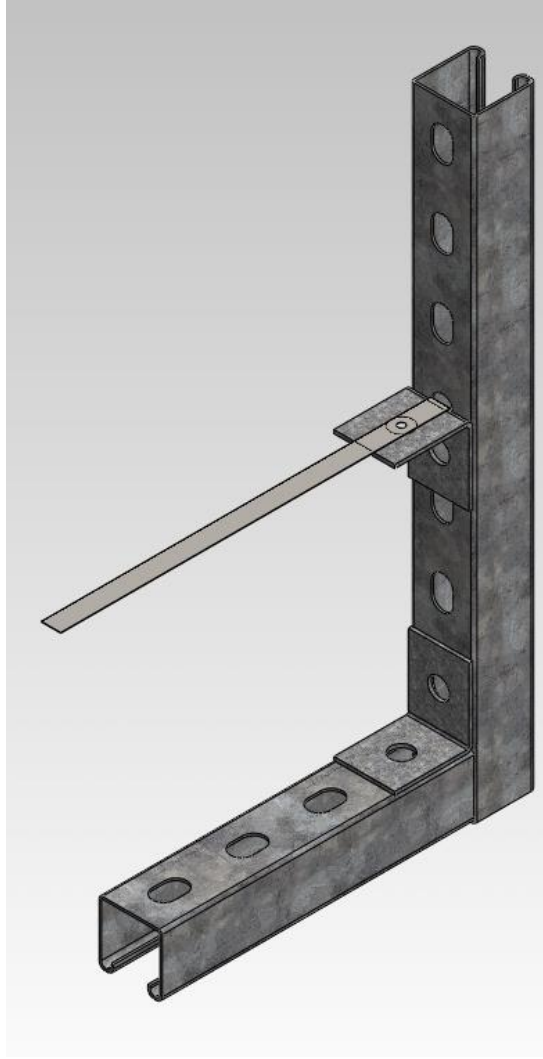


Figure 18: Isometric view of the leaf spring.

FACTOR 1: WEIGHT

Weights were introduced at certain points on the spring to induce deflection of the spring. Two different weights were used with significant gradient to observe the deflection of the spring. The weights chosen were 20.9g and 61.5g.

FACTOR 2: LOCATION OF THE WEIGHT

Different location points with equal distance with each other were set to place or hang the weights from the free end of the spring. This is to prove if moving close to the fixed end of the spring increased the stiffness of the spring. The locations that were chosen were 5in and 7in from the suspended end of the spring.

FACTOR 3: SPRING LENGTH

The length of the leaf spring was studied to determine if it will influence the performance of the spring. Two different spring lengths were chosen to observe for any variations in the readings. Spring lengths of 7.5in and 9.5in were selected for the experiment.

FACTOR 4: SPRING THICKNESS

Spring thicknesses were studied to monitor the influence of spring thickness on the deflection of the spring. The springs will be placed on top of each other to increase the thickness. Therefore the thickness was set to t_1 and $t_2 = 3t_1$ which is 1/16in and 3/16in.

Detailed side view of the leaf spring setting and the factor are shown in figure 19.

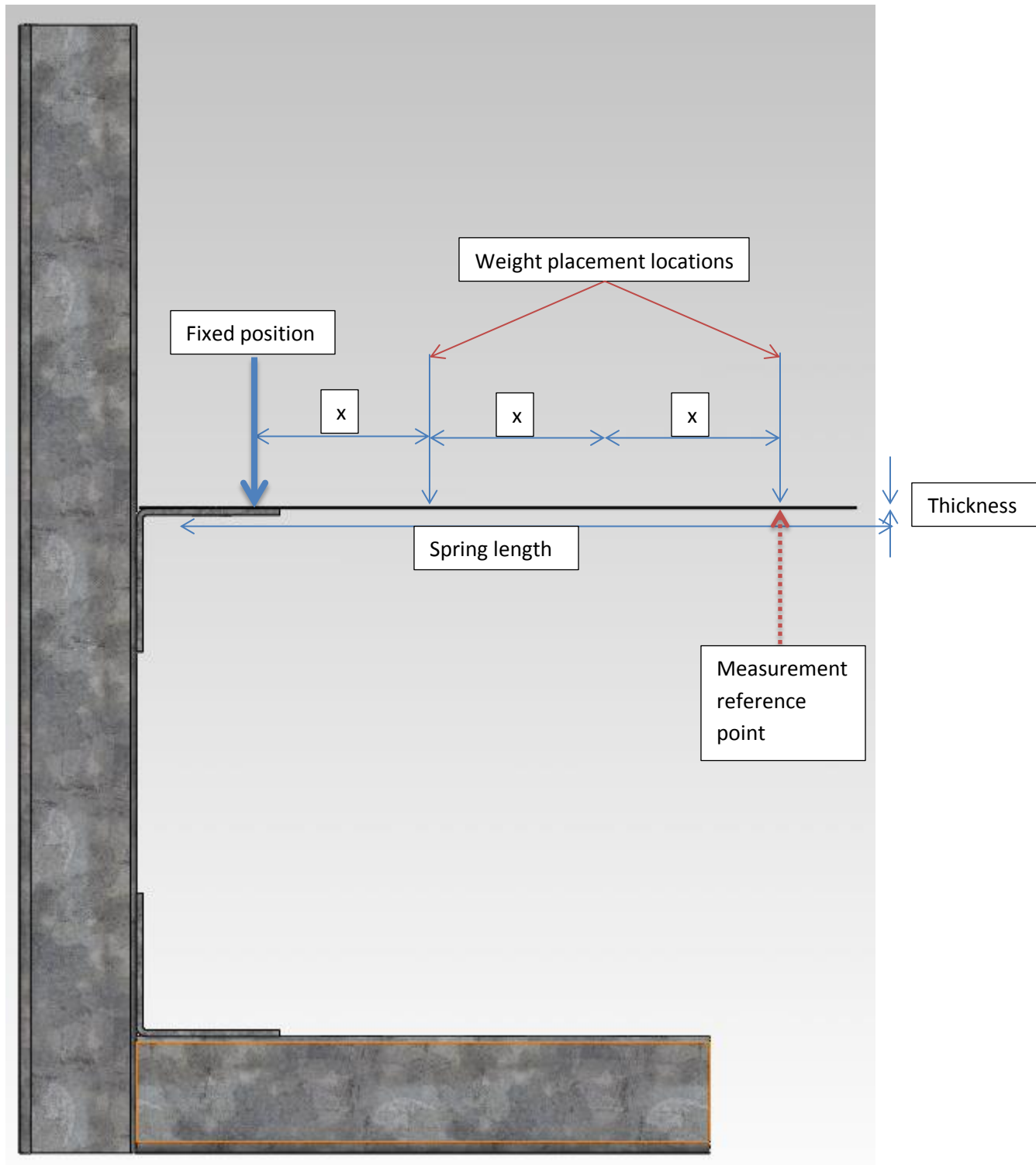


Figure 19: Side view of the spring setting.

EXPERIMENT DESIGN:

The experiment was run as a full factorial 2^4 design with a single replicate in Minitab. Since the full factorial design was decided for the final testing with four factors with one block and one replicate, the total number of runs that needed to be conducted was 16. The Minitab output for this full factorial design is given in the appendix B and C of Minitab output. All terms are free from aliasing.

EXPERIMENT PLAN:

The Minitab output of the experimental plan for the experiment with randomized run order is given in table 3 and in Appendix A of Minitab output. -1 denotes the lower level of the testing factor whereas 1 denotes the higher level of the factor that is being tested. The detailed experimental plan is given in table 4 for the ease of the experimenter.

StdOrder	RunOrder	CenterPt	Blocks	A	B	C	D
14	1	1	1	1	-1	1	1
7	2	1	1	-1	1	1	-1
6	3	1	1	1	-1	1	-1
10	4	1	1	1	-1	-1	1
2	5	1	1	1	-1	-1	-1
3	6	1	1	-1	1	-1	-1
11	7	1	1	-1	1	-1	1
13	8	1	1	-1	-1	1	1
12	9	1	1	1	1	-1	1
16	10	1	1	1	1	1	1
9	11	1	1	-1	-1	-1	1
5	12	1	1	-1	-1	1	-1
15	13	1	1	-1	1	1	1
8	14	1	1	1	1	1	-1
1	15	1	1	-1	-1	-1	-1
4	16	1	1	1	1	-1	-1

Table 3: Experimental plan from Minitab

StdOrder	RunOrder	CenterPt	Blocks	Weight(g)	Location Of the Weight (inch)	Spring length (inch)	Spring thickness (inch)
14	1	1	1	61.5	5	9.5	3/16
7	2	1	1	20.9	7	9.5	1/16
6	3	1	1	61.5	5	9.5	1/16
10	4	1	1	61.5	5	7.5	3/16
2	5	1	1	61.5	5	7.5	1/16
3	6	1	1	20.9	7	7.5	1/16
11	7	1	1	20.9	7	7.5	3/16
13	8	1	1	20.9	5	9.5	3/16
12	9	1	1	61.5	7	7.5	3/16
16	10	1	1	61.5	7	9.5	3/16
9	11	1	1	20.9	5	7.5	3/16
5	12	1	1	20.9	5	9.5	1/16
15	13	1	1	20.9	7	9.5	3/16
8	14	1	1	61.5	7	9.5	1/16
1	15	1	1	20.9	5	7.5	1/16
4	16	1	1	61.5	7	7.5	1/16

Table 4: Detailed experimental plan

DATA COLLECTION:

A	B	C	D	Deflection(mm)
1	-1	1	1	6
-1	1	1	-1	13
1	-1	1	-1	18
1	-1	-1	1	7
1	-1	-1	-1	19
-1	1	-1	-1	14
-1	1	-1	1	5
-1	-1	1	1	3
1	1	-1	1	15
1	1	1	1	12
-1	-1	-1	1	3
-1	-1	1	-1	7
-1	1	1	1	6
1	1	1	-1	38
-1	-1	-1	-1	7
1	1	-1	-1	35

Table 5: Data collected (12/6/2014 @ 3pm)

The experiment was run in the random order given by the Minitab software and the deflections of the beams were recorded in millimeters (mm) as show above.

STATISTICAL ANALYSIS:

Since the experiment was conducted with just one single run per case without any replicates, these resulted in zero degrees of freedom for error which is crucial in running the statistical analysis. Normal and half normal probability plots were constructed to identify the significant factors in this experiment in order to conduct the statistical analysis.

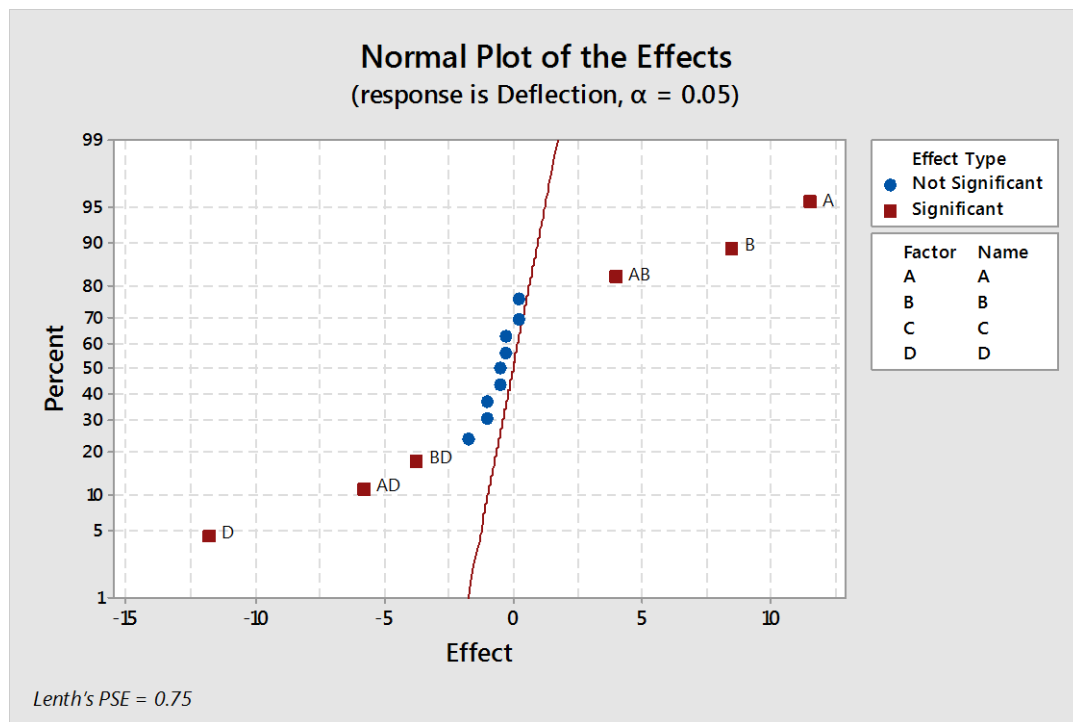


Figure 20: Normal probability plot

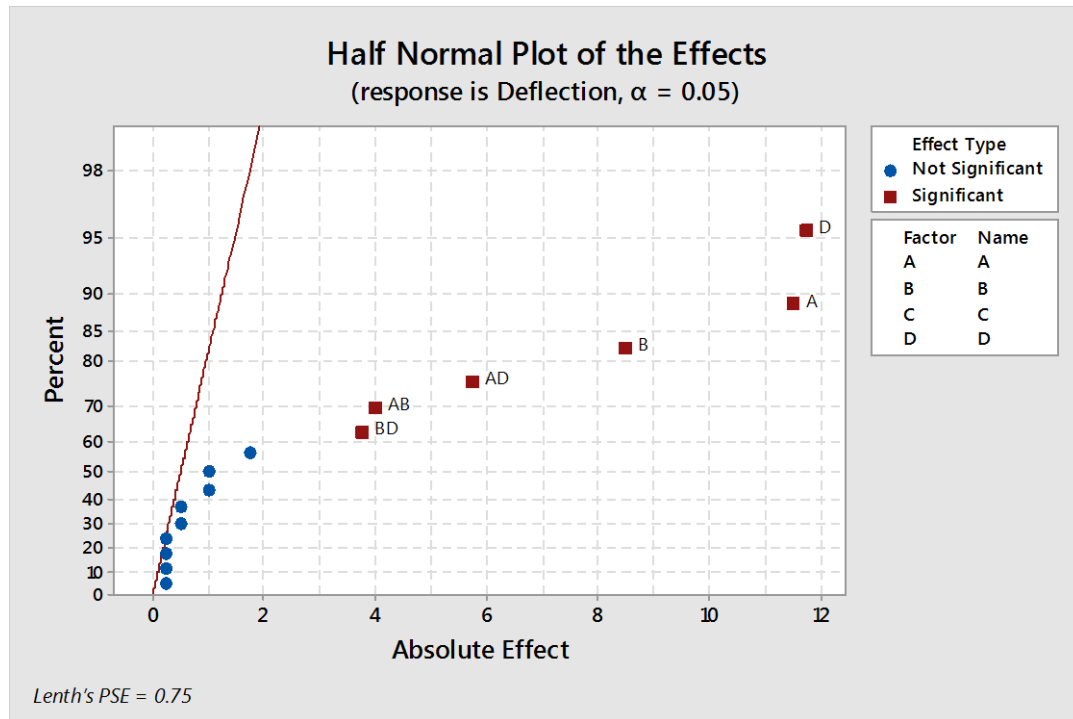


Figure 21: Half normal probability plot

The normal and half normal probability plot in figure 20 and 21 shows the significant and non-significant factors and the significant and non-significant interaction between the factors. This allowed for the identification and investigation of the significant factors and the interaction between them. The non-significant factor and interactions were combined together and included with the error term. The normal and half normal probability plot shows that factors A, B and D played significant roles in the magnitude of the deflection of the beam. The plots also indicate that the interaction between factors AB, AD and BD play a significant role in the deflection of the beam. Based on the results from the plot, another Design of Experiment (DOE) was ran with the selected factorials and interactions.

Based on the analysis of the variance, it can be seen that factors A, B and D and the interactions between them are significant since the P value for all those cases were below 5%. This means that the weight that was placed on the spring, the location where the weight was placed on, the spring thickness and their interactions are factors that significantly affect the deflection of the spring. The effect portion in the coded coefficients showed the magnitude of effect each factor and interaction had on the spring. It also shows the direction of effect when the factor was increases from lower level to upper level. For example, factor A and factor D has the highest effect on the deflection of the spring but factor A has a positive effect. This means that when the weight is increased, the spring had a higher deflection whereas when the thickness of the spring was increased, the spring had a lower deflection. From the R square value given above, it can be said that this is a sound model.

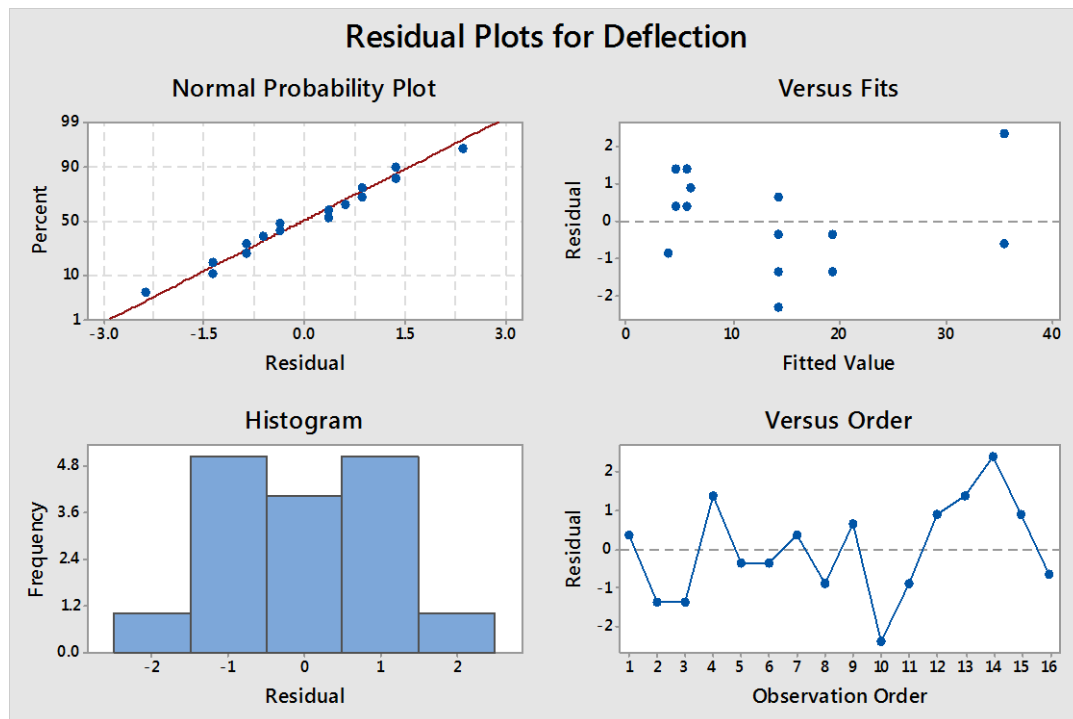


Figure 22: Residual plots for deflection

Figure 22 shows the residual plots for deflection. The deflection data for the Normal probability plot appear to follow a straight line. There is no evidence of non-normality, skewness, outliers, or unidentified variables. Based on the versus fit plot, the residuals appear to be randomly scattered about zero. There is no evidence of non-constant variance, missing terms, or outliers. The histogram shows an evenly distributed graph. For the residuals vs observation order, the residuals appear to be randomly scattered about zero. There is no evidence that the error terms are correlated with one another. Figure 23, 24, 25 and 26 shows the residual plots versus each factor. For all the factors, the residuals appear to be randomly scattered about zero. No evidence exists that there is a pattern in the residuals or curvature in the data.

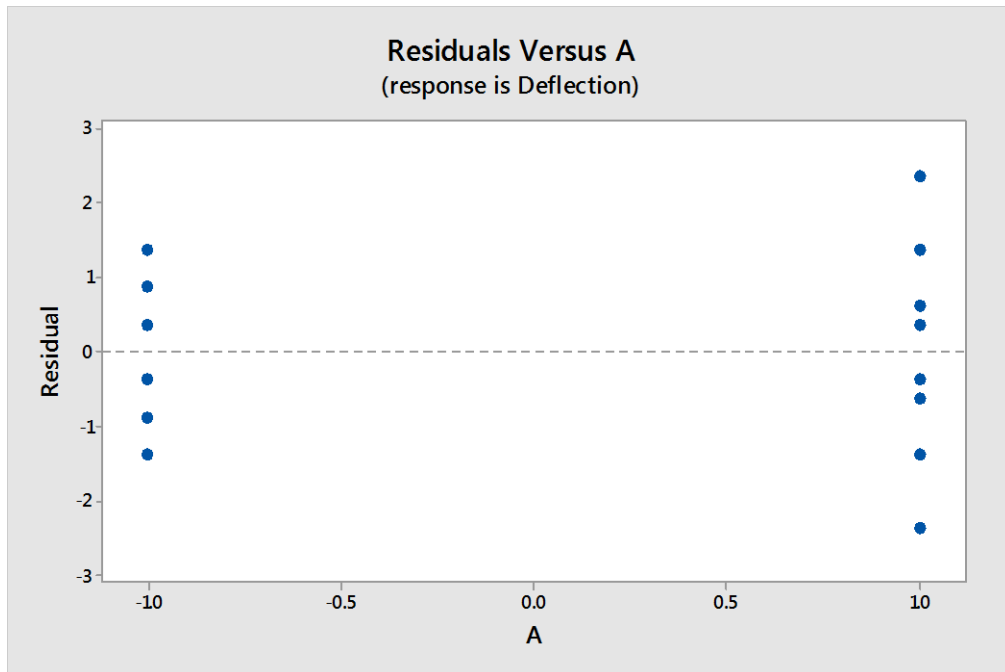


Figure 23: Residual versus A (Weight)

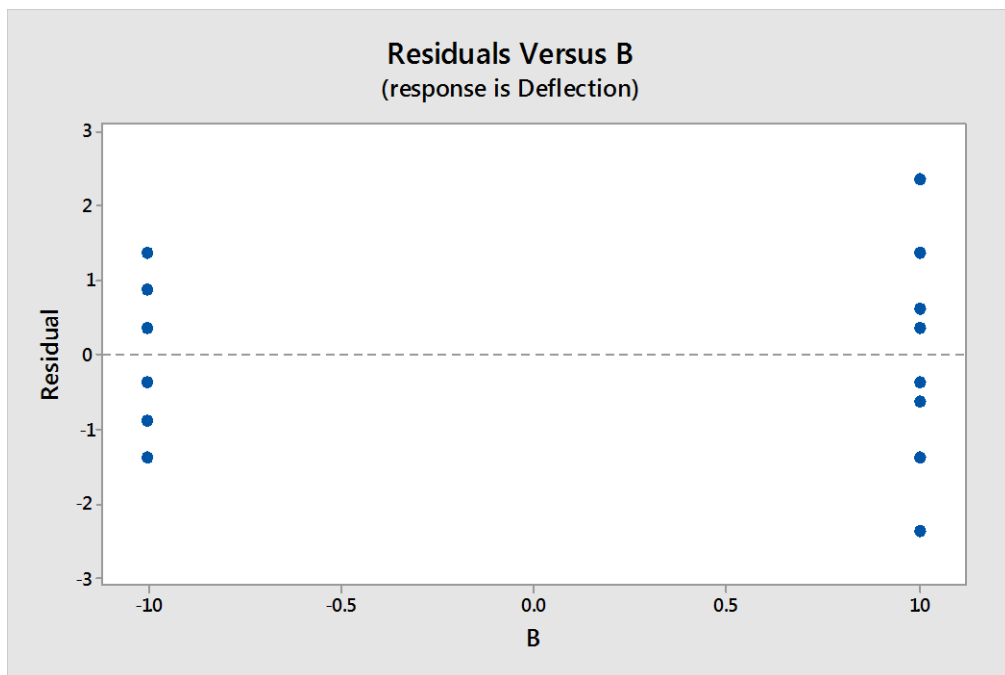


Figure 24: Residual versus B (Location of the weight)

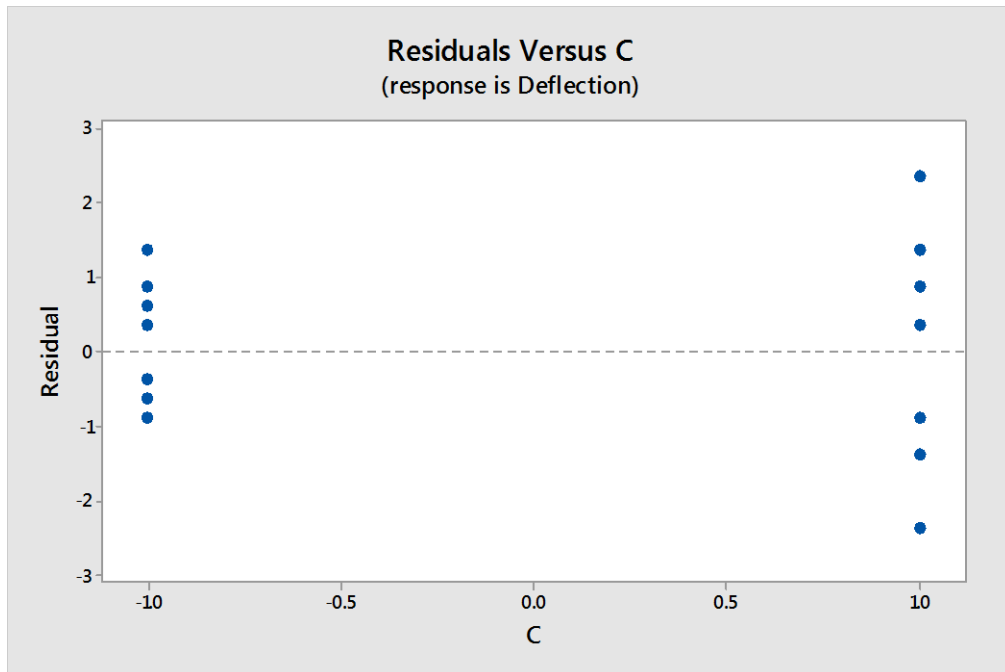


Figure 25: Residual versus C (Length of the spring)

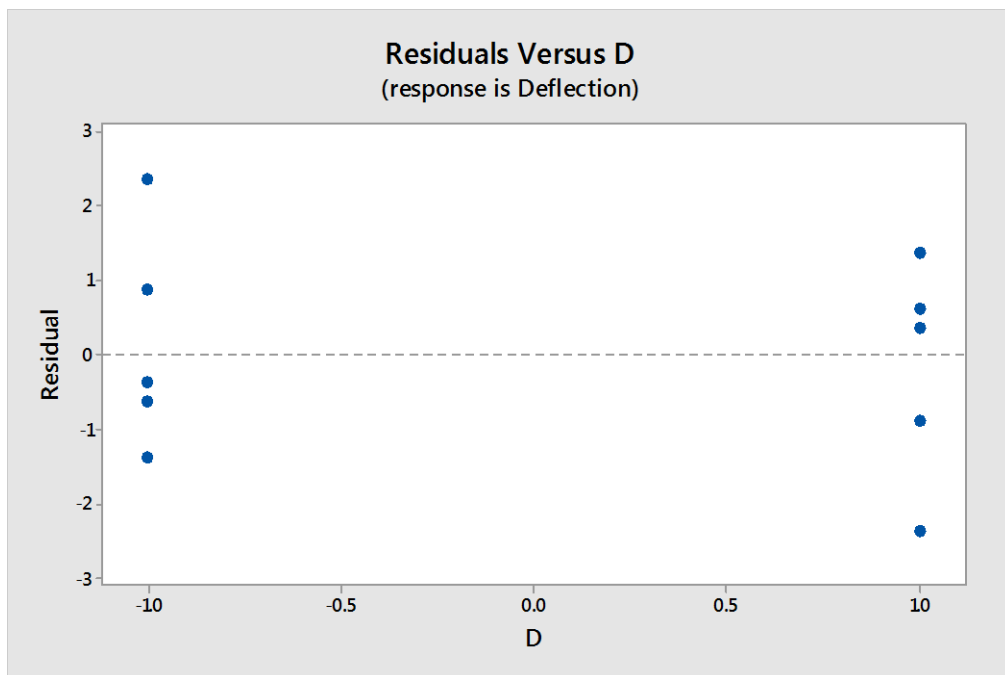


Figure 26: Residual versus D (Thickness of the spring)

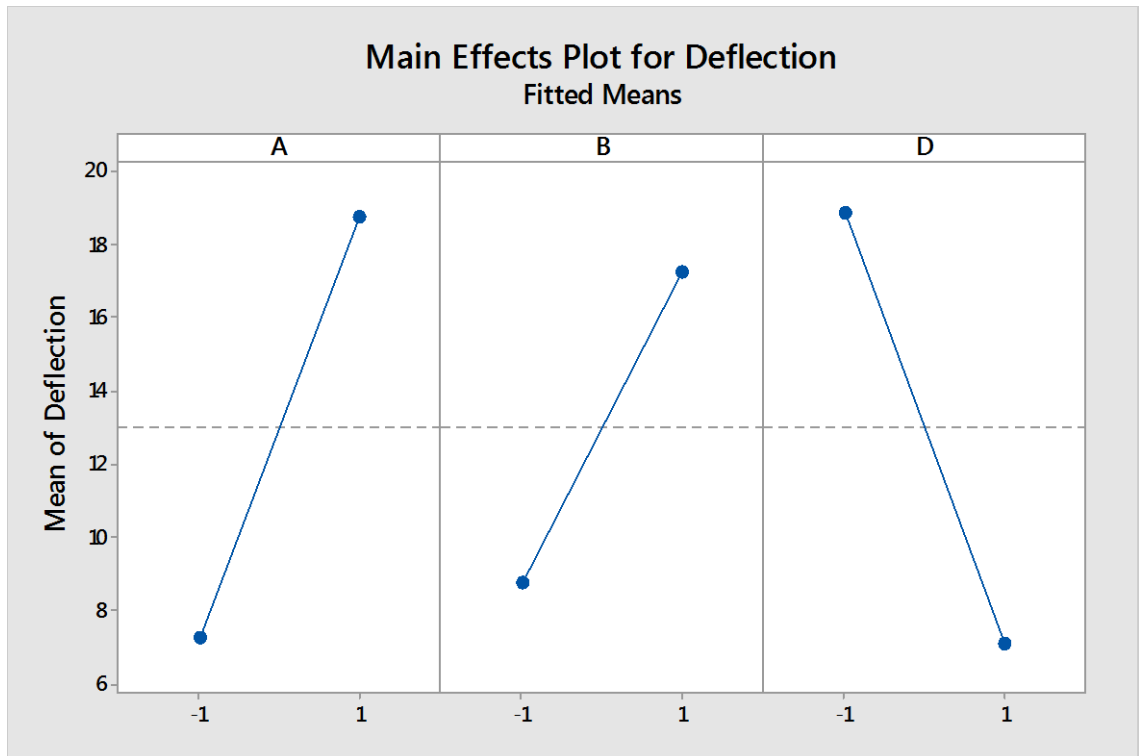


Figure 27: Main effect plot for deflection

Figure 27 shows the main effect plot for deflection of the spring. 1 and -1 in the figure above is defined as the higher and lower level of the factors. This indicates that when factor weight (A) is 20.9g which is indicated as 1 in figure 27, the mean value for deflection seems to be the highest. The plot for factor B shows that the further the location of the weight from the fixed position, the higher the deflection of the spring and it was shown that at 7 inch, the spring has the best deflection. The thickness factor of the spring which is denoted by the letter D has the opposite effect compared to factor A and B. The plot shows that when the thickness of the spring increased, the deflection property of the spring decreased and it is shown that a spring with 1/16 inch which is shown as -1, thickness has the best deflection magnitude. The plots also show that both factors A and

D have bigger presence in the deflection of the spring compared to B. The overall mean deflection of the spring of about 13mm was plotted across each panel.

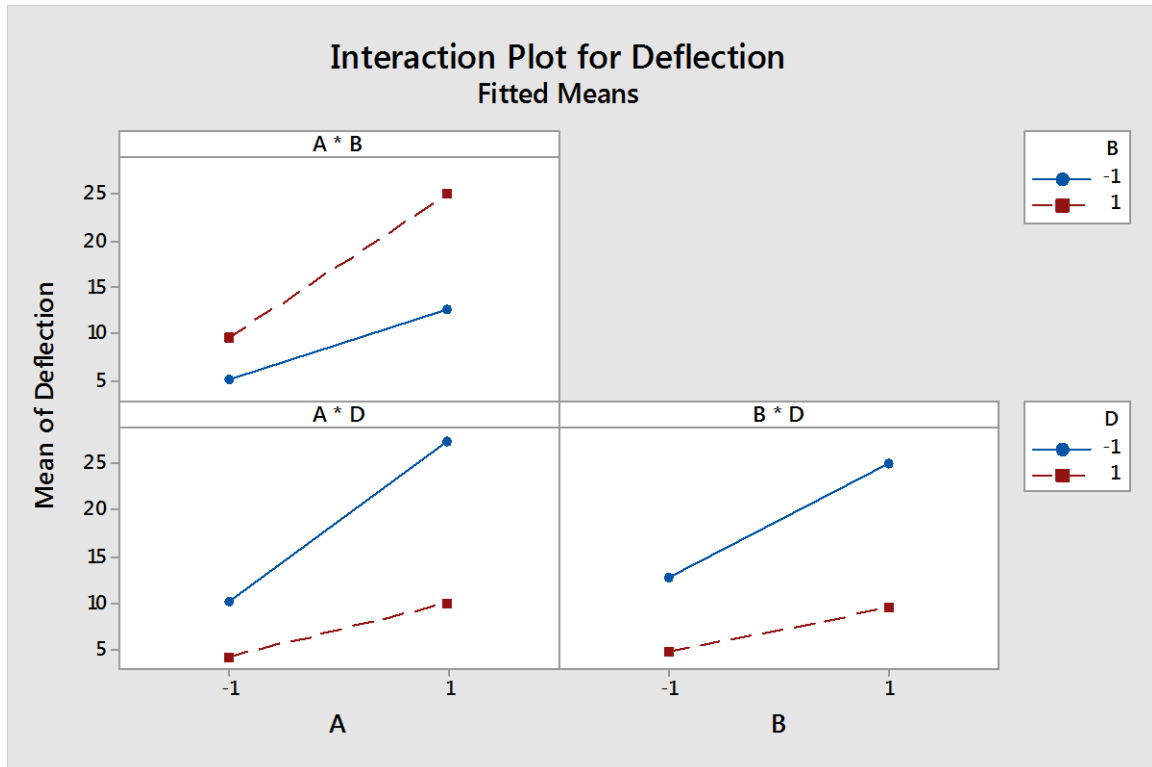


Figure 28: Interaction plot for deflection

The interaction plot in figure 28 shows that when both factors A and B are high, the deflection of the spring is around 25 mm. The interaction plot also shows that when factor D is low and both factors A and B are high, the deflection was high. The highest deflection was recorded when factor A is high and factor D is low. This was found to be above 25mm. This means that in order to achieve higher magnitude of deflection, the user has to use heavier weight (factor A) at the furthest location of the spring (factor B) on a thinner spring (factor D).

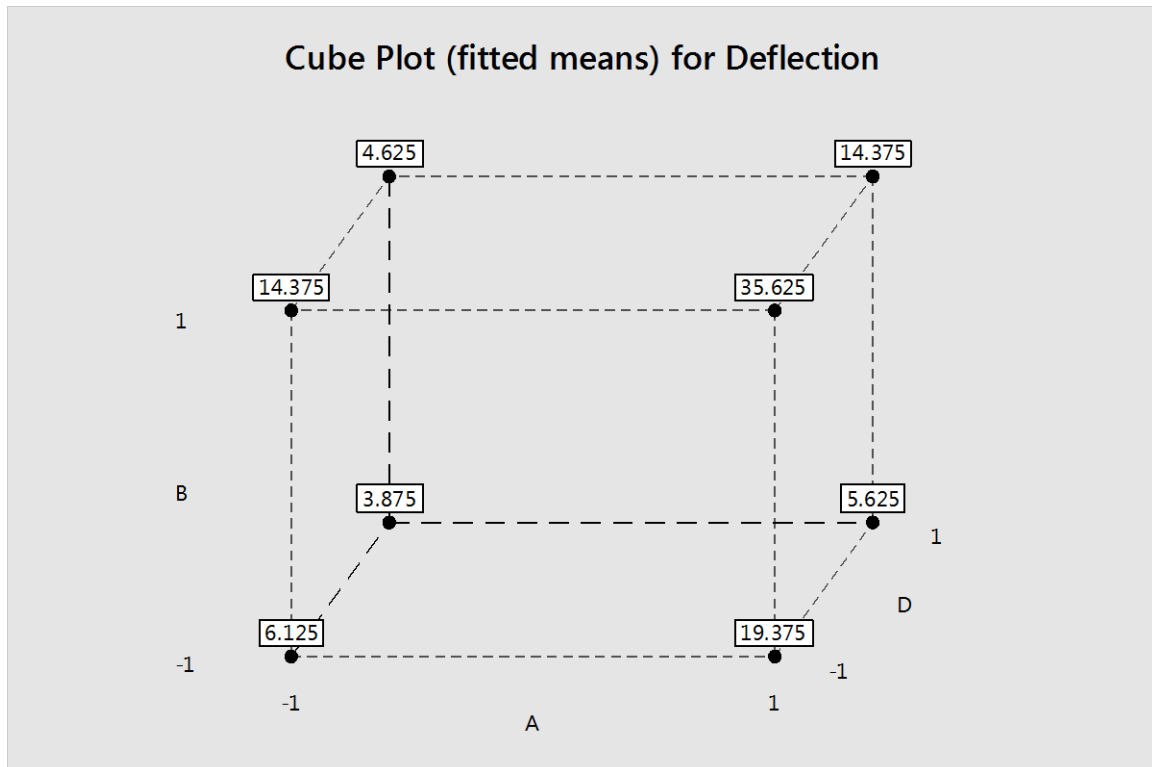


Figure 29: Box plot for deflection

The box plot above in figure 29 shows that with the current setting, the highest deflection that can be obtained is 35.625mm. This occurs when factors A and B were at its highest, and when factor D was at its lowest level. When the factors were reversed, the lowest deflection value that could be achieved is 3.875mm from figure 29 above.

CONCLUSION AND RECOMMENDATION:

The intent of this experiment was to determine which factors had the biggest influence in how much the leaf spring or beam deflects. It was found that out of the four factors suggested for evaluation, only three factors played a major role in affecting the deflection of the spring. The three main factors were weight, the location where the weight was placed on the spring and the thickness of the spring. The results show that the deflection increased as the weight increases and the location where the weight was placed gets further away from the fixed position. On the other hand, increasing the spring thickness reduced the deflection of the spring. Based on the results obtained, the user can decide if the leaf spring has to act as a spring or dampener by controlling the deflection of the system. The leaf spring acts more like a spring when the deflection is higher and acts more like a dampener when the deflection is lower or stiffer. The results obtained from the experiment are linear since only two level of each factor were tested. The experiment also shows that the stiffness of the leaf spring can be easily manipulated as per the convenience of the experimenter and it is more practical to implement on a full scale model compared to the other springs.

Bearing

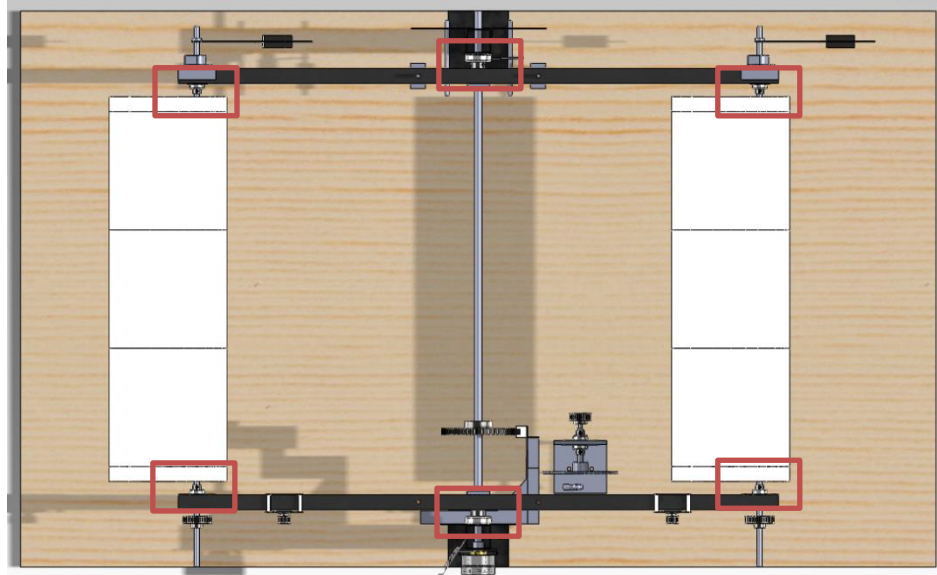


Figure 30: The top view of the system shows the locations on the bearings in Solidworks.

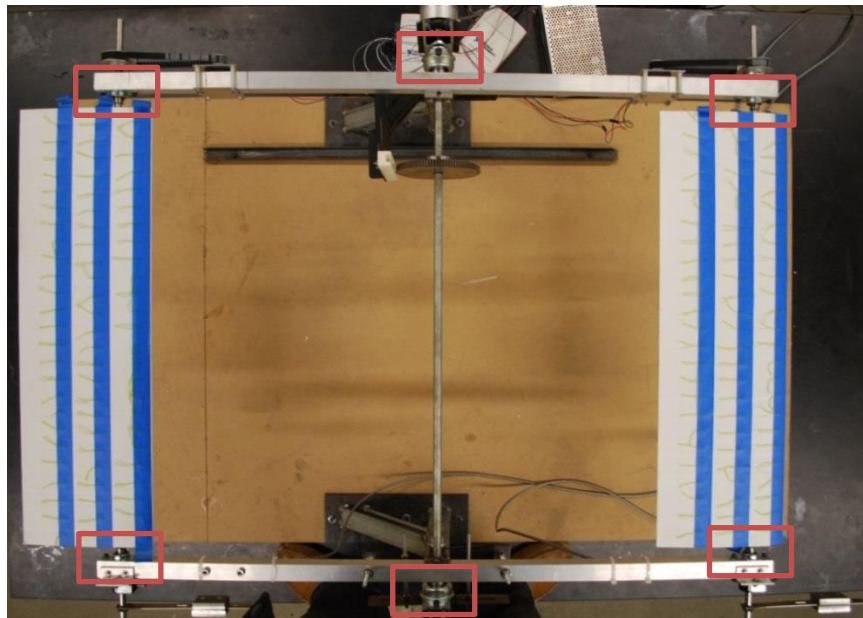


Figure 31: The actual location of the bearings on the device from top view.

Bearings play an important role in the movement of the whole system as the whole system has to be free moving as much as possible. Since this mechanical system was made out of moving parts, friction cannot be avoided but it can be reduced by choosing bearings with less friction. Flanged ball bearing were considered as it is not only easy to mount but also produces less friction as the ball bearing placed inside the bearings is only in contact with the surface at a single point. The locations of the bearing are shown in Solidworks drawing and on the actual model from the top view in figures 30 and 31 respectively. Two different sizes of flanged bearings were used in the device. Flanged bearing with a $\frac{3}{8}$ in bore diameter were not only used to hold the bar running through the wings but also to connect the wings to the arm. Two more flanged bearings with a bore diameter of 0.5in were used at the center of the arm to connect it to the legs of the device and to allow it to oscillate at that location. The close-up views of both bearings are shown in Solidworks drawing and on the actual model in figures 32 and 33 respectively.

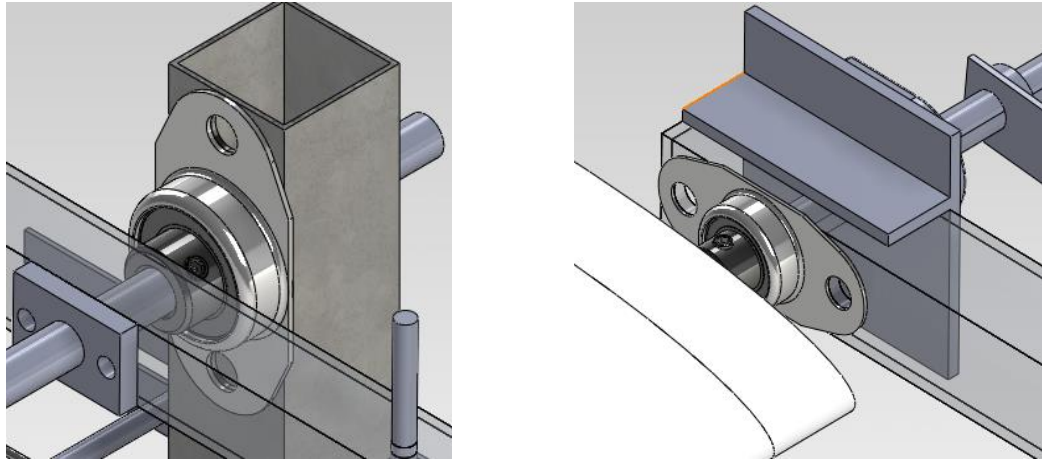


Figure 32: The location of the flanged ball bearings in detail Solidworks drawing.

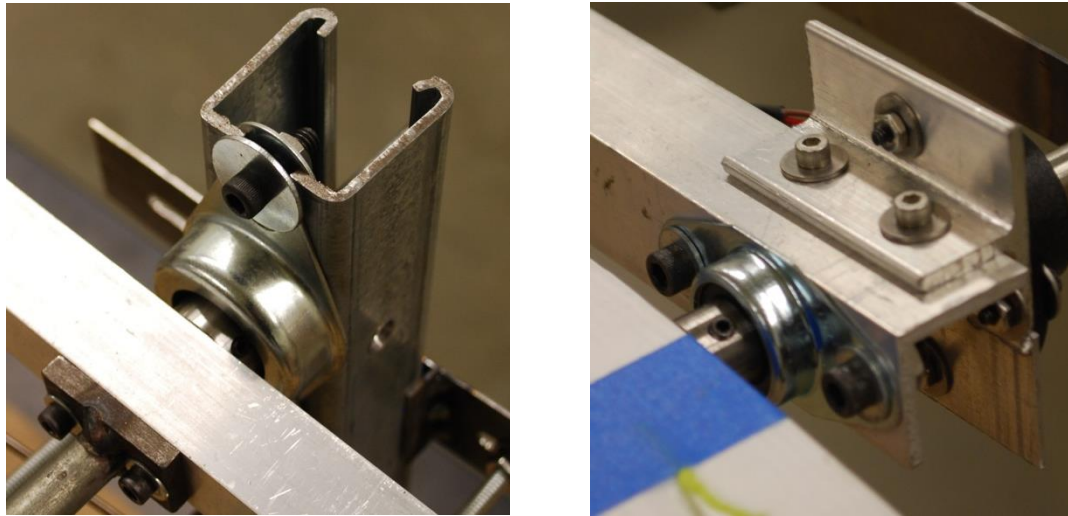


Figure 33: The actual location and setting of the bearings on the device.

Counter Weight



Figure 34: Isometric view of the model oscillator without counter balance.

Aerodynamic center (ac) and center of gravity (cg) of the wing had to be located on the same location for this device to work. The aerodynamic center is located at the quarter chord of the wing whereas the center of gravity depends on the distribution of material inside the wing. Since the wings were made using rapid prototype method, the material inside the wings were distributed in a honeycomb fashion to make sure that the wings are structurally stable and this made the center of gravity to not be in-line with the aerodynamic center of the wing. Figure 34 shows the isometric view if the model Wind

Oscillator where the aerodynamic center and center of gravity are not at the same location. This offset gave the wings natural moment when the wings are pivoted at the quarter chord as seen in the figure 34. If this moment is countered and balanced out, the motor that drives the wing would need more power to control its movement. Counter weights were added in the form of blocks in front of the wings to make sure that the wing is horizontally balanced. The weights also balanced out the whole system since the trailing wing section and the leading wing section had to be balanced for the system to operate in a harmonic frequency. Figure 35 and figure 36 shows the location and how the counter weights are attached to the wing in Solidworks drawing and on the device.

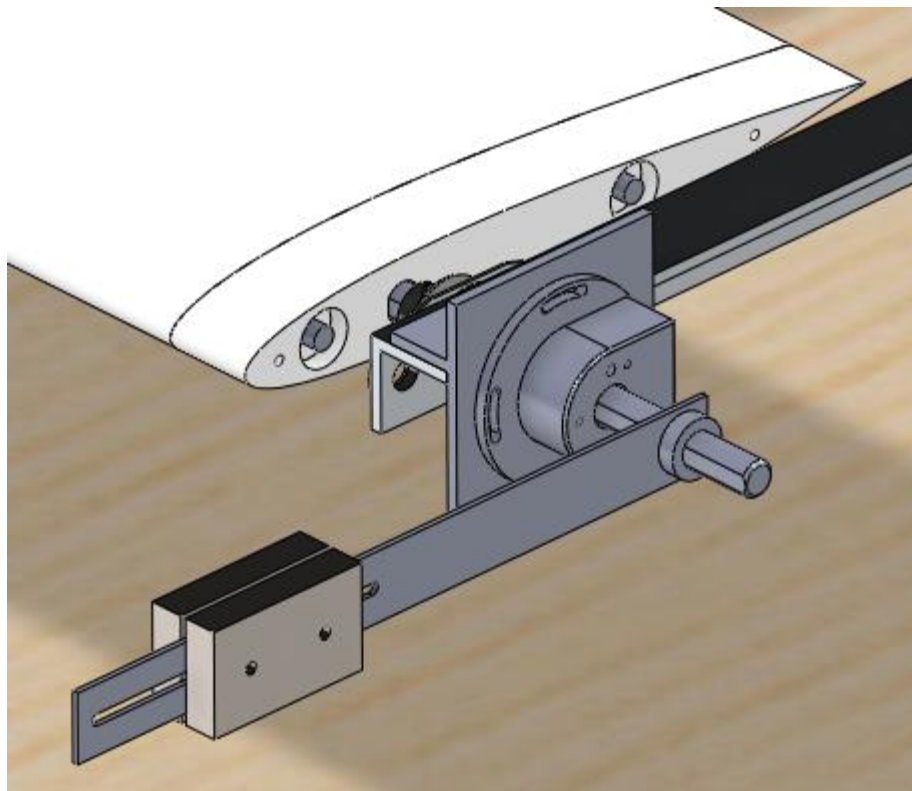


Figure 35: The attachment of counter weight to the wing in Solidworks.

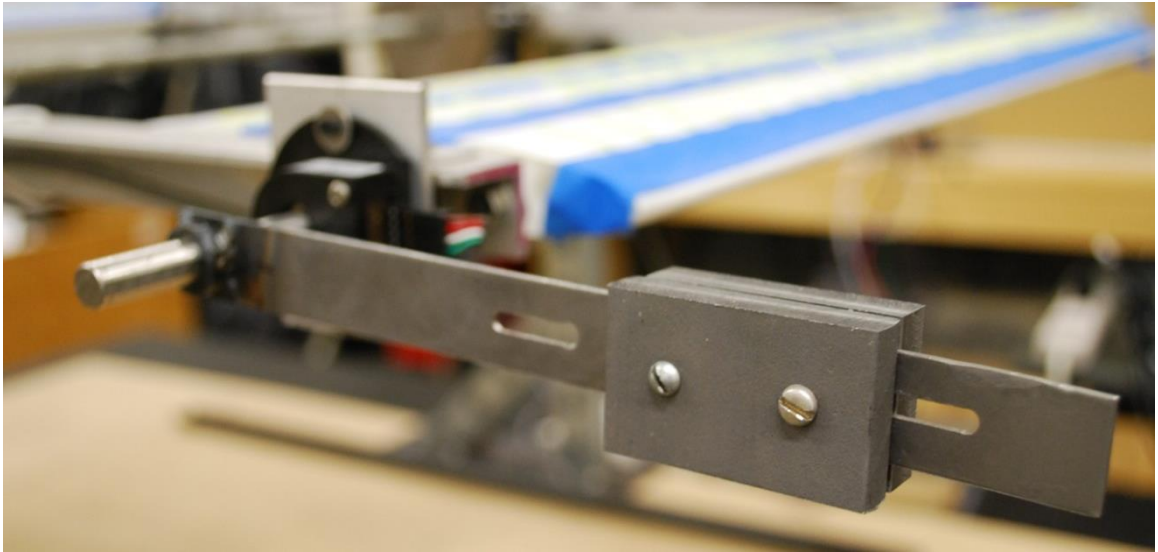


Figure 36: The actual location of the counter balance and how it is attached to the wing.

Gear and Belt

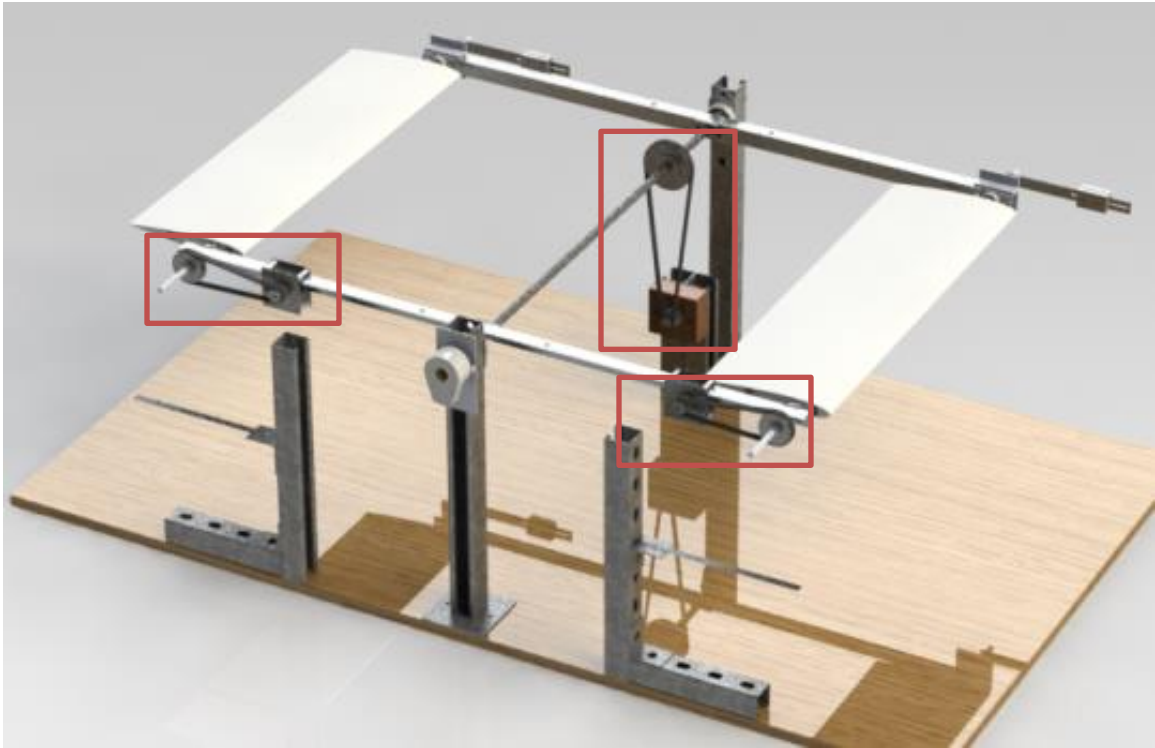


Figure 37 : Gear and belt mechanisms on the device.

The gear and belt play a crucial role as they not only help the motors to actuate the wings, but also amplify the angle of rotation of the motor by a ratio of 2:5. The gear that was fixed to the motor has 12 teeth. This is connected to the wing with a 30 teeth gear through the use of a 3/8in thick belt. The gear and belt system was also used to run the generator. A gear with 48 teeth was connected to the Direct Current (DC) motor generator with a 10 teeth gear through the use of a 3/8 inch thick belt. When the DC motor generator was replaced by a pendulum to generate mechanical power, the 10 teeth gear was replaced by an 18 teeth gear.

CHAPTER V

ELETRONIC DESIGN

Optical Encoder

The system uses two types of optical sensors to measure the angle and location of the wings and the arm. The type of optical sensors used for this device is optical encoders. The optical encoders were used at three different locations on the device. The main optical encoder was placed in the middle of the arm and the other two encoders were placed at the quarter chord of the wings.

Optical Encoder – Arm



Figure 38: HB6M Hollow Bore Optical Encoder [130].

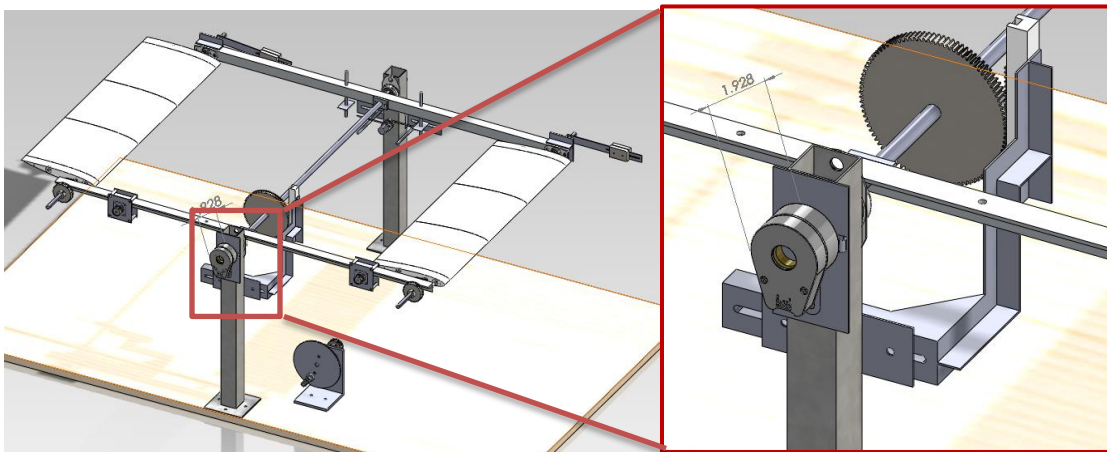


Figure 39: The optical encoder located at the end of the middle rod in Solidworks.

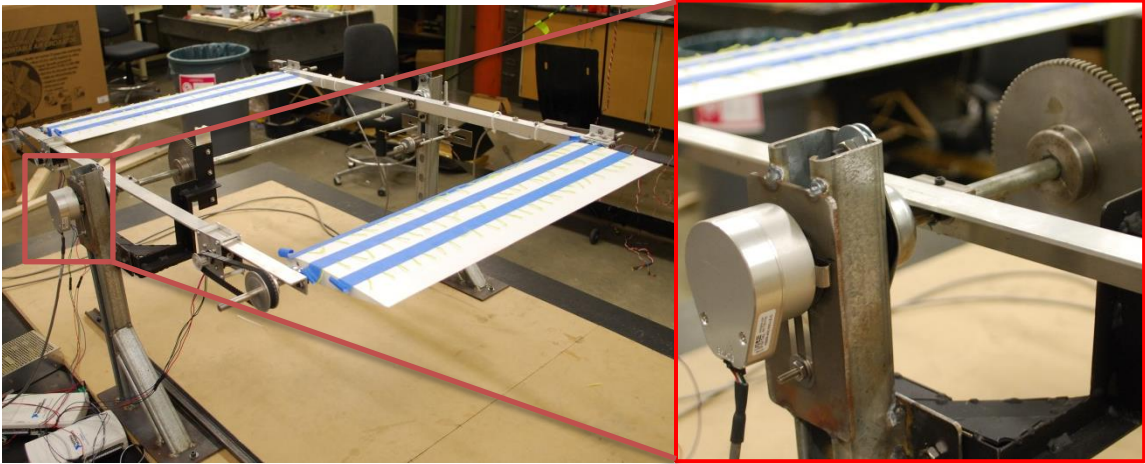


Figure 40: The location of the optical encoder which is located at the end of the middle rod.

The main optical encoder is a HB6M hollow bore optical encoder as shown in figure 38. This optical encoder was placed at the end of the middle rod which is also in the middle of the arm as shown in figures 39 and 40 in Solidworks drawing and on the actual device. The optical encoder allows the user to monitor the angle of the arm and also as a trigger for the motor controlling the wing as it is programmed to activate the motors when the arm moves past the arm angle set by the user. The optical encoder has a count per revolution(CPR) of 400, therefore as per the data sheet in table 6, it takes a supply current of about 27mA typically and a maximum of 33mA. It also has a rise time of 110nS and a fall time of about 35 nS. The dimensions for the optical encoder can be found in figure 41.

Parameter	Min.	Typ.	Max.	Units	Conditions
Supply Voltage	4.5	5.0	5.5	V	
Supply Current		27	33	mA	CPR < 1000, no load
		50	62	mA	CPR ≥ 1000, no load
Low-level Output			0.5	V	I _{OL} = 8mA max.
High-level Output	2.0			V	I _{OH} = -8mA max.
	4.2	4.8		V	no load
Output Current Per Channel	-8		8	mA	
Output Rise Time		110		nS	
Output Fall Time		35		nS	

Table 6: Parameters for the single ended electrical optical encoder [131].

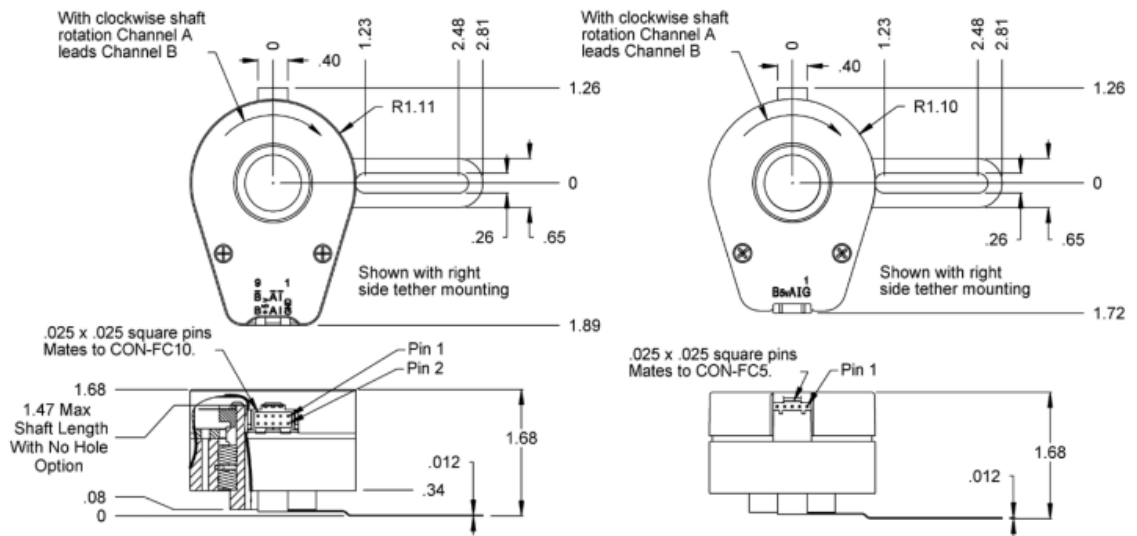


Figure 41: Dimensions of the HB6M Hollow Bore Optical Encoder [132].

Optical Encoder – Wing

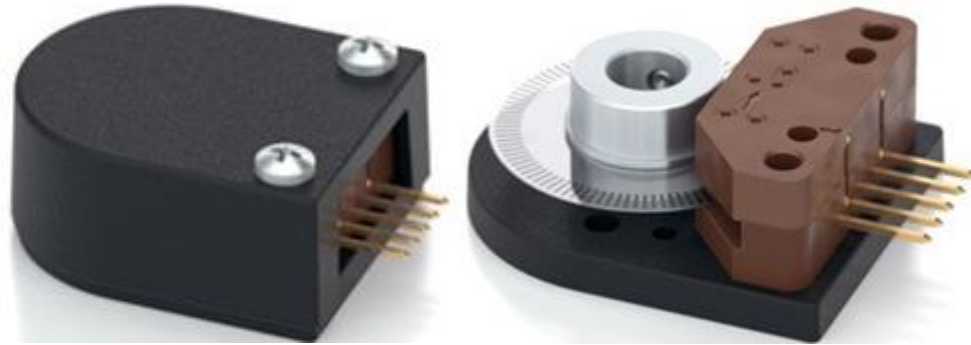


Figure 42: E2 Optical Kit Encoder with and without cover respectively [133].

The other two optical encoders placed at the quarter chord of the wings are the E2 optical kit encoder which are shown in figure 42. The placement of these optical encoders on the Wind Oscillator are shown in figures 44 and 45 in Solidworks drawing and on actual model respectively. These optical encoders allow the user to not only monitor the angle of the wings individually but also to control them individually which allow the wings to have different angle of attacks at any moment.

The dimensions for the encoders are shown in figure 43. The parameters for the encoder is given in table 7. The E2 optical encoder has a 400 count per revolution(CPR). Since it has a CPR that is less than 500, it takes a current supply of about 27mA typically and a maximum of 33mA. It also has an output rise time of 110nS and output fall time of about 100 nS since it has a CPR that is less than 2000. The timing characteristics of both E2 and HB6M optical encoders are given in figure 46.

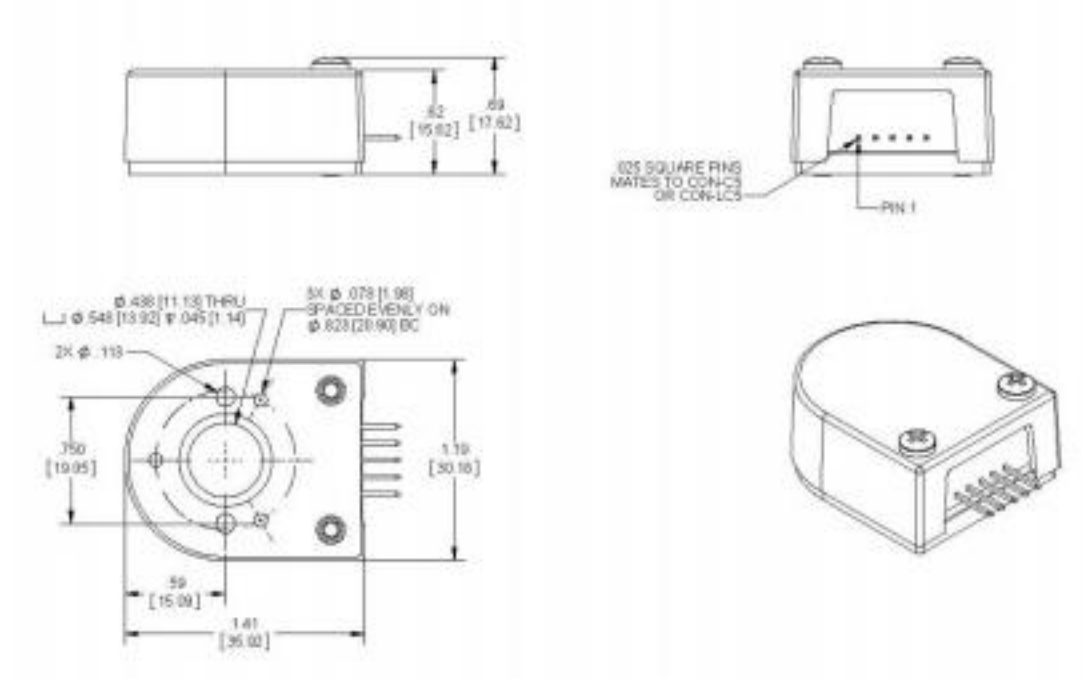


Figure 43: Dimensions of the E2 Optical Kit Encoder [134].

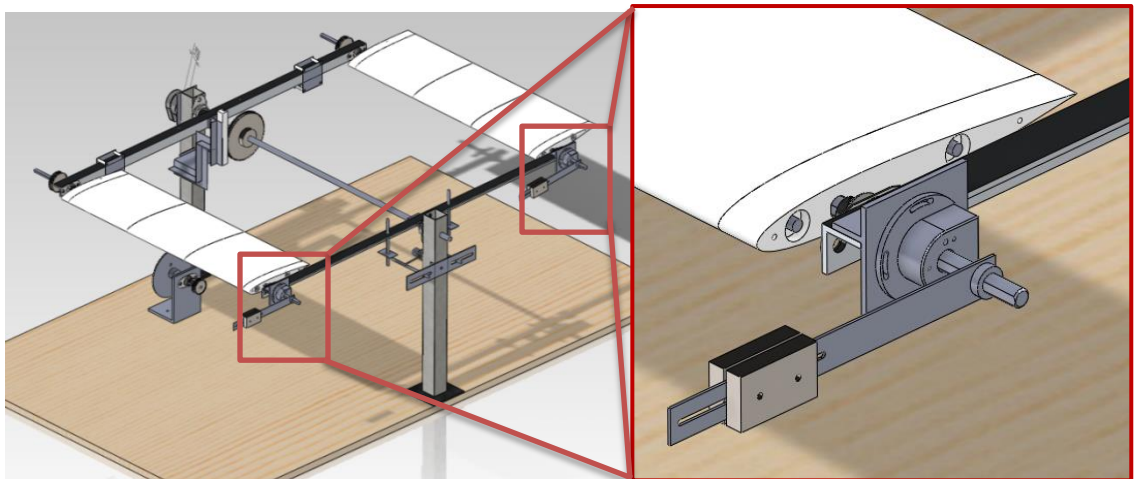


Figure 44: The optical encoder located at the quarter chord of the wing.

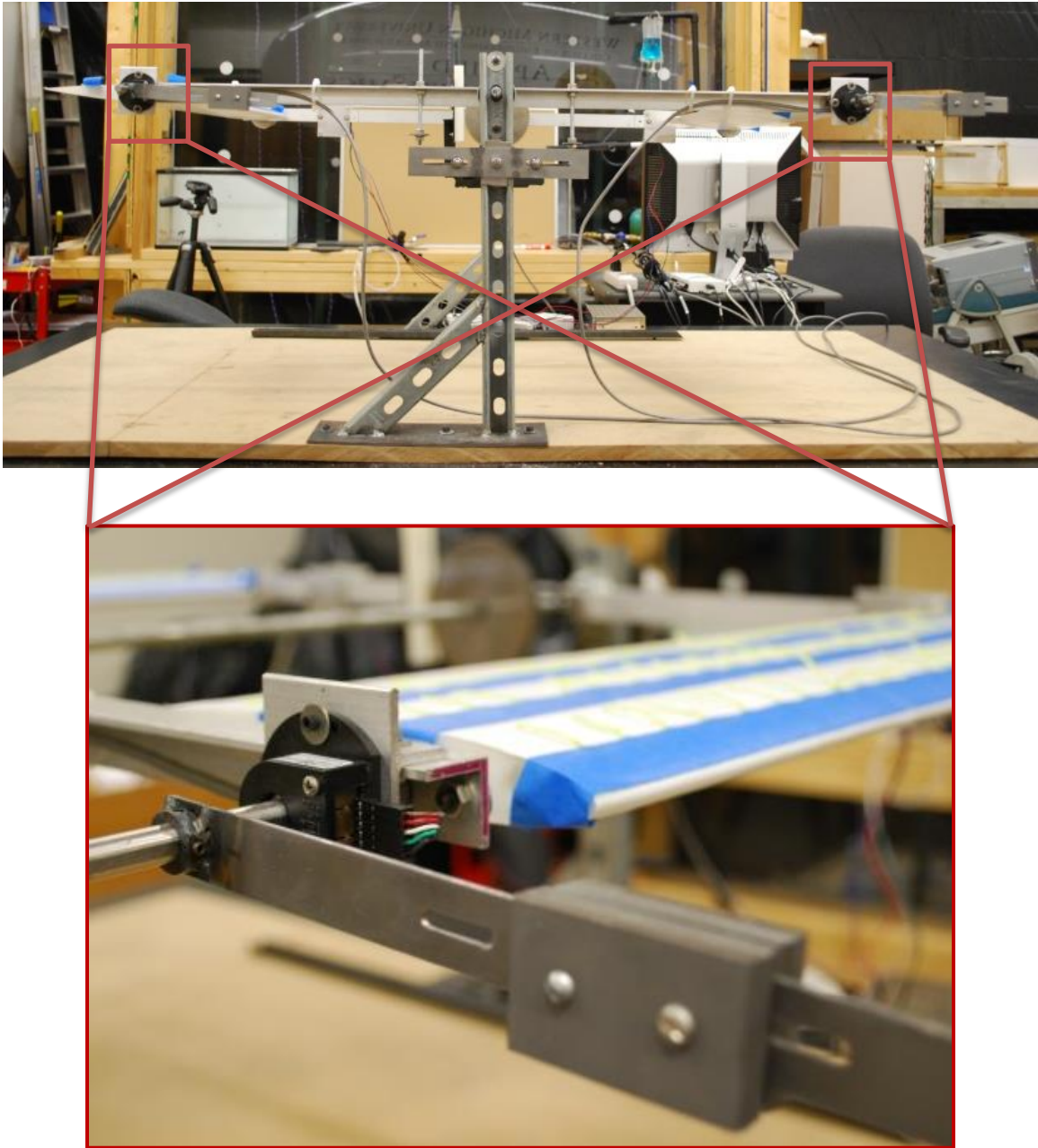


Figure 45: Optical encoders located at the quarter chord of the wings and a zoomed in view of the encoder.

Parameter	Min.	Typ.	Max.	Units	Conditions
Supply Voltage	4.5	5.0	5.5	V	
Supply Current		27	33	mA	CPR < 500, no load
		50	62	mA	CPR ≥ 500 and < 2000, no load
		72	85	mA	CPR ≥ 2000, no load
Low-level Output			0.5	V	I _{OL} = 8mA max., CPR < 2000
			0.5	V	I _{OL} = 5mA max., CPR ≥ 2000
		0.25		V	no load, CPR ≥ 2000
High-level Output	2.0			V	I _{OH} = -8mA max. and CPR < 2000
	2.0			V	I _{OH} = -5mA max. and CPR ≥ 2000
		4.8		V	no load and CPR < 2000
		3.5		V	no load and CPR ≥ 2000
Output Current Per Channel	-8		8	mA	CPR < 2000
	-5		5	mA	CPR ≥ 2000
Output Rise Time		110		nS	CPR < 2000
		50		nS	CPR ≥ 2000, ± 5mA load
Output Fall Time		100		nS	CPR < 2000
		50		nS	CPR ≥ 2000, ± 5mA load

Table 7: Parameters for E2 Optical Kit Encoder shown above [135].

Parameter	Symbol	Min.	Typ.	Max.	Units
Cycle Error	C		3.0	5.5	$^{\circ}\text{e}$
Symmetry	X, Y	150	180	210	$^{\circ}\text{e}$
Quadrature	Z	60	90	120	$^{\circ}\text{e}$
Index Pulse Width	Po	60	90	120	$^{\circ}\text{e}$
Ch. I Rise After Ch. B or Ch. A Fall	t1	50	100	200	ns
Ch. I Fall After Ch. B or Ch. A Rise	t2	-10	15	25	ns

Timing Diagram:

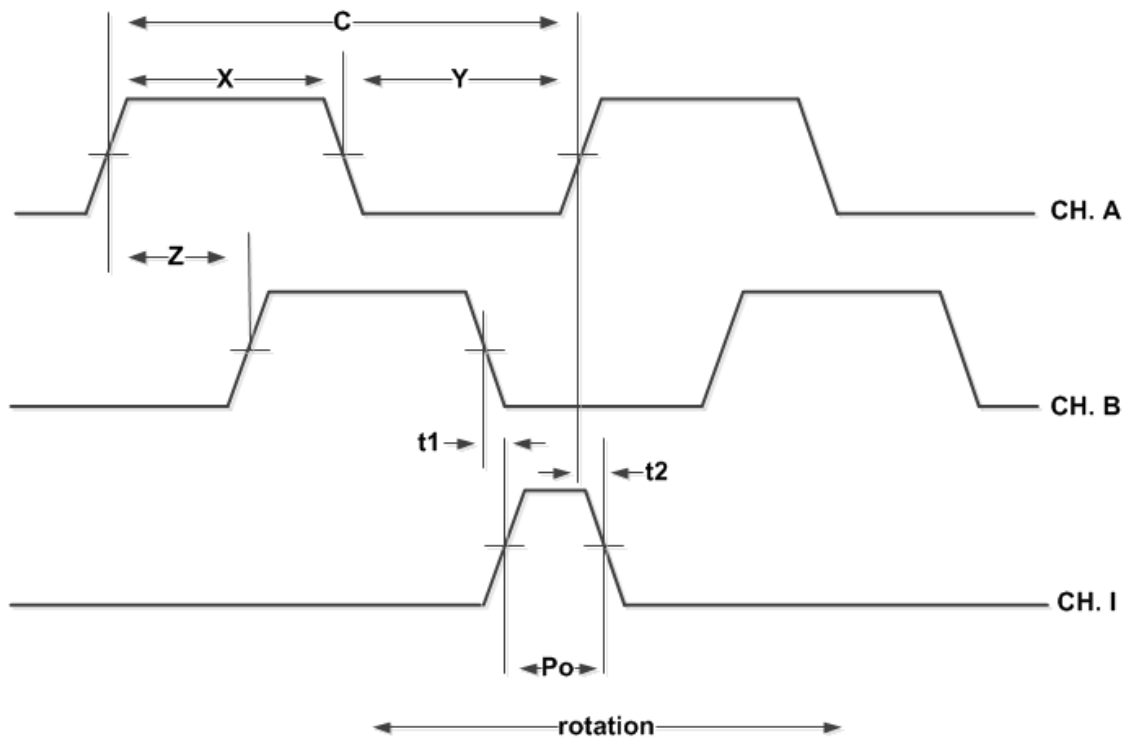


Figure 46: Timing characteristics of the encoders [136].

Digital IO & Power Drivers

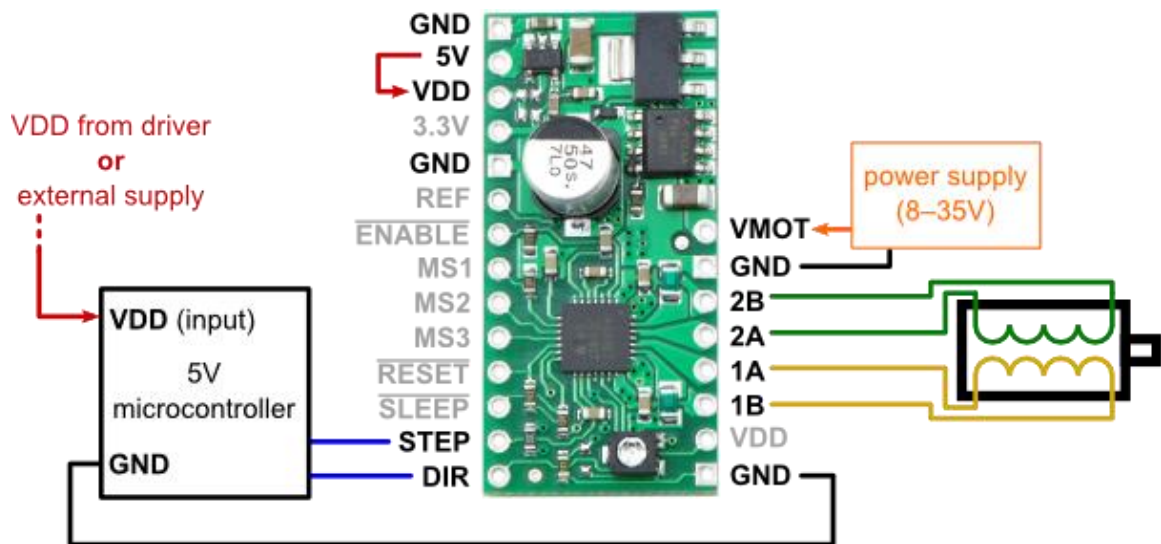


Figure 47: Simplified schematic of the motor controller [137].

The stepper motor driver (Polulu A4988) shown in figure 47 receive signals from the National Instruments (NI) Data Acquisition (DAQ) Modules based on the angular positions of the arm and wings using multiple optical encoders. As this project was done entirely in LabVIEW, it eliminated the need for various electronic components, and instead, a computer code in LabVIEW handled all the required functions. Although LabVIEW handled all the signals processing, the type of signal had to be known.

For example the direction input on the stepper motor driver is a logic input which can receive either I or O. One being clockwise and the other vice-versa. It is important that the direction signal should change at different locations of the arm. For example, when the arm is at high position, the stepper motor is required to turn the wing to

clockwise position to a lower angle of attack to facilitate the movement of the arm to a low position where it is repeated in an opposite fashion. The driver then translates a logical input for the direction, and translates it to the direction of current flow in each winding which ultimately determines the direction of motion of the motor. Likewise, the step input which commands the motor to travel a step is defined by a low to high signal transition which advances the motor one by increment.

Logic Input Voltage: -0.3 - 5.5V

Logic Supply Voltage: -0.3 - 5.5V

From the above specifications, it is clear that the low state is ideally at 0V, whereas high state is at 5V.

The diagram shown in figure 48 is the schematic of the complete stepper motor circuit. The STEP and direction (DIR) are logical inputs to the controller which in turn drives the direction of current flow in the motor windings. The voltage supplied to the motor is dependent on the voltage supplied to the motor controller. In this case, a 12V fixed DC voltage is supplied to the motors. The power source is rated up to 5Amperes. This provides for enough current so that the voltage may be split for both the motors, one for each wing. A simplified schematic of this is shown in figure 47.

Power Supply



Figure 49: 150W single output switching power supply [139].

Two different power supplies were used in the project. A 12V power supply was used to power the stepper motors through the motor voltage (VMOT) in the motor controllers shown in figure 47. The 12V power supply is a 150W single output switching power supply as shown in figure 49.

Table 8 shows the output specification of different power supply models with varying DC voltage output. The model that was used for the project is the S-150-12 which is capable of a 12V DC voltage output with the tolerance of plus minus one percent. The rated current and power for the power supply are 12.5A and 150W respectively.

The second type of power supply that was used in the project was the 5V USB power supply. The 5V was used to power all the three encoders and the circuitry in the

motor controllers through the National Instruments (NI) Data Acquisition (DAQ) Modules. The circuitries of the motor controllers were powered through the VDD located on the circuits.

MODEL		S-150-5	S-150-12
OUTPUT	DC VOLTAGE	5V	12V
	RATED CURRENT	30A	12.5A
	CURRENT RANGE	0 ~ 30A	0 ~ 12.5A
	RATED POWER	150W	150W
	RIPPLE & NOISE (max.) Note.2	150mVp-p	180mVp-p
	VOLTAGE ADJ. RANGE	4.5 ~ 5.5V	10.6 ~ 13.2V
	VOLTAGE TOLERANCE Note.3	±2.0%	±1.0%
	LINE REGULATION	±0.5%	±0.3%
	LOAD REGULATION	±0.5%	±0.3%
	SETUP, RISE TIME	100ms, 50ms at full load	
	HOLD UP TIME (Typ.)	28ms at full load	

Table 8: Specifications of different models for 150W power supply [140].

National Instruments (NI) Data Acquisition (DAQ) Modules

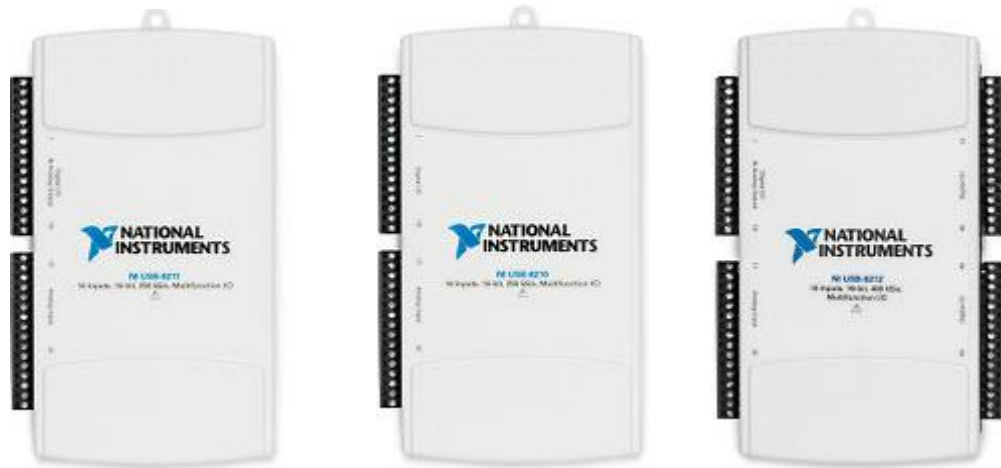


Figure 50: Three different models of the NI DAQs.

Three different NI DAQs shown in figure 50 were used in the device as the system required 5 timers to operate. Three timers were required for the encoders and two timers for controlling the stepper motors. The NI DAQ also provided the motors with two digital outputs to control the direction in the stepper motors. Also, the NI DAQ provided a 5V power supply to power the circuitry in the stepper motor drivers and grounding for all the devices connected to the system.

Stepper Motor

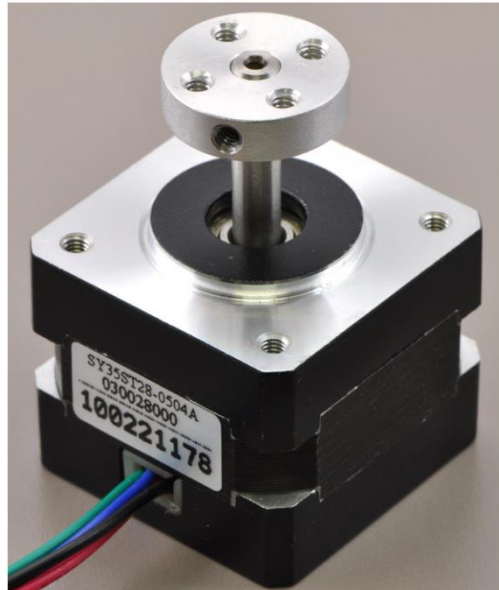


Figure 51: 14 oz-in hybrid stepper motor [141].

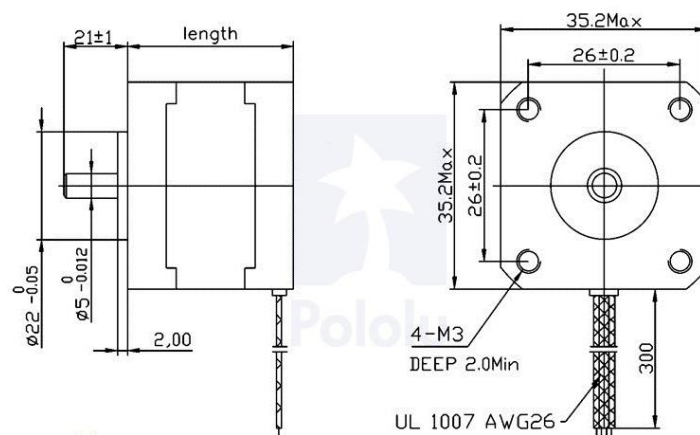


Figure 52: Schematics of the stepper motor [141].

The movement of the whole system depended on the angle of attack of the wings. The angle of attack of the wings depended on the wind direction, wind speed and the location of the wings on the arm. Therefore at a certain condition, both wings will have the same angle of attack at a given wind condition and opposite values depending on the location. Also, when the system is operating, the wings must be able to change angle at a certain rate and accurately for the system to keep on operating. The actuator must also be capable of operating in a small range since the smallest operating angle of attack of the wings is around plus minus 5 degrees. The Hybrid stepping motor allowed for smaller step size depending on steps per revolution of the motor, which in return increased the accuracy of the system. The holding torque of a motor is also crucial since once the wing changes angle, the motor had to hold the wings position until the arm reached the designated angle. The hybrid stepper motor used in this application has a 1.8 step angle or is capable of making 200 steps per revolution. Each phase draws 500 mA at 10 V, allowing for a holding torque of 1 kg-cm or 14 oz-in. Figure 53 shows the pullout torque of the stepper motor for a half step at 24VDC and 0.5A. Figures 51 and 52 show the image and schematics of the hybrid stepper motor. Figures 54 and 55 show the location of the stepper motor on the device in Solidworks drawing and on the actual model respectively

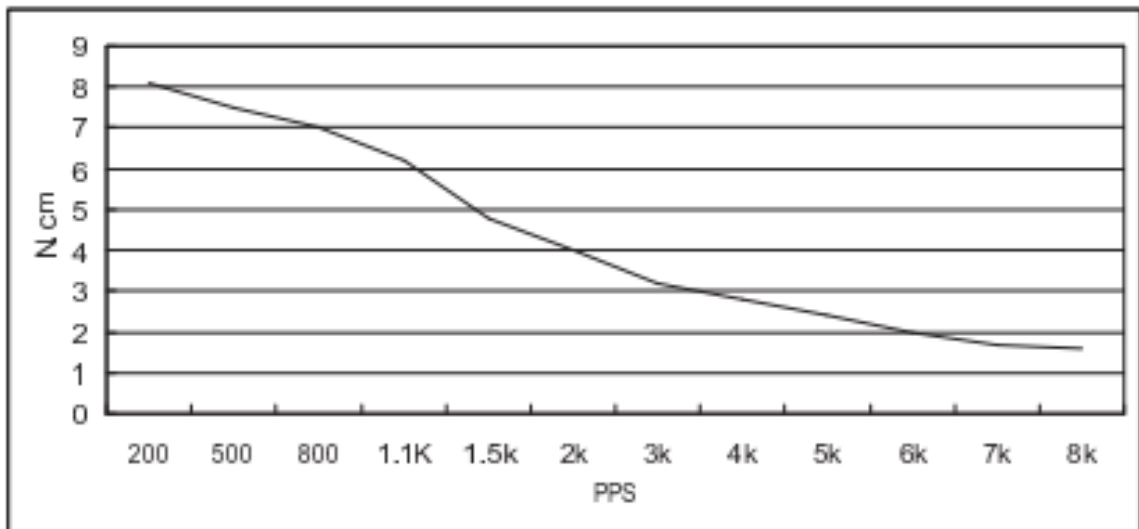


Figure 53: Pullout torque curve at 24VDC, 0.5A, half step [142].

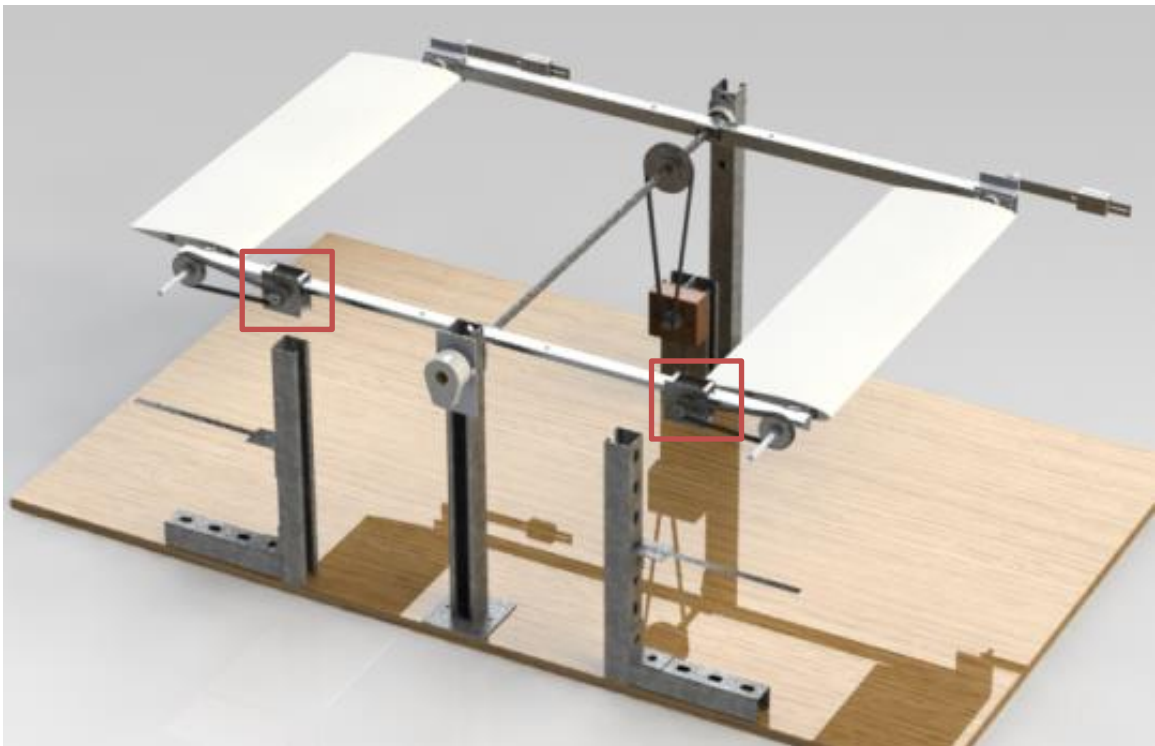


Figure 54: The location of the hybrid stepper motor with the covering.

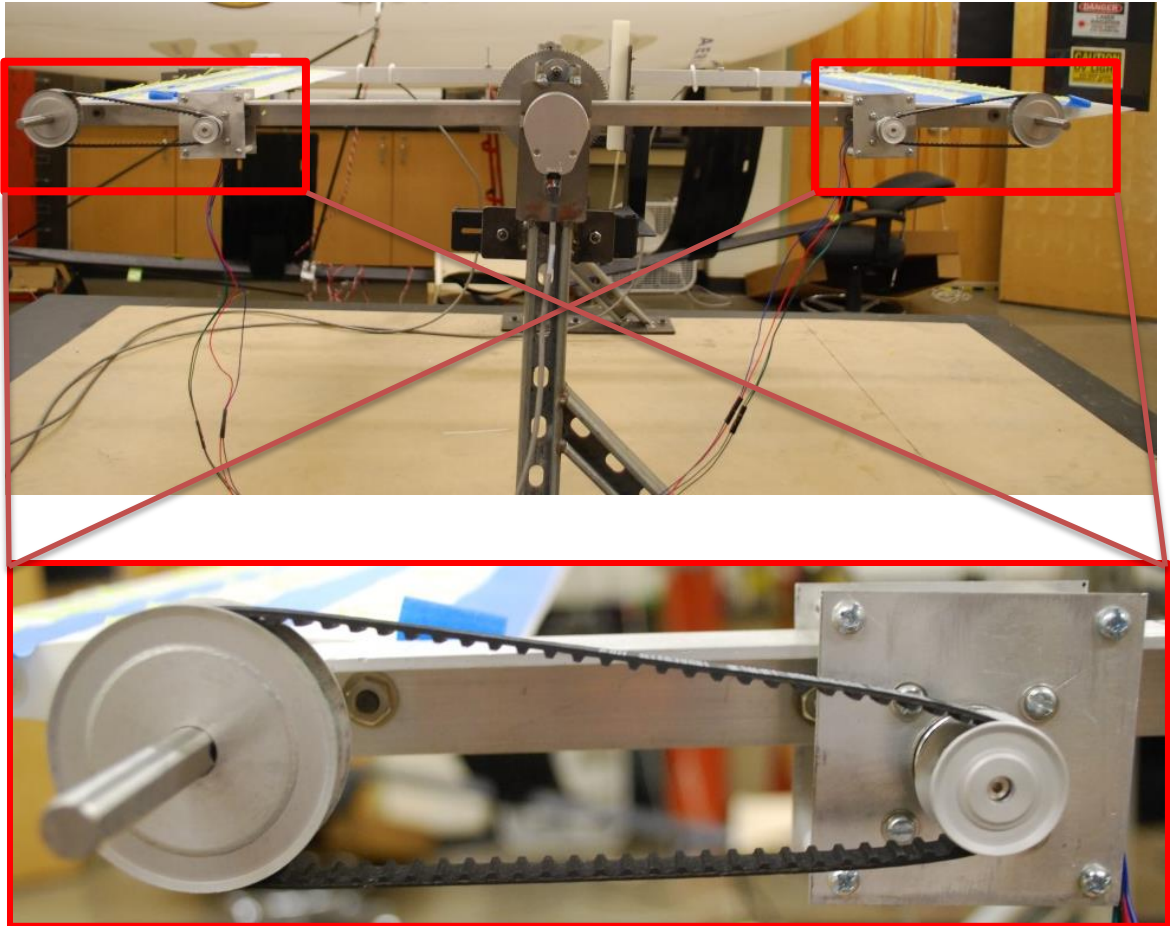


Figure 55: The location of the stepper motors on the arm and a zoomed in image showing how it is connected to the wing.

CHAPTER VI

GENERATOR DESIGN

Brushed dc Motor

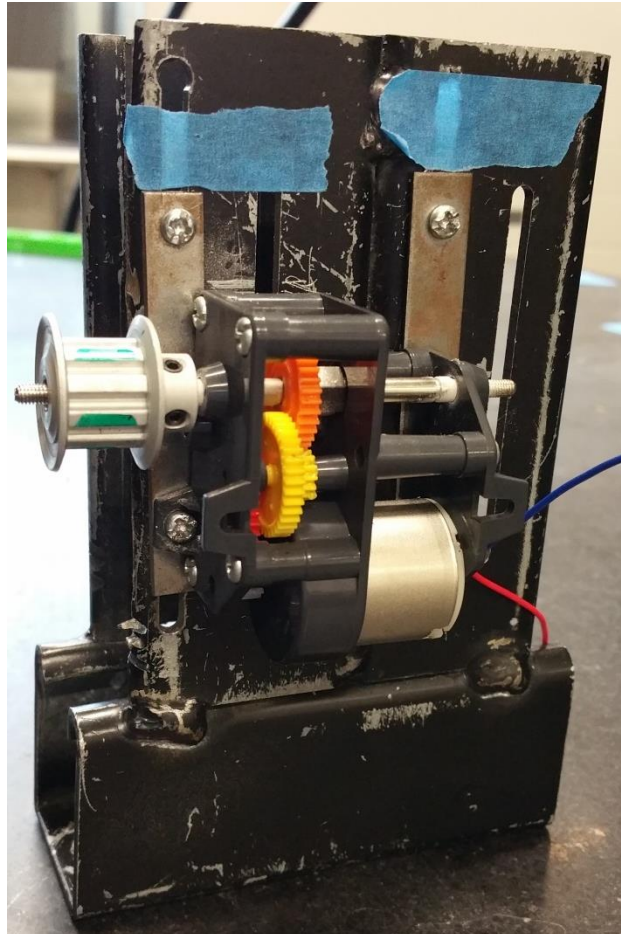


Figure 56: Brushed dc motor in Tamiya high power gearbox [143] set up on the motor stand.

A brushed DC motor shown in figure 56 was considered as a generator for testing to determine if the systems worked before investing in an actual generator or a high precision motor to be converted into generator based on the results. A brushed DC motor is not only cheap but also highly reliable. Brushless DC motor was not considered because a brushless DC motor will act as an alternator when driven compared to a brushed DC motor which will behave as a dc generator when driven. Since the dc motor was subjected to oscillating motion, the voltage output would be in the form of Alternating Current (AC) voltage as shown in figure 57.

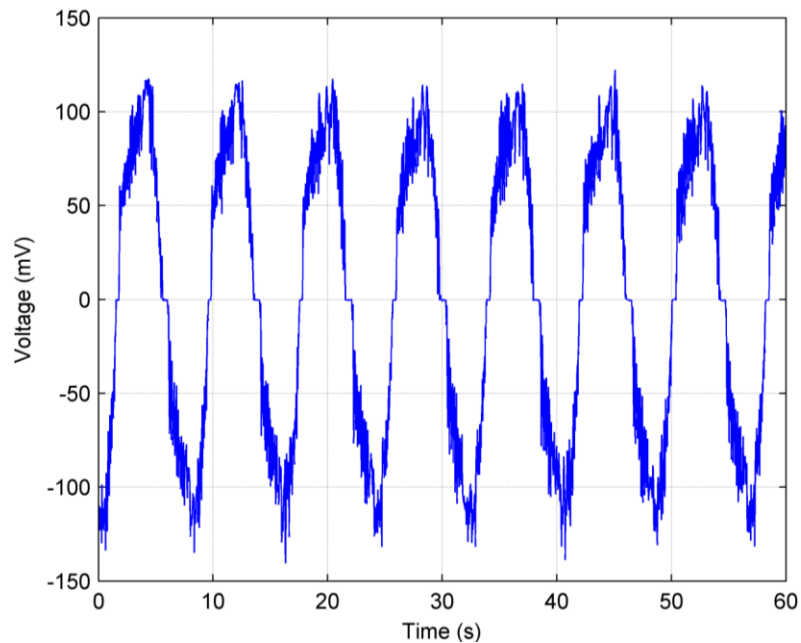


Figure 57: Typical voltage output from model wind oscillator through DC motor.

Pendulum



Figure 58: Pendulum setting of the device.

The DC motor generator was replaced by a pendulum system as shown in figure 58 to measure the mechanical power output since the voltage output by the generator was small. The pendulum would also give the absolute power output of the system compared to the generator output which might have losses due to the heating up of the generator.

CHAPTER VII

SOFTWARE DESIGN

LabVIEW (Laboratory Virtual Instrument Engineering Workbench)

LabVIEW is the programming language that was used to actuate the device and to collect data as required. LabVIEW is a visual programming language which uses graphical block diagrams and wires to program which is different from conventional programming. The visualization of the programming code helps the user to better understand the coding and sort out the errors much more easily compare to conventional programming. It is also much more convenient to manipulate the code and to further improve it or for others to understand the program just by looking at it.

LabVIEW - Control

Figure 59 shows the front panel of the LabVIEW program that enabled the user to control the angle of the arm and the wings. AoA set and AoA set 2 in figure 59 shows the user-set initializing angle of attack for the wing. The dial shows the active reading of the angle of the arm by the middle encoder. The value 5 in the y and y2 denotes the user-set response angle of attack of the wings. The values shown are positive but the system applies the same response for negative values. The fudge in the front panel denotes the orientation of the optical encoder disk inside the encoder. In this case, it is oriented 180 degrees from its index position. The upper and lower panel shows the active reading of the angle of attack by the wing encoders at the leading wing and the trailing wing at upper and lower positions respectively. The initial AOA shows the active angle of attack at quarter chord of the wing during the initialization process. The active readings shown in the front panel was used to see if the motor reached or over-shot the denoted angle of attack which was set earlier. The display of active readings of the system helps the user to reduce error and help to make the device more effective.

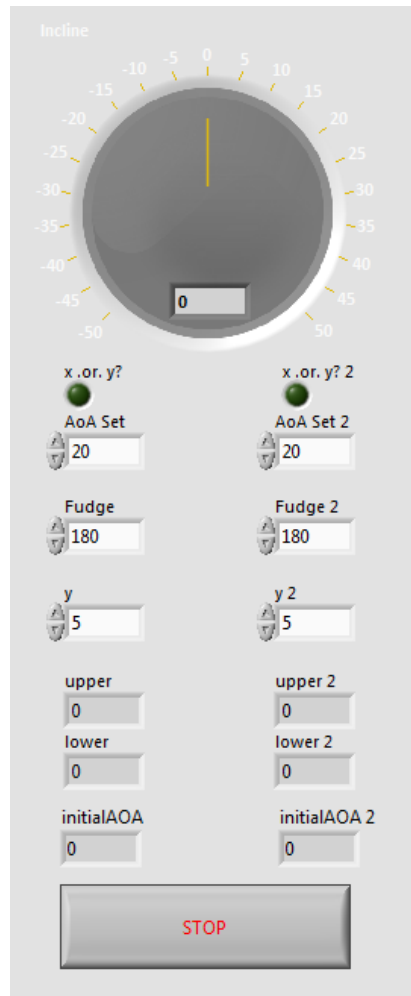


Figure 59: Front panel of the LabVIEW program controlling the device.

When the program is run, both motors controlling the wings are run simultaneously and go through an initializing process which sets the leading and trailing wings angle of attack as requested by the user in the front panel. The leading and trailing wings are set in the positive and negative angle of attack direction respectively which allowed the arm to rotate in a clockwise direction when the wind tunnel is activated. The device only goes through the initializing process once every time the program is run.

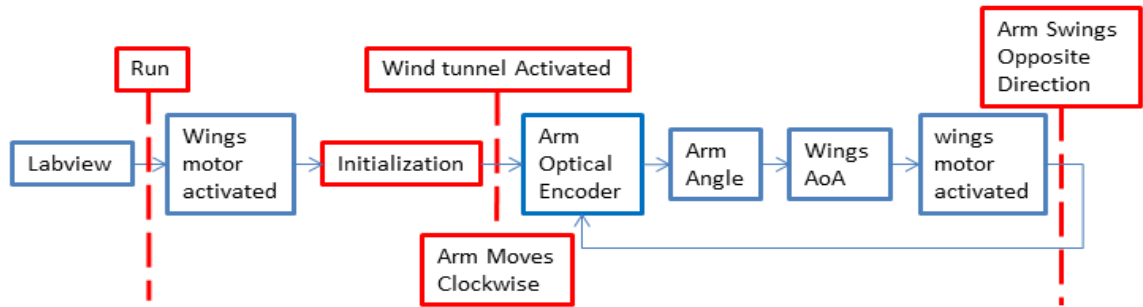


Figure 60: Simplified block diagram of the control system.

When the wind source is turned on, lift is created in the upwards direction for the front wing and downwards for the rear wing. Figure 60 shows the simplified block diagram of the process that the device goes through. The lift generated by the wings allow the arm to pivot at the middle point of the whole structure and the digital optical encoder attached at the pivoting point helps to monitor the angle of the arm. When the arm reaches the specific angle that was set in the program, the program executes the subsequent command that allow the stepper motor attached at the quarter chord of the wing, through a mechanism of gear and belt combination, to rotate the wing to a specific angle in the opposite direction. The rotation of the wing is monitored by another E2 digital optical encoder located at the quarter chord of the wing. This change in the wing angle of attack pushes the arm to rotate in the counterclockwise direction. The changes in the arm angle is again monitored by the middle optical encoder and the device goes through the whole process repeatedly until the wind speed is too low to have any effect on the device.

All the data, or input and output signals generated by the devices and the computer are connected through several National Instrument data acquisition system. The analog signals generated by the optical encoders are converted into digital numeric signals to be processed by the microprocessors in the computer and the digital signals generated by the microprocessors in the computer are converted to analog signal to actuate the motors in return. The microprocessor used in this application is the Intel® Xeon® Processor 5130 (4M Cache, 2.00 GHz, 1333 MHz FSB). The microprocessor used has the Harvard architecture with parallel connections.

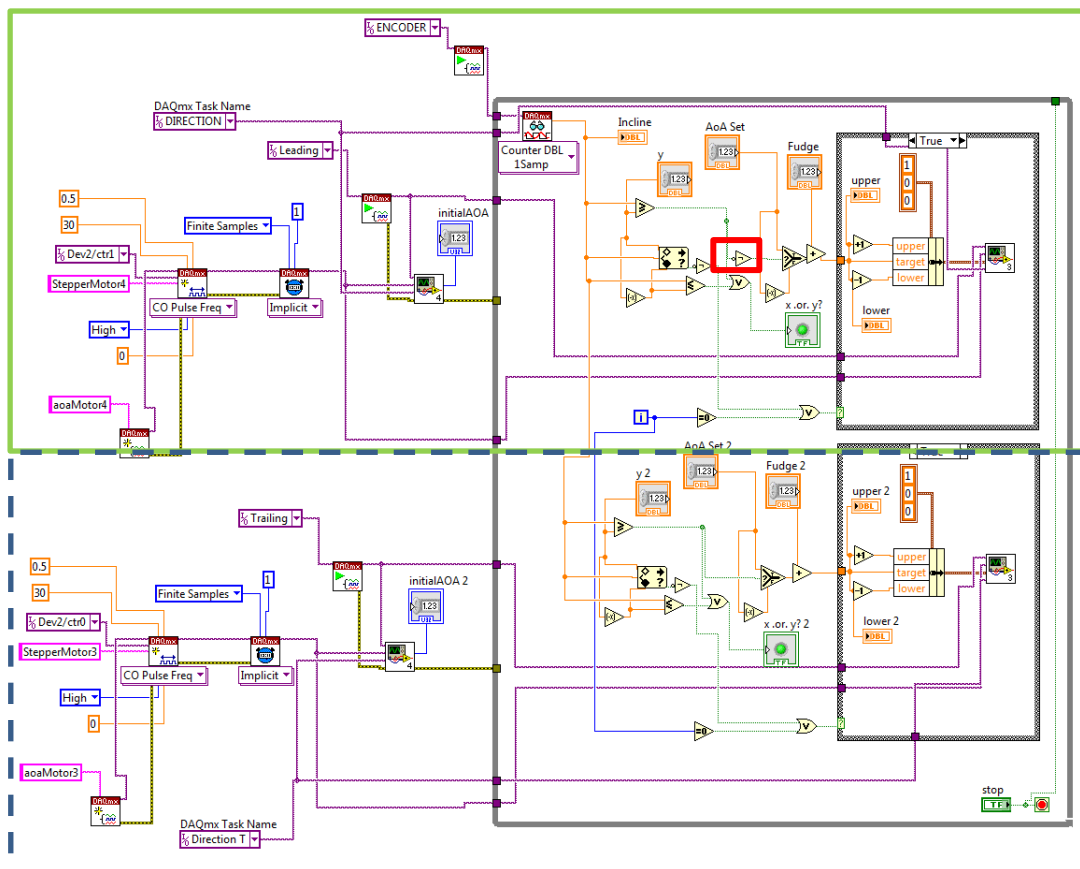


Figure 61: The main VI controlling the system.

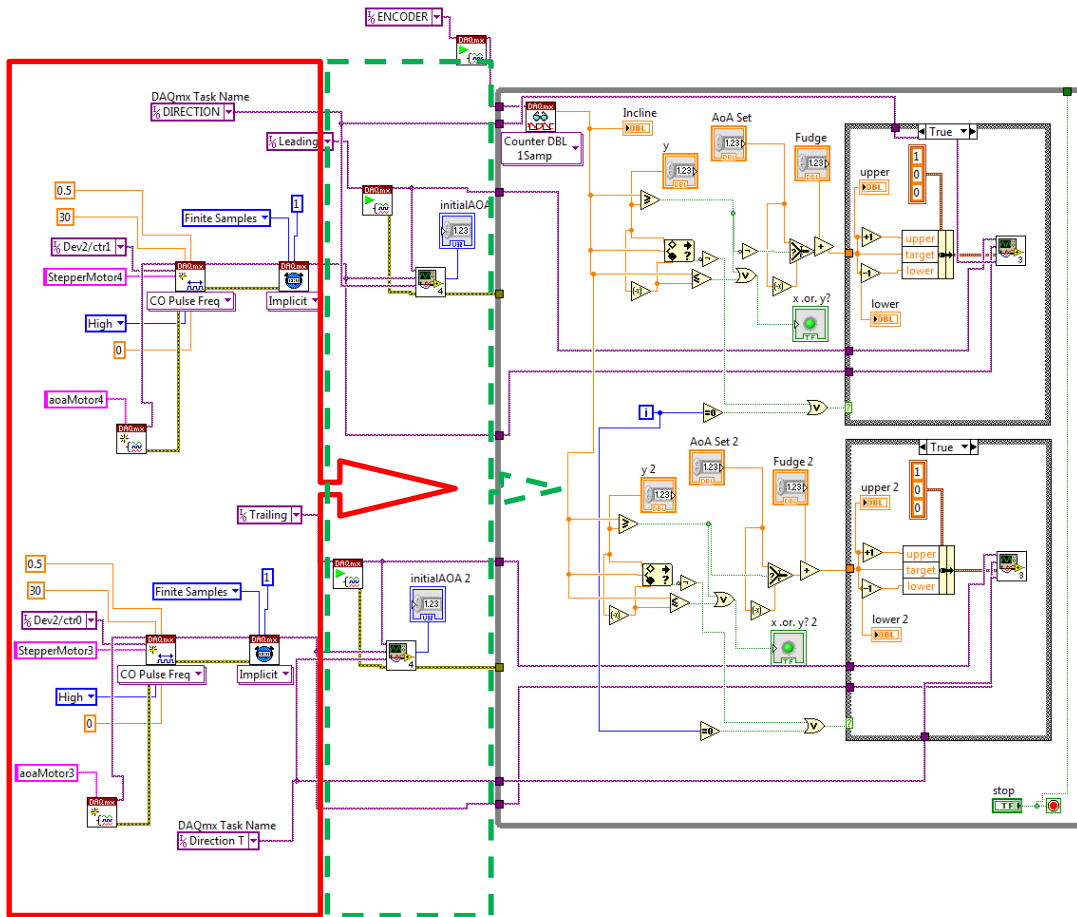


Figure 62: The sequence of event for the main VI controlling the system.

Figure 61 shows the schematic for the main virtual instruments (VI) that controlled the system. The green (solid line) and blue (dashed line) highlighted region shows two separate sections that are responsible of controlling the behavior of the leading and trailing wing respectively. The block diagrams used in both sections are the same except for the NOT symbol which is highlighted (red) and is used in the leading wing section (solid green line section) of the VI region so as to have an opposite angle or direction than the trailing wing. Figure 62 shows the sequence of events that takes place when the program is run. When the program is run, the motors start running which is

shown in the red (solid line) region, then the program goes through an initializing process to make sure that the leading and trailing wing has the same angle but in the opposite direction. The program runs through the while loop, which is activated if there is a change of angle in the middle encoder. The case structures of both leading and trailing wings are activated by the value recorded by the middle encoder.

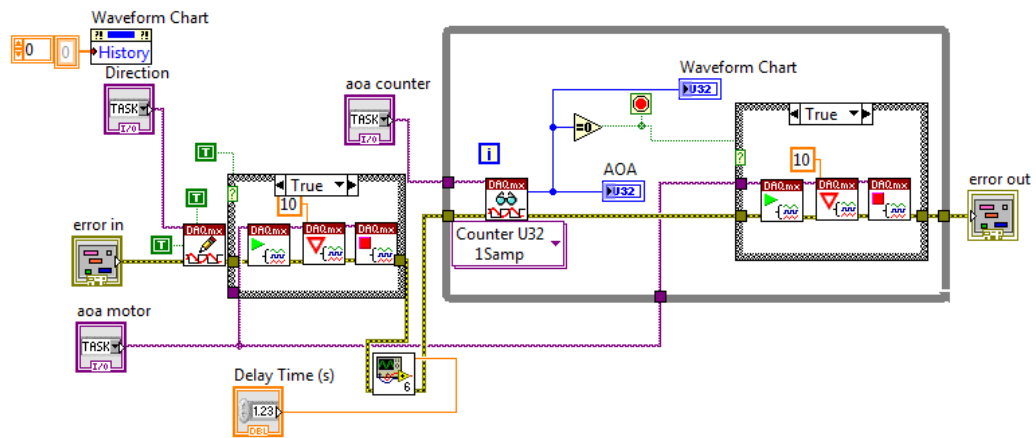


Figure 63: The sub VI that is responsible for initializing the system.

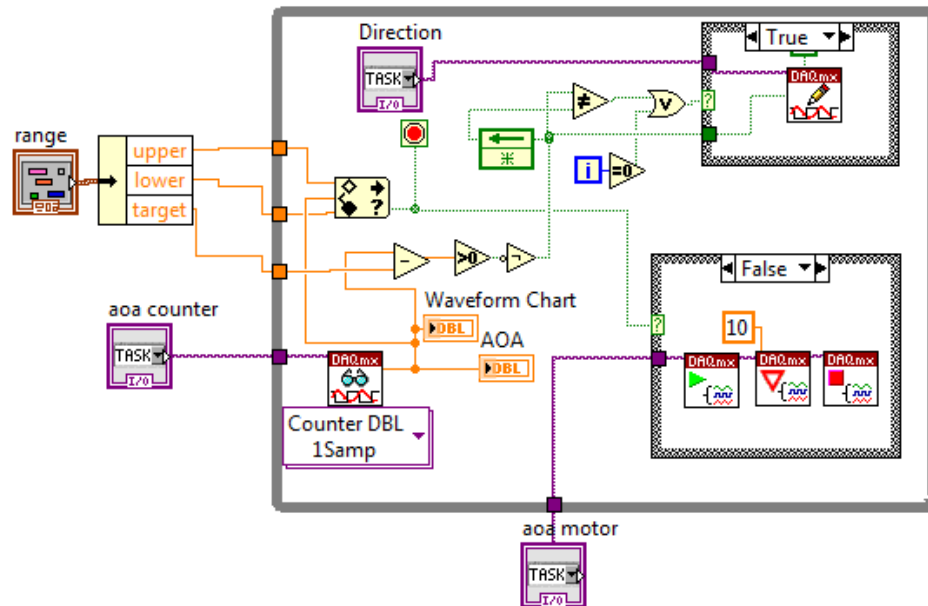


Figure 64: The sub VI that is controlling the angle of attack of the wings.

Figure 63 shows the sub VI that controlled the initialization process of the system. Figure 64 shows the sub VI inside the case structure of the main VI that is responsible for determining the direction of the wings based on the reading from the middle encoder, which is shown as range and the wing encoder which is shown as Counter DBL 1 Samp. The case structure on top changes if the angle of the wing meets the criteria of being TRUE whereas the case structure on the bottom runs the motor if it meets the criteria of being FALSE. Figures 65 and 66 show the breakdown of the process mentioned earlier in a detailed block diagram drawing.

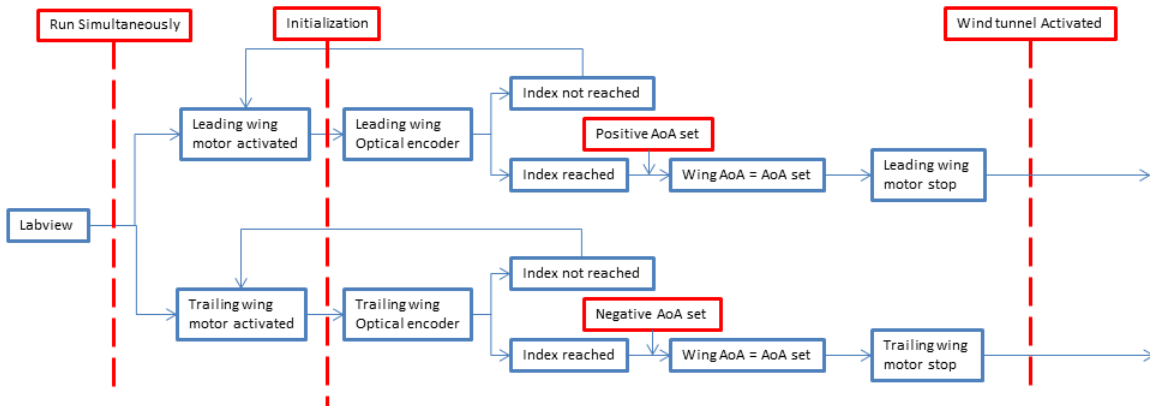


Figure 65 : Detailed block diagram of the control system.

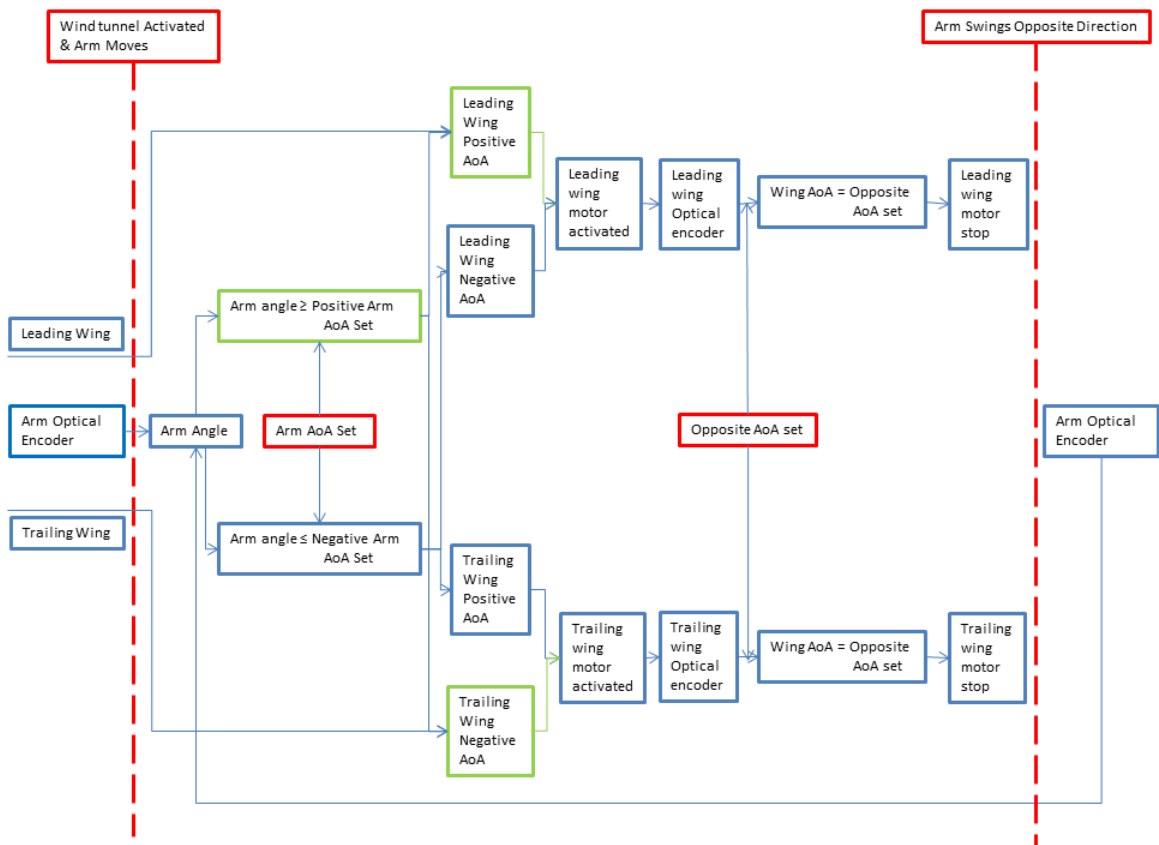


Figure 66: Detailed block diagram of the control system.

LabVIEW – Data Acquisition

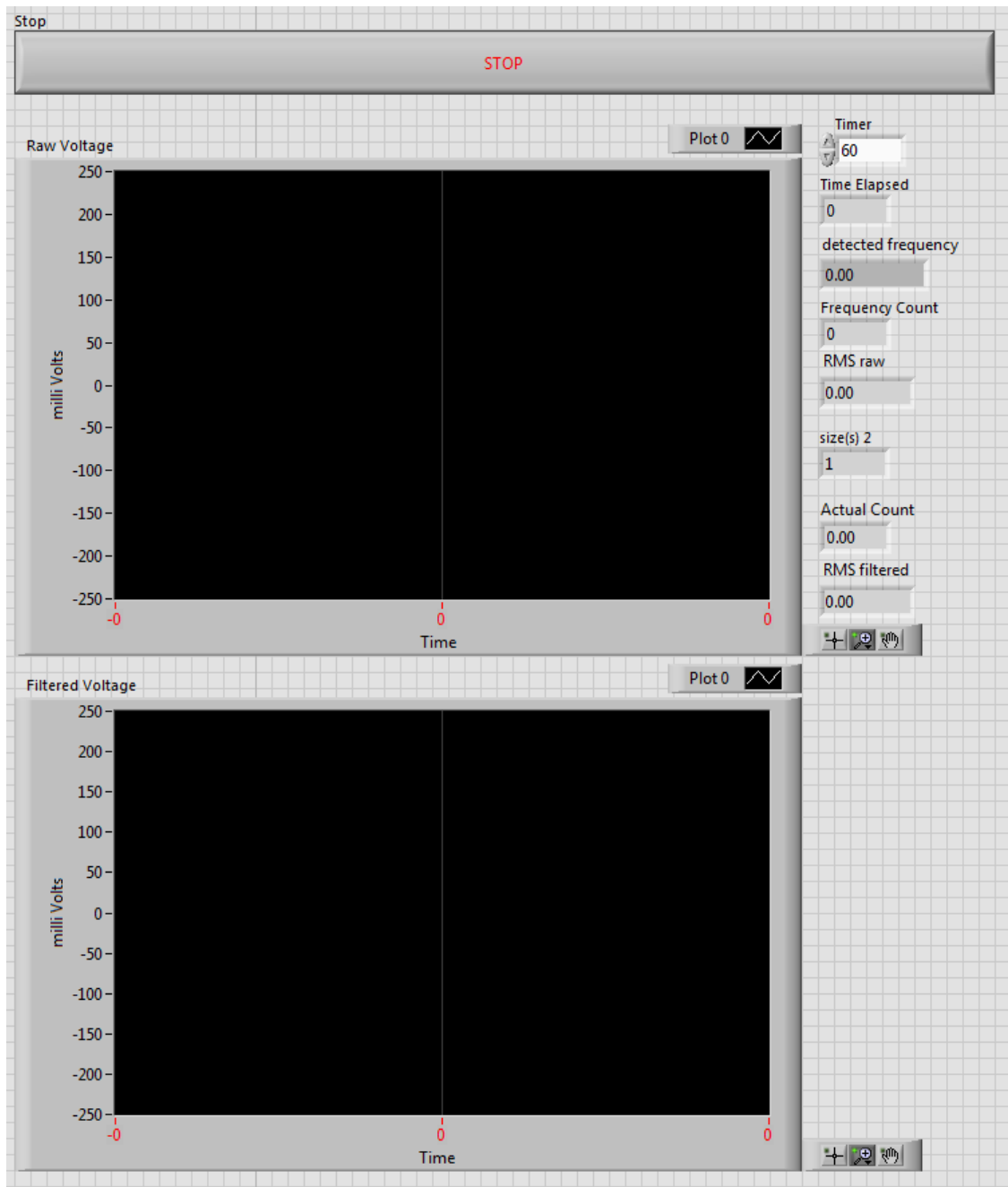


Figure 67: Front panel of the LabVIEW program used to collect data from the Wind Oscillator

The LabVIEW program was also used to record the voltage data obtained from the DC motor generator. The front panel of the LabVIEW data acquisition program is shown in figure 66. The program allowed the user to observe the live raw voltage data that is being generated by the Wind Oscillator. It also allowed the user to observe the filtered data of the raw voltage with a few millisecond delay. A low pass filter is used, as can be seen in figure 68, to filter the noise generated by the electronics and the user is responsible for setting the value for the filter before the data acquisition VI is run. The User can also set the duration of time that the data will be collected in the timer on the front panel as shown on figure 67. The front panel allows the user to observe the raw Root-Mean-Square (RMS) voltage, filtered RMS voltage, frequency and the frequency count of the device after each run. Figure 68 shows the schematic of the VI that collects, calculates and records the data that is obtained from the system. The program also writes the data obtained to a text file and saves it.

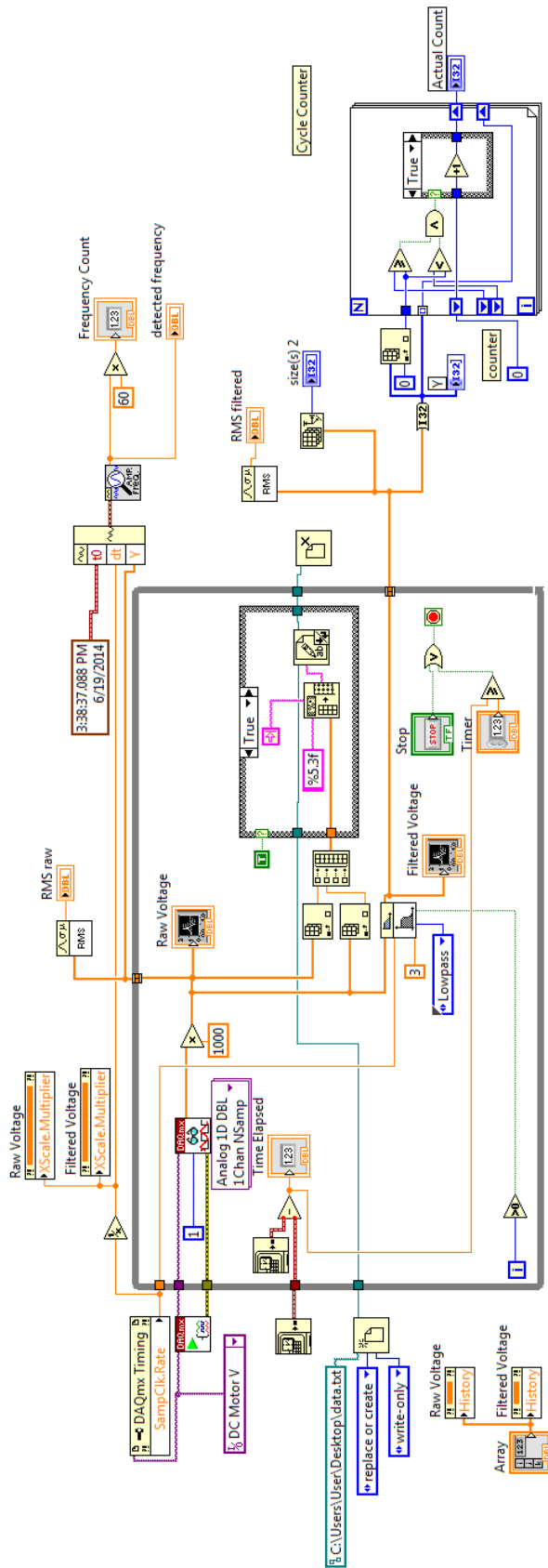


Figure 68: The VI that collects and records raw and calculated RMS voltage data

CHAPTER VIII

WIND TUNNEL TESTING

Model Set Up and Wind Tunnel Calibration

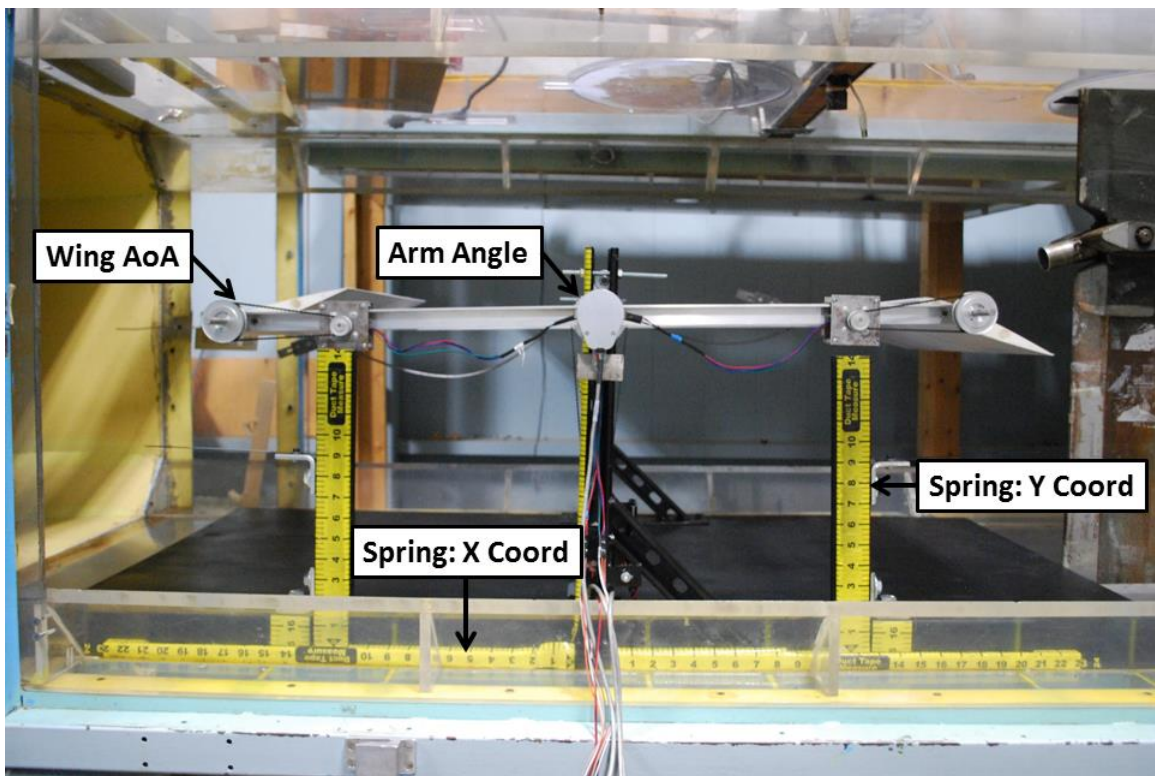


Figure 69: Model wind oscillator set up in the Advanced Design Wind Tunnel at WMU.

The device is put through a set of systematic testing in the Advanced Design Wind Tunnel (ADWT) facility which is owned by Western Michigan University (WMU). The wind tunnel test section measures about 0.813m high, 1.14m, wide and 2.44 m long, which are the main constraining design parameter for the model wind oscillator design. It is also a closed loop, low speed atmospheric tunnel. Figure 69 shows the Wind Oscillator placed inside the test section of the wind tunnel. The wind tunnel test section is walled in by the Plexiglas on the top and the sides to allow optical visualization to the test that is being conducted. Although the tunnel is capable of having a wind flow velocity of up to 73 m/s, due to the dimension constrain of the model, it was only run to a maximum wind speed of 6m/s. An anemometer by Ambient Weather shown in figure 70 was used to measure and calibrate the wind tunnel at lower wind speed since the range of wind speed tested was below the operating range of the manometer connected to the wind tunnel. The anemometer is capable of measuring wind speed in the range of 0.4mph to 67 mph with a resolution of 0.1mph and accuracy of $\pm 3\%$ [144] which falls within the range of wind speed that the model was tested in. The wind speed of the tunnel was calibrated in respect to the wind tunnel's fan speed which was shown on the ADWT control panel using the anemometer for the ease of the experiment being repeated multiple times with minimal error. The calibration graph is shown in figure 71 and the extrapolated version of the graph is shown in figure 72. The Matlab code for the calibration is given in the appendix B.



Figure 70: Anemometer[144].

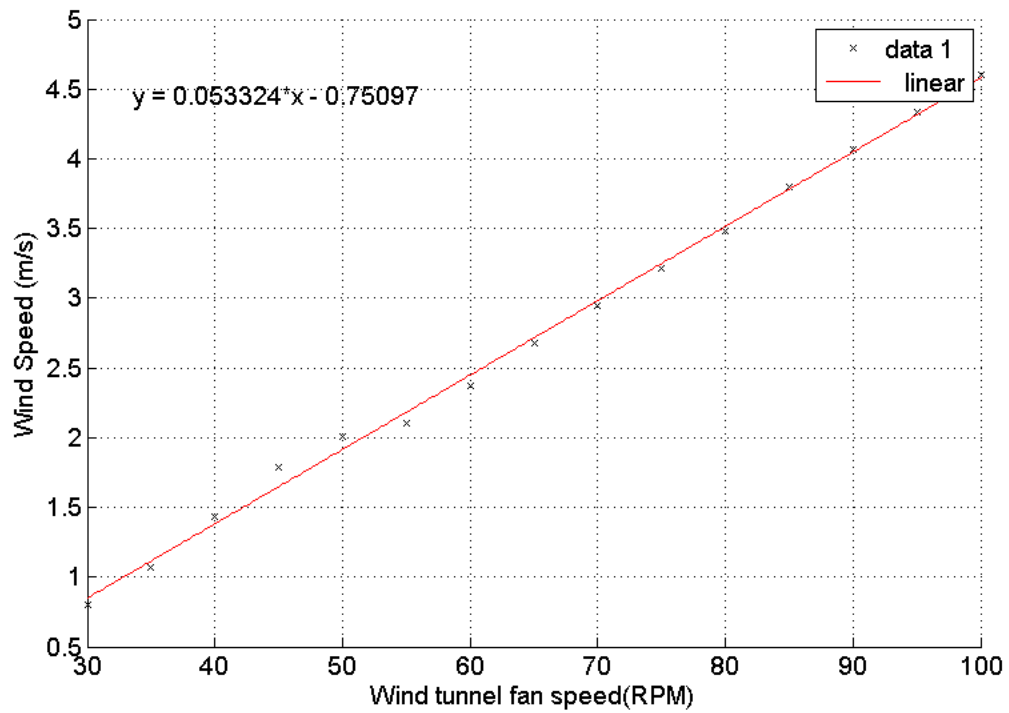


Figure 71: Wind speed inside wind tunnel calibration based on wind tunnel fan speed.

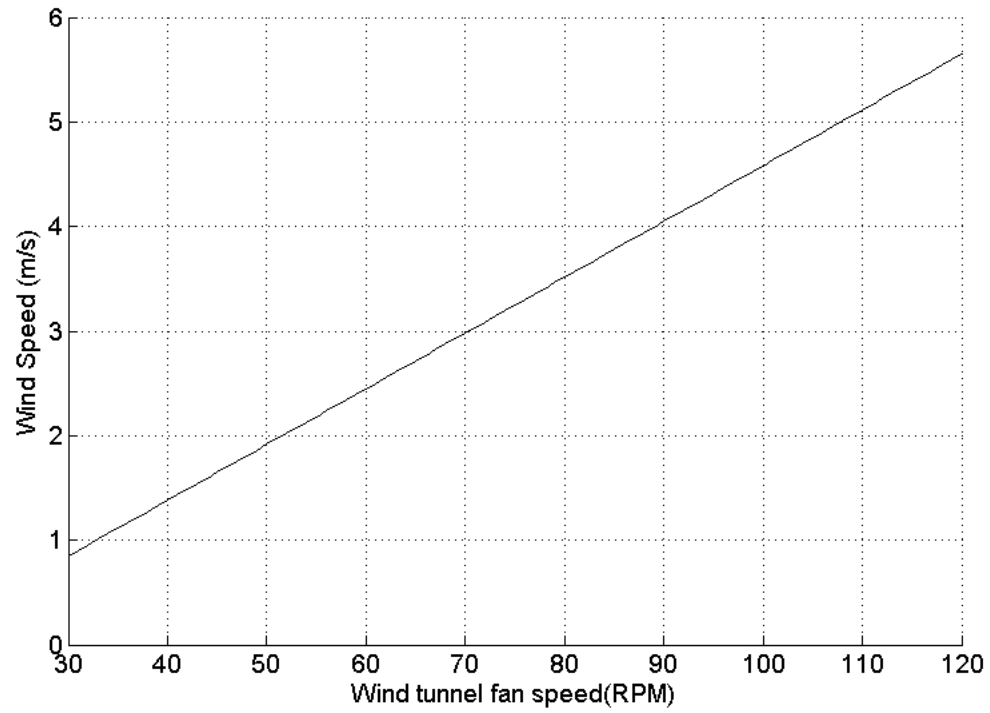


Figure 72: Extrapolated wind speed versus fan speed graph based on the calibration data

RMS Voltage Data Acquisition and Analysis

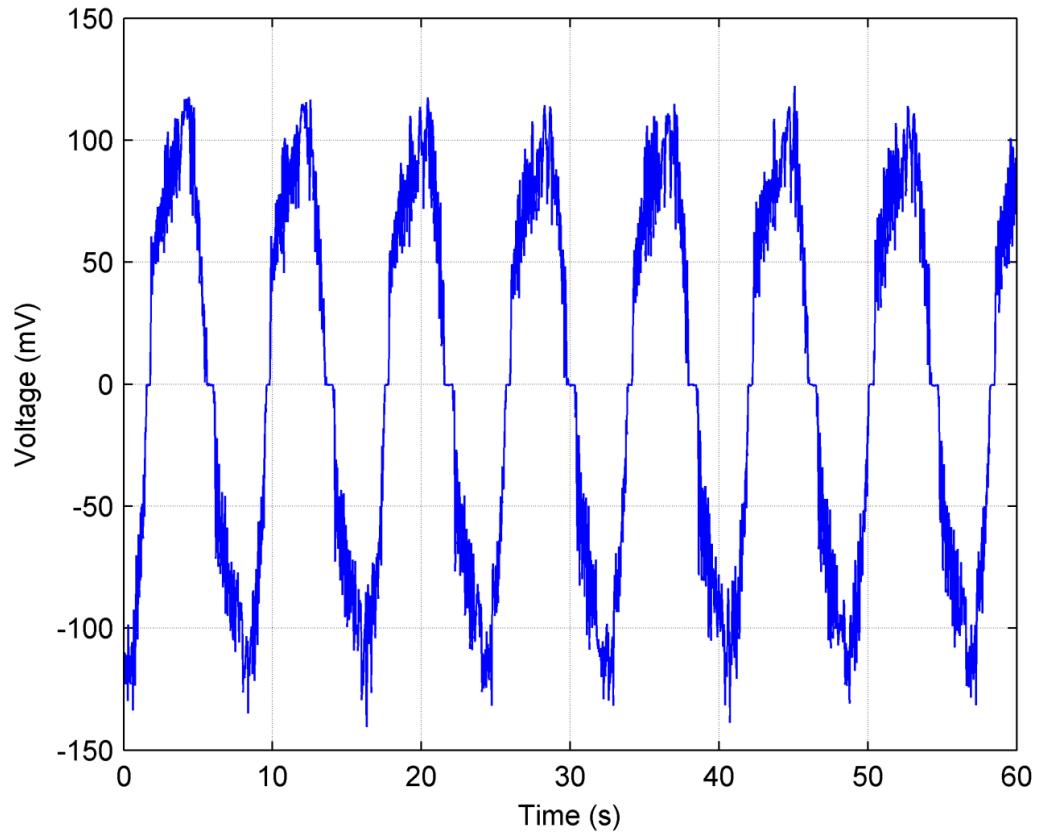


Figure 73: Typical voltage output from model wind oscillator through DC motor.

The LabVIEW data acquisition program, as mentioned earlier, collects and records the data produced by the DC motor generator. Figure 73 shows the typical raw voltage output produced by the generator. The program also calculates the RMS voltage value from the collected raw voltage data and shows the value on the front panel for the ease of the user to record the data.

Three different parameters were controlled and one parameter was kept constant for the experiment. The control parameters were AoA of the wing (wing AoA), AoA of the arm (arm angle) and the height of the leaf spring (spring: y coordinate) as shown in figure 69. The location of the spring in the x-axis was kept constant for all the cases. The controlled parameters were tested individually at different values while restraining the other two control parameters at a specific value for a range of wind speeds and a period of 60 seconds. The range of the wind speed for the experiment was determined by the starting speed of the wind tunnel and at the moment where the Wind Oscillator starts to hit the wind tunnel test section surface. This was done to avoid any damage to the model as well as the wind tunnel test section.

The three control parameters were tested at three different levels to understand the effect it might have on the RMS voltage output and each level was tested three times for the same range of wind speeds. The average value of the each wind speed was then obtained.

PARAMETER 1: HEIGHT OF THE LEAF SPRING

Three different leaf spring heights were tested to observe the effect of the spring stiffness on the system. The leaf spring heights were 7, 8 and 9 inches. The height of the spring was measured from the top surface of the Wind Oscillator base plate to the top surface of the leaf spring.

PARAMETER 2: AOA OF THE WING

The AoA of the wings were set and tested at ± 15 , ± 20 and ± 30 degrees. The values were set through the front panel of the LabVIEW control program. It was presumed that the higher the AoA the higher the output RMS voltage value.

PARAMETER 3: AOA OF THE ARM

The AoA of the arm was also set through the front panel of the LabVIEW program at ± 5 , ± 9 and ± 13 degrees. This parameter was tested not only to observe the RMS voltage output but also for the oscillation frequency of the system.

CONTROLLED PARAMETER: X COORDINATE OF THE LEAF SPRING

Both springs were placed 7 inches away from the side surface of the leg on both directions.

RESULT AND DISCUSSION

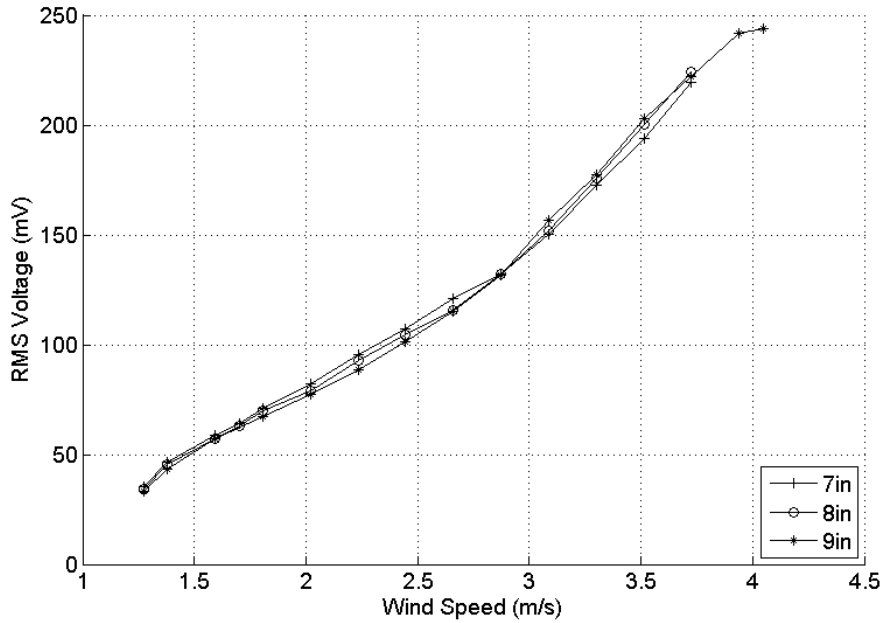


Figure 74: RMS voltage output for different leaf spring heights when arm AoA is ± 5 degree and wing AoA is ± 15 degree.

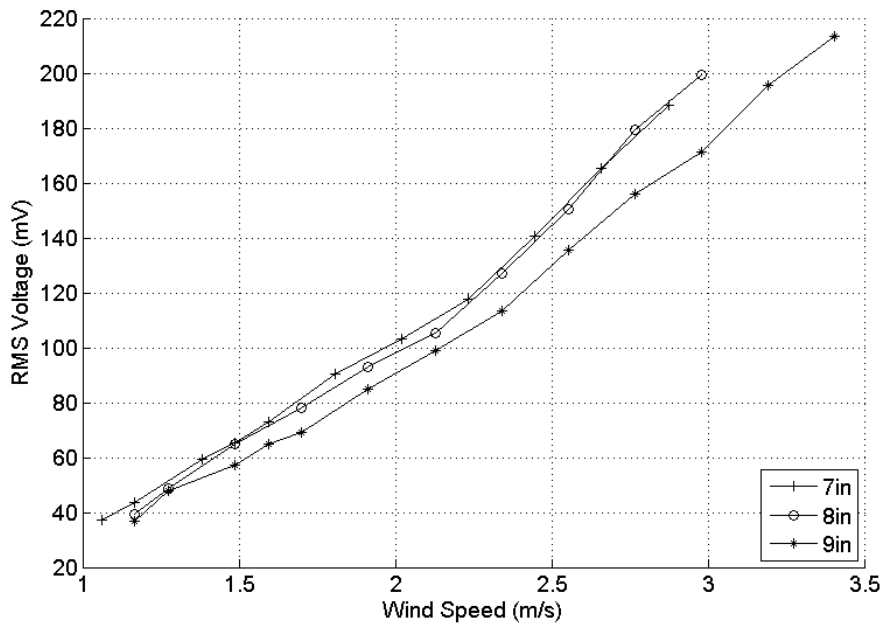


Figure 75: RMS voltage output for different leaf spring heights when arm AoA is ± 5 degree and wing AoA is ± 20 degree.

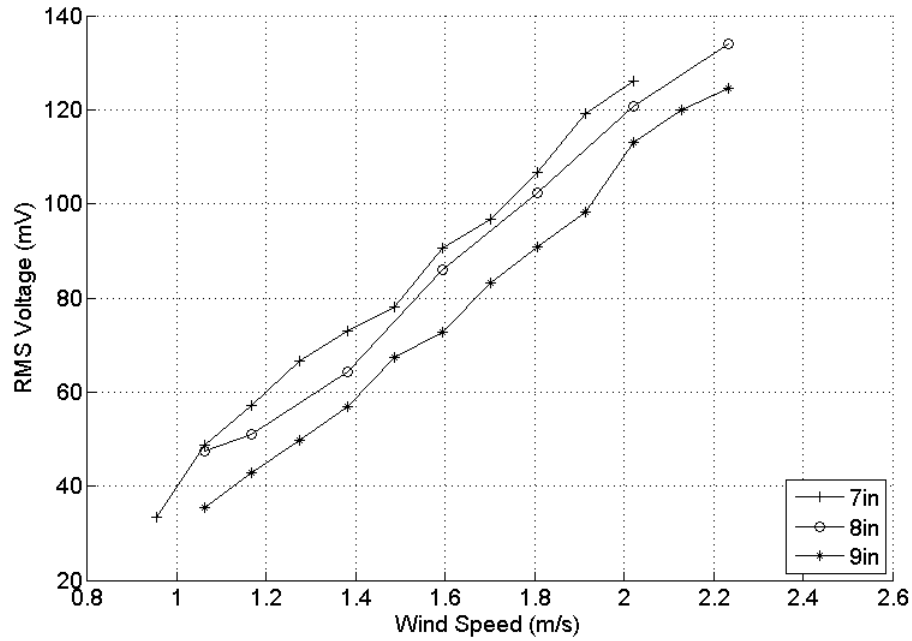


Figure 76: RMS voltage output for different leaf spring heights when arm AoA is ± 5 degree and wing AoA is ± 30 degree.

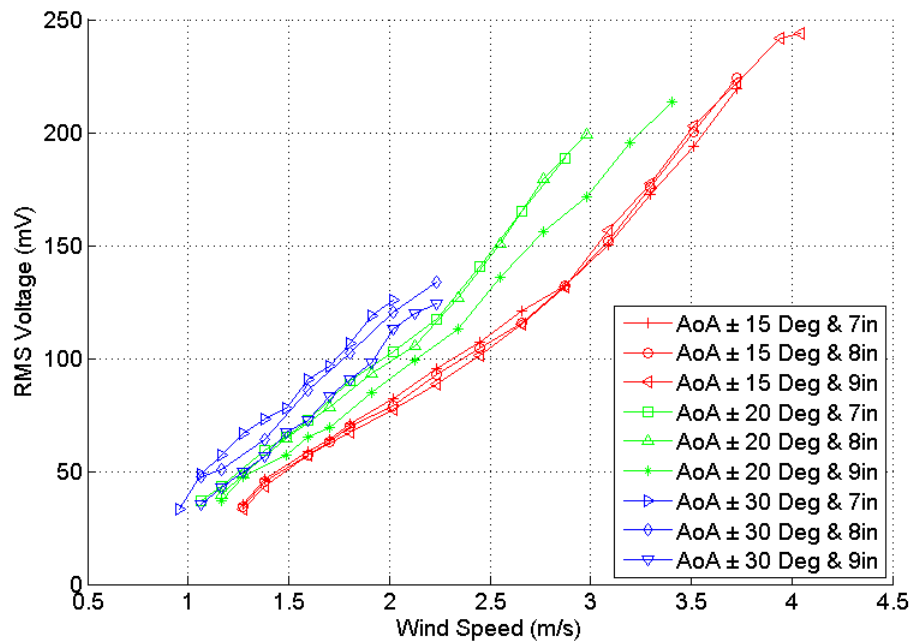


Figure 77: Comparison of all the RMS voltage output graphs when arm AoA is ± 5 degree.

Figure 74 shows the average RMS voltage output for a range of wind speeds when the AoA of the wing was set at ± 15 degree and the AoA of the arm was set at ± 5 degree using different heights for the leaf spring. The RMS voltage output for the three spring heights increased as the wind speed increases but there is no significant difference in the RMS voltage output with the different spring heights. Figures 75 and 76 have the same setting as figure 74 but the AoA of the wing was changed to ± 20 and ± 30 degrees respectively. Both figures show linear graphs for all three cases but they also show a significant increase in RMS voltage output for a specific wind speed when the height of the spring is reduced. This was more significant in figure 76. The increase in AoA of the wing also reduced the cut-off wind speed but increased the cut-in speed of the device, which can be seen in the comparison graph presented in figure 77. The comparison graph also shows that the RMS voltage is higher for a higher AoA of the wing at a specific wind speed.

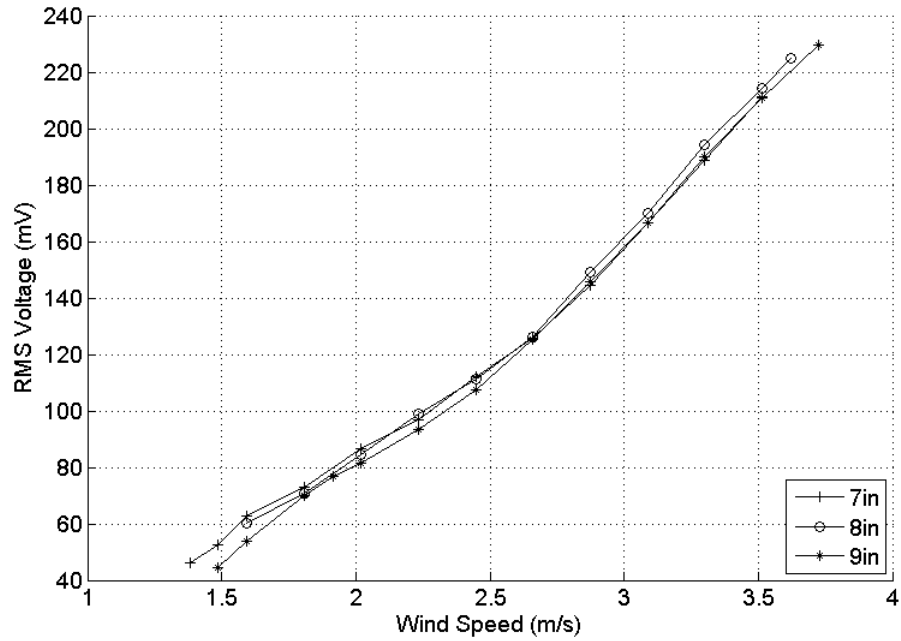


Figure 78: RMS voltage output for different leaf spring heights when arm AoA is ± 9 degree and wing AoA is ± 15 degree.

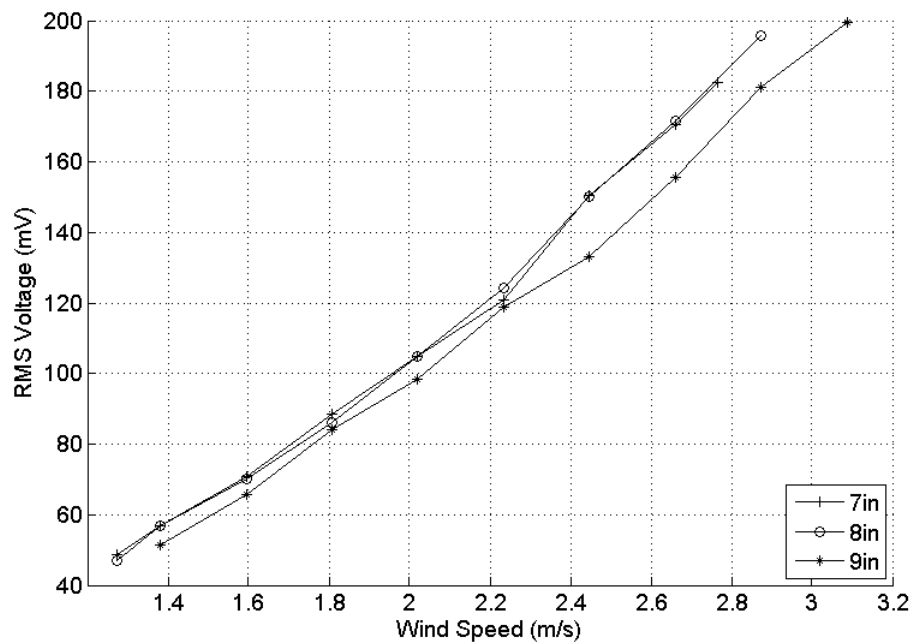


Figure 79: RMS voltage output for different leaf spring heights when arm AoA is ± 9 degree and wing AoA is ± 20 degree.

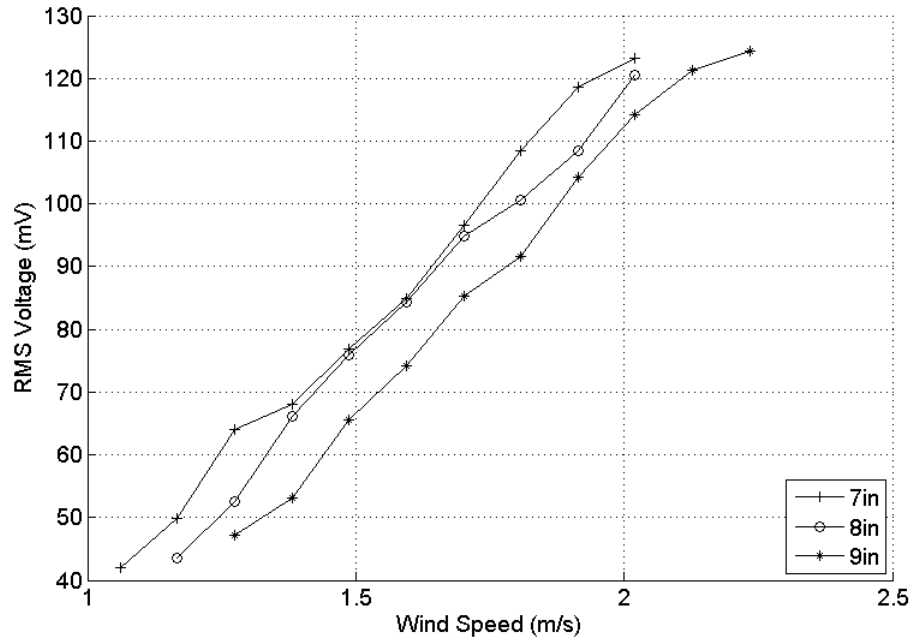


Figure 80: RMS voltage output for different leaf spring heights when arm AoA is ± 9 degree and wing AoA is ± 30 degree.

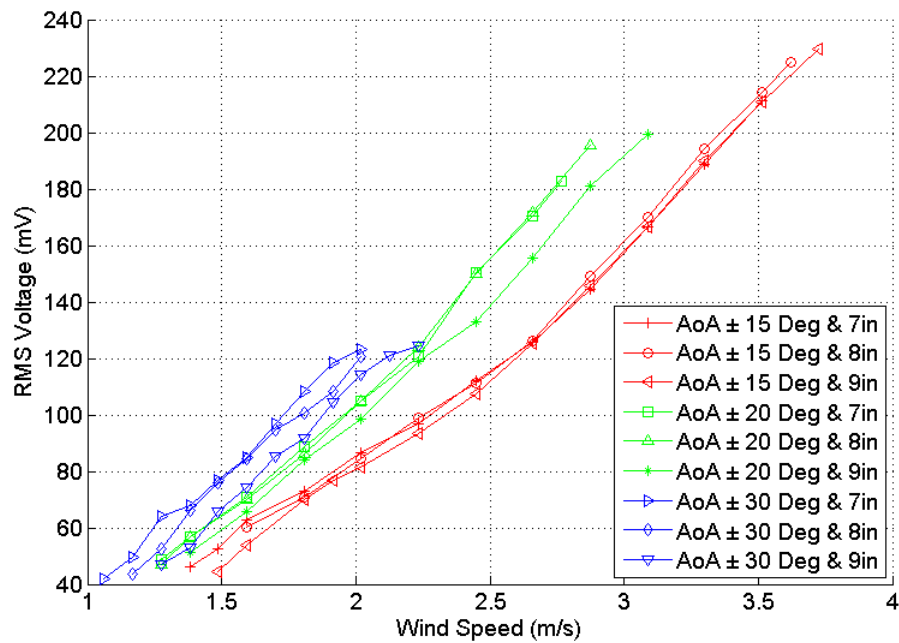


Figure 81: Comparison of all the RMS voltage output graphs when arm AoA is ± 9 degree.

Figures 78, 79 and 80 have similar settings as figures 74, 75 and 76 but with a different arm AoA value, which was set at ± 9 degrees. All three figures have a linear pattern for all three heights of the leaf spring but there is no significant difference in the RMS voltage output at a particular wind speed except for figure 80, which shows an increment in the RMS voltage output as the spring height decreases. The comparison graph for arm AoA set at ± 9 degree is shown in figure 81. It shows that as the AoA of the wing was increased, the RMS voltage output of the device increased for a specific wind speed. The increase in AoA of the wing also increased the cut-in speed of the device but also reduced the cut-off speed of the device.

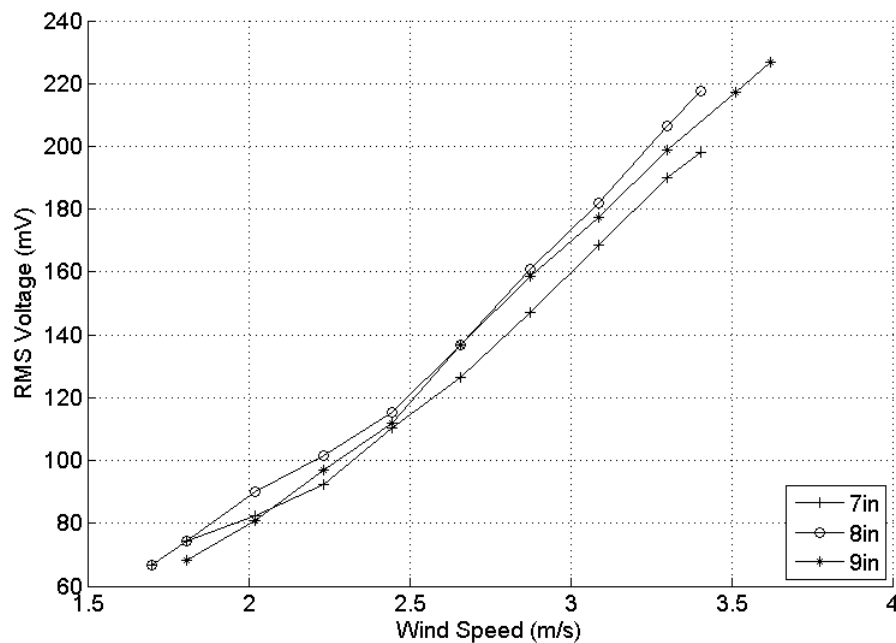


Figure 82: RMS voltage output for different leaf spring heights when arm AoA is ± 13 degree and wing AoA is ± 15 degree.

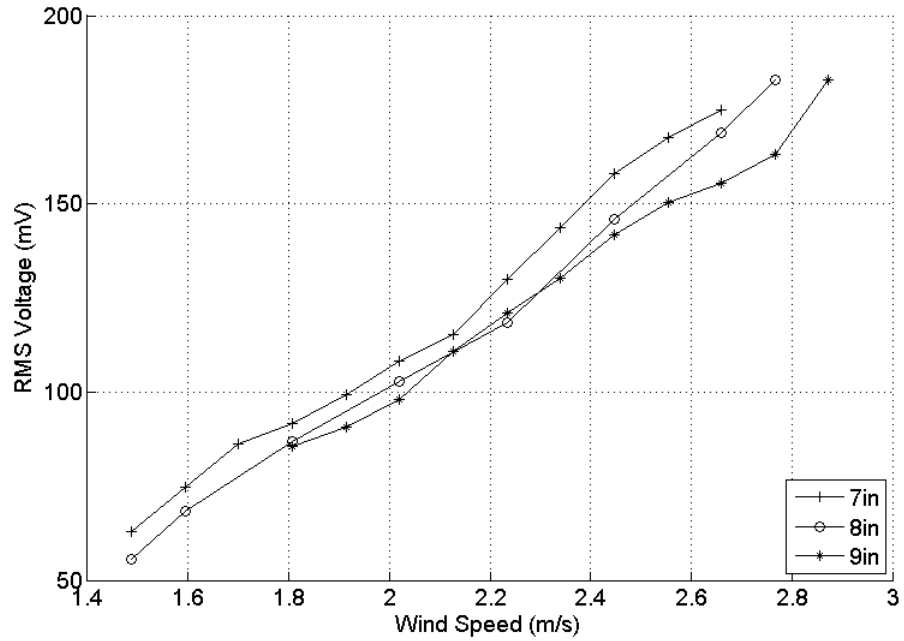


Figure 83: RMS voltage output for different leaf spring heights when arm AoA is ± 13 degree and wing AoA is ± 20 degree.

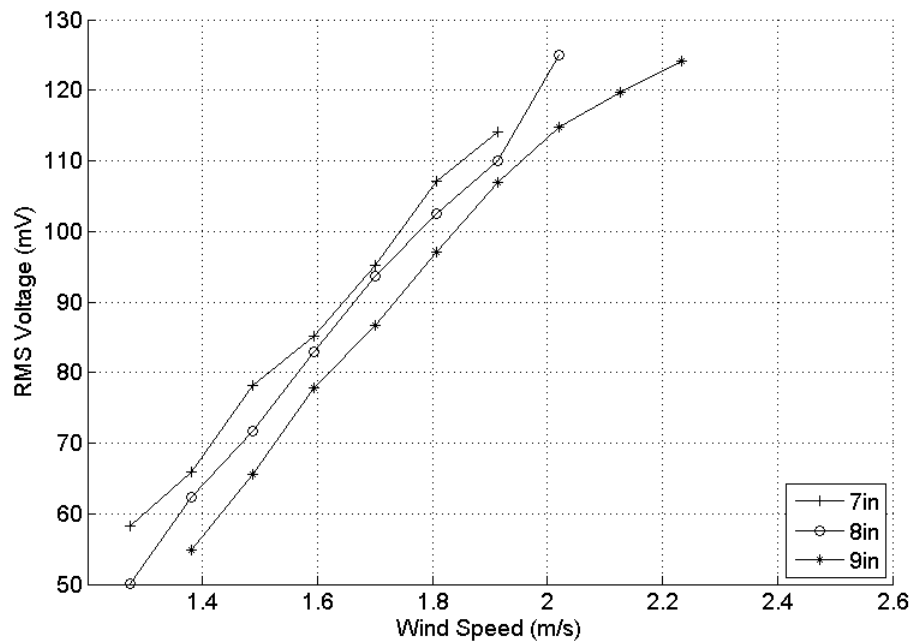


Figure 84: RMS voltage output for different leaf spring heights when arm AoA is ± 13 degree and wing AoA is ± 30 degree.

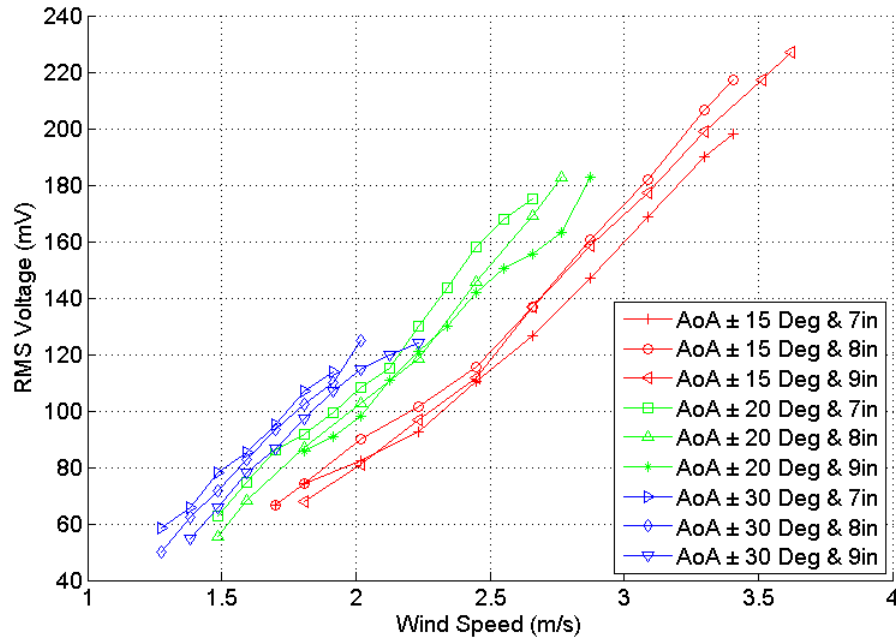


Figure 85: Comparison of all the RMS voltage output graphs when arm AoA is ± 13 degree.

Figures 82, 83 and 84 have similar settings as figures 74, 75 and 76 but with a different AoA of the arm, which was set at ± 13 degrees. All three figures have a significant difference in RMS voltage output at any particular wind speed. The comparison graph for arm AoA set at ± 13 degree in figure 85 shows that as the AoA of the wing increases, the RMS voltage output of the device also increases for a specific wind speed. The increase in AoA of the wing also increased the cut-in speed of the device but reduced the cut-off speed of the device, similar to the previous comparison graphs.

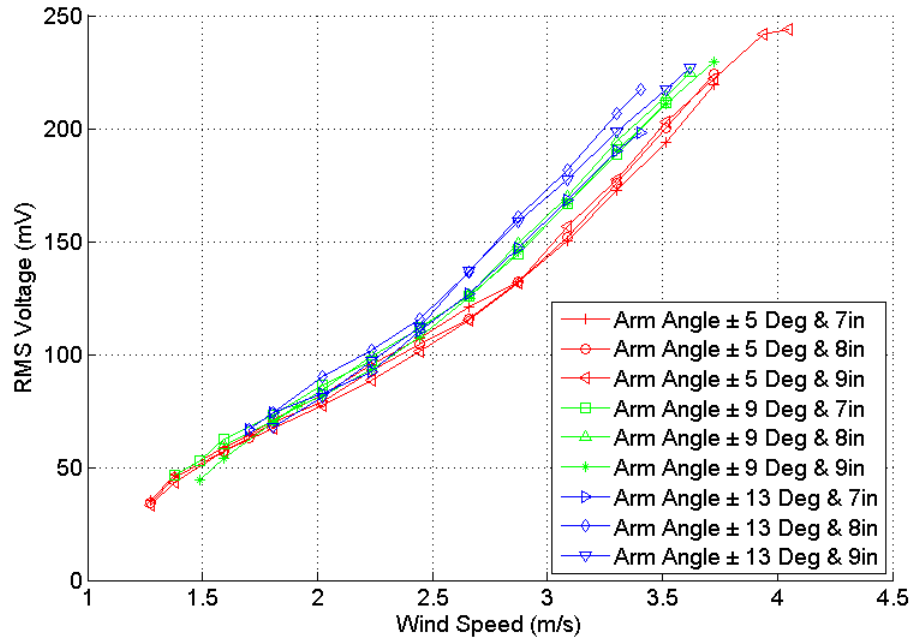


Figure 86: Comparison of all the RMS voltage output graphs when wing AoA is ± 15 degree.

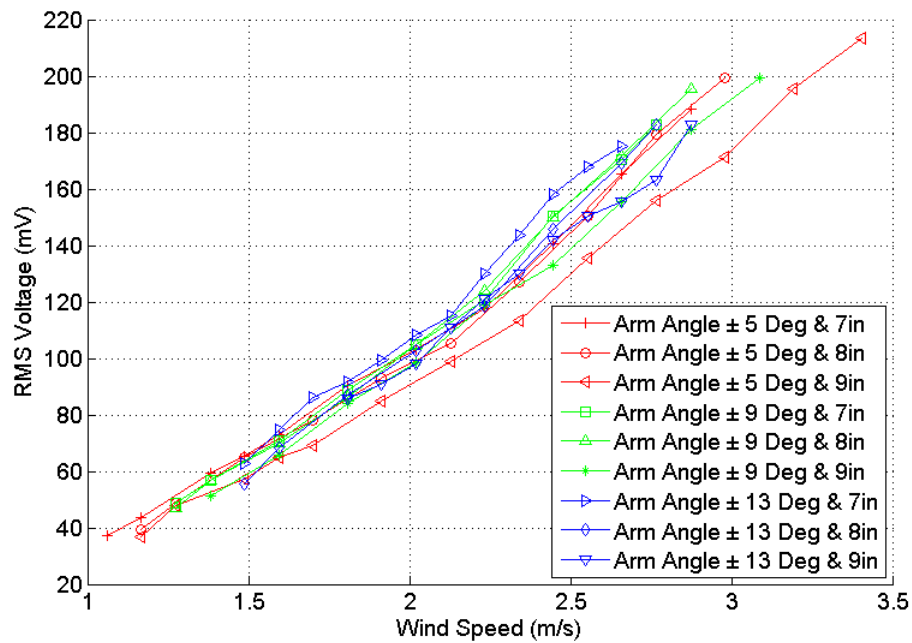


Figure 87: Comparison of all the RMS voltage output graphs when wing AoA is ± 20 degree.

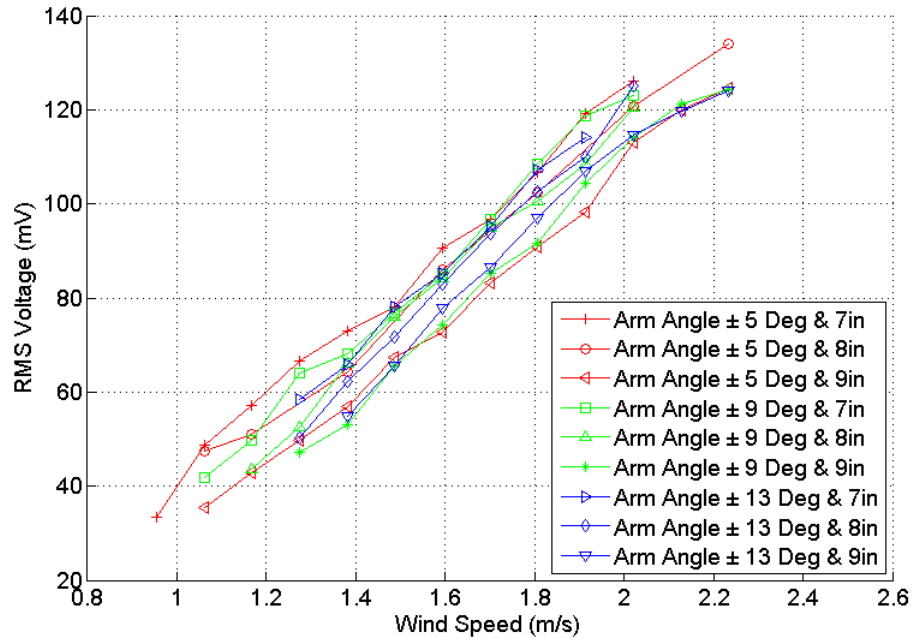


Figure 88: Comparison of all the RMS voltage output graphs when wing AoA is ± 30 degree.

Figures 86, 87 and 88 show the comparison graphs of wing AoA ± 15 , ± 20 and ± 30 degrees respectively. All three figures show that the increase in arm AoA increased the cut-in speed of the device. No other significant results were observed from these comparison plots as the graphs overlap each other.

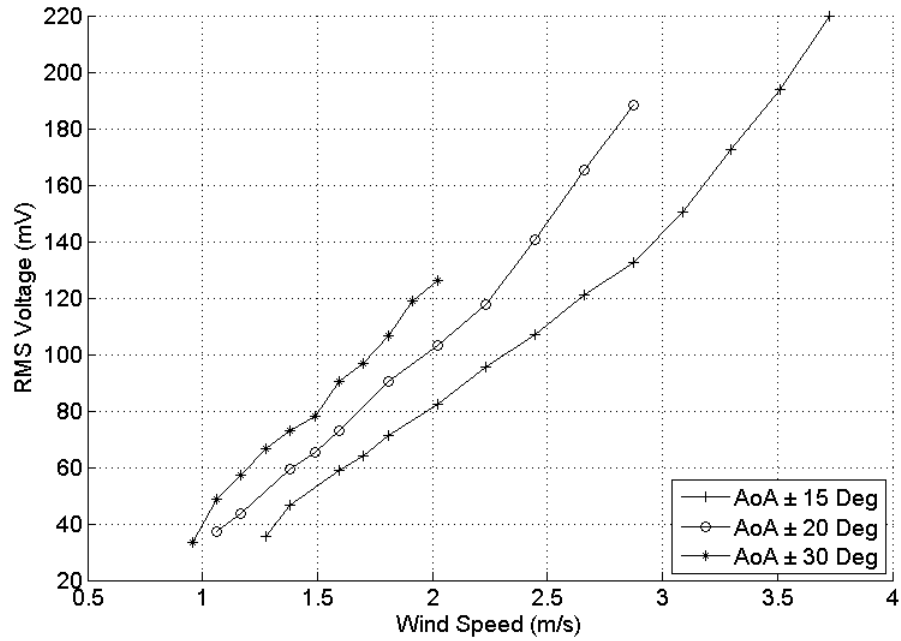


Figure 89: RMS voltage output for different wing AoA when arm AoA is ± 5 degree and leaf spring height is 7 in.

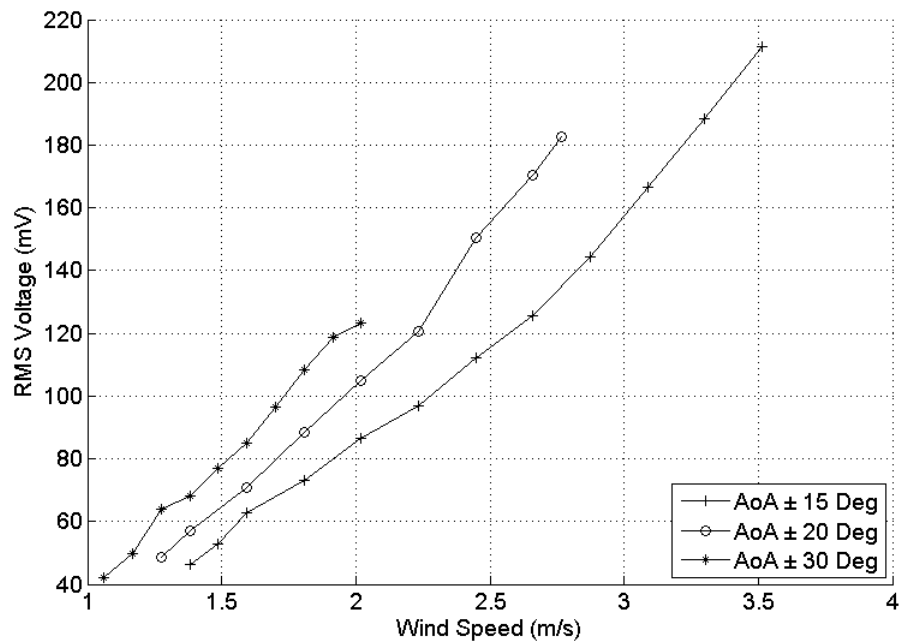


Figure 90: RMS voltage output for different wing AoA when arm AoA is ± 9 degree and leaf spring height is 7 in.

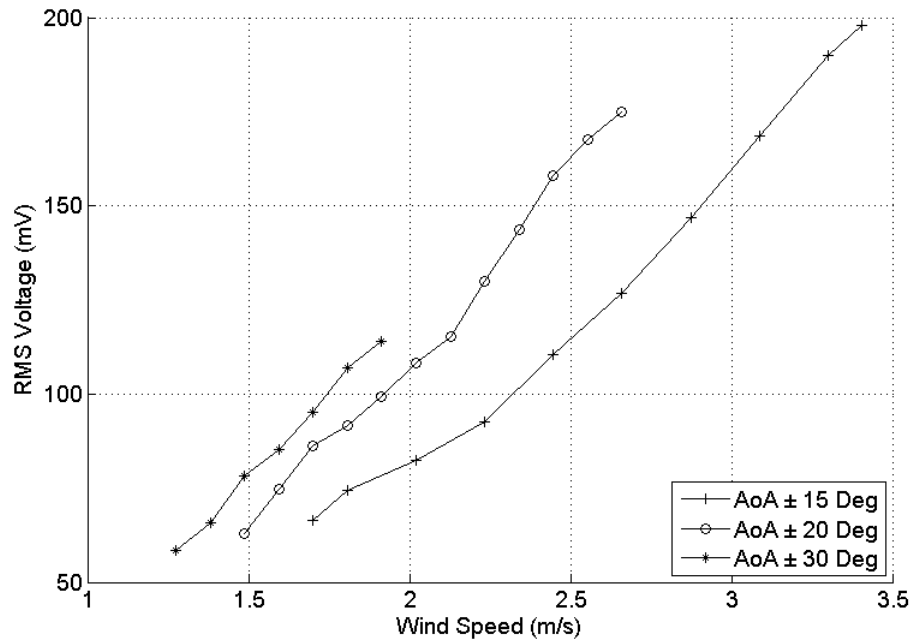


Figure 91: RMS voltage output for different wing AoA when arm AoA is ± 13 degree and leaf spring height is 7 in.

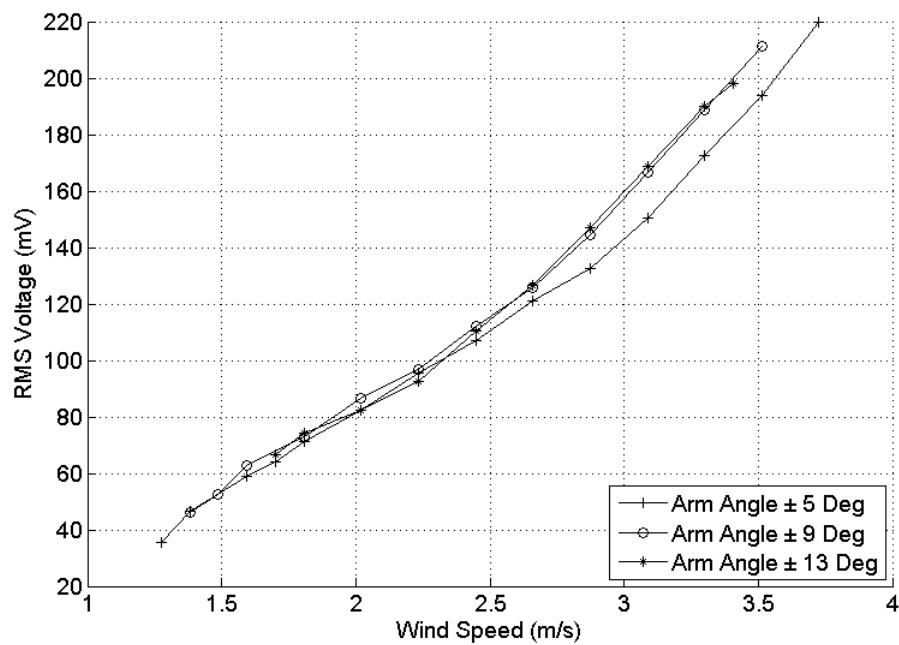


Figure 92: RMS voltage output for different arm AoA when wing AoA is ± 15 degree and leaf spring height is 7 in.

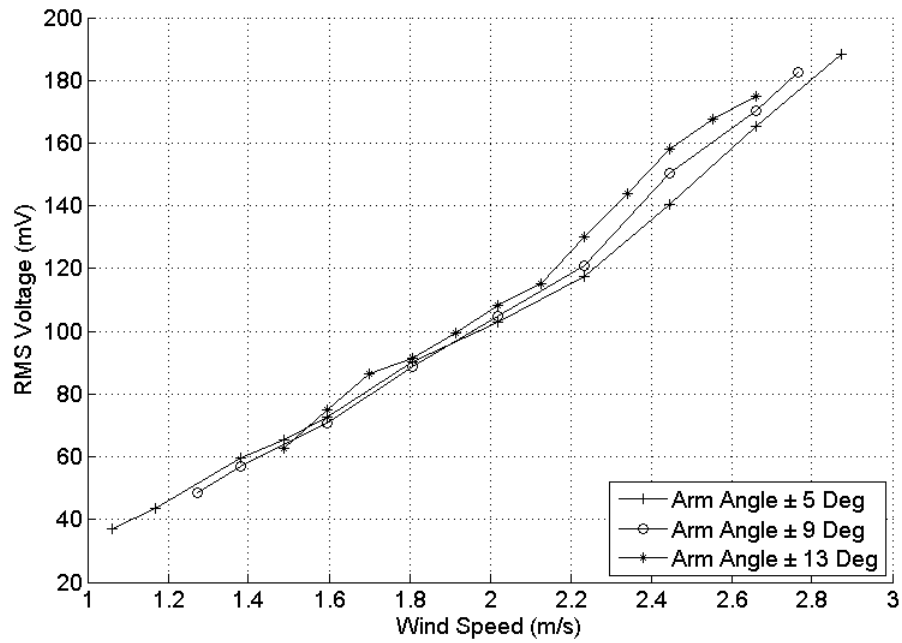


Figure 93: RMS voltage output for different arm AoA when wing AoA is ± 20 degree and leaf spring height is 7 in.

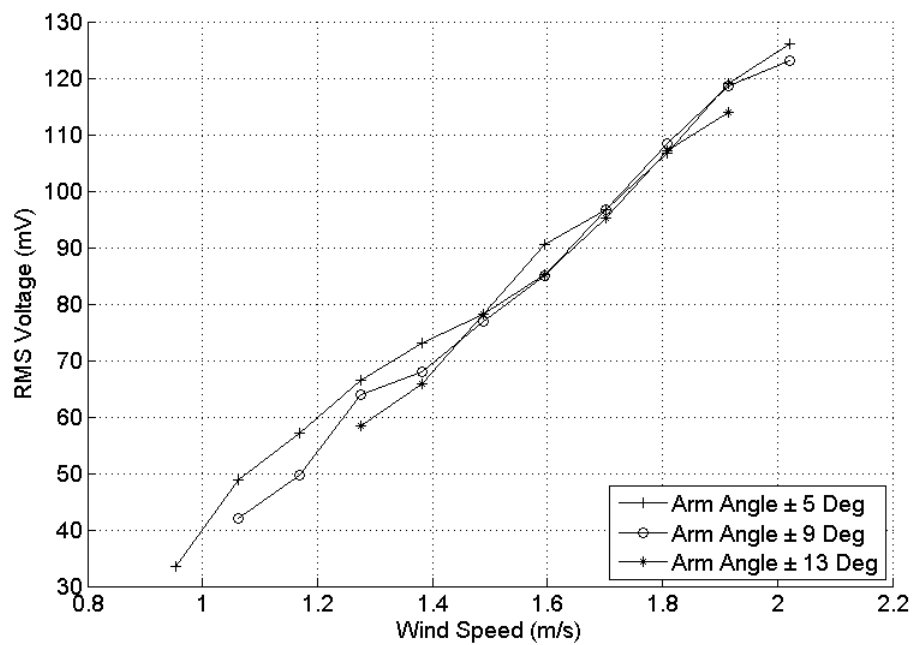


Figure 94: RMS voltage output for different arm AoA when wing AoA is ± 30 degree and leaf spring height is 7 in.

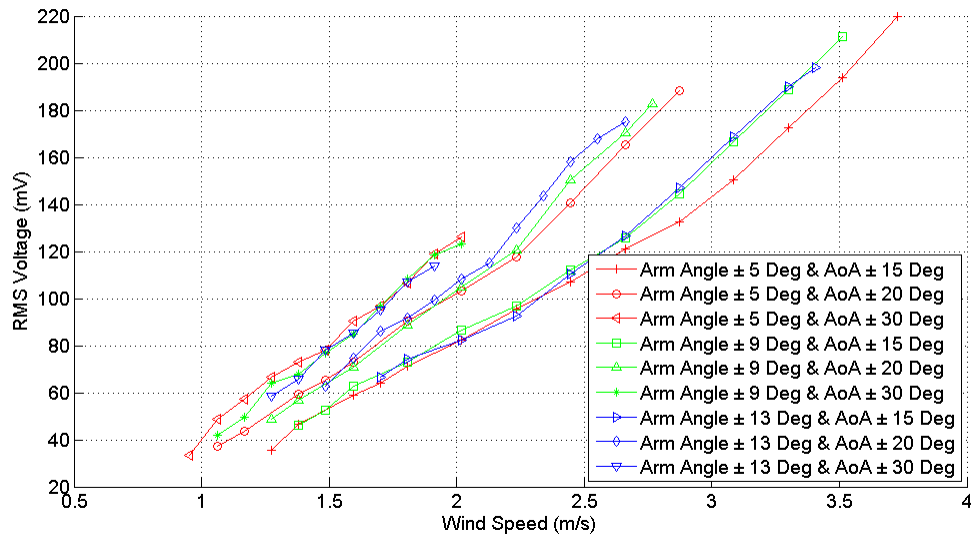


Figure 95: Comparison of all the RMS voltage output graphs when leaf spring height is 7 in.

Figures 89, 90 and 91 show the RMS voltage output for different AoA of the wing when the AoA of the arm is set at ± 5 , ± 9 and ± 13 degrees respectively. All three figures were set to have the leaf spring at 7 inches. The three figures also show that the RMS voltage output of the device increased as the AoA of the wing increases for a specific wind speed. The cut-in speed and the cut-off speed decreased as the AoA of the wing increases in all three figures. The RMS voltage output for different AoA of the arm were plotted in figures 92, 93 and 94 with wing AoA of ± 15 , ± 20 and ± 30 degrees respectively. The increase in arm AoA increased the cut-in speed and decreased the cut-off speed of the device according to the plots for the given conditions. The comparison graph in figure 95 for the leaf spring fixed at a height of 7 inches show that the AoA of the wing had a much bigger influence on the Wind Oscillator compared to the AoA of the arm.

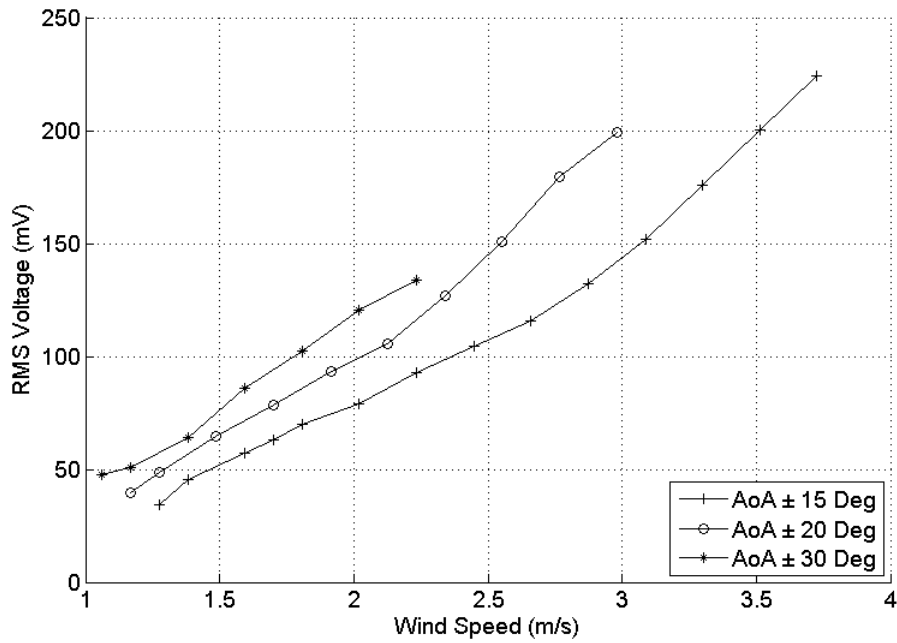


Figure 96: RMS voltage output for different wing AoA when arm AoA is ± 5 degree and leaf spring height is 8 in.

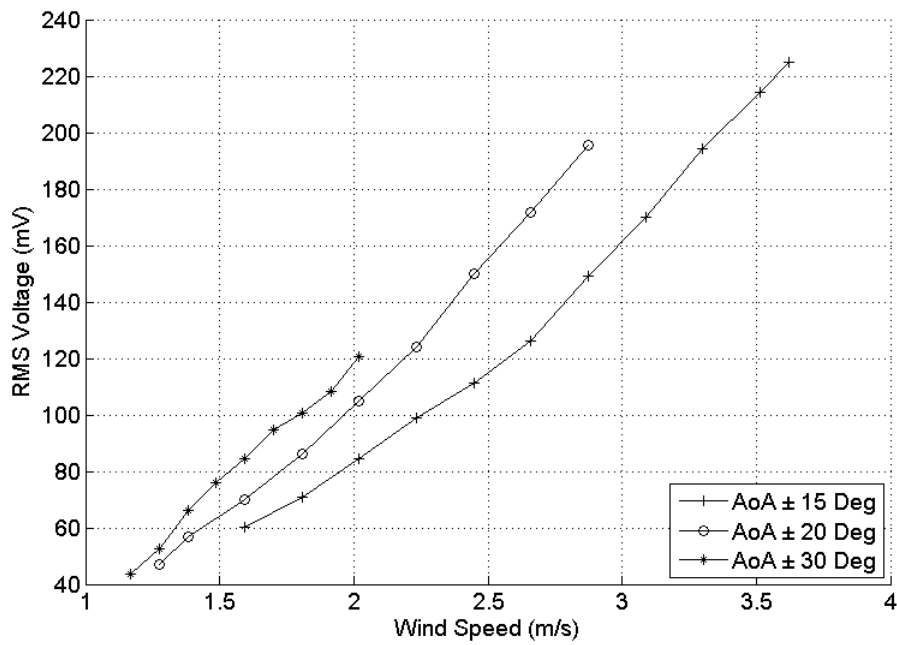


Figure 97: RMS voltage output for different wing AoA when arm AoA is ± 9 degree and leaf spring height is 8 in.

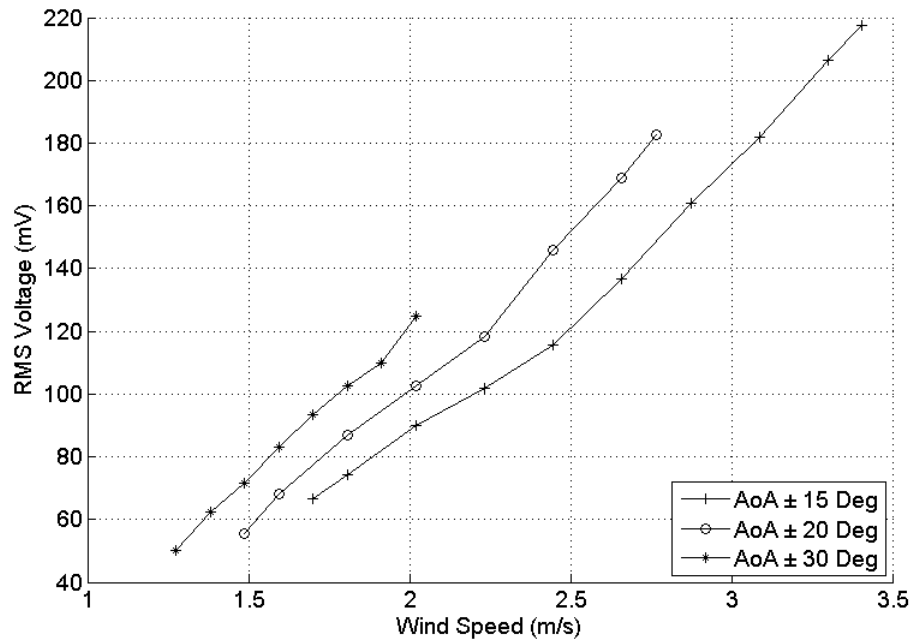


Figure 98: RMS voltage output for different wing AoA when arm AoA is ± 13 degree and leaf spring height is 8 in.

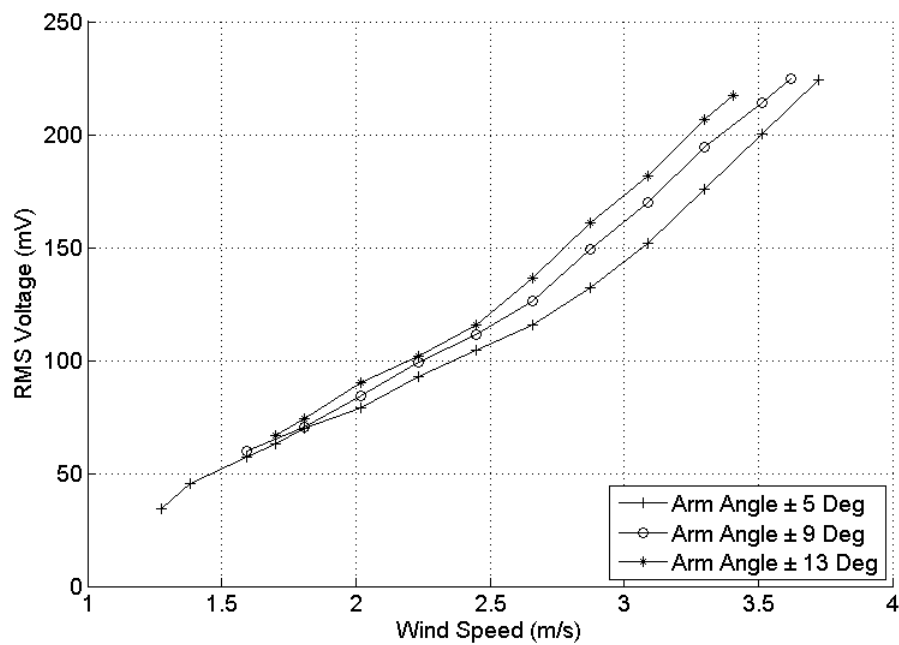


Figure 99: RMS voltage output for different arm AoA when wing AoA is ± 15 degree and leaf spring height is 8 in.

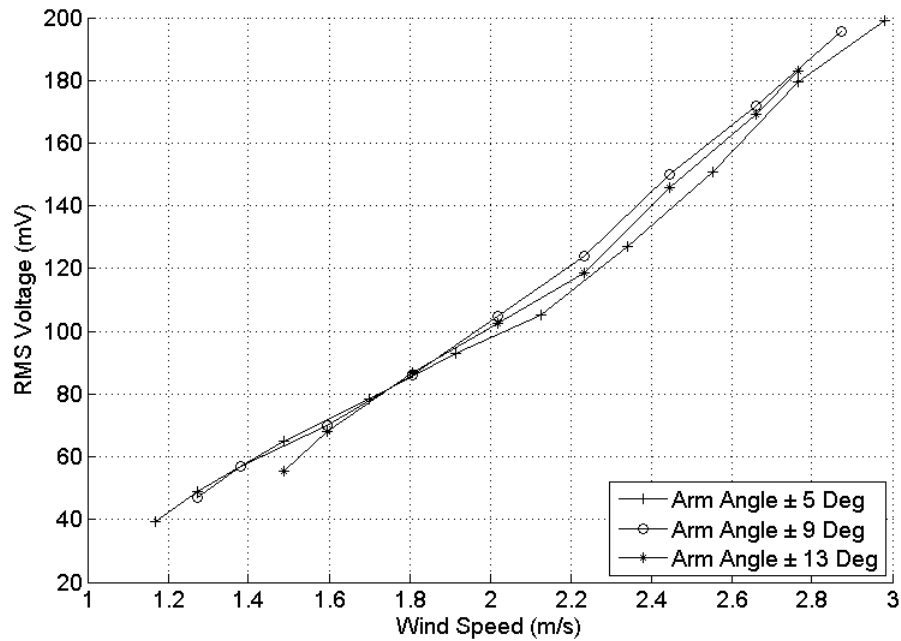


Figure 100: RMS voltage output for different arm AoA when wing AoA is ± 20 degree and leaf spring height is 8 in.

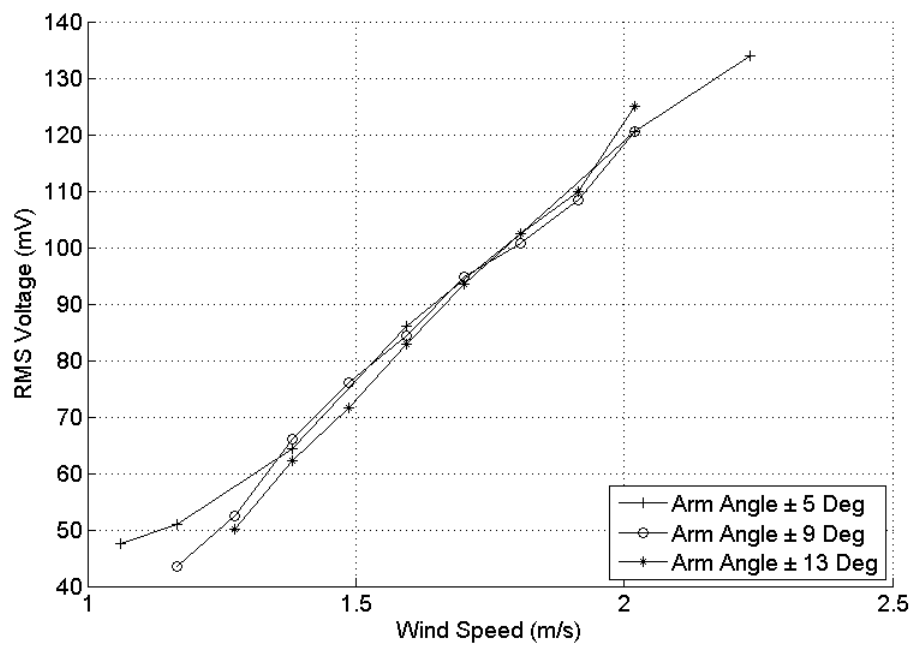


Figure 101: RMS voltage output for different arm AoA when wing AoA is ± 30 degree and leaf spring height is 8 in.

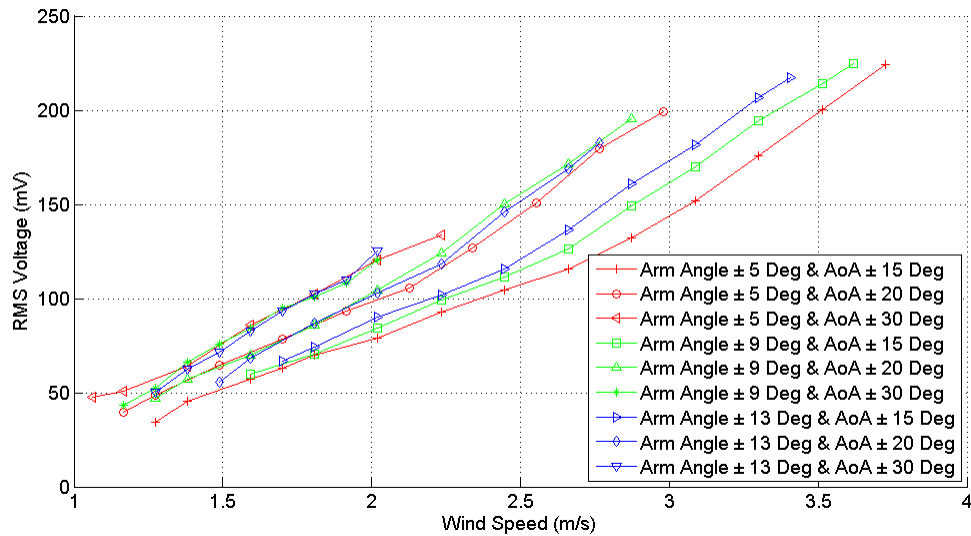


Figure 102: Comparison of all the RMS voltage output graphs when leaf spring height is 8 in.

The effect of the arm AoA and the wing AoA on the RMS voltage output when the spring height was set to 8 inches can be observed in figures 96, 97, 98, 99, 100 and 101. Figure 96, 97 and 98 show the RMS voltage output for three different levels of wing AoA when arm AoA was set to ± 5 , ± 9 , and ± 13 degrees respectively. The three figures show an increase in RMS voltage output when the AoA of the wing was increased. Similarly, the cut-in speed and the cut-off speed of the device inside the wind tunnel seem to increase with a decrease in wing AoA. Figures 99, 100 and 101 show the effect of increasing arm AoA for wing AoA of ± 15 , ± 20 and ± 30 degrees respectively. No major increase can be seen in the RMS voltage value with the increase of arm AoA for a specific wind speed since the graphs were closely plotted. However, the plots in all three figures show an increase in cut-off speed and a decrease in cut-in speed of the device

when the arm AoA was decreased. Figure 102 compares all the graphs plotted in earlier figure when the spring height was fixed to 8 inches. This figure also shows that the AoA of the wing had a more significant effect on the device compared to the arm AoA.

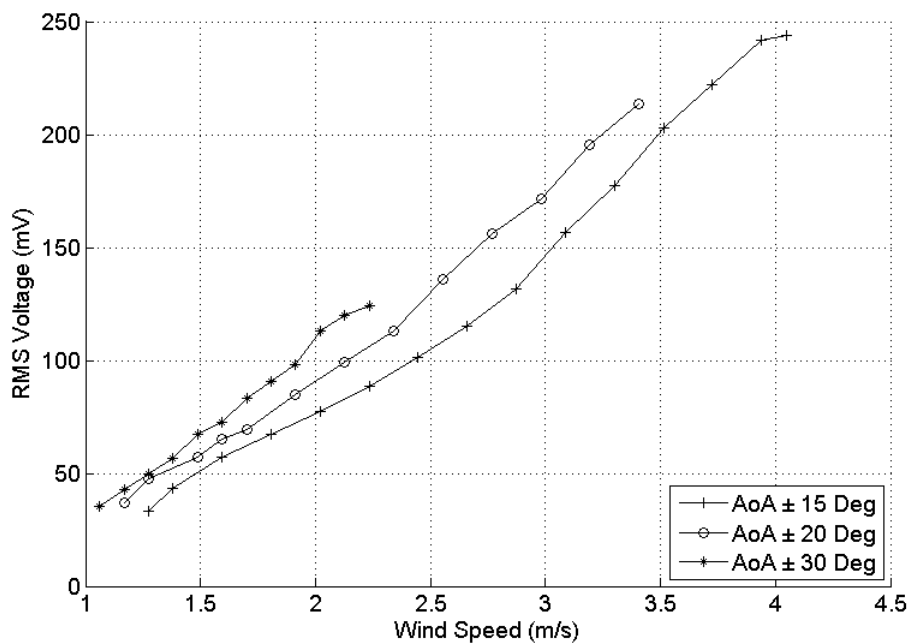


Figure 103: RMS voltage output for different wing AoA when arm AoA is ± 5 degree and leaf spring height is 9 in.

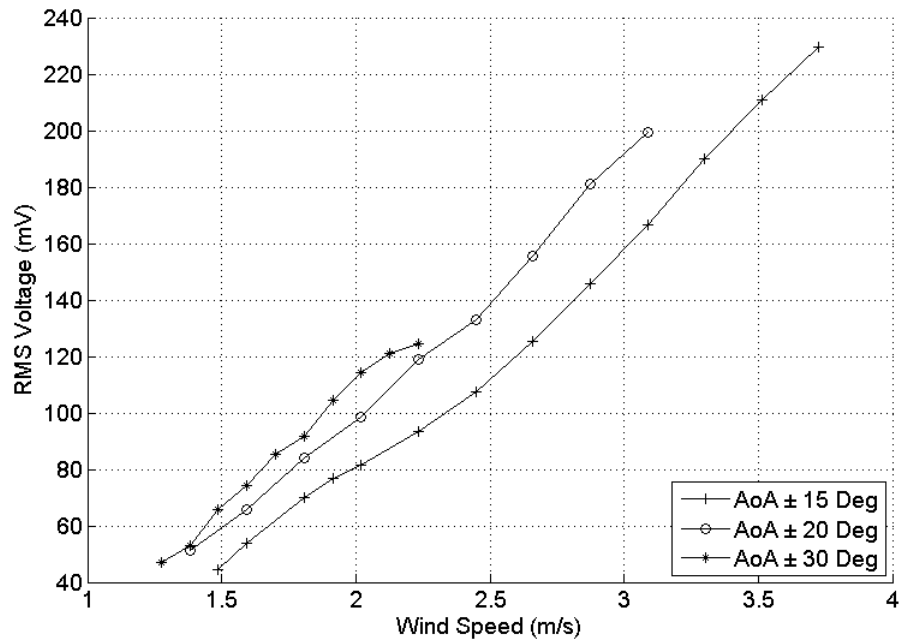


Figure 104: RMS voltage output for different wing AoA when arm AoA is ± 9 degree and leaf spring height is 9 in.

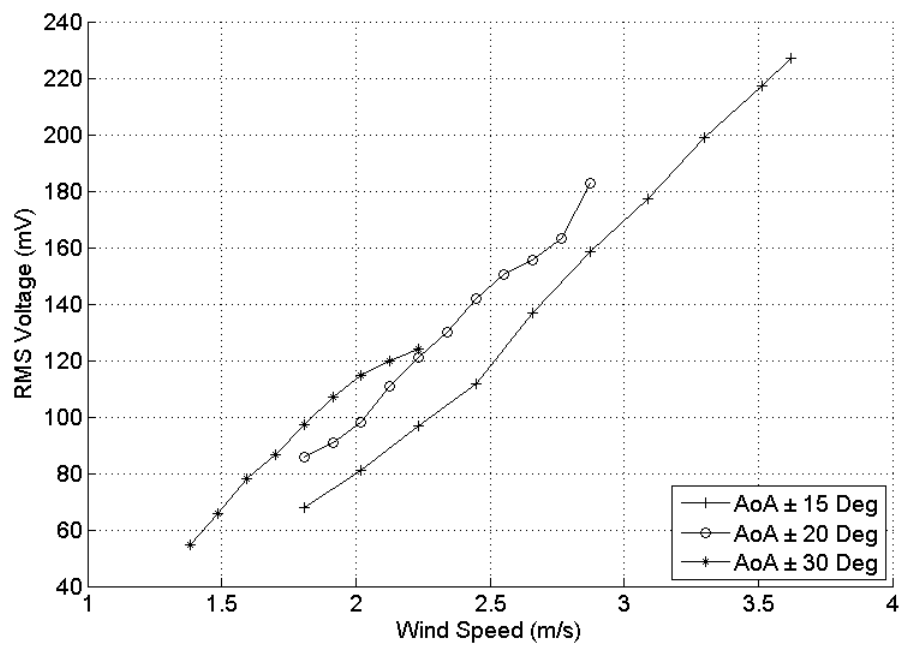


Figure 105: RMS voltage output for different wing AoA when arm AoA is ± 13 degree and leaf spring height is 9 in.

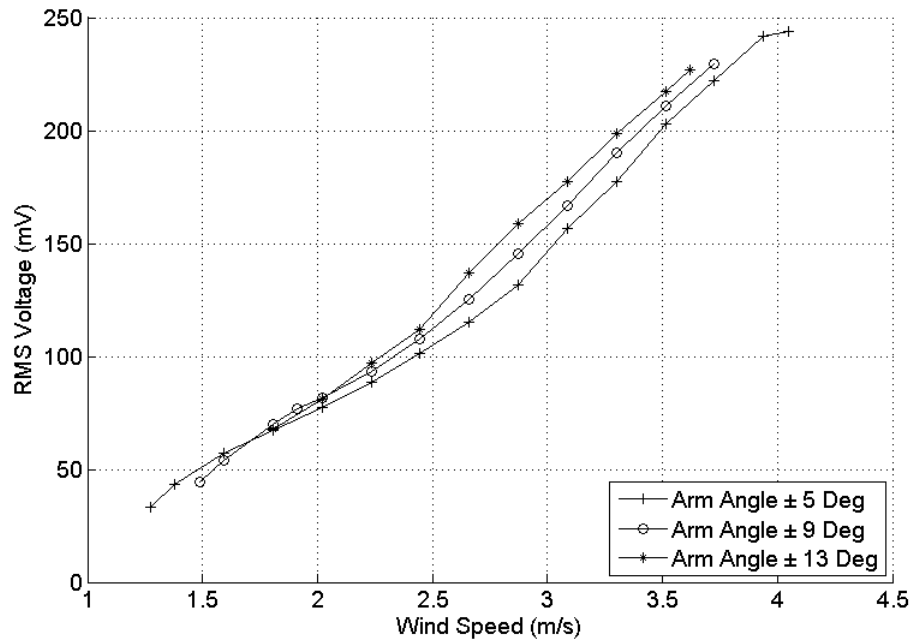


Figure 106: RMS voltage output for different arm AoA when wing AoA is ± 15 degree and leaf spring height is 9 in.

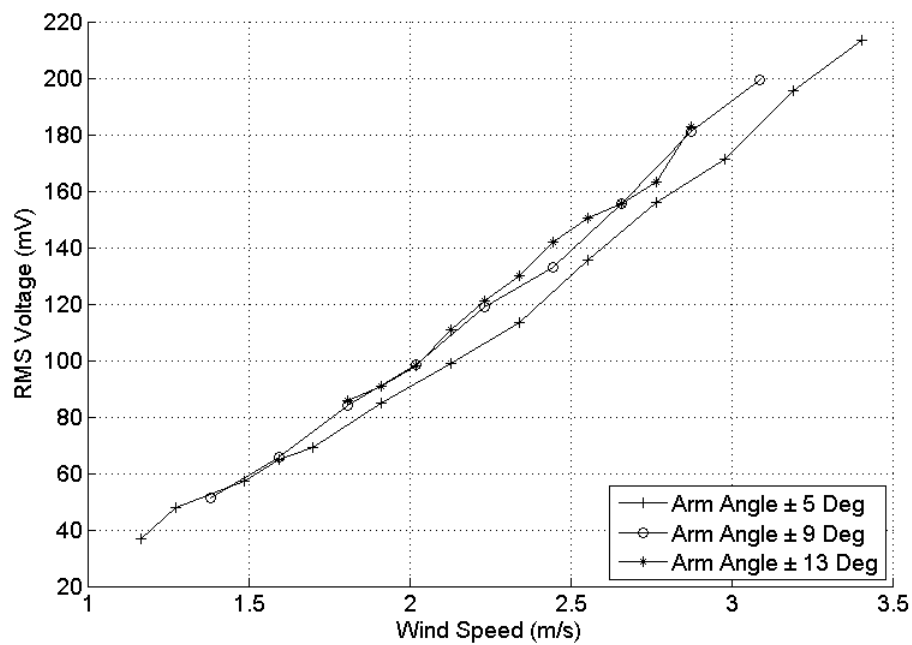


Figure 107: RMS voltage output for different arm AoA when wing AoA is ± 20 degree and leaf spring height is 9 in.

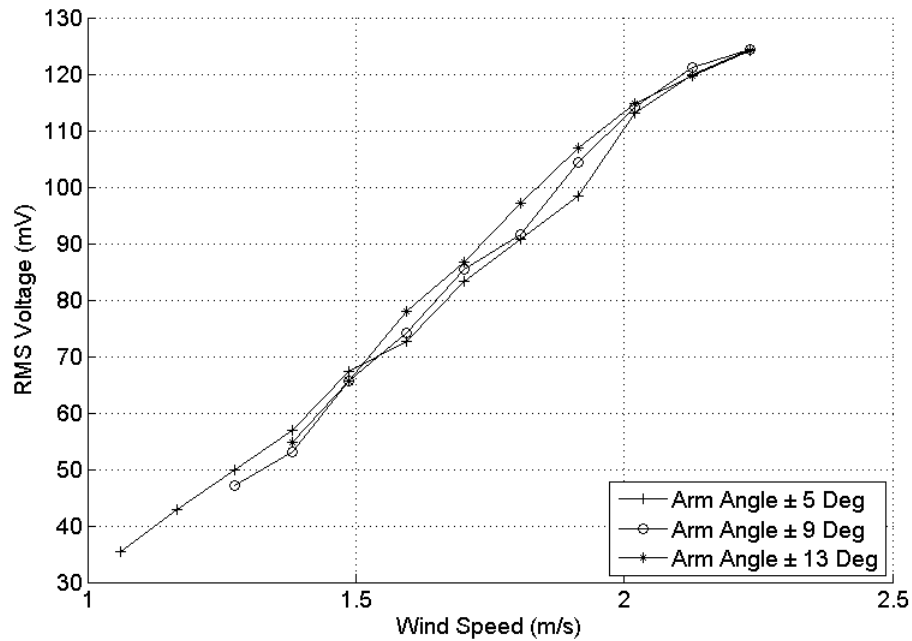


Figure 108: RMS voltage output for different arm AoA when wing AoA is ± 30 degree and leaf spring height is 9 in.

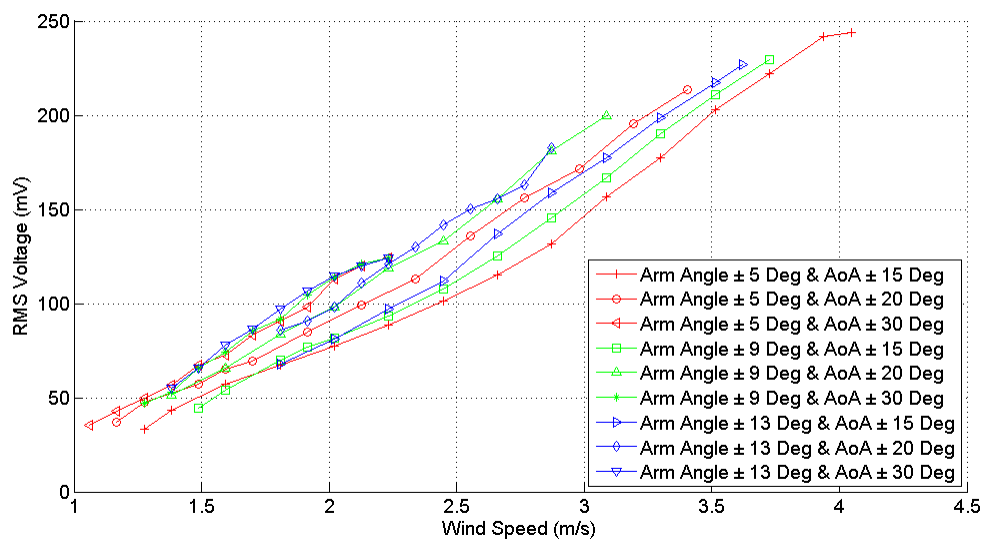


Figure 109: Comparison of all the RMS voltage output graphs when leaf spring height is 9 in.

The RMS voltage plot versus a range of wind speed was given in figures 103,104 and 105 for the three level wing AoA with the spring height fixed at 9 inches from the base and the arm AoA at ± 5 , ± 9 and ± 13 degrees respectively. An increase in cut-in speed and cut-off speed can be observed from the figures with the decrease in AoA of the wing. The RMS voltage output was observed to decrease with the decrease of the wing AoA. The study of arm AoA for wind AoA ± 15 , ± 20 and ± 30 degrees when the spring height was 9 inches can be seen in figures 106, 107, and 108 respectively. The figures show that the range of wind speed that the device can operate under was increased with the decrease of arm AoA. The comparison graph in figure 109 shows that the difference was that the RMS voltage output was lesser compared to earlier comparison graphs where the effect of the wing AoA was much more evident. The calculations in Matlab for all the results above are shown in the appendix C, D, E and F.

The results help to better understand the performance of the device and also to identify the suitable set up for the parameters for a given wind speed.

Photogrammetry

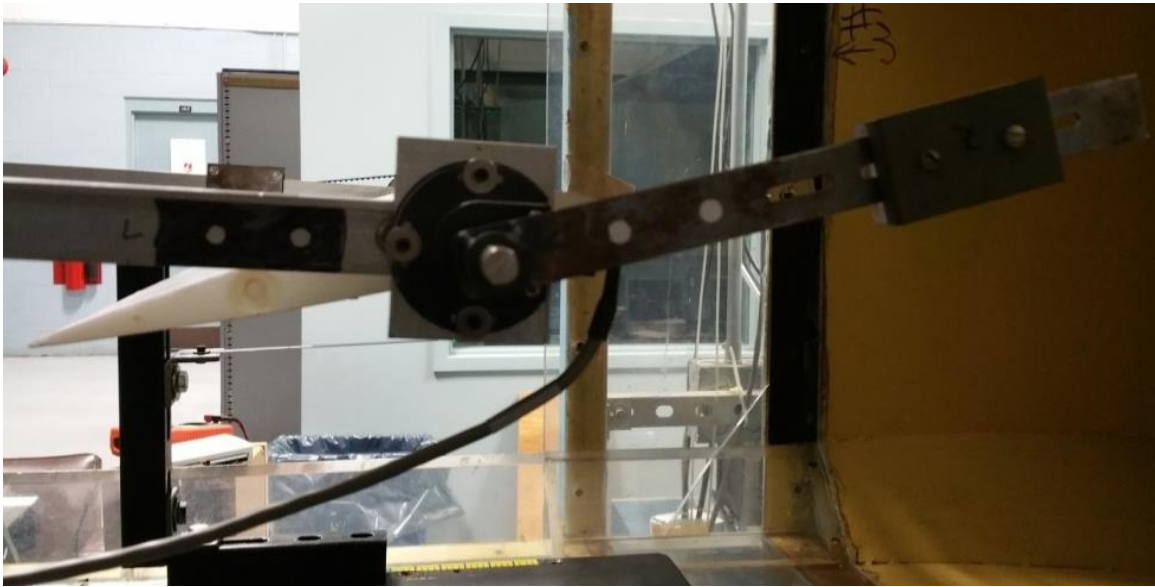
WING AND ARM

Figure 110: Leading wing and arm photogrammetry target point locations.

The AoA of the arm and the wing were set by the user on the front panel of the LabVIEW control program, as mentioned earlier in the software design chapter. Photogrammetry study was conducted on both the wing and the arm to determine if the device was behaving as commanded on the LabVIEW control. Figure 110 shows the section on the arm and the wing where the photogrammetry study was conducted on. Target points with reflective surface were placed on the arm and the counterweight arm as seen on figure 110 which allowed the Matlab code given in Appendix G to track the target points and extract coordinate points. The coordinate points were later fed into another Matlab code, which is shown in Appendix H, to calculate and plot the AoA of the

arm, AoA of the wing with respect to the arm and AoA of the wing with respect to incoming wind direction which is given in the results below as arm, aoa res arm and abs aoa respectively. The AoA of the arm was set as the trip angle whereas the arm passed the set AoA of the arm, it sends a signal back to the LabVIEW control program to switch the AoA of the wing in the opposite direction. Therefore, the actual AoA of the arm was expected to be higher than the set value and it was also expected to increase with an increase of wind speed. Two different AoA of the wing were studied with each in respect to the arm and to the incoming wind direction. The AoA of the wing, which was set by the user in the LabVIEW control program, was the AoA with respect to the arm measured with the help of the optical encoder. The AoA of the wing with respect to the incoming wind direction was calculated to observe the total AoA achieved by the wing. The photogrammetry test was conducted on the arm and the wing for a duration of 8 seconds at several different wind speeds to determine if the wind speed affects the performance of the device. The AoA of the wing and the arm were set at 20 and 5 degrees respectively throughout the photogrammetry experiment and it was also used as the baseline for the experiment. The height of the spring was fixed at 9in.

RESULT AND DISCUSSION

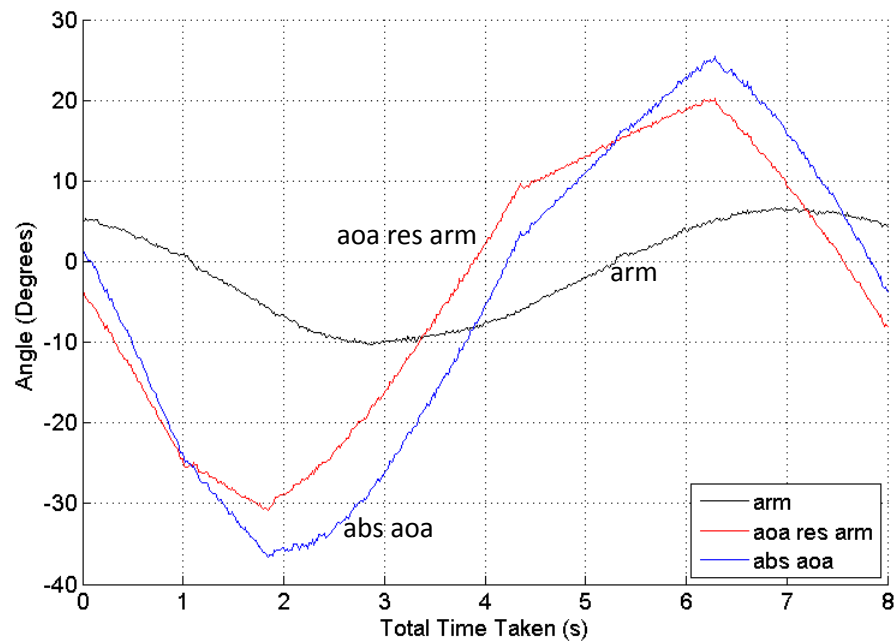


Figure 111: Actual angle of the wing and arm when the incoming wind speed is 1.06m/s (34rpm).

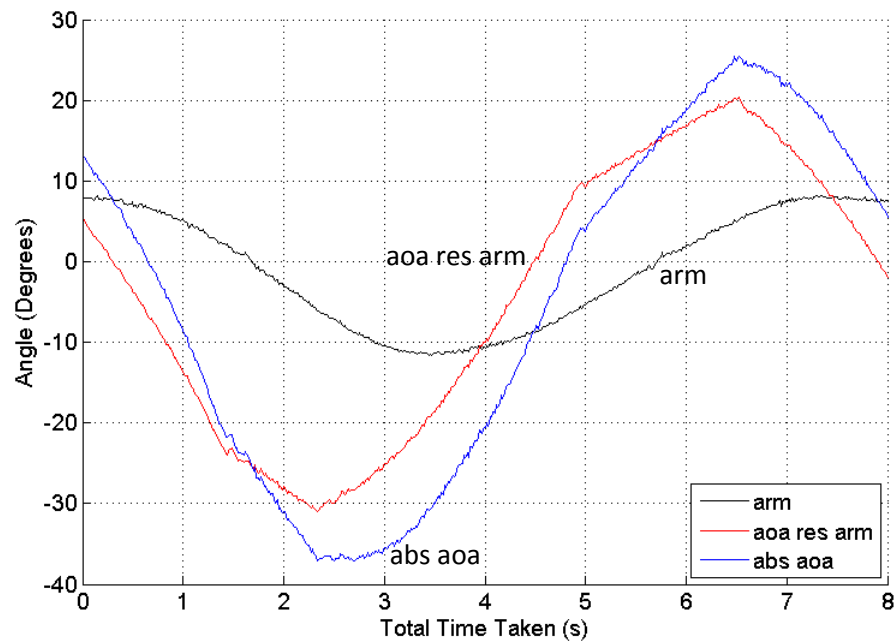


Figure 112: Actual angle of the wing and arm when the incoming wind speed is 1.17m/s (36rpm).

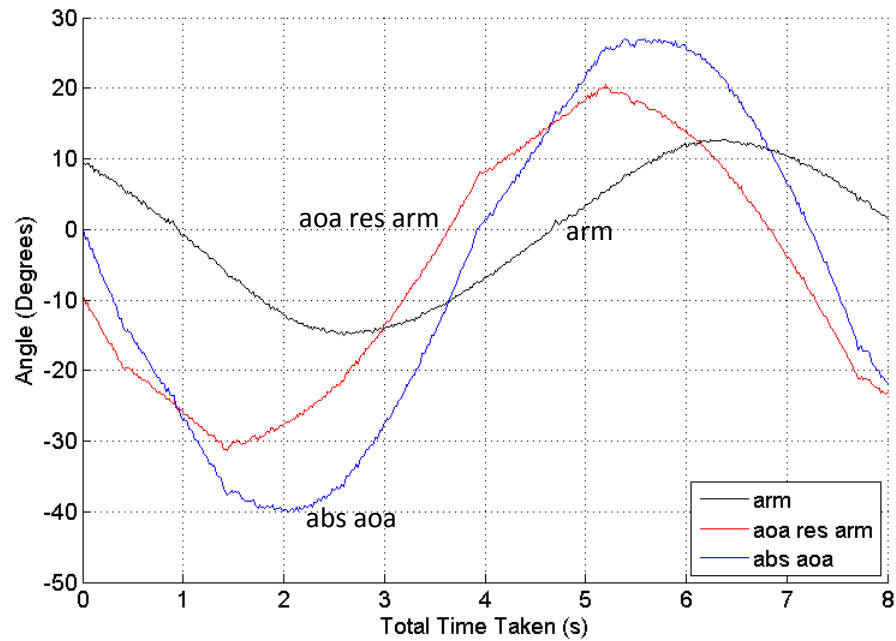


Figure 113: Actual angle of the wing and arm when the incoming wind speed is 1.38m/s (40rpm).

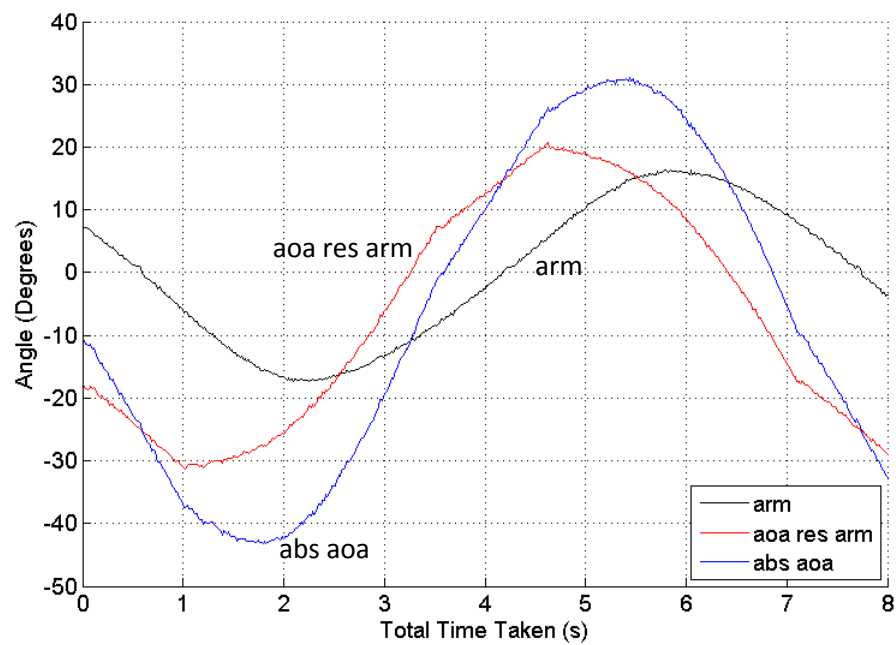


Figure 114: Actual angle of the wing and arm when the incoming wind speed is 1.59m/s (44rpm).

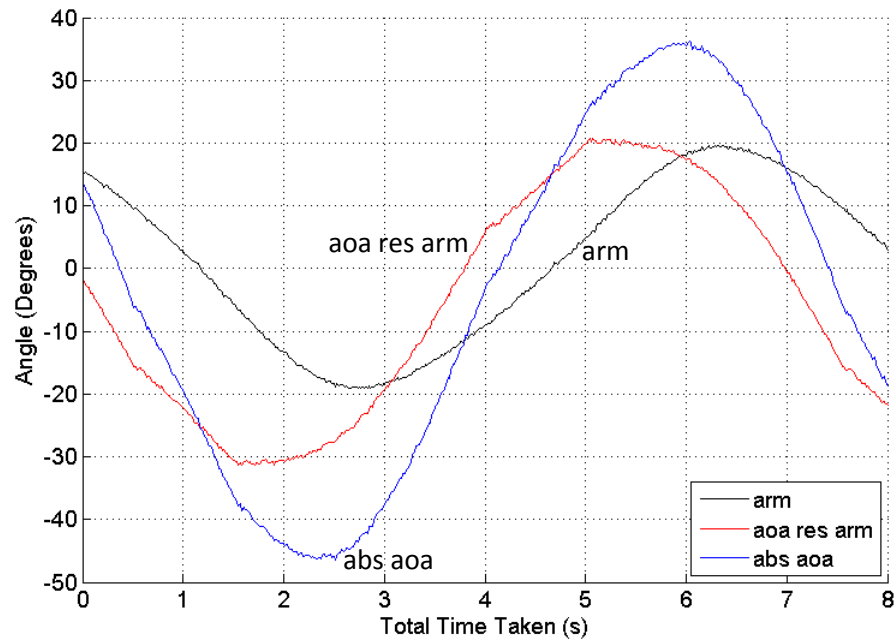


Figure 115: Actual angle of the wing and arm when incoming wind speed is 1.81m/s (48rpm).

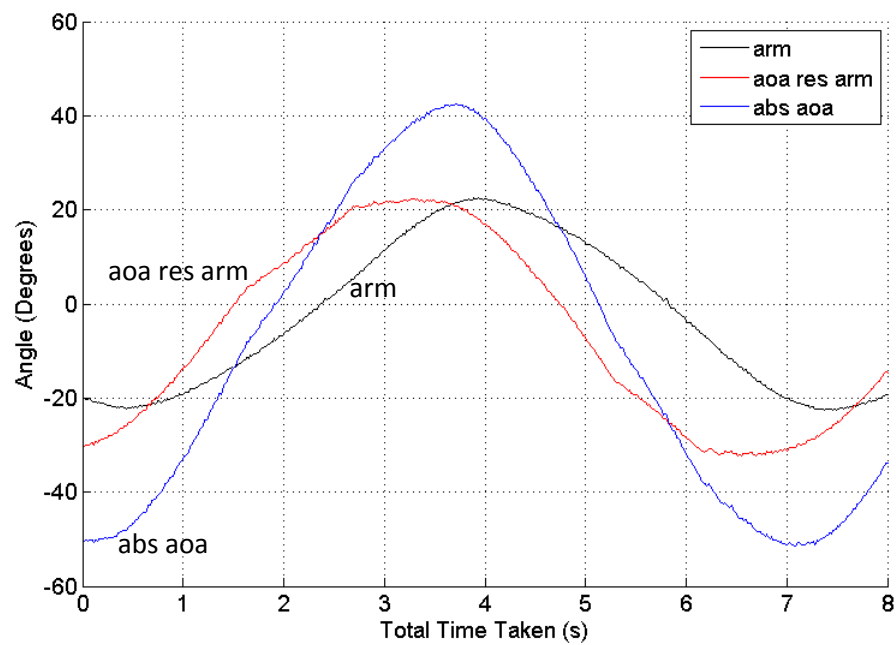


Figure 116: Actual angle of the wing and arm when the incoming wind speed is 2.02m/s (52rpm).

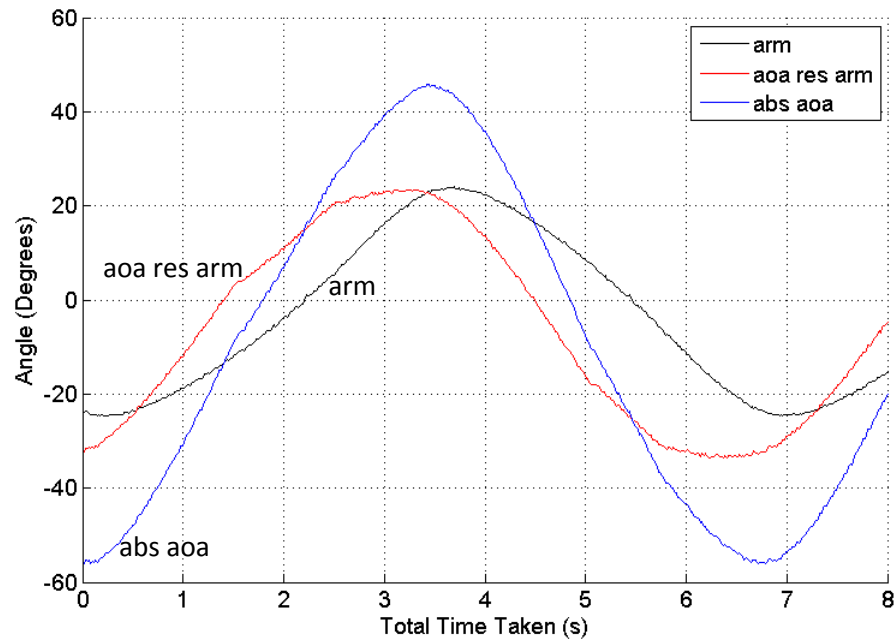


Figure 117: Actual angle of the wing and arm when the incoming wind speed is 2.23m/s (56rpm).

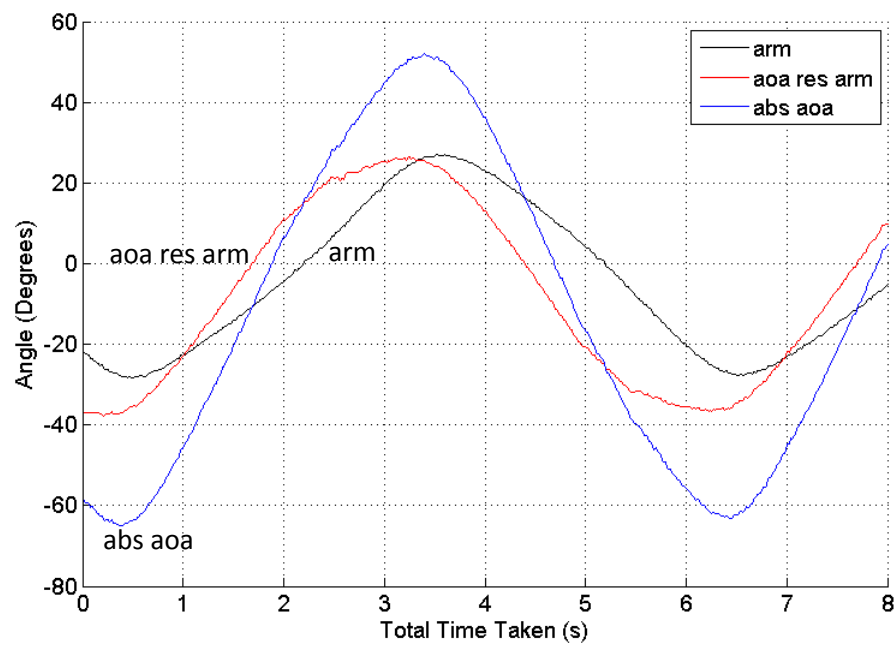


Figure 118: Actual angle of the wing and arm when the incoming wind speed is 2.45m/s (60rpm).

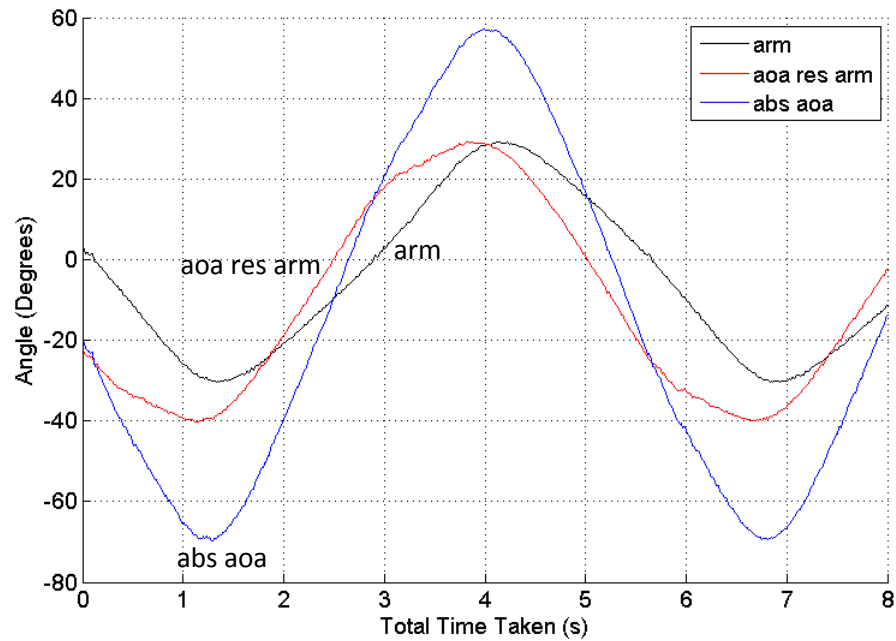


Figure 119: Actual angle of the wing and arm when the incoming wind speed is 2.66m/s (64rpm).

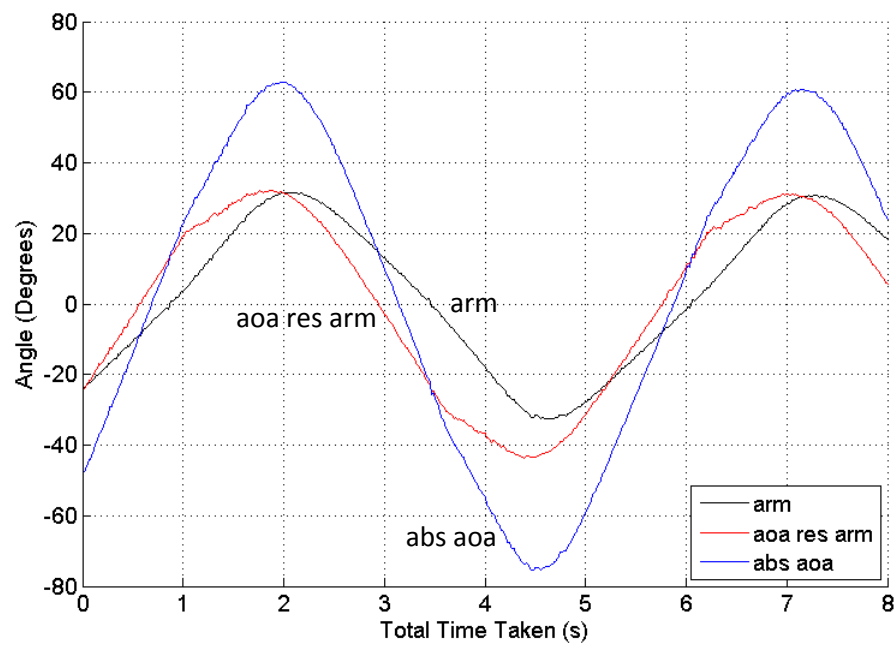


Figure 120: Actual angle of the wing and arm when the incoming wind speed is 2.87m/s (68rpm).

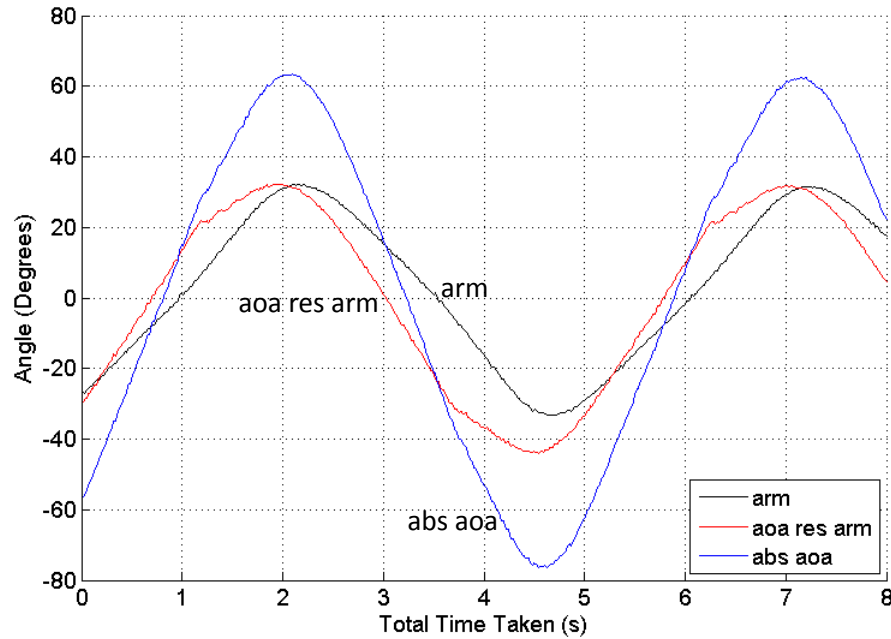


Figure 121: Actual angle of the wing and arm when the incoming wind speed is 2.98m/s (70rpm).

Figures 111 to 121 show the arm, aoa res arm and abs aoa with respect to time for a range of wind speed from 1.06m/s to 2.98m/s in a progressive manner. It can be seen from the figures above that as the wind speed increases, the number of oscillations that the device was able to make also increases for the same time period. The figures also show that the magnitude of the AoA of the arm is distributed evenly on the top and bottom along the zero y-axis value for all the cases, even though they were not the set value by the user which was expected at the beginning of the experiment. The comparison between all the recorded AoA of the arm and the set AoA of the arm in respect to wind speed can be seen in figure 122 below. It also shows that as the wind speed increased, the recorded AoA of the arm also increased even though the set arm

angle remained the same. The increase in aoa res arm and abs aoa, with the increase of wind speed, was much more evident from figures 111 to 121. This was also confirmed by the comparison graph between the set wing AoA and the recorded wing AoA with respect to the arm and the incoming wind direction in figure 123. Figure 111 to 121 also show that the maximum and the minimum values of the aoa res arm and abs aoa were not equal in magnitude. This difference can also be clearly seen in the comparison graph in figure 123. Both AoA of the wing with respect to the arm and the wind direction values in the maximum region were closer to the user-set value than compared to the minimum region. This may be due to a minor imbalance in the setup of the device or the spring. The abs aoa value is much higher than the aoa res arm since it is the cumulative value of arm and aoa res arm at any time period.

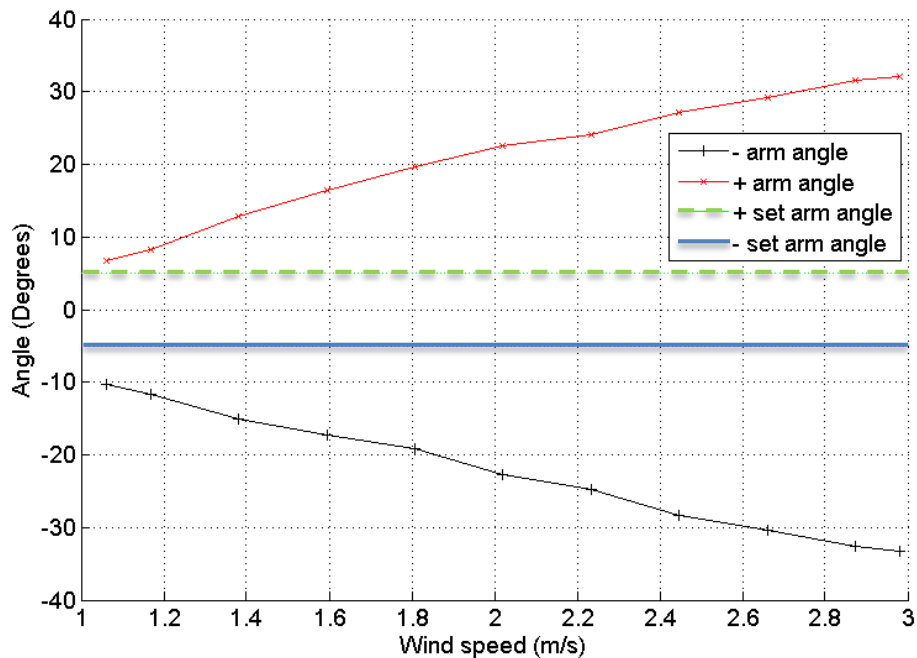


Figure 122: Comparison between set arm angle and actual arm angle

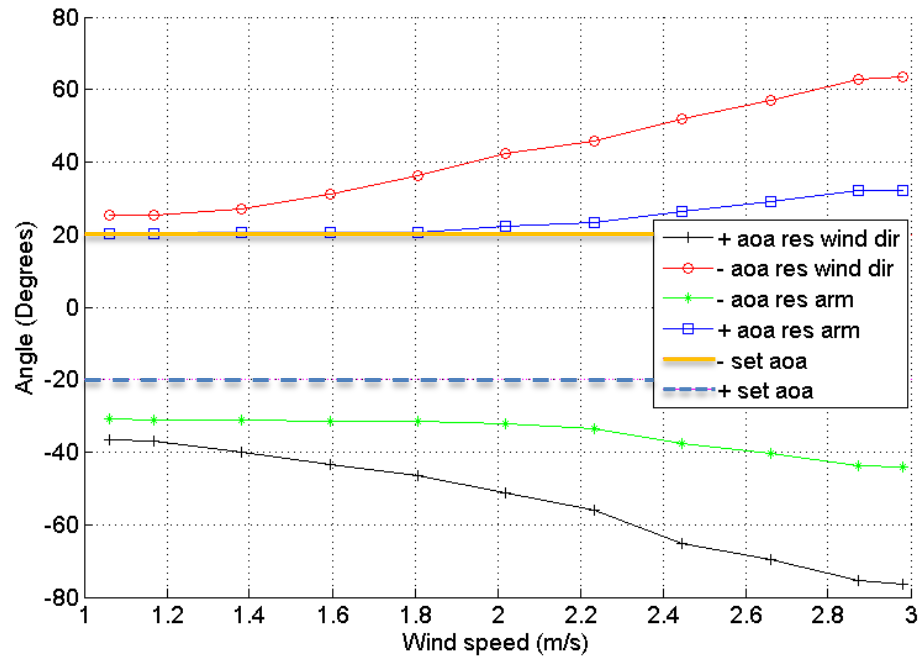


Figure 123: Comparison between set wing AoA and AoA respective to arm and incoming wind direction.

PENDULUM

Figure 124: Pendulum photogrammetry target point setting for calculating mechanical power.

Photogrammetry was conducted on the pendulum system which replaced the DC motor generator to measure the mechanical power output of the device. Similar to the photogrammetry study that was conducted on the wing and the arm, reflective target points were placed on the pendulum system. The reflective target points were placed at

the middle of the weight and around the middle point of the pendulum. Weights of 23.2g and 70.2g were used on the system. The AoA of the arm and the wing for this experiment were set at 5 and 20 degrees respectively, similar to the previous experiment. The Matlab code in appendix I was used to process the images captured and convert the target points into coordinates which was used to calculate the mechanical power output through the Matlab code in appendix J.

RESULT AND DISCUSSION

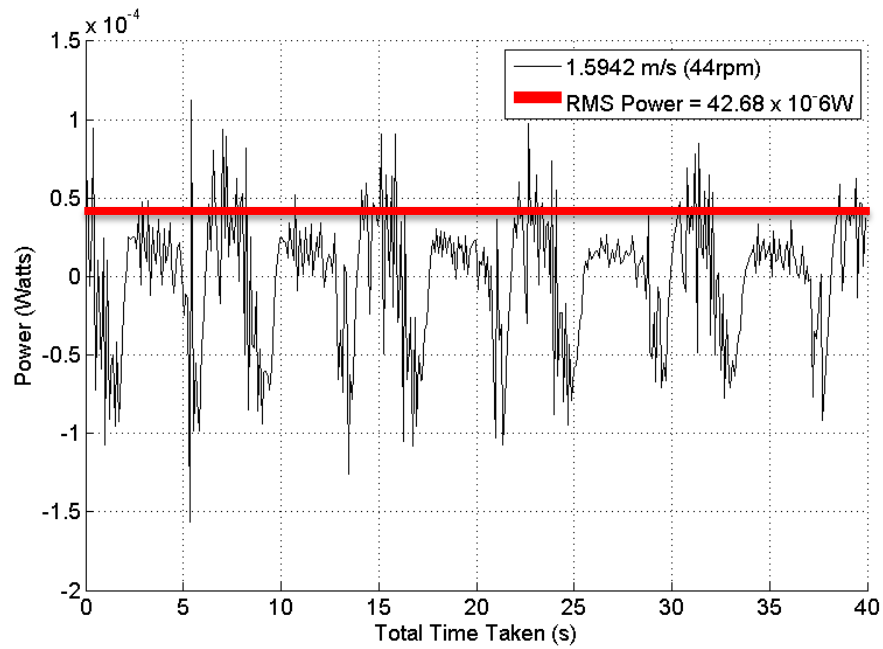


Figure 125: Mechanical power output of the system with a mass of 32.2g on each side on the pendulum for incoming wind speed of 1.6m/s (44rpm)

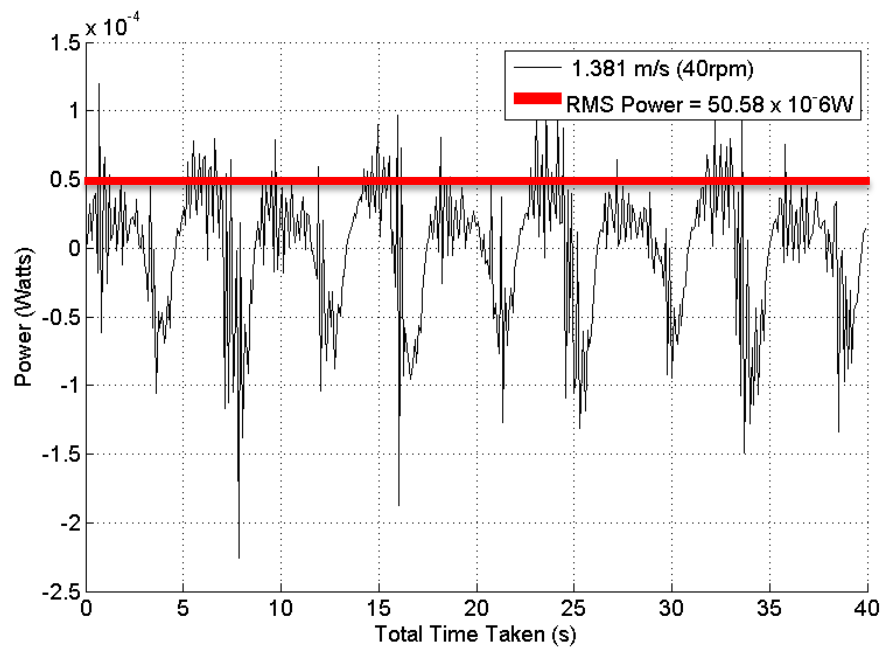


Figure 126: Mechanical power output of the system with a mass of 70.2g on each side on the pendulum for incoming wind speed of 1.6m/s (40rpm)

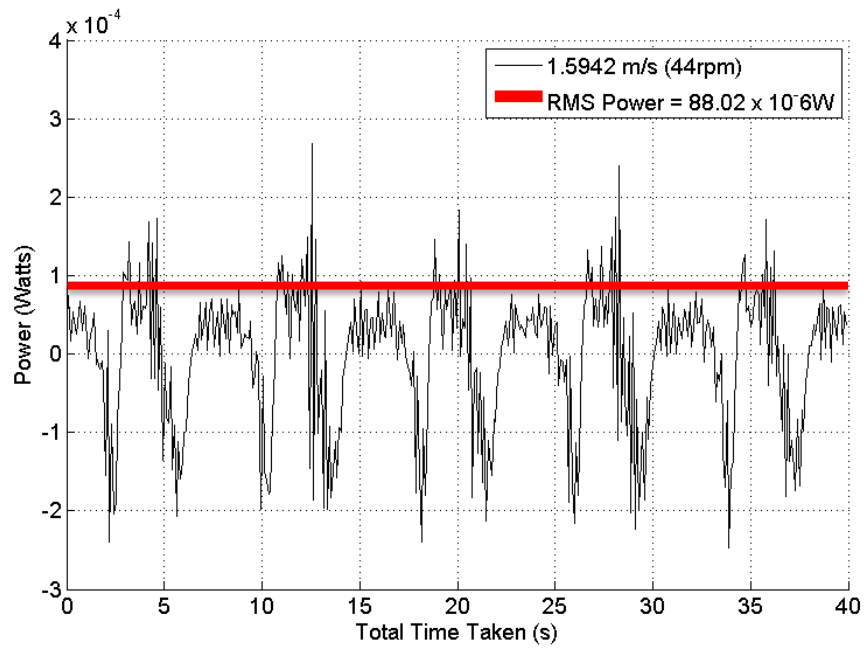


Figure 127: Mechanical power output of the system with a mass of 70.2g on each side on the pendulum for incoming wind speed of 1.6m/s (44rpm)

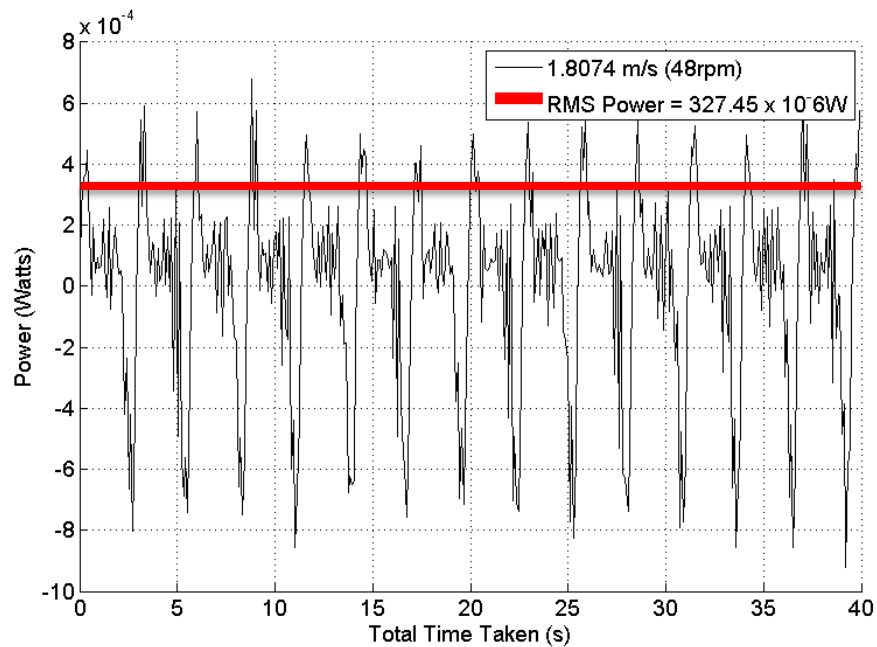


Figure 128: Mechanical power output of the system with a mass of 70.2g on each side on the pendulum for incoming wind speed of 1.6m/s (48rpm)

The mechanical power outputs of the system with respect to time for a range of wind speed and for the two different weights were given in figures 125 to 128. The power output was converted to RMS power output so that the values could be easily compared. Figures 126 to 128 show an increase in RMS power output with an increase in wind speed for the mass of 70.2g. An RMS power output increase was also seen when the weights on the pendulum were increased from 32.2g to 70.2g; all while the wind speed was fixed as can be seen in figures 125 and 127. The comparisons mentioned above can also be seen in figures 129 and 130 which show the mechanical power output trend in respect to wind speed for half of the system and for the whole system respectively.

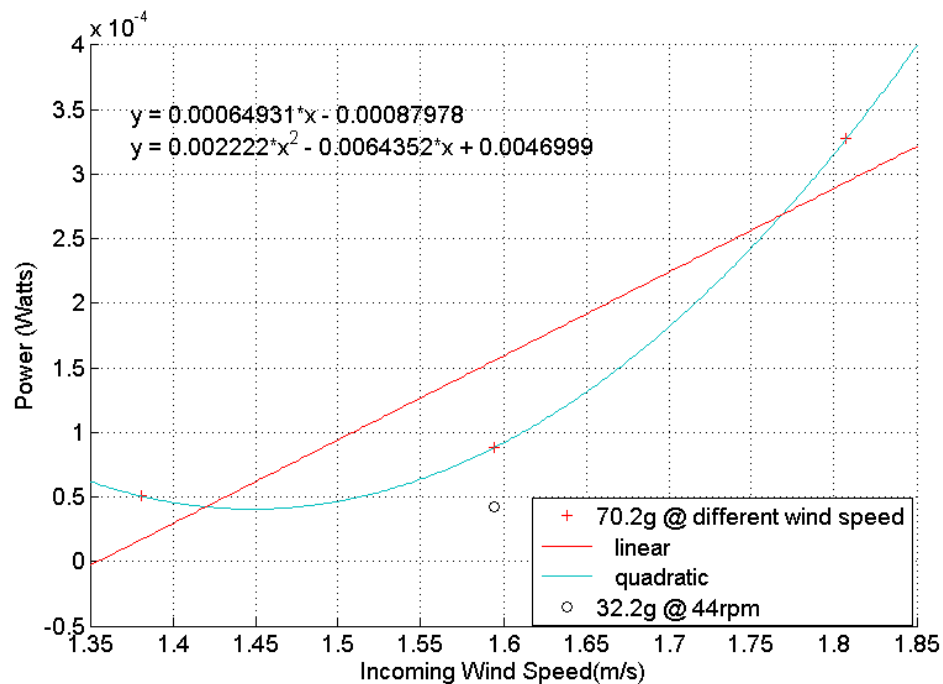


Figure 129: Mechanical power output trend in respective to wind speed for half of the system.

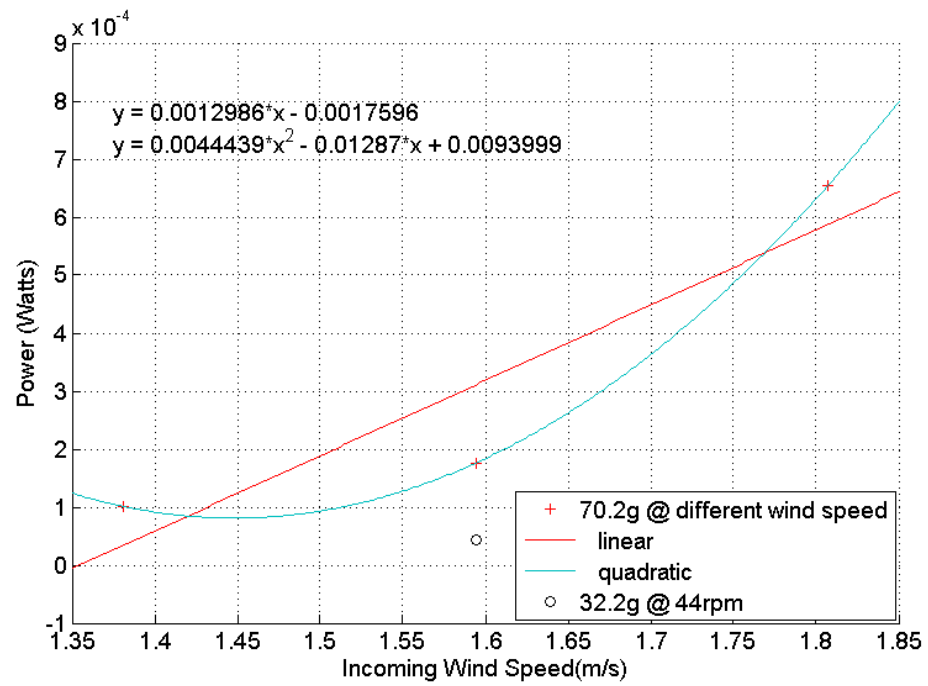


Figure 130: Mechanical power output trend in respective to wind speed for the whole system.

CHAPTER IX

CONCLUSION AND FUTURE WORK

Conclusion

The practicality of the Wind Oscillator was proven with the experiments conducted in the wind tunnel. The RMS voltage data acquisition from the DC motor generator and analysis of the data show that the device can be easily controlled based on the incoming wind speed to maximize the performance of the device. The photogrammetry studies of the arm and the wing gave the user a look into the actual reading of the AoA of the arm and the wing which helped to identify the problems with the device and also helped to improve the overall performance of the device. Photogrammetry study on the pendulum showed the actual power output capable by the device.

Further detailed wind tunnel testing will be required to further study the device. More data needs to be analyzed on how the system will behave at different or higher wind speeds and with sudden changes in wind speed. Further study will also be required to see how the wake created by the front wing will affect the performance of the rear wing. The current device loses its efficiency mainly due to friction. The loss of efficiency caused by friction is unavoidable and is pretty significant because this was the small scale model. The loss caused by friction would be manageable if the model is fully scaled up as the force that will be produced is significantly higher and better materials could be used

to reduce the loss caused by friction. This device is not only capable of operating with a gas medium, but also underwater where the higher density of the water will allow the device to output higher torque. This can then be converted into higher voltage output.

Future Work

There is a lot of room for improvement that can be implemented to the project since it is the first working model of the concept. Further development can be made to both the mechanical aspect of the project and the electrical and software aspect of the project. The mechanical development for the future model will be given in the breakdown below. Future development in the electrical aspect can be done by having an actual generator but this can only be implemented for larger scale model. As the device gets larger, the software controlling the device might also need to go through some changes as the components on the device might change.

Bearing:

Low friction bearing is required to reduce the loss in the system. For this type of system, air bearings are much more suitable but it is very expensive and not practical to be implemented for this small scale model. Air bearings would be a logical choice for the full scale model so as to reduce the loss of efficiency due to friction in the device. Even a regular low friction bearing would be less efficient for a small scale model but would be highly efficient for a large scale or full scale model.

Wing and counter weight:

The construction of a wing which has both its aerodynamic center and center of gravity at its quarter chord position would eliminate the need of counter weights. The wing also needs to be light so that the wings will not put strains and stresses on the arms holding the wing. The wings also need to be light as it takes a longer time to build the momentum to get the wing oscillating if the wing is heavy. Multiple layers of wings like bi or tri-wing can also be considered for the system as it would increase the lift created by the wings.

Piston motion:

The current oscillating motion might be reducing the power output by the generator and might also reduce the lifetime of the generator in the long run. This is another hypothesis that has to be tested. Converting oscillating motion into a circular motion is also not applicable for the current system as the whole system behaves as a single rigid system and the operating speed is very low. Separating the system into 2 systems, oscillating side by side or up and down, will create a piston like movement. This will then be able to run a flywheel so as to maintain the frequency of the system and a generator subsequently.

BIBLIOGRAPHY

- [1] Ramasamy, RS Vewen. Wind Oscillator and Rotor for Power Generation. Tianshu Liu, assignee. Patent US 2011/0064576 A1. 17 Mar. 2011.
- [2] Twidell, J. (2009). Offshore wind power. Brentwood: Multi-Science Pub.
- [3] Morris, C. (2006). Energy switch: Proven solutions for a renewable future. Gabriola Island, B.C.: New Society.
- [4] Nicholson, M. (2009). Energy in a changing climate. Dural Delivery Centre, N.S.W.: Rosenberg.
- [5] Manwell, J., & McGowan, J. (2002). Wind energy explained theory, design and application. Chichester: Wiley.
- [6] Fox, B., Flynn, D., Bryans, L., Jenkins, N., Milborrow, D., O'Malley, M., Watson, R., Anaya-Lara, O. (2007). Wind power integration connection and system operational aspects. London: Institution of Engineering and Technology.
- [7] Rensen, B. (2007). Renewable energy conversion, transmission, and storage. Amsterdam: Elsevier/Academic Press.
- [8] Tiwari, G., & Ghosal, M. (2007). Fundamentals of renewable energy sources. Oxford, U.K.: Alpha Science International.
- [9] Twidell, J., & Weir, A. (2006). Renewable energy resources (2nd ed.). London: Taylor & Francis.
- [10] Elliott, D. (2007). Sustainable energy: Opportunities and limitations. Basingstoke, Hampshire: Palgrave Macmillan.
- [11] Kaltschmitt, M. (2007). Renewable energy technology, economics, and environment. Berlin: Springer.
- [12] E-82 E3 / 3,000 kW. (n.d.). Retrieved January 31, 2015, from <http://www.enercon.de/enen/64.htm>

- [13] MM100. (2014, February 1). Retrieved March 4, 2015, from http://www.senvion.com/fileadmin/user_upload/02_WindPowerSolutions/DataSheets/Senvion_MM100_Datasheet_EN.pdf
- [14] Acciona-Windpower-Brochure-2012 (n.d.). Retrieved March 5, 2015, from <http://www.acciona.us/pdf/Acciona-Windpower-Brochure-2012.aspx>
- [15] ACSA - A27/225 kW WINDTURBINE (n.d.). Retrieved March 5, 2015, from http://www.acsaeolica.com/en/productos_aerogeneradores.htm
- [16] SMALL WIND TURBINES. (n.d.). Retrieved March 5, 2015, from <http://www.acsaeolica.com/en/pdf/miniturbinas.pdf>
- [17] AIR - Specification. (n.d.). Retrieved March 5, 2015, from <http://www.air-windpower.com/specification.html>
- [18] ECO 80 & ECO 86 Wind Turbines. (n.d.). Retrieved March 5, 2015, from <http://www.alstom.com/Global/Power/Resources/Documents/Brochures/eco-80-wind-turbine-platform.pdf>
- [19] ECO 100, ECO 110 & ECO 122 wind turbines (n.d.). Retrieved March 5, 2015, from <http://www.alstom.com/Global/Power/Resources/Documents/Brochures/eco-100-wind-turbine-platform.pdf>
- [20] Haliade™ 150-6MW Offshore wind turbine. (n.d.). Retrieved March 5, 2015, from <http://www.alstom.com/Global/Power/Resources/Documents/Brochures/offshore-wind-turbine-6mw-robust-simple-efficient.pdf>
- [21] AWE 52-750 Wind Turbine. (n.d.). Retrieved March 5, 2015, from <http://www.awewind.com/Products/AWE52750/tabid/60/Default.aspx>
- [22] AWE 52-900 Wind Turbine. (n.d.). Retrieved March 5, 2015, from <http://www.awewind.com/Products/AWE52900/tabid/78/Default.aspx>
- [23] AWE 54-900 Wind Turbine. (n.d.). Retrieved March 5, 2015, from <http://www.awewind.com/Products/AWE54900/tabid/62/Default.aspx>
- [24] wt1650df. (n.d.). Retrieved March 5, 2015, from <http://www.amsc.com/documents/wt1650df-data-sheet/>

- [25] Wt2000df and wt2000fc. (n.d.). Retrieved March 5, 2015, from <http://www.amsc.com/documents/wt2000-data-sheet/>
- [26] Wt3000df and wt3000fc. (n.d.). Retrieved March 5, 2015, from <http://www.amsc.com/documents/wt3000-data-sheet/>
- [27] Wt5500df and wt5500fc. (n.d.). Retrieved March 5, 2015, from <http://www.amsc.com/documents/wt5500-data-sheet/>
- [28] SeaTitan™ 10 MW Wind Turbine. (n.d.). Retrieved March 5, 2015, from <http://www.amsc.com/documents/seatitan-10-mw-wind-turbine-data-sheet/>
- [29] SW 3.5 GT Small Wind Turbine. (n.d.). Retrieved March 5, 2015, from http://www.allsmallwindturbines.com/images/uploads/turbine_data_sheet/data_sheet_314.pdf
- [30] 100kW Wind Turbine. (n.d.). Retrieved March 5, 2015, from [http://www.argolabe.es/pdf/Argolabe\(en\).pdf](http://www.argolabe.es/pdf/Argolabe(en).pdf)
- [31] Aventa. (n.d.). Retrieved March 5, 2015, from <http://aventa.ch/en/technische-daten.html>
- [32] BERGEY EXCEL 6 The wise choice for Performance, Reliability, and Ruggedness. (n.d.). Retrieved March 5, 2015, from http://bergey.com/documents/2013/10/excel-6-spec-sheet_2013.pdf
- [33] BERGEY EXCEL 6 The wise choice for Performance, Reliability, and Ruggedness. (n.d.). Retrieved March 5, 2015, from http://bergey.com/documents/2013/10/excel-10-spec-sheet_2013.pdf
- [34] WIND TURBINE BEE 800. (n.d.). Retrieved March 5, 2015, from <http://www.bornay.com/en/products/small-wind-turbines/wind-turbine-bee-800>
- [35] Súmate a la experiencia Bornay. (n.d.). Retrieved March 5, 2015, from <http://www.bornay.com/media/download/431>
- [36] CF_Green_Energy_50-100_Brochure. (n.d.). Retrieved March 5, 2015, from http://www.cfgreenenergy.com/sites/default/files/CF_Green_Energy_50-100_Brochure.pdf

- [37] CF_Green_Energy_Brochure.pdf. (n.d.). Retrieved March 5, 2015, from http://www.cfgreenenergy.com/sites/default/files/CF_Green_Energy_Brochure.pdf
- [38] TECHNICAL DATA CARTER WIND TURBINE MODEL 300. (n.d.). Retrieved March 5, 2015, from http://www.carterwindenergy.com/site/pdf/cwe_300kw_100ft_specification.2009-05-20.pdf
- [39] TECHNICAL DATA CARTER WIND TURBINE MODEL 500. (n.d.). Retrieved March 5, 2015, from http://www.carterwindenergy.com/site/pdf/cwe_500kw_120ft_specification.2011-04-08.pdf
- [40] DeWind_Brochure_D8_2_eng. (n.d.). Retrieved March 5, 2015, from http://windturbine.com/download/8112/55dewind_brochure_d8_2_eng_x_1328001063_x_.pdf.
- [41] DeWind D9 Series English[1]. (n.d.). Retrieved March 5, 2015, from <http://www.scribd.com/doc/131960841/DeWind-D9-Series-English-1#scribd>
- [42] DOOSAN WIND TURBINE CREATING VALUE FOR THE WORLD WinDS3000TM. (n.d.). Retrieved March 5, 2015, from http://www.doosan.com/doosanheavybiz/attach_files/services/green_energy/en_wind_turbine.pdf
- [43] E-53 / 800 kW | ENERCON. (n.d.). Retrieved March 5, 2015, from <http://www.enercon.de/en-en/59.htm>
- [44] E-44 / 900 kW | ENERCON. (n.d.). Retrieved March 5, 2015, from <http://www.enercon.de/en-en/60.htm>
- [45] E-48 / 800 kW | ENERCON. (n.d.). Retrieved March 5, 2015, from <http://www.enercon.de/en-en/492.htm>
- [46] E-70 / 2,300 kW | ENERCON. (n.d.). Retrieved March 5, 2015, from <http://www.enercon.de/en-en/61.htm>
- [47] E-82 E2 / 2,000 kW | ENERCON. (n.d.). Retrieved March 5, 2015, from <http://www.enercon.de/en-en/62.htm>
- [48] E-82 E2 / 2,300 kW | ENERCON. (n.d.). Retrieved March 5, 2015, from <http://www.enercon.de/en-en/63.htm>

- [49] E-82 E3 / 3,000 kW | ENERCON. (n.d.). Retrieved March 5, 2015, from <http://www.enercon.de/en-en/64.htm>
- [50] E-82 E4 / 3,000 kW | ENERCON. (n.d.). Retrieved March 5, 2015, from <http://www.enercon.de/en-en/2040.htm>
- [51] E-82 E5 / 2,350 kW | ENERCON. (n.d.). Retrieved March 5, 2015, from <http://www.enercon.de/en-en/2429.htm>
- [52] E-92 / 2,350 kW | ENERCON. (n.d.). Retrieved March 5, 2015, from <http://www.enercon.de/en-en/1865.htm>
- [53] E-101 / 3,050 kW | ENERCON. (n.d.). Retrieved March 5, 2015, from <http://www.enercon.de/en-en/65.htm>
- [54] E-101 E2 / 3,500 kW | ENERCON. (n.d.). Retrieved March 5, 2015, from <http://www.enercon.de/en-en/2439.htm>
- [55] E-115 / 3,000 kW | ENERCON. (n.d.). Retrieved March 5, 2015, from <http://www.enercon.de/en-en/2290.htm>
- [56] E-126 / 7,580 kW | ENERCON. (n.d.). Retrieved March 5, 2015, from <http://www.enercon.de/en-en/66.htm>
- [57] G114-2.5 MW Boosting production in medium wind sites. (n.d.). Retrieved March 5, 2015, from <http://www.gamesacorp.com/recursos/doc/productos-servicios/aerogeneradores/brochure-g114-25-mw-eng.pdf>
- [58] Catalogo-g5x-850-kw-eng. (n.d.). Retrieved March 5, 2015, from <http://pdf.archiexpo.com/pdf/gamesa/catalogo-g5x-850-kw-eng/88576-145771.html>
- [59] Gamesa 2.0-2.5 MW. (n.d.). Retrieved March 5, 2015, from <http://www.gamesacorp.com/recursos/doc/productos-servicios/aerogeneradores/catalogo-g9x-20-mw-eng.pdf>
- [60] Gamesa 5.0 MW. (n.d.). Retrieved March 5, 2015, from <http://www.gamesacorp.com/recursos/doc/productos-servicios/aerogeneradores/catalogo-g10x-45mw-eng.pdf>
- [61] Gamesa Offshore Cutting edge technology solutions. (n.d.). Retrieved March 5, 2015, from <http://www.gamesacorp.com/recursos/doc/productos-servicios/aerogeneradores/catalogo-offshore-eng.pdf>

- [62] GE's 1.6-100 and 1.7-100. (n.d.). Retrieved March 5, 2015, from <http://www.niagarawind.com/wp-content/uploads/2012/03/GE-1.7-100-Brochure.pdf>
- [63] GE's 1.85-82.5 Capacity factor leadership in Class II winds. (n.d.). Retrieved March 5, 2015, from https://renewables.gepower.com/content/dam/gepower-renewables/global/en_US/documents/GEA18755D_L_1.85-82.5.pdf
- [64] Introducing GE's 2.85 MW Wind Turbines 2.85-100 2.85-103. (n.d.). Retrieved March 5, 2015, from http://www.ge-renewable-energy.com/uploads/tx_spdownloads/1_2.85_100_103.pdf
- [65] GE's 1.85-87 Capacity factor leadership in Class S winds. (n.d.). Retrieved March 5, 2015, from https://renewables.gepower.com/content/dam/gepower-renewables/global/en_US/documents/GEA30627A_Wind_1.85-87_Brochure_LR.pdf
- [66] Introducing GE's 3.2-103... a powerful turbine. (n.d.). Retrieved March 5, 2015, from http://www.ge-renewable-energy.com/uploads/tx_spdownloads/GE_Wind_3.2-103_Brochure.pdf
- [67] GE's 2.75-120 Smarter and more powerful. (n.d.). Retrieved March 5, 2015, from https://renewables.gepower.com/content/dam/gepower-renewables/global/en_US/documents/GEA31073A_Wind_2.75-120_Brochure_LR.pdf
- [68] GE's 2.3-107. (n.d.). Retrieved March 5, 2015, from http://www.ge-renewable-energy.com/uploads/tx_spdownloads/9_GEA31219_Wind_2.3-107_Brochure_LR.pdf
- [69] HYOSUNG WIND TURBINE. (n.d.). Retrieved March 5, 2015, from <http://pdf.directindustry.com/pdf/hyosung-power-industrial-systems-pg-industrial/hyosung-wind-turbine/52755-348767.html>
- [70] Hyundai Wind Turbine System - Generated from abundant experience. (n.d.). Retrieved March 5, 2015, from <http://pdf.archiexpo.com/pdf/hyundai/hyundai-wind-turbine-system-generated-from-abundant-experience/69960-189561.html>
- [71] L82-2.0 MW - Lagerwey Wind. (n.d.). Retrieved March 5, 2015, from <http://www.lagerweywind.nl/products/windturbines/l82-2-0-mw/>

- [72] L93-1.5 MW - Lagerwey Wind. (n.d.). Retrieved March 5, 2015, from <http://www.lagerweywind.nl/products/windturbines/l93-1-5-mw/>
- [73] L93-2.6 MW - Lagerwey Wind. (n.d.). Retrieved March 5, 2015, from <http://www.lagerweywind.nl/products/windturbines/l93-2-6-mw/>
- [74] L100-1.5 MW - Lagerwey Wind. (n.d.). Retrieved March 5, 2015, from <http://www.lagerweywind.nl/products/windturbines/l100-1-5-mw/>
- [75] L100-2.5 MW - Lagerwey Wind. (n.d.). Retrieved March 5, 2015, from <http://www.lagerweywind.nl/products/windturbines/l100-2-5-mw/>
- [76] LELY AIRCON 10 Wind turbines. (n.d.). Retrieved March 5, 2015, from http://www.lely.com/uploads/original/documents/Brochures/Energy/Lely_Aircon_03_EN.pdf
- [77] Technical data of the M5000 product platform. (n.d.). Retrieved March 5, 2015, from <http://de.aveva.com/EN/aveva-wind-313/m5000-technical-data.html?MEDIADetail=1440>
- [78] MAPNA-Wind-Turbine-Catalogue. (n.d.). Retrieved March 5, 2015, from <http://www.mapnagroup.com/files/2014/04/MAPNA-Wind-Turbine-Catalogue.pdf>
- [79] Mingyang 1.5MW Series Wind Turbine Generator. (n.d.). Retrieved March 5, 2015, from http://www.mywind.com.cn/upfile/File/2012/Mingyang_1.5MW_Series_Wind_Turbine_Generator.pdf
- [80] Mingyang SCD Series Wind Turbine Generator. (n.d.). Retrieved March 5, 2015, from http://www.mywind.com.cn/upfile/File/2012/SCD_Series_Wind_Turbine_Generator.pdf
- [81] Mitsubishi mwt1000a. (n.d.). Retrieved March 5, 2015, from <https://www.mhi-global.com/products/pdf/mwt1000a.pdf>
- [82] Mitsubishi MWT92_24. (n.d.). Retrieved March 5, 2015, from https://www.mhi-global.com/products/pdf/MWT92_24.pdf
- [83] Mitsubishi MWT95_24.pdf Mitsubishi MWT95_24. (n.d.). Retrieved March 5, 2015, from https://www.mhi-global.com/products/pdf/MWT95_24.pdf
- [84] Mitsubishi MWT100_24.pdf Mitsubishi MWT100_24. (n.d.). Retrieved March 5, 2015, from https://www.mhi-global.com/products/pdf/MWT100_24.pdf

- [85] Mitsubishi MWT102_24.pdf Mitsubishi MWT102_24. (n.d.). Retrieved March 5, 2015, from https://www.mhi-global.com/products/pdf/MWT102_24.pdf
- [86] Nordex_Delta_Broschuere_en. (n.d.). Retrieved March 5, 2015, from http://www.nordex-online.com/fileadmin/MEDIA/Produktinfos/EN/Nordex_Delta_Broschuere_en.pdf
- [87] Nordex_Gamma_en.pdf Nordex_Gamma_en. (n.d.). Retrieved March 5, 2015, from http://www.nordex-online.com/fileadmin/MEDIA/Gamma/Nordex_Gamma_en.pdf
- [88] NPS 100-21 Arctic Class S. (n.d.). Retrieved March 5, 2015, from http://www.northernpower.com/wp-content/uploads/2014/09/brochure-NPS100-21-Arctic_EU-online.pdf
- [89] NPS 100-24 Arctic Class S. (n.d.). Retrieved March 5, 2015, from http://www.northernpower.com/wp-content/uploads/2014/09/brochure-NPS100-24-Arctic_EU-online.pdf
- [90] NPS 100-24 Class III/S. (n.d.). Retrieved March 5, 2015, from <http://www.northernpower.com/wp-content/uploads/2014/04/brochure-NPS-100-24-US-online.pdf>
- [91] Performance _ Wind Turbine _ Hitachi. (n.d.). Retrieved March 5, 2015, from <http://www.hitachi.com/products/power/wind-turbine/performance/index.html>
- [92] 1.5MW series wind turbine onshore. (n.d.). Retrieved March 5, 2015, from <http://down.sanygroup.com/files/20101214173039214.pdf>
- [93] 2.0 MW Series Wind Turbine [Onshore) SE8220III, SE8720III, SE9320III-3. (n.d.). Retrieved March 5, 2015, from <http://pdf.directindustry.com/pdf/sany-heavy-industry/20-mw-series-wind-turbine-onshore-se8220iii-se8720iii-y-se9320iii-3-y/52887-565695.html>
- [94] 2.0MW 60Hz: SE8720III E 60HZ. (n.d.). Retrieved March 5, 2015, from <http://down.sanygroup.com/down.jsp?filename=http://resource.sanygroup.com/files/20101214174711792.pdf&flag=1&title=SE8720IIIE60HZ>
- [95] 2.0MW Wind Turbine SE9320III-S3. (n.d.). Retrieved March 5, 2015, from <http://resource.sanygroup.com/files/20101214175524157.pdf>

- [96] 3.0MW Wind Turbine SE11030III-S. (n.d.). Retrieved March 5, 2015, from <http://resource.sanygroup.com/files/20101215104331666.pdf>
- [97] Senvion_3.0M122_Datasheet. (n.d.). Retrieved March 5, 2015, from http://www.senvion.com/fileadmin/user_upload/02_WindPowerSolutions/DataSheets/Senvion_3.0M122_Datasheet_EN.pdf
- [98] Senvion_3.2M114_Datasheet. (n.d.). Retrieved March 5, 2015, from http://www.senvion.com/fileadmin/user_upload/02_WindPowerSolutions/DataSheets/Senvion_3.2M114_Datasheet_EN.pdf
- [99] Senvion_3.4M104_Datasheet. (n.d.). Retrieved March 5, 2015, from http://www.senvion.com/fileadmin/user_upload/02_WindPowerSolutions/DataSheets/Senvion_3.4M104_Datasheet_EN.pdf
- [100] Senvion_6.2M126_Datasheet. (n.d.). Retrieved March 5, 2015, from http://www.senvion.com/fileadmin/user_upload/02_WindPowerSolutions/DataSheets/Senvion_6.2M126_Datasheet_EN.pdf
- [101] Senvion_6.2M152_Datasheet_EN. (n.d.). Retrieved March 5, 2015, from http://www.senvion.com/fileadmin/user_upload/02_WindPowerSolutions/DataSheets/Senvion_6.2M152_Datasheet_EN.pdf
- [102] Senvion_MM82_Datasheet. (n.d.). Retrieved March 5, 2015, from http://www.senvion.com/fileadmin/user_upload/02_WindPowerSolutions/DataSheets/Senvion_MM82_Datasheet_EN.pdf
- [103] Senvion_MM92_Datasheet. (n.d.). Retrieved March 5, 2015, from http://www.senvion.com/fileadmin/user_upload/02_WindPowerSolutions/DataSheets/Senvion_MM92_Datasheet_EN.pdf
- [104] Senvion_MM100_Datasheet. (n.d.). Retrieved March 5, 2015, from http://www.senvion.com/fileadmin/user_upload/02_WindPowerSolutions/DataSheets/Senvion_MM100_Datasheet_EN.pdf
- [105] Senvion_Product_Portfolio. (n.d.). Retrieved March 5, 2015, from http://www.senvion.com/fileadmin/user_upload/02_WindPowerSolutions/ProductBrochures/Senvion_Product_Portfolio_EN.pdf
- [106] Senvion_References_Q1_2014. (n.d.). Retrieved March 5, 2015, from http://www.senvion.com/fileadmin/user_upload/02_WindPowerSolutions/References/Senvion_References_Q4_2014.pdf

- [107] Siemens D3 platform – 3.0-MW and 3.2-MW direct drive wind turbine. Reduced complexity, increased profitability. (n.d.). Retrieved March 5, 2015, from [http://www.energy.siemens.com/us/pool/hq/power-generation/renewables/wind-power/platform brochures/D3 Onshore brochure_ENGLISH_Apr2014_WEB.pdf](http://www.energy.siemens.com/us/pool/hq/power-generation/renewables/wind-power/platform%20brochures/D3%20Onshore%20brochure_ENGLISH_Apr2014_WEB.pdf)
- [108] Siemens D6 platform – 6.0-MW direct drive wind turbin. The new standard for offshore. (n.d.). Retrieved March 5, 2015, from [http://www.energy.siemens.com/ru/pool/hq/power-generation/renewables/wind-power/platform brochures/D6 Offshore brochure_English_Apr2014_WEB.pdf](http://www.energy.siemens.com/ru/pool/hq/power-generation/renewables/wind-power/platform%20brochures/D6%20Offshore%20brochure_English_Apr2014_WEB.pdf)
- [109] Siemens G2 platform – 2.3-MW geared wind turbines. Exceptional performance, proven reliability. (n.d.). Retrieved March 5, 2015, from [http://www.energy.siemens.com/us/pool/hq/power-generation/renewables/wind-power/platform brochures/G2 Onshore Platform brochure_English_Apr2014_WEB.pdf](http://www.energy.siemens.com/us/pool/hq/power-generation/renewables/wind-power/platform%20brochures/G2%20Onshore%20Platform%20brochure_English_Apr2014_WEB.pdf)
- [110] Siemens G4 platform – 3.6-MW and 4.0-MW geared wind turbines The offshore workhorse – redefined. (n.d.). Retrieved March 5, 2015, from [http://www.energy.siemens.com/ru/pool/hq/power-generation/renewables/wind-power/platform brochures/G4 Offshore brochure_English_Apr2014_WEB.pdf](http://www.energy.siemens.com/ru/pool/hq/power-generation/renewables/wind-power/platform%20brochures/G4%20Offshore%20brochure_English_Apr2014_WEB.pdf)
- [111] Suzlon S97-Proven Reliability, Higher Profitability. (n.d.). Retrieved March 5, 2015, from http://www.suzlon.com/pdf/S97-Product_brochure_FV5.pdf
- [112] Suzlon-S52-600 kW Technical Overview. (n.d.). Retrieved March 5, 2015, from <http://www.suzlon.com/pdf/Suzlon-S52-product-brochure.pdf>
- [113] S66 MARK II - 1.25 MW TECHNICAL OVERVIEW. (n.d.). Retrieved March 5, 2015, from <http://www.suzlon.com/pdf/Suzlon-S66-Mark-II-product-brochure.pdf>
- [114] S82 - 1.5 MW TECHNICAL OVERVIEW. (n.d.). Retrieved March 5, 2015, from <http://www.suzlon.com/pdf/Suzlon-S82-product-brochure.pdf>
- [115] S88 - 2.1 MW TECHNICAL OVERVIEW. (n.d.). Retrieved March 5, 2015, from <http://www.suzlon.com/pdf/Suzlon-S88-2.1MW-product-brochure.pdf>
- [116] GEV HP 1 MW Technical description. (n.d.). Retrieved March 5, 2015, from <http://www.vergnet.com/pdf/specs-hp.pdf>

- [117] GEV MP C 200 kW 250 kW 275 kW Technical description. (n.d.). Retrieved March 5, 2015, from <http://www.vergnet.com/pdf/specs-mpc.pdf>
- [118] GEV MP R 200 kW 250 kW 275 kW Technical description. (n.d.). Retrieved March 5, 2015, from <http://www.vergnet.com/pdf/specs-mpr.pdf>
- [119] Vestas 2MW platform. (n.d.). Retrieved March 5, 2015, from <http://nozebra.ipapercms.dk/Vestas/Communication/Productbrochure/2MWbrochure/2MWProductBrochure/>
- [120] Vestas 3MW Platform. (n.d.). Retrieved March 5, 2015, from http://www.eolien-en-correze.fr/doc/3_MW_Product_Brochurepdf.pdf
- [121] Building on 60 GW of experience Track record as of 31 December 2013. (n.d.). Retrieved March 5, 2015, from <http://www.vestas.com/en/media/~media/0461be729dbd4e72a5e2c7d3e1583b0c.ashx>
- [122] PENDULAR WIND TURBINE 60 kW - 335 kW. (n.d.). Retrieved March 5, 2015, from <http://pdf.archiexpo.com/pdf/ades/wind-turbines/125833-194581.html>
- [123] Windflow 500 The next generation in wind turbine design. (n.d.). Retrieved March 5, 2015, from http://www.windflow.co.nz/pdf-folder/misc/Windflow_Brochure_Mar_07.pdf
- [124] WWD-1 Wind Turbine Fact sheet. (n.d.). Retrieved March 5, 2015, from http://www.winwind.com/support_files/pdf/WWD1_Fact_sheet.pdf
- [125] WWD-3 Wind Turbine Fact sheet. (n.d.). Retrieved March 5, 2015, from http://www.winwind.com/support_files/pdf/WWD-3_Fact_sheet1.pdf
- [126] Annual average wind speed at 30m elevation. Retrieved April 21,2014, from <http://www.nrel.gov/gis/wind.html> on 04/21/2014
- [127] Annual average wind speed at 80m elevation. Retrieved April 21,2014, from http://www.nrel.gov/gis/images/80m_wind/USwind300dpe4-11.jpg on
- [128] Cross section of NACA 0012 airfoil. Retrieved April 21,2014, from <http://airfoiltools.com/airfoil/details?airfoil=n0012-il> on 04/21/2014
- [129] Characteristic graphs for NACA 0012 at different Reynolds Numbers. Retrieved April 21,2014, from <http://airfoiltools.com/airfoil/details?airfoil=n0012-il>

- [130] HB6M Hollow Bore Optical Encoder. Retrieved April 21,2014, from http://www.usdigital.com/assets/datasheets/HB6M_datasheet.pdf?k=635336289918424585
- [131] Parameters for the single ended electrical optical encoder. Retrieved April 21, 2014, from http://www.usdigital.com/assets/datasheets/HB6M_datasheet.pdf?k=635336289918424585
- [132] Dimensions of the HB6M Hollow Bore Optical Encoder. Retrieved April 21, 2014, from http://www.usdigital.com/assets/datasheets/HB6M_datasheet.pdf?k=635336289918424585
- [133] E2 Optical Kit Encoder with and without cover. Retrieved April 21,2014, from http://www.usdigital.com/assets/datasheets/E2_datasheet.pdf?k=635336297060882132
- [134] Dimensions of the E2 Optical Kit Encoder. Retrieved April 21,2014,from http://www.usdigital.com/assets/datasheets/E2_datasheet.pdf?k=635336297060882132
- [135] Parameters for E2 Optical Kit Encoder. Retrieved April 21,2014, from http://www.usdigital.com/assets/datasheets/E2_datasheet.pdf?k=635336297060882132on
- [136] Timing characteristics of the encoders. Retrieved April 21,2014, from http://www.usdigital.com/assets/datasheets/E2_datasheet.pdf?k=635336297060882132
- [137] Simplified schematic of the motor controller. Retrieved April 21,2014, from http://www.pololu.com/file/0J450/a4988_DMOS_microstepping_driver_with_translator.pdf
- [138] Schematic Diagram of A4988 Stepper Motor Driver. Retrieved April 21,2014, from http://www.pololu.com/file/0J450/a4988_DMOS_microstepping_driver_with_translator.pdf
- [139] 150W single output switching power supply. Retrieved April 21,2014, from <http://www.meanwell.com/search/S-150/S-150-spec.pdf>
- [140] Specifications of different models for 150W power supply. Retrieved April 21,2014,from <http://www.meanwell.com/search/S-150/S-150-spec.pdf>

- [141] 14 oz-in hybrid stepper motor and schematics of the motor. Retrieved April 21,2014,from <http://www.pololu.com/file/OJ688/SY35ST28-0504A.pdf>
- [142] Pullout torque curve at 24VDC, 0.5A, half step. Retrieved April 21,2014, from <http://www.pololu.com/file/OJ688/SY35ST28-0504A.pdf> on 04/21/2014
- [143] Ambient Weather WM-2 Handheld Wind Meter User Manual. (n.d.). Retrieved May 6, 2015, from <http://site.ambientweatherstore.com/Manuals/wm-2.pdf>
- [144] High Power Gearbox H.E. User Manual. (n.d.). Retrieved May 6, 2015, from <http://www.tamiyausa.com/pdf/manuals/72003ml.pdf>

APPENDICES: Minitab Output

Appendix A

Full factorial design

12/5/2014 3:01:15 PM

Full Factorial Design

Factors: 4 Base Design: 4, 16
 Runs: 16 Replicates: 1
 Blocks: 1 Center pts (total): 0

All terms are free from aliasing.

StdOrder	RunOrder	CenterPt	Blocks	A	B	C	D
14	1	1	1	1	-1	1	1
7	2	1	1	-1	1	1	-1
6	3	1	1	1	-1	1	-1
10	4	1	1	1	-1	-1	1
2	5	1	1	1	-1	-1	-1
3	6	1	1	-1	1	-1	-1
11	7	1	1	-1	1	-1	1
13	8	1	1	-1	-1	1	1
12	9	1	1	1	1	-1	1
16	10	1	1	1	1	1	1
9	11	1	1	-1	-1	-1	1
5	12	1	1	-1	-1	1	-1
15	13	1	1	-1	1	1	1
8	14	1	1	1	1	1	-1
1	15	1	1	-1	-1	-1	-1
4	16	1	1	1	1	-1	-1

Appendix B

DOE for all the factorials

DOE for all the factorials

 12/6/2014 4:06:39 PM

Factorial Regression: Deflection versus A, B, C, D

Analysis of Variance

Source	DF	Adj SS	Adj MS	F-Value	P-Value
Model	15	1646.00	109.733	*	*
Linear	4	1370.50	342.625	*	*
A	1	529.00	529.000	*	*
B	1	289.00	289.000	*	*
C	1	0.25	0.250	*	*
D	1	552.25	552.250	*	*
2-Way Interactions	6	254.00	42.333	*	*
A*B	1	64.00	64.000	*	*
A*C	1	0.25	0.250	*	*
A*D	1	132.25	132.250	*	*
B*C	1	0.25	0.250	*	*
B*D	1	56.25	56.250	*	*
C*D	1	1.00	1.000	*	*
3-Way Interactions	4	17.50	4.375	*	*
A*B*C	1	0.25	0.250	*	*
A*B*D	1	12.25	12.250	*	*
A*C*D	1	4.00	4.000	*	*
B*C*D	1	1.00	1.000	*	*
4-Way Interactions	1	4.00	4.000	*	*
A*B*C*D	1	4.00	4.000	*	*
Error	0	*	*		
Total	15	1646.00			

Model Summary

S	R-sq	R-sq(adj)	R-sq(pred)
*	100.00%	*	*

Coded Coefficients

Term	Effect	Coef	SE	T-Value	P-Value	VIF
Constant		13.00	*	*	*	
A	11.500	5.750	*	*	*	1.00
B	8.500	4.250	*	*	*	1.00
C	-0.2500	-0.1250	*	*	*	1.00
D	-11.750	-5.875	*	*	*	1.00
A*B	4.000	2.000	*	*	*	1.00
A*C	-0.2500	-0.1250	*	*	*	1.00
A*D	-5.750	-2.875	*	*	*	1.00
B*C	0.2500	0.1250	*	*	*	1.00
B*D	-3.750	-1.875	*	*	*	1.00
C*D	-0.5000	-0.2500	*	*	*	1.00
A*B*C	0.2500	0.1250	*	*	*	1.00
A*B*D	-1.7500	-0.8750	*	*	*	1.00
A*C*D	-1.0000	-0.5000	*	*	*	1.00

B*C*D	-0.5000	-0.2500	*	*	*	1.00
A*B*C*D	-1.0000	-0.5000	*	*	*	1.00

Regression Equation in Uncoded Units

$$\begin{aligned} \text{Deflection} = & 13.00 + 5.750 A + 4.250 B - 0.1250 C - 5.875 D + 2.000 A*B - \\ & 0.1250 A*C \\ & - 2.875 A*D + 0.1250 B*C - 1.875 B*D - 0.2500 C*D + 0.1250 A*B*C - \\ & 0.8750 A*B*D \\ & - 0.5000 A*C*D - 0.2500 B*C*D - 0.5000 A*B*C*D \end{aligned}$$

Alias Structure

Factor Name

A	A
B	B
C	C
D	D

Aliases

I
A
B
C
D
AB
AC
AD
BC
BD
CD
ABC
ABD
ACD
BCD
ABCD

Appendix C

DOE for selected factorials

DOE for selected factorials**Factorial Regression: Deflection versus A, B, D**

Analysis of Variance

Source	DF	Adj SS	Adj MS	F-Value	P-Value
Model	6	1622.75	270.458	104.69	0.000
Linear	3	1370.25	456.750	176.81	0.000
A	1	529.00	529.000	204.77	0.000
B	1	289.00	289.000	111.87	0.000
D	1	552.25	552.250	213.77	0.000
2-Way Interactions	3	252.50	84.167	32.58	0.000
A*B	1	64.00	64.000	24.77	0.001
A*D	1	132.25	132.250	51.19	0.000
B*D	1	56.25	56.250	21.77	0.001
Error	9	23.25	2.583		
Total	15	1646.00			

Model Summary

S	R-sq	R-sq(adj)	R-sq(pred)
1.60728	98.59%	97.65%	95.54%

Coded Coefficients

Term	Effect	Coef	SE Coef	T-Value	P-Value	VIF
Constant		13.000	0.402	32.35	0.000	
A	11.500	5.750	0.402	14.31	0.000	1.00
B	8.500	4.250	0.402	10.58	0.000	1.00
D	-11.750	-5.875	0.402	-14.62	0.000	1.00
A*B	4.000	2.000	0.402	4.98	0.001	1.00
A*D	-5.750	-2.875	0.402	-7.15	0.000	1.00
B*D	-3.750	-1.875	0.402	-4.67	0.001	1.00

Regression Equation in Uncoded Units

$$\text{Deflection} = 13.000 + 5.750 A + 4.250 B - 5.875 D + 2.000 A*B - 2.875 A*D - 1.875 B*D$$

Alias Structure

Factor Name

A	A
B	B
C	C
D	D

Aliases

I
A
B
D
AB
AD

APPENDICES: Matlab Code

Appendix A

Benchmark

Benchmark

```
clear;
clc;
load('G:\wind turbine benchmark/benchmark.dat');

A = benchmark;
B = A(:,1)/1000;
figure(1);
hold on;
plot(A(:,2),B,'ok');figure(gcf);
xlabel('Rotor diameter (m)');
ylabel('Power (MW)');
legend('Rated Power of HAWT (12-14 m/s)', 'Location', 'northeast');
grid on

figure(2);
hold on;
plot(A(:,3),B,'ok');figure(gcf);
xlabel('Actuator area (m^2)');
ylabel('Power (MW)');
legend('Rated Power of HAWT (12-14 m/s)', 'Location', 'northeast');
grid on
```

Appendix B

Wind tunnel speed calibration

Wind Tunnel speed calibration

```
clc;
load 'G:\New ossilator reading/tunnel_calib.dat';

figure(1);
hold on;
plot(tunnel_calib(:,1),tunnel_calib(:,3),'xk');figure(gcf);
xlabel('Wind tunnel fan speed(RPM)');
ylabel('Wind Speed (m/s)');
grid on

x=30:1:120
y=0.053324*x-0.75097
figure(2);
hold on;
plot(x,y,'-k');figure(gcf);
xlabel('Wind tunnel fan speed(RPM)');
ylabel('Wind Speed (m/s)');
grid on
```

Appendix C

LabVIEW data acquisition analysis 1 (leaf spring height 7,8 and 9)

LabVIEW data acquisition analysis 1 (leaf spring height7,8 and 9)

```

clc;
load 'G:\New ossilator
reading\arm_AoA_x7_y7_41_7_filtered\Arm5_AoA15_x7_y7_41_7.dat';
load 'G:\New ossilator
reading\arm_AoA_x7_y7_41_7_filtered\Arm5_AoA20_x7_y7_41_7.dat';
load 'G:\New ossilator
reading\arm_AoA_x7_y7_41_7_filtered\Arm5_AoA30_x7_y7_41_7.dat';
load 'G:\New ossilator
reading\arm_AoA_x7_y7_41_7_filtered\Arm9_AoA15_x7_y7_41_7.dat';
load 'G:\New ossilator
reading\arm_AoA_x7_y7_41_7_filtered\Arm9_AoA20_x7_y7_41_7.dat';
load 'G:\New ossilator
reading\arm_AoA_x7_y7_41_7_filtered\Arm9_AoA30_x7_y7_41_7.dat';
load 'G:\New ossilator
reading\arm_AoA_x7_y7_41_7_filtered\Arm13_AoA15_x7_y7_41_7.dat';
load 'G:\New ossilator
reading\arm_AoA_x7_y7_41_7_filtered\Arm13_AoA20_x7_y7_41_7.dat';
load 'G:\New ossilator
reading\arm_AoA_x7_y7_41_7_filtered\Arm13_AoA30_x7_y7_41_7.dat';

load 'G:\New ossilator
reading\arm_AoA_x7_y9_41_7_filtered\Arm5_AoA15_x7_y9_41_7.dat';
load 'G:\New ossilator
reading\arm_AoA_x7_y9_41_7_filtered\Arm5_AoA20_x7_y9_41_7.dat';
load 'G:\New ossilator
reading\arm_AoA_x7_y9_41_7_filtered\Arm5_AoA30_x7_y9_41_7.dat';
load 'G:\New ossilator
reading\arm_AoA_x7_y9_41_7_filtered\Arm9_AoA15_x7_y9_41_7.dat';
load 'G:\New ossilator
reading\arm_AoA_x7_y9_41_7_filtered\Arm9_AoA20_x7_y9_41_7.dat';
load 'G:\New ossilator
reading\arm_AoA_x7_y9_41_7_filtered\Arm9_AoA30_x7_y9_41_7.dat';
load 'G:\New ossilator
reading\arm_AoA_x7_y9_41_7_filtered\Arm13_AoA15_x7_y9_41_7.dat';
load 'G:\New ossilator
reading\arm_AoA_x7_y9_41_7_filtered\Arm13_AoA20_x7_y9_41_7.dat';
load 'G:\New ossilator
reading\arm_AoA_x7_y9_41_7_filtered\Arm13_AoA30_x7_y9_41_7.dat';

load 'G:\New ossilator
reading\arm_AoA_x7_y8_41_7_filtered\Arm5_AoA15_x7_y8_41_7.dat';
load 'G:\New ossilator
reading\arm_AoA_x7_y8_41_7_filtered\Arm5_AoA20_x7_y8_41_7.dat';
load 'G:\New ossilator
reading\arm_AoA_x7_y8_41_7_filtered\Arm5_AoA30_x7_y8_41_7.dat';
load 'G:\New ossilator
reading\arm_AoA_x7_y8_41_7_filtered\Arm9_AoA15_x7_y8_41_7.dat';
load 'G:\New ossilator
reading\arm_AoA_x7_y8_41_7_filtered\Arm9_AoA20_x7_y8_41_7.dat';
load 'G:\New ossilator
reading\arm_AoA_x7_y8_41_7_filtered\Arm9_AoA30_x7_y8_41_7.dat';

```



```

load 'G:\New ossilator
reading\arm_AoA_x7_y8_41_7_filtered\Arm13_AoA15_x7_y8_41_7.dat';
load 'G:\New ossilator
reading\arm_AoA_x7_y8_41_7_filtered\Arm13_AoA20_x7_y8_41_7.dat';
load 'G:\New ossilator
reading\arm_AoA_x7_y8_41_7_filtered\Arm13_AoA30_x7_y8_41_7.dat';

%fanrpm %windspeed(mph) %windspeed(m/s) %freq(mHz)1 %RMS(milivolt)1
%Count1 %freq(mHz)2 %RMS(milivolt)2 %Count2 %freq(mHz)3 %RMS(milivolt)3
%Count3 %avg RMS(milivolt)

%effect of y(height of the spring from the ground) change in RMS when
arm angle is 5 degree & AoA is 15 degree
%avg RMS vs windspeed (m/s):Arm5_AoA15_x7_y_41_7
figure(1);
hold on;
plot(Arm5_AoA15_x7_y7_41_7(:,3),Arm5_AoA15_x7_y7_41_7(:,end),'-
k+');figure(gcf);
plot(Arm5_AoA15_x7_y8_41_7(:,3),Arm5_AoA15_x7_y8_41_7(:,end),'-
ko');figure(gcf);
plot(Arm5_AoA15_x7_y9_41_7(:,3),Arm5_AoA15_x7_y9_41_7(:,end),'-
k*');figure(gcf);

xlabel('Wind Speed (m/s)');
ylabel('RMS Voltage (mV)');
legend('7in','8in','9in','Location','southeast');
grid on

%effect of y(height of the spring from the ground) change in RMS when
arm angle is 5 degree & AoA is 20 degree
%avg RMS vs windspeed (m/s):Arm5_AoA20_x7_y_41_7
figure(2);
hold on;
plot(Arm5_AoA20_x7_y7_41_7(:,3),Arm5_AoA20_x7_y7_41_7(:,end),'-
k+');figure(gcf);
plot(Arm5_AoA20_x7_y8_41_7(:,3),Arm5_AoA20_x7_y8_41_7(:,end),'-
ko');figure(gcf);
plot(Arm5_AoA20_x7_y9_41_7(:,3),Arm5_AoA20_x7_y9_41_7(:,end),'-
k*');figure(gcf);

xlabel('Wind Speed (m/s)');
ylabel('RMS Voltage (mV)');
legend('7in','8in','9in','Location','southeast');
grid on

%effect of y(height of the spring from the ground) change in RMS when
arm angle is 5 degree & AoA is 30 degree
%avg RMS vs windspeed (m/s):Arm5_AoA30_x7_y_41_7
figure(3);
hold on;

```

```

plot(Arm5_AoA30_x7_y7_41_7(:,3),Arm5_AoA30_x7_y7_41_7(:,end),'-
k+');figure(gcf);
plot(Arm5_AoA30_x7_y8_41_7(:,3),Arm5_AoA30_x7_y8_41_7(:,end),'-
ko');figure(gcf);
plot(Arm5_AoA30_x7_y9_41_7(:,3),Arm5_AoA30_x7_y9_41_7(:,end),'-
k*');figure(gcf);

xlabel('Wind Speed (m/s)');
ylabel('RMS Voltage (mV)');
legend('7in','8in','9in','Location','southeast');
grid on

%effect of y(height of the spring from the ground) change in RMS when
arm angle is 9 degree & AoA is 15 degree
%avg RMS vs windspeed (m/s):Arm9_AoA15_x7_y9_41_7
figure(4);
hold on;
plot(Arm9_AoA15_x7_y7_41_7(:,3),Arm9_AoA15_x7_y7_41_7(:,end),'-
k+');figure(gcf);
plot(Arm9_AoA15_x7_y8_41_7(:,3),Arm9_AoA15_x7_y8_41_7(:,end),'-
ko');figure(gcf);
plot(Arm9_AoA15_x7_y9_41_7(:,3),Arm9_AoA15_x7_y9_41_7(:,end),'-
k*');figure(gcf);

xlabel('Wind Speed (m/s)');
ylabel('RMS Voltage (mV)');
legend('7in','8in','9in','Location','southeast');
grid on

%effect of y(height of the spring from the ground) change in RMS when
arm angle is 9 degree & AoA is 20 degree
%avg RMS vs windspeed (m/s):Arm5_AoA20_x7_y9_41_7
figure(5);
hold on;
plot(Arm9_AoA20_x7_y7_41_7(:,3),Arm9_AoA20_x7_y7_41_7(:,end),'-
k+');figure(gcf);
plot(Arm9_AoA20_x7_y8_41_7(:,3),Arm9_AoA20_x7_y8_41_7(:,end),'-
ko');figure(gcf);
plot(Arm9_AoA20_x7_y9_41_7(:,3),Arm9_AoA20_x7_y9_41_7(:,end),'-
k*');figure(gcf);

xlabel('Wind Speed (m/s)');
ylabel('RMS Voltage (mV)');
legend('7in','8in','9in','Location','southeast');
grid on

%effect of y(height of the spring from the ground) change in RMS when
arm angle is 9 degree & AoA is 30 degree
%avg RMS vs windspeed (m/s):Arm5_AoA30_x7_y9_41_7
figure(6);
hold on;
plot(Arm9_AoA30_x7_y7_41_7(:,3),Arm9_AoA30_x7_y7_41_7(:,end),'-
k+');figure(gcf);

```

```

plot(Arm9_AoA30_x7_y8_41_7(:,3),Arm9_AoA30_x7_y8_41_7(:,end),'-
ko');figure(gcf);
plot(Arm9_AoA30_x7_y9_41_7(:,3),Arm9_AoA30_x7_y9_41_7(:,end),'-
k*');figure(gcf);

xlabel('Wind Speed (m/s)');
ylabel('RMS Voltage (mV)');
legend('7in','8in','9in','Location','southeast');
grid on

%effect of y(height of the spring from the ground) change in RMS when
arm angle is 13 degree & AoA is 15 degree
%avg RMS vs windspeed (m/s):Arm9_AoA15_x7_y9_41_7
figure(7);
hold on;
plot(Arm13_AoA15_x7_y7_41_7(:,3),Arm13_AoA15_x7_y7_41_7(:,end),'-
k+');figure(gcf);
plot(Arm13_AoA15_x7_y8_41_7(:,3),Arm13_AoA15_x7_y8_41_7(:,end),'-
ko');figure(gcf);
plot(Arm13_AoA15_x7_y9_41_7(:,3),Arm13_AoA15_x7_y9_41_7(:,end),'-
k*');figure(gcf);

xlabel('Wind Speed (m/s)');
ylabel('RMS Voltage (mV)');
legend('7in','8in','9in','Location','southeast');
grid on

%effect of y(height of the spring from the ground) change in RMS when
arm angle is 13 degree & AoA is 20 degree
%avg RMS vs windspeed (m/s):Arm5_AoA20_x7_y9_41_7
figure(8);
hold on;
plot(Arm13_AoA20_x7_y7_41_7(:,3),Arm13_AoA20_x7_y7_41_7(:,end),'-
k+');figure(gcf);
plot(Arm13_AoA20_x7_y8_41_7(:,3),Arm13_AoA20_x7_y8_41_7(:,end),'-
ko');figure(gcf);
plot(Arm13_AoA20_x7_y9_41_7(:,3),Arm13_AoA20_x7_y9_41_7(:,end),'-
k*');figure(gcf);

xlabel('Wind Speed (m/s)');
ylabel('RMS Voltage (mV)');
legend('7in','8in','9in','Location','southeast');
grid on

%effect of y(height of the spring from the ground) change in RMS when
arm angle is 13 degree & AoA is 30 degree
%avg RMS vs windspeed (m/s):Arm5_AoA30_x7_y9_41_7
figure(9);
hold on;
plot(Arm13_AoA30_x7_y7_41_7(:,3),Arm13_AoA30_x7_y7_41_7(:,end),'-
k+');figure(gcf);
plot(Arm13_AoA30_x7_y8_41_7(:,3),Arm13_AoA30_x7_y8_41_7(:,end),'-
ko');figure(gcf);

```

```

plot(Arm13_AoA30_x7_y9_41_7(:,3),Arm13_AoA30_x7_y9_41_7(:,end),'-
k*');figure(gcf);

xlabel('Wind Speed (m/s)');
ylabel('RMS Voltage (mV)');
legend('7in','8in','9in','Location','southeast');
grid on

%effect of y(height of the spring from the ground) change in RMS when
arm angle is 5 degree & AoA is (10,20,30) degree
%avg RMS vs windspeed (m/s):Arm5_AoA(15,20,30)_x7_y(7,8,9)_41_7
figure(10);
hold on;
plot(Arm5_AoA15_x7_y7_41_7(:,3),Arm5_AoA15_x7_y7_41_7(:,end),'-
r+');figure(gcf);
plot(Arm5_AoA15_x7_y8_41_7(:,3),Arm5_AoA15_x7_y8_41_7(:,end),'-
ro');figure(gcf);
plot(Arm5_AoA15_x7_y9_41_7(:,3),Arm5_AoA15_x7_y9_41_7(:,end),'-
r*');figure(gcf);
plot(Arm5_AoA20_x7_y7_41_7(:,3),Arm5_AoA20_x7_y7_41_7(:,end),'-
g+');figure(gcf);
plot(Arm5_AoA20_x7_y8_41_7(:,3),Arm5_AoA20_x7_y8_41_7(:,end),'-
go');figure(gcf);
plot(Arm5_AoA20_x7_y9_41_7(:,3),Arm5_AoA20_x7_y9_41_7(:,end),'-
g*');figure(gcf);
plot(Arm5_AoA30_x7_y7_41_7(:,3),Arm5_AoA30_x7_y7_41_7(:,end),'-
b+');figure(gcf);
plot(Arm5_AoA30_x7_y8_41_7(:,3),Arm5_AoA30_x7_y8_41_7(:,end),'-
bo');figure(gcf);
plot(Arm5_AoA30_x7_y9_41_7(:,3),Arm5_AoA30_x7_y9_41_7(:,end),'-
b*');figure(gcf);

xlabel('Wind Speed (m/s)');
ylabel('RMS Voltage (mV)');
legend('AoA ± 15 Degree & 7in','AoA ± 15 Degree & 8in','AoA ± 15 Degree
& 9in','AoA ± 20 Degree & 7in','AoA ± 20 Degree & 8in','AoA ± 20 Degree
& 9in','AoA ± 30 Degree & 7in','AoA ± 30 Degree & 8in','AoA ± 30 Degree
& 9in','Location','southeast');
grid on

%effect of y(height of the spring from the ground) change in RMS when
arm angle is 9 degree & AoA is (10,20,30) degree
%avg RMS vs windspeed (m/s):Arm9_AoA(15,20,30)_x7_y(7,8,9)_41_7
figure(11);
hold on;
plot(Arm9_AoA15_x7_y7_41_7(:,3),Arm9_AoA15_x7_y7_41_7(:,end),'-
r+');figure(gcf);
plot(Arm9_AoA15_x7_y8_41_7(:,3),Arm9_AoA15_x7_y8_41_7(:,end),'-
ro');figure(gcf);
plot(Arm9_AoA15_x7_y9_41_7(:,3),Arm9_AoA15_x7_y9_41_7(:,end),'-
r*');figure(gcf);
plot(Arm9_AoA20_x7_y7_41_7(:,3),Arm9_AoA20_x7_y7_41_7(:,end),'-
g+');figure(gcf);

```

```

plot(Arm9_AoA20_x7_y8_41_7(:,3),Arm9_AoA20_x7_y8_41_7(:,end),'-
go');figure(gcf);
plot(Arm9_AoA20_x7_y9_41_7(:,3),Arm9_AoA20_x7_y9_41_7(:,end),'-
g*');figure(gcf);
plot(Arm9_AoA30_x7_y7_41_7(:,3),Arm9_AoA30_x7_y7_41_7(:,end),'-
b+');figure(gcf);
plot(Arm9_AoA30_x7_y8_41_7(:,3),Arm9_AoA30_x7_y8_41_7(:,end),'-
bo');figure(gcf);
plot(Arm9_AoA30_x7_y9_41_7(:,3),Arm9_AoA30_x7_y9_41_7(:,end),'-
b*');figure(gcf);

xlabel('Wind Speed (m/s)');
ylabel('RMS Voltage (mV)');
legend('AoA ± 15 Degree & 7in','AoA ± 15 Degree & 8in','AoA ± 15 Degree
& 9in','AoA ± 20 Degree & 7in','AoA ± 20 Degree & 8in','AoA ± 20 Degree
& 9in','AoA ± 30 Degree & 7in','AoA ± 30 Degree & 8in','AoA ± 30 Degree
& 9in','Location','southeast');
grid on

%effect of y(height of the spring from the ground) change in RMS when
arm angle is 13 degree & AoA is (10,20,30) degree
%avg RMS vs windspeed (m/s):Arm13_AoA(15,20,30)_x7_y(7,8,9)_41_7
figure(12);
hold on;
plot(Arm13_AoA15_x7_y7_41_7(:,3),Arm13_AoA15_x7_y7_41_7(:,end),'-
r+');figure(gcf);
plot(Arm13_AoA15_x7_y8_41_7(:,3),Arm13_AoA15_x7_y8_41_7(:,end),'-
ro');figure(gcf);
plot(Arm13_AoA15_x7_y9_41_7(:,3),Arm13_AoA15_x7_y9_41_7(:,end),'-
r*');figure(gcf);
plot(Arm13_AoA20_x7_y7_41_7(:,3),Arm13_AoA20_x7_y7_41_7(:,end),'-
g+');figure(gcf);
plot(Arm13_AoA20_x7_y8_41_7(:,3),Arm13_AoA20_x7_y8_41_7(:,end),'-
go');figure(gcf);
plot(Arm13_AoA20_x7_y9_41_7(:,3),Arm13_AoA20_x7_y9_41_7(:,end),'-
g*');figure(gcf);
plot(Arm13_AoA30_x7_y7_41_7(:,3),Arm13_AoA30_x7_y7_41_7(:,end),'-
b+');figure(gcf);
plot(Arm13_AoA30_x7_y8_41_7(:,3),Arm13_AoA30_x7_y8_41_7(:,end),'-
bo');figure(gcf);
plot(Arm13_AoA30_x7_y9_41_7(:,3),Arm13_AoA30_x7_y9_41_7(:,end),'-
b*');figure(gcf);

xlabel('Wind Speed (m/s)');
ylabel('RMS Voltage (mV)');
legend('AoA ± 15 Degree & 7in','AoA ± 15 Degree & 8in','AoA ± 15 Degree
& 9in','AoA ± 20 Degree & 7in','AoA ± 20 Degree & 8in','AoA ± 20 Degree
& 9in','AoA ± 30 Degree & 7in','AoA ± 30 Degree & 8in','AoA ± 30 Degree
& 9in','Location','southeast');
grid on

%effect of y(height of the spring from the ground) change in RMS when
AoA is 15 degree & arm angle is (5,9,13) degree
%avg RMS vs windspeed (m/s):Arm(5,9,13)_AoA15_x7_y(7,8,9)_41_7

```

```

figure(13);
hold on;
plot(Arm5_AoA15_x7_y7_41_7(:,3),Arm5_AoA15_x7_y7_41_7(:,end),'-r+');figure(gcf);
plot(Arm5_AoA15_x7_y8_41_7(:,3),Arm5_AoA15_x7_y8_41_7(:,end),'-ro');figure(gcf);
plot(Arm5_AoA15_x7_y9_41_7(:,3),Arm5_AoA15_x7_y9_41_7(:,end),'-r*');figure(gcf);
plot(Arm9_AoA15_x7_y7_41_7(:,3),Arm9_AoA15_x7_y7_41_7(:,end),'-g+');figure(gcf);
plot(Arm9_AoA15_x7_y8_41_7(:,3),Arm9_AoA15_x7_y8_41_7(:,end),'-go');figure(gcf);
plot(Arm9_AoA15_x7_y9_41_7(:,3),Arm9_AoA15_x7_y9_41_7(:,end),'-g*');figure(gcf);
plot(Arm13_AoA15_x7_y7_41_7(:,3),Arm13_AoA15_x7_y7_41_7(:,end),'-b+');figure(gcf);
plot(Arm13_AoA15_x7_y8_41_7(:,3),Arm13_AoA15_x7_y8_41_7(:,end),'-bo');figure(gcf);
plot(Arm13_AoA15_x7_y9_41_7(:,3),Arm13_AoA15_x7_y9_41_7(:,end),'-b*');figure(gcf);

xlabel('Wind Speed (m/s)');
ylabel('RMS Voltage (mV)');
legend('Arm Angle ± 5 Degree & 7in','Arm Angle ± 5 Degree & 8in','Arm Angle ± 5 Degree & 9in','Arm Angle ± 9 Degree & 7in','Arm Angle ± 9 Degree & 8in','Arm Angle ± 9 Degree & 9in','Arm Angle ± 13 Degree & 7in','Arm Angle ± 13 Degree & 8in','Arm Angle ± 13 Degree & 9in','Location','southeast');
grid on

%effect of y(height of the spring from the ground) change in RMS when
AoA is 20 degree & arm angle is (5,9,13) degree
%avg RMS vs windspeed (m/s):Arm(5,9,13)_AoA20_x7_y(7,8,9)_41_7
figure(14);
hold on;
plot(Arm5_AoA20_x7_y7_41_7(:,3),Arm5_AoA20_x7_y7_41_7(:,end),'-r+');figure(gcf);
plot(Arm5_AoA20_x7_y8_41_7(:,3),Arm5_AoA20_x7_y8_41_7(:,end),'-ro');figure(gcf);
plot(Arm5_AoA20_x7_y9_41_7(:,3),Arm5_AoA20_x7_y9_41_7(:,end),'-r*');figure(gcf);
plot(Arm9_AoA20_x7_y7_41_7(:,3),Arm9_AoA20_x7_y7_41_7(:,end),'-g+');figure(gcf);
plot(Arm9_AoA20_x7_y8_41_7(:,3),Arm9_AoA20_x7_y8_41_7(:,end),'-go');figure(gcf);
plot(Arm9_AoA20_x7_y9_41_7(:,3),Arm9_AoA20_x7_y9_41_7(:,end),'-g*');figure(gcf);
plot(Arm13_AoA20_x7_y7_41_7(:,3),Arm13_AoA20_x7_y7_41_7(:,end),'-b+');figure(gcf);
plot(Arm13_AoA20_x7_y8_41_7(:,3),Arm13_AoA20_x7_y8_41_7(:,end),'-bo');figure(gcf);
plot(Arm13_AoA20_x7_y9_41_7(:,3),Arm13_AoA20_x7_y9_41_7(:,end),'-b*');figure(gcf);

```

```

xlabel('Wind Speed (m/s)');
ylabel('RMS Voltage (mV)');
legend('Arm Angle ± 5 Degree & 7in','Arm Angle ± 5 Degree & 8in','Arm
Angle ± 5 Degree & 9in','Arm Angle ± 9 Degree & 7in','Arm Angle ± 9
Degree & 8in','Arm Angle ± 9 Degree & 9in','Arm Angle ± 13 Degree &
7in','Arm Angle ± 13 Degree & 8in','Arm Angle ± 13 Degree &
9in','Location','southeast');
grid on

%effect of y(height of the spring from the ground) change in RMS when
AoA is 30 degree & arm angle is (5,9,13) degree
%avg RMS vs windspeed (m/s):Arm(5,9,13)_AoA30_x7_y(7,8,9)_41_7
figure(15);
hold on;
plot(Arm5_AoA30_x7_y7_41_7(:,3),Arm5_AoA30_x7_y7_41_7(:,end),'-
r+');figure(gcf);
plot(Arm5_AoA30_x7_y8_41_7(:,3),Arm5_AoA30_x7_y8_41_7(:,end),'-
ro');figure(gcf);
plot(Arm5_AoA30_x7_y9_41_7(:,3),Arm5_AoA30_x7_y9_41_7(:,end),'-
r*');figure(gcf);
plot(Arm9_AoA30_x7_y7_41_7(:,3),Arm9_AoA30_x7_y7_41_7(:,end),'-
g+');figure(gcf);
plot(Arm9_AoA30_x7_y8_41_7(:,3),Arm9_AoA30_x7_y8_41_7(:,end),'-
go');figure(gcf);
plot(Arm9_AoA30_x7_y9_41_7(:,3),Arm9_AoA30_x7_y9_41_7(:,end),'-
g*');figure(gcf);
plot(Arm13_AoA30_x7_y7_41_7(:,3),Arm13_AoA30_x7_y7_41_7(:,end),'-
b+');figure(gcf);
plot(Arm13_AoA30_x7_y8_41_7(:,3),Arm13_AoA30_x7_y8_41_7(:,end),'-
bo');figure(gcf);
plot(Arm13_AoA30_x7_y9_41_7(:,3),Arm13_AoA30_x7_y9_41_7(:,end),'-
b*');figure(gcf);

xlabel('Wind Speed (m/s)');
ylabel('RMS Voltage (mV)');
legend('Arm Angle ± 5 Degree & 7in','Arm Angle ± 5 Degree & 8in','Arm
Angle ± 5 Degree & 9in','Arm Angle ± 9 Degree & 7in','Arm Angle ± 9
Degree & 8in','Arm Angle ± 9 Degree & 9in','Arm Angle ± 13 Degree &
7in','Arm Angle ± 13 Degree & 8in','Arm Angle ± 13 Degree &
9in','Location','southeast');
grid on

```

Appendix D

LabVIEW data acquisition analysis 2 (leaf spring height7in)

LabVIEW data acquisition analysis 2 (leaf spring height 7in)

```

clc;
load 'G:\New ossilator
reading\arm_AoA_x7_y7_41_7_filtered\Arm5_AoA15_x7_y7_41_7.dat';
load 'G:\New ossilator
reading\arm_AoA_x7_y7_41_7_filtered\Arm5_AoA20_x7_y7_41_7.dat';
load 'G:\New ossilator
reading\arm_AoA_x7_y7_41_7_filtered\Arm5_AoA30_x7_y7_41_7.dat';
load 'G:\New ossilator
reading\arm_AoA_x7_y7_41_7_filtered\Arm9_AoA15_x7_y7_41_7.dat';
load 'G:\New ossilator
reading\arm_AoA_x7_y7_41_7_filtered\Arm9_AoA20_x7_y7_41_7.dat';
load 'G:\New ossilator
reading\arm_AoA_x7_y7_41_7_filtered\Arm9_AoA30_x7_y7_41_7.dat';
load 'G:\New ossilator
reading\arm_AoA_x7_y7_41_7_filtered\Arm13_AoA15_x7_y7_41_7.dat';
load 'G:\New ossilator
reading\arm_AoA_x7_y7_41_7_filtered\Arm13_AoA20_x7_y7_41_7.dat';
load 'G:\New ossilator
reading\arm_AoA_x7_y7_41_7_filtered\Arm13_AoA30_x7_y7_41_7.dat';

%fanrpm %windspeed(mph) %windspeed(m/s) %freq(mHz)1 %RMS(milivolt)1
%Count1 %freq(mHz)2 %RMS(milivolt)2 %Count2 %freq(mHz)3 %RMS(milivolt)3
%Count3 %avg RMS(milivolt)

%effect of AoA change in RMS when arm angle is 5 degree
%avg RMS vs windspeed (m/s):Arm5_AoAX_x7_y7_41_7
figure(1);
hold on;
plot(Arm5_AoA15_x7_y7_41_7(:,3),Arm5_AoA15_x7_y7_41_7(:,end),'-
k+');figure(gcf);
plot(Arm5_AoA20_x7_y7_41_7(:,3),Arm5_AoA20_x7_y7_41_7(:,end),'-
ko');figure(gcf);
plot(Arm5_AoA30_x7_y7_41_7(:,3),Arm5_AoA30_x7_y7_41_7(:,end),'-
k*');figure(gcf);

xlabel('Wind Speed (m/s)');
ylabel('RMS Voltage (mV)');
legend('AoA ± 15 Degree','AoA ± 20 Degree','AoA ± 30
Degree','Location','southeast');
grid on

%effect of AoA change in RMS when arm angle is 9 degree
%avg RMS vs windspeed (m/s):Arm9_AoAX_x7_y7_41_7
figure(2);
hold on;
plot(Arm9_AoA15_x7_y7_41_7(:,3),Arm9_AoA15_x7_y7_41_7(:,end),'-
k+');figure(gcf);
plot(Arm9_AoA20_x7_y7_41_7(:,3),Arm9_AoA20_x7_y7_41_7(:,end),'-
ko');figure(gcf);

```

```

plot(Arm9_AoA30_x7_y7_41_7(:,3),Arm9_AoA30_x7_y7_41_7(:,end),'-
k*');figure(gcf);

xlabel('Wind Speed (m/s)');
ylabel('RMS Voltage (mV)');
legend('AoA ± 15 Degree','AoA ± 20 Degree','AoA ± 30
Degree','Location','southeast');
grid on

%effect of AoA change in RMS when arm angle is 13 degree
%avg RMS vs windspeed (m/s):Arm13_AoAX_x7_y7_41_7
figure(3);
hold on;
plot(Arm13_AoA15_x7_y7_41_7(:,3),Arm13_AoA15_x7_y7_41_7(:,end),'-
k+');figure(gcf);
plot(Arm13_AoA20_x7_y7_41_7(:,3),Arm13_AoA20_x7_y7_41_7(:,end),'-
ko');figure(gcf);
plot(Arm13_AoA30_x7_y7_41_7(:,3),Arm13_AoA30_x7_y7_41_7(:,end),'-
k*');figure(gcf);

xlabel('Wind Speed (m/s)');
ylabel('RMS Voltage (mV)');
legend('AoA ± 15 Degree','AoA ± 20 Degree','AoA ± 30
Degree','Location','southeast');
grid on

%effect of AoA change in RMS when arm angle is 5,9&13 degree
%avg RMS vs windspeed (m/s):Arm(5,9,13)_AoAX_x7_y7_41_7
figure(4);
hold on;
plot(Arm5_AoA15_x7_y7_41_7(:,3),Arm5_AoA15_x7_y7_41_7(:,end),'-
r+');figure(gcf);
plot(Arm5_AoA20_x7_y7_41_7(:,3),Arm5_AoA20_x7_y7_41_7(:,end),'-
ro');figure(gcf);
plot(Arm5_AoA30_x7_y7_41_7(:,3),Arm5_AoA30_x7_y7_41_7(:,end),'-
r*');figure(gcf);
plot(Arm9_AoA15_x7_y7_41_7(:,3),Arm9_AoA15_x7_y7_41_7(:,end),'-
g+');figure(gcf);
plot(Arm9_AoA20_x7_y7_41_7(:,3),Arm9_AoA20_x7_y7_41_7(:,end),'-
go');figure(gcf);
plot(Arm9_AoA30_x7_y7_41_7(:,3),Arm9_AoA30_x7_y7_41_7(:,end),'-
g*');figure(gcf);
plot(Arm13_AoA15_x7_y7_41_7(:,3),Arm13_AoA15_x7_y7_41_7(:,end),'-
b+');figure(gcf);
plot(Arm13_AoA20_x7_y7_41_7(:,3),Arm13_AoA20_x7_y7_41_7(:,end),'-
bo');figure(gcf);
plot(Arm13_AoA30_x7_y7_41_7(:,3),Arm13_AoA30_x7_y7_41_7(:,end),'-
b*');figure(gcf);

xlabel('Wind Speed (m/s)');
ylabel('RMS Voltage (mV)');
legend('Arm Angle ± 5 Degree & AoA ± 15 Degree','Arm Angle ± 5 Degree &
AoA ± 20 Degree','Arm Angle ± 5 Degree & AoA ± 30 Degree','Arm Angle ±

```

```

9 Degree & AoA ± 15 Degree', 'Arm Angle ± 9 Degree & AoA ± 20
Degree', 'Arm Angle ± 9 Degree & AoA ± 30 Degree', 'Arm Angle ± 13 Degree
& AoA ± 15 Degree', 'Arm Angle ± 13 Degree & AoA ± 20 Degree', 'Arm Angle
± 13 Degree & AoA ± 30 Degree', 'Location', 'southeast');
grid on

%effect of Arm change in RMS when AoA is 15 degree
%avg RMS vs windspeed (m/s):ArmX_AoA15_x7_y7_41_7
figure(5);
hold on;
plot(Arm5_AoA15_x7_y7_41_7(:,3),Arm5_AoA15_x7_y7_41_7(:,end), '-
k+');figure(gcf);
plot(Arm9_AoA15_x7_y7_41_7(:,3),Arm9_AoA15_x7_y7_41_7(:,end), '-
ko');figure(gcf);
plot(Arm13_AoA15_x7_y7_41_7(:,3),Arm13_AoA15_x7_y7_41_7(:,end), '-
k*');figure(gcf);

xlabel('Wind Speed (m/s)');
ylabel('RMS Voltage (mV)');
legend('Arm Angle ± 5 Degree', 'Arm Angle ± 9 Degree', 'Arm Angle ± 13
Degree', 'Location', 'southeast');
grid on

%effect of Arm change in RMS when AoA is 20 degree
%avg RMS vs windspeed (m/s):ArmX_AoA20_x7_y7_41_7
figure(6);
hold on;
plot(Arm5_AoA20_x7_y7_41_7(:,3),Arm5_AoA20_x7_y7_41_7(:,end), '-
k+');figure(gcf);
plot(Arm9_AoA20_x7_y7_41_7(:,3),Arm9_AoA20_x7_y7_41_7(:,end), '-
ko');figure(gcf);
plot(Arm13_AoA20_x7_y7_41_7(:,3),Arm13_AoA20_x7_y7_41_7(:,end), '-
k*');figure(gcf);

xlabel('Wind Speed (m/s)');
ylabel('RMS Voltage (mV)');
legend('Arm Angle ± 5 Degree', 'Arm Angle ± 9 Degree', 'Arm Angle ± 13
Degree', 'Location', 'southeast');
grid on

%effect of Arm change in RMS when AoA is 30 degree
%avg RMS vs windspeed (m/s):ArmX_AoA30_x7_y7_41_7
figure(7);
hold on;
plot(Arm5_AoA30_x7_y7_41_7(:,3),Arm5_AoA30_x7_y7_41_7(:,end), '-
k+');figure(gcf);
plot(Arm9_AoA30_x7_y7_41_7(:,3),Arm9_AoA30_x7_y7_41_7(:,end), '-
ko');figure(gcf);
plot(Arm13_AoA30_x7_y7_41_7(:,3),Arm13_AoA30_x7_y7_41_7(:,end), '-
k*');figure(gcf);

xlabel('Wind Speed (m/s)');
ylabel('RMS Voltage (mV)');

```

```
legend('Arm Angle ± 5 Degree','Arm Angle ± 9 Degree','Arm Angle ± 13  
Degree','Location','southeast');  
grid on
```

Appendix E

LabVIEW data acquisition analysis 3 (leaf spring height 8in)

LabVIEW data acquisition analysis 3(leaf spring height 8in)

```

clc;
load 'G:\New ossilator
reading\arm_AoA_x7_y8_41_7_filtered\Arm5_AoA15_x7_y8_41_7.dat';
load 'G:\New ossilator
reading\arm_AoA_x7_y8_41_7_filtered\Arm5_AoA20_x7_y8_41_7.dat';
load 'G:\New ossilator
reading\arm_AoA_x7_y8_41_7_filtered\Arm5_AoA30_x7_y8_41_7.dat';
load 'G:\New ossilator
reading\arm_AoA_x7_y8_41_7_filtered\Arm9_AoA15_x7_y8_41_7.dat';
load 'G:\New ossilator
reading\arm_AoA_x7_y8_41_7_filtered\Arm9_AoA20_x7_y8_41_7.dat';
load 'G:\New ossilator
reading\arm_AoA_x7_y8_41_7_filtered\Arm9_AoA30_x7_y8_41_7.dat';
load 'G:\New ossilator
reading\arm_AoA_x7_y8_41_7_filtered\Arm13_AoA15_x7_y8_41_7.dat';
load 'G:\New ossilator
reading\arm_AoA_x7_y8_41_7_filtered\Arm13_AoA20_x7_y8_41_7.dat';
load 'G:\New ossilator
reading\arm_AoA_x7_y8_41_7_filtered\Arm13_AoA30_x7_y8_41_7.dat';

%fanrpm %windspeed(mph) %windspeed(m/s) %freq(mHz)1 %RMS(milivolt)1
%Count1 %freq(mHz)2 %RMS(milivolt)2 %Count2 %freq(mHz)3 %RMS(milivolt)3
%Count3 %avg RMS(milivolt)

%effect of AoA change in RMS when arm angle is 5 degree
%avg RMS vs windspeed (m/s):Arm5_AoAX_x7_y8_41_7
figure(1);
hold on;
plot(Arm5_AoA15_x7_y8_41_7(:,3),Arm5_AoA15_x7_y8_41_7(:,end),'-
k+');figure(gcf);
plot(Arm5_AoA20_x7_y8_41_7(:,3),Arm5_AoA20_x7_y8_41_7(:,end),'-
ko');figure(gcf);
plot(Arm5_AoA30_x7_y8_41_7(:,3),Arm5_AoA30_x7_y8_41_7(:,end),'-
k*');figure(gcf);

xlabel('Wind Speed (m/s)');
ylabel('RMS Voltage (mV)');
legend('AoA ± 15 Degree','AoA ± 20 Degree','AoA ± 30
Degree','Location','southeast');
grid on

%effect of AoA change in RMS when arm angle is 9 degree
%avg RMS vs windspeed (m/s):Arm9_AoAX_x7_y8_41_7
figure(2);
hold on;
plot(Arm9_AoA15_x7_y8_41_7(:,3),Arm9_AoA15_x7_y8_41_7(:,end),'-
k+');figure(gcf);
plot(Arm9_AoA20_x7_y8_41_7(:,3),Arm9_AoA20_x7_y8_41_7(:,end),'-
ko');figure(gcf);

```

```

plot(Arm9_AoA30_x7_y8_41_7(:,3),Arm9_AoA30_x7_y8_41_7(:,end),'-
k*');figure(gcf);

xlabel('Wind Speed (m/s)');
ylabel('RMS Voltage (mV)');
legend('AoA ± 15 Degree','AoA ± 20 Degree','AoA ± 30
Degree','Location','southeast');
grid on

%effect of AoA change in RMS when arm angle is 13 degree
%avg RMS vs windspeed (m/s):Arm13_AoAX_x7_y8_41_7
figure(3);
hold on;
plot(Arm13_AoA15_x7_y8_41_7(:,3),Arm13_AoA15_x7_y8_41_7(:,end),'-
k+');figure(gcf);
plot(Arm13_AoA20_x7_y8_41_7(:,3),Arm13_AoA20_x7_y8_41_7(:,end),'-
ko');figure(gcf);
plot(Arm13_AoA30_x7_y8_41_7(:,3),Arm13_AoA30_x7_y8_41_7(:,end),'-
k*');figure(gcf);

xlabel('Wind Speed (m/s)');
ylabel('RMS Voltage (mV)');
legend('AoA ± 15 Degree','AoA ± 20 Degree','AoA ± 30
Degree','Location','southeast');
grid on

%effect of AoA change in RMS when arm angle is 5,9&13 degree
%avg RMS vs windspeed (m/s):Arm(5,9,13)_AoAX_x7_y8_41_7
figure(4);
hold on;
plot(Arm5_AoA15_x7_y8_41_7(:,3),Arm5_AoA15_x7_y8_41_7(:,end),'-
r+');figure(gcf);
plot(Arm5_AoA20_x7_y8_41_7(:,3),Arm5_AoA20_x7_y8_41_7(:,end),'-
ro');figure(gcf);
plot(Arm5_AoA30_x7_y8_41_7(:,3),Arm5_AoA30_x7_y8_41_7(:,end),'-
r*');figure(gcf);
plot(Arm9_AoA15_x7_y8_41_7(:,3),Arm9_AoA15_x7_y8_41_7(:,end),'-
g+');figure(gcf);
plot(Arm9_AoA20_x7_y8_41_7(:,3),Arm9_AoA20_x7_y8_41_7(:,end),'-
go');figure(gcf);
plot(Arm9_AoA30_x7_y8_41_7(:,3),Arm9_AoA30_x7_y8_41_7(:,end),'-
g*');figure(gcf);
plot(Arm13_AoA15_x7_y8_41_7(:,3),Arm13_AoA15_x7_y8_41_7(:,end),'-
b+');figure(gcf);
plot(Arm13_AoA20_x7_y8_41_7(:,3),Arm13_AoA20_x7_y8_41_7(:,end),'-
bo');figure(gcf);
plot(Arm13_AoA30_x7_y8_41_7(:,3),Arm13_AoA30_x7_y8_41_7(:,end),'-
b*');figure(gcf);

xlabel('Wind Speed (m/s)');
ylabel('RMS Voltage (mV)');
legend('Arm Angle ± 5 Degree & AoA ± 15 Degree','Arm Angle ± 5 Degree &
AoA ± 20 Degree','Arm Angle ± 5 Degree & AoA ± 30 Degree','Arm Angle ±

```

```

9 Degree & AoA ± 15 Degree', 'Arm Angle ± 9 Degree & AoA ± 20
Degree', 'Arm Angle ± 9 Degree & AoA ± 30 Degree', 'Arm Angle ± 13 Degree
& AoA ± 15 Degree', 'Arm Angle ± 13 Degree & AoA ± 20 Degree', 'Arm Angle
± 13 Degree & AoA ± 30 Degree', 'Location', 'southeast');
grid on

%effect of Arm change in RMS when AoA is 15 degree
%avg RMS vs windspeed (m/s):ArmX_AoA15_x7_y8_41_7
figure(5);
hold on;
plot(Arm5_AoA15_x7_y8_41_7(:,3),Arm5_AoA15_x7_y8_41_7(:,end), '-
k+');figure(gcf);
plot(Arm9_AoA15_x7_y8_41_7(:,3),Arm9_AoA15_x7_y8_41_7(:,end), '-
ko');figure(gcf);
plot(Arm13_AoA15_x7_y8_41_7(:,3),Arm13_AoA15_x7_y8_41_7(:,end), '-
k*');figure(gcf);

xlabel('Wind Speed (m/s)');
ylabel('RMS Voltage (mV)');
legend('Arm Angle ± 5 Degree', 'Arm Angle ± 9 Degree', 'Arm Angle ± 13
Degree', 'Location', 'southeast');
grid on

%effect of Arm change in RMS when AoA is 20 degree
%avg RMS vs windspeed (m/s):ArmX_AoA20_x7_y8_41_7
figure(6);
hold on;
plot(Arm5_AoA20_x7_y8_41_7(:,3),Arm5_AoA20_x7_y8_41_7(:,end), '-
k+');figure(gcf);
plot(Arm9_AoA20_x7_y8_41_7(:,3),Arm9_AoA20_x7_y8_41_7(:,end), '-
ko');figure(gcf);
plot(Arm13_AoA20_x7_y8_41_7(:,3),Arm13_AoA20_x7_y8_41_7(:,end), '-
k*');figure(gcf);

xlabel('Wind Speed (m/s)');
ylabel('RMS Voltage (mV)');
legend('Arm Angle ± 5 Degree', 'Arm Angle ± 9 Degree', 'Arm Angle ± 13
Degree', 'Location', 'southeast');
grid on

%effect of Arm change in RMS when AoA is 30 degree
%avg RMS vs windspeed (m/s):ArmX_AoA30_x7_y8_41_7
figure(7);
hold on;
plot(Arm5_AoA30_x7_y8_41_7(:,3),Arm5_AoA30_x7_y8_41_7(:,end), '-
k+');figure(gcf);
plot(Arm9_AoA30_x7_y8_41_7(:,3),Arm9_AoA30_x7_y8_41_7(:,end), '-
ko');figure(gcf);
plot(Arm13_AoA30_x7_y8_41_7(:,3),Arm13_AoA30_x7_y8_41_7(:,end), '-
k*');figure(gcf);

xlabel('Wind Speed (m/s)');
ylabel('RMS Voltage (mV)');

```



```
legend('Arm Angle ± 5 Degree','Arm Angle ± 9 Degree','Arm Angle ± 13  
Degree','Location','southeast');  
grid on
```

Appendix F

LabVIEW data acquisition analysis 4 (leaf spring height 9in)

LabVIEW data acquisition analysis 4(leaf spring height 9in)

```

clc;
load 'G:\New ossilator
reading\arm_AoA_x7_y9_41_7_filtered\Arm5_AoA15_x7_y9_41_7.dat';
load 'G:\New ossilator
reading\arm_AoA_x7_y9_41_7_filtered\Arm5_AoA20_x7_y9_41_7.dat';
load 'G:\New ossilator
reading\arm_AoA_x7_y9_41_7_filtered\Arm5_AoA30_x7_y9_41_7.dat';
load 'G:\New ossilator
reading\arm_AoA_x7_y9_41_7_filtered\Arm9_AoA15_x7_y9_41_7.dat';
load 'G:\New ossilator
reading\arm_AoA_x7_y9_41_7_filtered\Arm9_AoA20_x7_y9_41_7.dat';
load 'G:\New ossilator
reading\arm_AoA_x7_y9_41_7_filtered\Arm9_AoA30_x7_y9_41_7.dat';
load 'G:\New ossilator
reading\arm_AoA_x7_y9_41_7_filtered\Arm13_AoA15_x7_y9_41_7.dat';
load 'G:\New ossilator
reading\arm_AoA_x7_y9_41_7_filtered\Arm13_AoA20_x7_y9_41_7.dat';
load 'G:\New ossilator
reading\arm_AoA_x7_y9_41_7_filtered\Arm13_AoA30_x7_y9_41_7.dat';

%fanrpm %windspeed(mph) %windspeed(m/s) %freq(mHz)1 %RMS(milivolt)1
%Count1 %freq(mHz)2 %RMS(milivolt)2 %Count2 %freq(mHz)3 %RMS(milivolt)3
%Count3 %avg RMS(milivolt)

%effect of AoA change in RMS when arm angle is 5 degree
%avg RMS vs windspeed (m/s):Arm5_AoAX_x7_y9_41_7
figure(1);
hold on;
plot(Arm5_AoA15_x7_y9_41_7(:,3),Arm5_AoA15_x7_y9_41_7(:,end),'-
k+');figure(gcf);
plot(Arm5_AoA20_x7_y9_41_7(:,3),Arm5_AoA20_x7_y9_41_7(:,end),'-
ko');figure(gcf);
plot(Arm5_AoA30_x7_y9_41_7(:,3),Arm5_AoA30_x7_y9_41_7(:,end),'-
k*');figure(gcf);

xlabel('Wind Speed (m/s)');
ylabel('RMS Voltage (mV)');
legend('AoA ± 15 Degree','AoA ± 20 Degree','AoA ± 30
Degree','Location','southeast');
grid on

%effect of AoA change in RMS when arm angle is 9 degree
%avg RMS vs windspeed (m/s):Arm9_AoAX_x7_y9_41_7
figure(2);
hold on;
plot(Arm9_AoA15_x7_y9_41_7(:,3),Arm9_AoA15_x7_y9_41_7(:,end),'-
k+');figure(gcf);
plot(Arm9_AoA20_x7_y9_41_7(:,3),Arm9_AoA20_x7_y9_41_7(:,end),'-
ko');figure(gcf);

```

```

plot(Arm9_AoA30_x7_y9_41_7(:,3),Arm9_AoA30_x7_y9_41_7(:,end),'-
k*');figure(gcf);

xlabel('Wind Speed (m/s)');
ylabel('RMS Voltage (mV)');
legend('AoA ± 15 Degree','AoA ± 20 Degree','AoA ± 30
Degree','Location','southeast');
grid on

%effect of AoA change in RMS when arm angle is 13 degree
%avg RMS vs windspeed (m/s):Arm13_AoAX_x7_y9_41_7
figure(3);
hold on;
plot(Arm13_AoA15_x7_y9_41_7(:,3),Arm13_AoA15_x7_y9_41_7(:,end),'-
k+');figure(gcf);
plot(Arm13_AoA20_x7_y9_41_7(:,3),Arm13_AoA20_x7_y9_41_7(:,end),'-
ko');figure(gcf);
plot(Arm13_AoA30_x7_y9_41_7(:,3),Arm13_AoA30_x7_y9_41_7(:,end),'-
k*');figure(gcf);

xlabel('Wind Speed (m/s)');
ylabel('RMS Voltage (mV)');
legend('AoA ± 15 Degree','AoA ± 20 Degree','AoA ± 30
Degree','Location','southeast');
grid on

%effect of AoA change in RMS when arm angle is 5,9&13 degree
%avg RMS vs windspeed (m/s):Arm(5,9,13)_AoAX_x7_y9_41_7
figure(4);
hold on;
plot(Arm5_AoA15_x7_y9_41_7(:,3),Arm5_AoA15_x7_y9_41_7(:,end),'-
r+');figure(gcf);
plot(Arm5_AoA20_x7_y9_41_7(:,3),Arm5_AoA20_x7_y9_41_7(:,end),'-
ro');figure(gcf);
plot(Arm5_AoA30_x7_y9_41_7(:,3),Arm5_AoA30_x7_y9_41_7(:,end),'-
r*');figure(gcf);
plot(Arm9_AoA15_x7_y9_41_7(:,3),Arm9_AoA15_x7_y9_41_7(:,end),'-
g+');figure(gcf);
plot(Arm9_AoA20_x7_y9_41_7(:,3),Arm9_AoA20_x7_y9_41_7(:,end),'-
go');figure(gcf);
plot(Arm9_AoA30_x7_y9_41_7(:,3),Arm9_AoA30_x7_y9_41_7(:,end),'-
g*');figure(gcf);
plot(Arm13_AoA15_x7_y9_41_7(:,3),Arm13_AoA15_x7_y9_41_7(:,end),'-
b+');figure(gcf);
plot(Arm13_AoA20_x7_y9_41_7(:,3),Arm13_AoA20_x7_y9_41_7(:,end),'-
bo');figure(gcf);
plot(Arm13_AoA30_x7_y9_41_7(:,3),Arm13_AoA30_x7_y9_41_7(:,end),'-
b*');figure(gcf);

xlabel('Wind Speed (m/s)');
ylabel('RMS Voltage (mV)');
legend('Arm Angle ± 5 Degree & AoA ± 15 Degree','Arm Angle ± 5 Degree &
AoA ± 20 Degree','Arm Angle ± 5 Degree & AoA ± 30 Degree','Arm Angle ±

```

```

9 Degree & AoA ± 15 Degree', 'Arm Angle ± 9 Degree & AoA ± 20
Degree', 'Arm Angle ± 9 Degree & AoA ± 30 Degree', 'Arm Angle ± 13 Degree
& AoA ± 15 Degree', 'Arm Angle ± 13 Degree & AoA ± 20 Degree', 'Arm Angle
± 13 Degree & AoA ± 30 Degree', 'Location', 'southeast');
grid on

```

```

%effect of Arm change in RMS when AoA is 15 degree

```

```

%avg RMS vs windspeed (m/s):ArmX_AoA15_x7_y9_41_7

```

```

figure(5);

```

```

hold on;

```

```

plot(Arm5_AoA15_x7_y9_41_7(:,3),Arm5_AoA15_x7_y9_41_7(:,end),'-
k+');figure(gcf);

```

```

plot(Arm9_AoA15_x7_y9_41_7(:,3),Arm9_AoA15_x7_y9_41_7(:,end),'-
ko');figure(gcf);

```

```

plot(Arm13_AoA15_x7_y9_41_7(:,3),Arm13_AoA15_x7_y9_41_7(:,end),'-
k*');figure(gcf);

```

```


```

```


```

```


```

```

xlabel('Wind Speed (m/s)');

```

```

ylabel('RMS Voltage (mV)');

```

```

legend('Arm Angle ± 5 Degree', 'Arm Angle ± 9 Degree', 'Arm Angle ± 13
Degree', 'Location', 'southeast');

```

```

grid on

```

```

%effect of Arm change in RMS when AoA is 20 degree

```

```

%avg RMS vs windspeed (m/s):ArmX_AoA20_x7_y9_41_7

```

```

figure(6);

```

```

hold on;

```

```

plot(Arm5_AoA20_x7_y9_41_7(:,3),Arm5_AoA20_x7_y9_41_7(:,end),'-
k+');figure(gcf);

```

```

plot(Arm9_AoA20_x7_y9_41_7(:,3),Arm9_AoA20_x7_y9_41_7(:,end),'-
ko');figure(gcf);

```

```

plot(Arm13_AoA20_x7_y9_41_7(:,3),Arm13_AoA20_x7_y9_41_7(:,end),'-
k*');figure(gcf);

```

```


```

```


```

```


```

```

xlabel('Wind Speed (m/s)');

```

```

ylabel('RMS Voltage (mV)');

```

```

legend('Arm Angle ± 5 Degree', 'Arm Angle ± 9 Degree', 'Arm Angle ± 13
Degree', 'Location', 'southeast');

```

```

grid on

```

```

%effect of Arm change in RMS when AoA is 30 degree

```

```

%avg RMS vs windspeed (m/s):ArmX_AoA30_x7_y9_41_7

```

```

figure(7);

```

```

hold on;

```

```

plot(Arm5_AoA30_x7_y9_41_7(:,3),Arm5_AoA30_x7_y9_41_7(:,end),'-
k+');figure(gcf);

```

```

plot(Arm9_AoA30_x7_y9_41_7(:,3),Arm9_AoA30_x7_y9_41_7(:,end),'-
ko');figure(gcf);

```

```

plot(Arm13_AoA30_x7_y9_41_7(:,3),Arm13_AoA30_x7_y9_41_7(:,end),'-
k*');figure(gcf);

```

```


```

```


```

```


```

```

xlabel('Wind Speed (m/s)');

```

```

ylabel('RMS Voltage (mV)');

```

```
legend('Arm Angle ± 5 Degree','Arm Angle ± 9 Degree','Arm Angle ± 13  
Degree','Location','southeast');  
grid on
```

Appendix G

Wing and arm photogrammetry target tracking

Wing and arm photogrammetry target tracking

```

%%%%%%%%%%%%%%%%%%%%%%%%%%%%%%%%%%%%%%%%%%%%%%%%%%%%%%%%%%%%%%%%%%%%%%%%
%%%%%%%%
% centroids by mouse selection
%
% Inputs:
%   (1) 'imag', image name after loading an image file
%   (2) 'No_targets', total number of targets to be selected
%       (clicked)
%   (3) 'bk_size_0', bolck size for initial searching a target
%       (such as 10 pixels)
%
% Outputs:
%   [xc,yc], two-column array of target centroids in pixels
%
% Developed by Western Michigan University for NASA Langley Research
% Center
% Email: tianshu.liu@wmich.edu or aburner@cox.net to report bugs or
% suggest improvements
% Version date: August 28, 2006
% Primary author: Tianshu Liu
%%%%%%%%%%%%%%%%%%%%%%%%%%%%%%%%%%%%%%%%%%%%%%%%%%%%%%%%%%%%%%%%%%%%%%%%
%%%%%%%%

% open the file where the x, y data will be stored
clear all;
close all;

% set relevant parameters
No_targets=4; % No of targets for tracking
bk_size_0=5; % search area size
i_start=1; % starting image no
i_end=500; % ending image no

FileHead=strcat('C:\Documents and
Settings\Administrator\Desktop\Photogrammetry\videogrammetry\arm5_AoA20
_x7_y9_41_7_10fps_1500xps\arm5_AoA20_x7_y9_41_7_10fps_1500xps_70rpm_t\B
asler_avA1000-100gm_21113973_20150312_151534868_0');
FileName=strcat(FileHead,num2str(i_start),'.tiff');
imag=imread(FileName);

% convert rgb image to intensity image
if isrgb(imag)==1
    I=rgb2gray(imag);
elseif isgray(imag)==1
    I=imag;
end

% show image
imshow(I);
title(strcat('Click on','.. ', num2str(No_targets), '.. Targets'));

```



```

% click targets and calculate their centroids by calling
'locating_target1_fun.m'
i=1;
while (i<=No_targets)
    [x_p,y_p]=ginput(1);
    row_p=round(y_p);
    col_p=round(x_p);

    [xc1_shifted,yc1_shifted]=locating_target1_fun(I,row_p,col_p,bk_size_0)
; %Function locates centroid of target

    xc(i)=xc1_shifted;
    yc(i)=yc1_shifted;

% superimpose the calculated centroids on targets

    hold on;
    plot(round(xc(i)),round(yc(i)),'+r');
    i=i+1;
end

%%%%%%%%%%%%%%%%%%%%%%%%%%%%%%%%%%%%%%%%%%%%%%%%%%%%%%%%%%%%%%%%%%%%%%%%
sequence =[];
sequence2 =[];
% tracking targets in a time sequence
for k=i_start:i_end

    FileName=strcat(FileHead,num2str(k),'.tiff');

    imag = imread(FileName);

    % convert rgb image to intensity image
    if isrgb(imag)==1
        I=rgb2gray(imag);
    elseif isgray(imag)==1
        I=imag;
    end

    i=1;
    while (i<=No_targets)
        row_p=round(yc(i));
        col_p=round(xc(i));

        [xc1_shifted,yc1_shifted]=locating_target1_fun(I,row_p,col_p,bk_size_0)
; %Function locates centroid of target
        xc(i)=xc1_shifted;
        yc(i)=yc1_shifted;
        i=i+1;
    end
end

```

```

        %calculation
        degreearm=(atan((yc(1)-yc(2))/(xc(2)-xc(1))))*(180/pi);
        degreeAoA=(atan((yc(3)-yc(4))/(xc(4)-xc(3))))*(180/pi);

    end

    figure(2);
    imshow(I);
    hold on;
    plot(round(xc),round(yc),'+r');
    hold off;

    %write to a file the centroid of the targets
    output=[xc(1) xc(2) xc(3) xc(4) yc(1) yc(2) yc(3) yc(4)];
    [sequence] = [sequence; output];
    FileHead_out=strcat('C:\Documents and
Settings\Administrator\Desktop\Photogrammetry\videogrammetry\arm5_AoA20
_x7_y9_41_7_10fps_1500xps\arm5_AoA20_x7_y9_41_7_10fps_1500xps_70rpm_t\o
utput\xy_centroid-');
    FileName_out=strcat(FileHead_out,num2str(k),'.dat');
    dlmwrite(FileName_out, output,'delimiter','\t','precision',
'%6.4f','newline','pc');

    output=[degreearm' degreeAoA'];
    [sequence2] = [sequence2; output];
    FileHead_out=strcat('C:\Documents and
Settings\Administrator\Desktop\Photogrammetry\videogrammetry\arm5_AoA20
_x7_y9_41_7_10fps_1500xps\arm5_AoA20_x7_y9_41_7_10fps_1500xps_70rpm_t\angl
e\xy-');
    FileName_out=strcat(FileHead_out,num2str(k),'.dat');
    dlmwrite(FileName_out, output,'delimiter','\t','precision',
'%6.4f','newline','pc');

    k

end

```

Appendix H

Wing and arm photogrammetry data analysis

Wing and arm photogrammetry data analysis

```
load('arm5_AoA20_x7_y9_41_7_10fps_1500xps_34rpm_angle_t.mat');
load('arm5_AoA20_x7_y9_41_7_10fps_1500xps_36rpm_angle_t.mat');
load('arm5_AoA20_x7_y9_41_7_10fps_1500xps_40rpm_angle_t.mat');
load('arm5_AoA20_x7_y9_41_7_10fps_1500xps_44rpm_angle_t.mat');
load('arm5_AoA20_x7_y9_41_7_10fps_1500xps_44rpm_angle_t.mat');
load('arm5_AoA20_x7_y9_41_7_10fps_1500xps_48rpm_angle_t.mat');
load('arm5_AoA20_x7_y9_41_7_10fps_1500xps_52rpm_angle_t.mat');
load('arm5_AoA20_x7_y9_41_7_10fps_1500xps_56rpm_angle_t.mat');
load('arm5_AoA20_x7_y9_41_7_10fps_1500xps_60rpm_angle_t.mat');
load('arm5_AoA20_x7_y9_41_7_10fps_1500xps_64rpm_angle_t.mat');
load('arm5_AoA20_x7_y9_41_7_10fps_1500xps_68rpm_angle_t.mat');
load('arm5_AoA20_x7_y9_41_7_10fps_1500xps_70rpm_angle_t.mat');
```

%angle separately

```
rpm34_t=arm5_AoA20_x7_y9_41_7_10fps_1500xps_34rpm_angle_t;
rpm36_t=arm5_AoA20_x7_y9_41_7_10fps_1500xps_36rpm_angle_t;
rpm40_t=arm5_AoA20_x7_y9_41_7_10fps_1500xps_40rpm_angle_t;
rpm44_t=arm5_AoA20_x7_y9_41_7_10fps_1500xps_44rpm_angle_t;
rpm48_t=arm5_AoA20_x7_y9_41_7_10fps_1500xps_48rpm_angle_t;
rpm52_t=arm5_AoA20_x7_y9_41_7_10fps_1500xps_52rpm_angle_t;
rpm56_t=arm5_AoA20_x7_y9_41_7_10fps_1500xps_56rpm_angle_t;
rpm60_t=arm5_AoA20_x7_y9_41_7_10fps_1500xps_60rpm_angle_t;
rpm64_t=arm5_AoA20_x7_y9_41_7_10fps_1500xps_64rpm_angle_t;
rpm68_t=arm5_AoA20_x7_y9_41_7_10fps_1500xps_68rpm_angle_t;
rpm70_t=arm5_AoA20_x7_y9_41_7_10fps_1500xps_70rpm_angle_t;
```

%total angle

```
rpm34=arm5_AoA20_x7_y9_41_7_10fps_1500xps_34rpm_angle_t(:,1)+arm5_AoA20
_x7_y9_41_7_10fps_1500xps_34rpm_angle_t(:,2);
rpm36=arm5_AoA20_x7_y9_41_7_10fps_1500xps_36rpm_angle_t(:,1)+arm5_AoA20
_x7_y9_41_7_10fps_1500xps_36rpm_angle_t(:,2);
rpm40=arm5_AoA20_x7_y9_41_7_10fps_1500xps_40rpm_angle_t(:,1)+arm5_AoA20
_x7_y9_41_7_10fps_1500xps_40rpm_angle_t(:,2);
rpm44=arm5_AoA20_x7_y9_41_7_10fps_1500xps_44rpm_angle_t(:,1)+arm5_AoA20
_x7_y9_41_7_10fps_1500xps_44rpm_angle_t(:,2);
rpm48=arm5_AoA20_x7_y9_41_7_10fps_1500xps_48rpm_angle_t(:,1)+arm5_AoA20
_x7_y9_41_7_10fps_1500xps_48rpm_angle_t(:,2);
rpm52=arm5_AoA20_x7_y9_41_7_10fps_1500xps_52rpm_angle_t(:,1)+arm5_AoA20
_x7_y9_41_7_10fps_1500xps_52rpm_angle_t(:,2);
rpm56=arm5_AoA20_x7_y9_41_7_10fps_1500xps_56rpm_angle_t(:,1)+arm5_AoA20
_x7_y9_41_7_10fps_1500xps_56rpm_angle_t(:,2);
rpm60=arm5_AoA20_x7_y9_41_7_10fps_1500xps_60rpm_angle_t(:,1)+arm5_AoA20
_x7_y9_41_7_10fps_1500xps_60rpm_angle_t(:,2);
rpm64=arm5_AoA20_x7_y9_41_7_10fps_1500xps_64rpm_angle_t(:,1)+arm5_AoA20
_x7_y9_41_7_10fps_1500xps_64rpm_angle_t(:,2);
rpm68=arm5_AoA20_x7_y9_41_7_10fps_1500xps_68rpm_angle_t(:,1)+arm5_AoA20
_x7_y9_41_7_10fps_1500xps_68rpm_angle_t(:,2);
rpm70=arm5_AoA20_x7_y9_41_7_10fps_1500xps_70rpm_angle_t(:,1)+arm5_AoA20
_x7_y9_41_7_10fps_1500xps_70rpm_angle_t(:,2);
```

```
%max and min arm and AoA res arm
```

```
%min
```

```
rpm34_min=min(rpm34_t);
rpm36_min=min(rpm36_t);
rpm40_min=min(rpm40_t);
rpm44_min=min(rpm44_t);
rpm48_min=min(rpm48_t);
rpm52_min=min(rpm52_t);
rpm56_min=min(rpm56_t);
rpm60_min=min(rpm60_t);
rpm64_min=min(rpm64_t);
rpm68_min=min(rpm68_t);
rpm70_min=min(rpm70_t);
```

```
min_arm_AoA=[rpm34_min;rpm36_min;rpm40_min;rpm44_min;rpm48_min;rpm52_min;
rpm56_min;rpm60_min;rpm64_min;rpm68_min;rpm70_min];
```

```
%max
```

```
rpm34_max=max(rpm34_t);
rpm36_max=max(rpm36_t);
rpm40_max=max(rpm40_t);
rpm44_max=max(rpm44_t);
rpm48_max=max(rpm48_t);
rpm52_max=max(rpm52_t);
rpm56_max=max(rpm56_t);
rpm60_max=max(rpm60_t);
rpm64_max=max(rpm64_t);
rpm68_max=max(rpm68_t);
rpm70_max=max(rpm70_t);
```

```
max_arm_AoA=[rpm34_max;rpm36_max;rpm40_max;rpm44_max;rpm48_max;rpm52_max;
rpm56_max;rpm60_max;rpm64_max;rpm68_max;rpm70_max];
```

```
%max and min AoA total
```

```
%min
```

```
rpm34_min_total=min(rpm34);
rpm36_min_total=min(rpm36);
rpm40_min_total=min(rpm40);
rpm44_min_total=min(rpm44);
rpm48_min_total=min(rpm48);
rpm52_min_total=min(rpm52);
rpm56_min_total=min(rpm56);
rpm60_min_total=min(rpm60);
rpm64_min_total=min(rpm64);
rpm68_min_total=min(rpm68);
rpm70_min_total=min(rpm70);
```

```
min_total=[rpm34_min_total;rpm36_min_total;rpm40_min_total;rpm44_min_to
tal;rpm48_min_total;rpm52_min_total;rpm56_min_total;rpm60_min_total;rpm
64_min_total;rpm68_min_total;rpm70_min_total];
```

```
%max
```

```

rpm34_max_total=max(rpm34);
rpm36_max_total=max(rpm36);
rpm40_max_total=max(rpm40);
rpm44_max_total=max(rpm44);
rpm48_max_total=max(rpm48);
rpm52_max_total=max(rpm52);
rpm56_max_total=max(rpm56);
rpm60_max_total=max(rpm60);
rpm64_max_total=max(rpm64);
rpm68_max_total=max(rpm68);
rpm70_max_total=max(rpm70);

max_total=[rpm34_max_total;rpm36_max_total;rpm40_max_total;rpm44_max_to
tal;rpm48_max_total;rpm52_max_total;rpm56_max_total;rpm60_max_total;rpm
64_max_total;rpm68_max_total;rpm70_max_total];
%graphs
A = [0.016:0.016:8]';

figure(1);
hold on;
plot(A,arm5_AoA20_x7_y9_41_7_10fps_1500xps_34rpm_angle_t(:,1),'-
k');figure(gcf);
plot(A,arm5_AoA20_x7_y9_41_7_10fps_1500xps_34rpm_angle_t(:,2),'-
r');figure(gcf);
plot(A,rpm34,'-b');figure(gcf);

xlabel('Total Time Taken (s)');
ylabel('Angle (Degrees) ');
legend('arm','AoA res arm','abs AoA','Location','southeast');
grid on

figure(2);
hold on;
plot(A,arm5_AoA20_x7_y9_41_7_10fps_1500xps_36rpm_angle_t(:,1),'-
k');figure(gcf);
plot(A,arm5_AoA20_x7_y9_41_7_10fps_1500xps_36rpm_angle_t(:,2),'-
r');figure(gcf);
plot(A,rpm36,'-b');figure(gcf);

xlabel('Total Time Taken (s)');
ylabel('Angle (Degrees)');
legend('arm','AoA res arm','abs AoA','Location','southeast');
grid on

figure(3);
hold on;
plot(A,arm5_AoA20_x7_y9_41_7_10fps_1500xps_40rpm_angle_t(:,1),'-
k');figure(gcf);
plot(A,arm5_AoA20_x7_y9_41_7_10fps_1500xps_40rpm_angle_t(:,2),'-
r');figure(gcf);
plot(A,rpm40,'-b');figure(gcf);

xlabel('Total Time Taken (s)');

```

```

ylabel('Angle (Degrees)');
legend('arm', 'AoA res arm', 'abs AoA', 'Location', 'southeast');
grid on

figure(4);
hold on;
plot(A, arm5_AoA20_x7_y9_41_7_10fps_1500xps_44rpm_angle_t(:,1), '-k'); figure(gcf);
plot(A, arm5_AoA20_x7_y9_41_7_10fps_1500xps_44rpm_angle_t(:,2), '-r'); figure(gcf);
plot(A, rpm44, '-b'); figure(gcf);

xlabel('Total Time Taken (s)');
ylabel('Angle (Degrees)');
legend('arm', 'AoA res arm', 'abs AoA', 'Location', 'southeast');
grid on

figure(5);
hold on;
plot(A, arm5_AoA20_x7_y9_41_7_10fps_1500xps_48rpm_angle_t(:,1), '-k'); figure(gcf);
plot(A, arm5_AoA20_x7_y9_41_7_10fps_1500xps_48rpm_angle_t(:,2), '-r'); figure(gcf);
plot(A, rpm48, '-b'); figure(gcf);

xlabel('Total Time Taken (s)');
ylabel('Angle (Degrees)');
legend('arm', 'AoA res arm', 'abs AoA', 'Location', 'southeast');
grid on

figure(6);
hold on;
plot(A, arm5_AoA20_x7_y9_41_7_10fps_1500xps_52rpm_angle_t(:,1), '-k'); figure(gcf);
plot(A, arm5_AoA20_x7_y9_41_7_10fps_1500xps_52rpm_angle_t(:,2), '-r'); figure(gcf);
plot(A, rpm52, '-b'); figure(gcf);

xlabel('Total Time Taken (s)');
ylabel('Angle (Degrees)');
legend('arm', 'AoA res arm', 'abs AoA', 'Location', 'northeast');
grid on

figure(7);
hold on;
plot(A, arm5_AoA20_x7_y9_41_7_10fps_1500xps_56rpm_angle_t(:,1), '-k'); figure(gcf);
plot(A, arm5_AoA20_x7_y9_41_7_10fps_1500xps_56rpm_angle_t(:,2), '-r'); figure(gcf);
plot(A, rpm56, '-b'); figure(gcf);

xlabel('Total Time Taken (s)');
ylabel('Angle (Degrees)');

```

```

legend('arm', 'AoA res arm', 'abs AoA', 'Location', 'northeast');
grid on

figure(8);
hold on;
plot(A, arm5_AoA20_x7_y9_41_7_10fps_1500xps_60rpm_angle_t(:,1), '-k'); figure(gcf);
plot(A, arm5_AoA20_x7_y9_41_7_10fps_1500xps_60rpm_angle_t(:,2), '-r'); figure(gcf);
plot(A, rpm60, '-b'); figure(gcf);

xlabel('Total Time Taken (s)');
ylabel('Angle (Degrees)');
legend('arm', 'AoA res arm', 'abs AoA', 'Location', 'northeast');
grid on

figure(9);
hold on;
plot(A, arm5_AoA20_x7_y9_41_7_10fps_1500xps_64rpm_angle_t(:,1), '-k'); figure(gcf);
plot(A, arm5_AoA20_x7_y9_41_7_10fps_1500xps_64rpm_angle_t(:,2), '-r'); figure(gcf);
plot(A, rpm64, '-b'); figure(gcf);

xlabel('Total Time Taken (s)');
ylabel('Angle (Degrees)');
legend('arm', 'AoA res arm', 'abs AoA', 'Location', 'northeast');
grid on

figure(10);
hold on;
plot(A, arm5_AoA20_x7_y9_41_7_10fps_1500xps_68rpm_angle_t(:,1), '-k'); figure(gcf);
plot(A, arm5_AoA20_x7_y9_41_7_10fps_1500xps_68rpm_angle_t(:,2), '-r'); figure(gcf);
plot(A, rpm68, '-b'); figure(gcf);

xlabel('Total Time Taken (s)');
ylabel('Angle (Degrees)');
legend('arm', 'AoA res arm', 'abs AoA', 'Location', 'southeast');
grid on

figure(11);
hold on;
plot(A, arm5_AoA20_x7_y9_41_7_10fps_1500xps_70rpm_angle_t(:,1), '-k'); figure(gcf);
plot(A, arm5_AoA20_x7_y9_41_7_10fps_1500xps_70rpm_angle_t(:,2), '-r'); figure(gcf);
plot(A, rpm70, '-b'); figure(gcf);

xlabel('Total Time Taken (s)');
ylabel('Angle (Degrees)');
legend('arm', 'AoA res arm', 'abs AoA', 'Location', 'southeast');

```



```

grid on

w = [34 1.0612;36 1.1678;40 1.381;44 1.5942;48 1.8074;52 2.0206;56
2.2338;60 2.447;64 2.6602;68 2.8734;70 2.98];
B = [1:0.01:3]';
figure(12);
hold on;
plot(w(:,2),min_arm_AoA(:,1),'+-k');figure(gcf);
plot(w(:,2),max_arm_AoA(:,1),'x-r');figure(gcf);
plot(B,5,'g');figure(gcf);
plot(B,-5,'b');figure(gcf);
xlabel('Wind speed (m/s)');
ylabel('Angle (Degrees)');
legend('- arm angle','+ arm angle','+ set arm angle','- set arm
angle','Location','northeast');
grid on

figure(13);
hold on;
plot(w(:,2),min_total,'+-k');figure(gcf);
plot(w(:,2),max_total,'o-r');figure(gcf);
plot(w(:,2),min_arm_AoA(:,2),'*-g');figure(gcf);
plot(w(:,2),max_arm_AoA(:,2),'s-b');figure(gcf);
plot(B,-20,'-m');figure(gcf);
plot(B,20,'-r');figure(gcf);
xlabel('Wind speed (m/s)');
ylabel('Angle (Degrees)');
legend('+ AoA res wind dir','- AoA res wind dir','- AoA res arm','+ AoA
res arm','- set AoA','+ set AoA ','Location','northeast');
grid on

```

Appendix I

Pendulum photogrammetry target tracking

Pendulum photogrammetry target tracking

```

%%%%%%%%%%%%%%%%%%%%%%%%%%%%%%%%%%%%%%%%%%%%%%%%%%%%%%%%%%%%%%%%%%%%%%%%
%%%%%%%%%%%%%%%%%%%%%%%%%%%%%%%%%%%%%%%%%%%%%%%%%%%%%%%%%%%%%%%%%%%%%%%%
% centroids by mouse selection
%
% Inputs:
%   (1) 'imag', image name after loading an image file
%   (2) 'No_targets', total number of targets to be selected
%       (clicked)
%   (3) 'bk_size_0', bolck size for initial searching a target
%       (such as 10 pixels)
%
% Outputs:
%   [xc,yc], two-column array of target centroids in pixels
%
% Developed by Western Michigan University for NASA Langley Research
% Center
% Email: tianshu.liu@wmich.edu or aburner@cox.net to report bugs or
% suggest improvements
% Version date: August 28, 2006
% Primary author: Tianshu Liu
%%%%%%%%%%%%%%%%%%%%%%%%%%%%%%%%%%%%%%%%%%%%%%%%%%%%%%%%%%%%%%%%%%%%%%%%
%%%%%%%%%%%%%%%%%%%%%%%%%%%%%%%%%%%%%%%%%%%%%%%%%%%%%%%%%%%%%%%%%%%%%%%%

% open the file where the x, y data will be stored
clear all;
close all;

% set relevant parameters
No_targets=2; % No of targets for tracking
bk_size_0=28; % search area size
i_start=100; % starting image no
i_end=500;   % ending image no

FileHead=strcat('C:\Documents and
Settings\Administrator\Desktop\Photogrammetry\videogrammetry\weight\70_
3g\arm5_AoA20_x7_y9_10fps_15000xps_70.3g_52rpm\Basler_avA1000-
100gm_21452483_20150424_174250066_0');
FileName=strcat(FileHead,num2str(i_start),'.tiff');
imag=imread(FileName);

% convert rgb image to intensity image
if isrgb(imag)==1
    I=rgb2gray(imag);
elseif isgray(imag)==1
    I=imag;
end

% show image

```

```

imshow(I);
title(strcat('Click on', '.. ', num2str(No_targets), '.. Targets'));

% click targets and calculate their centroids by calling
'locating_target1_fun.m'
i=1;
while (i<=No_targets)
    [x_p,y_p]=ginput(1);
    row_p=round(y_p);
    col_p=round(x_p);

    [xc1_shifted,yc1_shifted]=locating_target1_fun(I,row_p,col_p,bk_size_0)
    ; %Function locates centroid of target

    xc(i)=xc1_shifted;
    yc(i)=yc1_shifted;

% superimpose the calculated centroids on targets

    hold on;
    plot(round(xc(i)),round(yc(i)),'+r');
    i=i+1;
end

%%%%%%%%%%%%%%%%%%%%%%%%%%%%%%%%%%%%%%%%%%%%%%%%%%%%%%%%%%%%%%%%%%%%%%%%
sequence =[];
sequence2 =[];
% tracking targets in a time sequence
for k=i_start:i_end

    FileName=strcat(FileHead,num2str(k),'.tiff');

    imag = imread(FileName);

% convert rgb image to intensity image
if isrgb(imag)==1
    I=rgb2gray(imag);
elseif isgray(imag)==1
    I=imag;
end

    i=1;
    while (i<=No_targets)
        row_p=round(yc(i));
        col_p=round(xc(i));

        [xc1_shifted,yc1_shifted]=locating_target1_fun(I,row_p,col_p,bk_size_0)
        ;%Function locates centroid of target
        xc(i)=xc1_shifted;

```

```

yc(i)=yc1_shifted;
i=i+1;
    %calculation
degree=(atan((yc(1)-yc(2))/(xc(2)-xc(1))))*(180/pi);
%degreeAoA=(atan((yc(3)-yc(4))/(xc(4)-xc(3))))*(180/pi);

end

figure(2);
imshow(I);
hold on;
plot(round(xc),round(yc),'+r');
hold off;

%write to a file the centroid of the targets
output=[xc(1) xc(2) yc(1) yc(2)];
[sequence] = [sequence; output];
FileHead_out=strcat('C:\Documents and
Settings\Administrator\Desktop\Photogrammetry\videogrammetry\weight\70_
3g\arm5_AoA20_x7_y9_10fps_15000xps_70.3g_52rpm\output\xy_centroid-');
FileName_out=strcat(FileHead_out,num2str(k),'.dat');
dlmwrite(FileName_out, output,'delimiter','\t','precision',
'%6.4f','newline','pc');

output=[degree'];
[sequence2] = [sequence2; output];
FileHead_out=strcat('C:\Documents and
Settings\Administrator\Desktop\Photogrammetry\videogrammetry\weight\70_
3g\arm5_AoA20_x7_y9_10fps_15000xps_70.3g_52rpm\angle\xy-');
FileName_out=strcat(FileHead_out,num2str(k),'.dat');
dlmwrite(FileName_out, output,'delimiter','\t','precision',
'%6.4f','newline','pc');

k

end

```

Appendix J

Pendulum photogrammetry data analysis

Pendulum photogrammetry data analysis

```

load('arm5_AoA20_x7_y9_10fps_15000xps_70_3g_40rpm_angle.mat');
load('arm5_AoA20_x7_y9_10fps_15000xps_70_3g_40rpm_data.mat');
load('arm5_AoA20_x7_y9_10fps_15000xps_70_3g_44rpm_angle.mat');
load('arm5_AoA20_x7_y9_10fps_15000xps_70_3g_44rpm_data.mat');
load('arm5_AoA20_x7_y9_10fps_15000xps_70_3g_48rpm_angle.mat');
load('arm5_AoA20_x7_y9_10fps_15000xps_70_3g_48rpm_data.mat');
load('arm5_AoA20_x7_y9_10fps_15000xps_23_3g_angle.mat');
load('arm5_AoA20_x7_y9_10fps_15000xps_23_3g_data.mat');

x_40=arm5_AoA20_x7_y9_10fps_15000xps_70_3g_40rpm_angle;%degree
x_44=arm5_AoA20_x7_y9_10fps_15000xps_70_3g_44rpm_angle;%degree
x_48=arm5_AoA20_x7_y9_10fps_15000xps_70_3g_48rpm_angle;%degree
x=arm5_AoA20_x7_y9_10fps_15000xps_23_3g_angle;%degree

theta_40=x_40*pi/180;%radian
theta_44=x_44*pi/180;%radian
theta_48=x_48*pi/180;%radian
theta=x*pi/180;%radian

r_1=0.0889;%m
r=0.073025;%m

s_40=r*theta_40;%m
s_44=r*theta_44;%m
s_48=r*theta_48;%m
s=r_1*theta;%m

t=1/10;%s

v_40=diff(s_40)/t;%m/s
v_44=diff(s_44)/t;%m/s
v_48=diff(s_48)/t;%m/s
v=diff(s)/t;%m/s

m=70.3/1000;%kg
m_1=23.3/1000;%kg

p_40=m*v_40;
p_44=m*v_44;
p_48=m*v_48;
p=m_1*v;

KE_40=0.5*m*(v_40.^2);%kgm^2/s^2
KE_44=0.5*m*(v_44.^2);%kgm^2/s^2
KE_48=0.5*m*(v_48.^2);%kgm^2/s^2
KE=0.5*m_1*(v.^2);%kgm^2/s^2

pwr_40=diff(KE_40)/t;

```

```

pwr_44=diff(KE_44)/t;
pwr_48=diff(KE_48)/t;
pwr=diff(KE)/t;

n_40=length(pwr_40)
n_44=length(pwr_44)
n_48=length(pwr_48)
n=length(pwr)

rms_40=norm(pwr_40)/sqrt(n_40)
rms_44=norm(pwr_44)/sqrt(n_44)
rms_48=norm(pwr_48)/sqrt(n_48)
rms=norm(pwr)/sqrt(n)
%angle=abs(min(arm5_AoA20_x7_y9_10fps_15000xps_23_3g_angle))+max(arm5_A
oA20_x7_y9_10fps_15000xps_23_3g_angle);

A = [0:0.1:40]';
figure(1);
hold on;
plot(A,theta_40(:,1),'-k');figure(gcf);
xlabel('Total Time Taken (s)');
ylabel('Angle (Radian)');
legend('1.381 m/s (40rpm)', 'Location', 'northeast');
grid on

figure(2);
hold on;
plot(A,theta_44(:,1),'-k');figure(gcf);
xlabel('Total Time Taken (s)');
ylabel('Angle (Radian)');
legend('1.5942 m/s (44rpm)', 'Location', 'northeast');
grid on

figure(3);
hold on;
plot(A,theta_48(:,1),'-k');figure(gcf);
xlabel('Total Time Taken (s)');
ylabel('Angle (Radian)');
legend('1.8074 m/s (48rpm)', 'Location', 'northeast');
grid on

figure(4);
hold on;
plot(A,theta(:,1),'-k');figure(gcf);
xlabel('Total Time Taken (s)');
ylabel('Angle (Radian)');
legend('1.5942 m/s (40rpm)', 'Location', 'northeast');
grid on

```



```

figure(5);
hold on;
plot(A,theta_40(:,1),'r');figure(gcf);
plot(A,theta_44(:,1),'g');figure(gcf);
plot(A,theta_48(:,1),'b');figure(gcf);
plot(A,theta(:,1),'k');figure(gcf);
xlabel('Total Time Taken (s)');
ylabel('Angle (Radian)');
legend('1.381 m/s (70.2g)', '1.5942 m/s (70.2g)', '1.8074 m/s
(70.2g)', '1.5942 m/s (32.2g)', 'Location', 'northeast');
grid on

```

```

figure(6);
hold on;
plot(A,s_40(:,1),'k');figure(gcf);
xlabel('Total Time Taken (s)');
ylabel('Circumference (m)');
legend('1.381 m/s (40rpm)', 'Location', 'northeast');
grid on

```

```

figure(7);
hold on;
plot(A,s_44(:,1),'k');figure(gcf);
xlabel('Total Time Taken (s)');
ylabel('Circumference (m)');
legend('1.5942 m/s (44rpm)', 'Location', 'northeast');
grid on

```

```

figure(8);
hold on;
plot(A,s_48(:,1),'k');figure(gcf);
xlabel('Total Time Taken (s)');
ylabel('Circumference (m)');
legend('1.8074 m/s (48rpm)', 'Location', 'northeast');
grid on

```

```

figure(9);
hold on;
plot(A,s(:,1),'k');figure(gcf);
xlabel('Total Time Taken (s)');
ylabel('Circumference (m)');
legend('1.5942 m/s (44rpm)', 'Location', 'northeast');
grid on

```

```

figure(10);
hold on;
plot(A,s_40(:,1),'r');figure(gcf);
plot(A,s_44(:,1),'g');figure(gcf);
plot(A,s_48(:,1),'b');figure(gcf);
plot(A,s(:,1),'b');figure(gcf);
xlabel('Total Time Taken (s)');
ylabel('Circumference (m)');

```

```

legend('1.381 m/s (70.2g)', '1.5942 m/s (70.2g)', '1.8074 m/s
(70.2g)', '1.5942 m/s (32.2g)', 'Location', 'northeast');
grid on

```

```

C = [0.1:0.1:40]';
figure(11);
hold on;
plot(C, v_40(:,1), '-k'); figure(gcf);
xlabel('Total Time Taken (s)');
ylabel('Velocity(m/s)');
legend('1.381 m/s (40rpm)', 'Location', 'northeast');
grid on

```

```

figure(12);
hold on;
plot(C, v_44(:,1), '-k'); figure(gcf);
xlabel('Total Time Taken (s)');
ylabel('Velocity(m/s)');
legend('1.5942 m/s (44rpm)', 'Location', 'northeast');
grid on

```

```

figure(13);
hold on;
plot(C, v_48(:,1), '-k'); figure(gcf);
xlabel('Total Time Taken (s)');
ylabel('Velocity(m/s)');
legend('1.8074 m/s (48rpm)', 'Location', 'northeast');
grid on

```

```

figure(14);
hold on;
plot(C, v(:,1), '-k'); figure(gcf);
xlabel('Total Time Taken (s)');
ylabel('Velocity(m/s)');
legend('1.5942 m/s (44rpm)', 'Location', 'northeast');
grid on

```

```

figure(15);
hold on;
plot(C, v_40(:,1), '-r'); figure(gcf);
plot(C, v_44(:,1), '-g'); figure(gcf);
plot(C, v_48(:,1), '-b'); figure(gcf);
plot(C, v(:,1), '-k'); figure(gcf);
xlabel('Total Time Taken (s)');
ylabel('Velocity(m/s)');
legend('1.381 m/s (70.2g)', '1.5942 m/s (70.2g)', '1.8074 m/s
(70.2g)', '1.5942 m/s (32.2g)', 'Location', 'northeast');
grid on

```

```

figure(16);
hold on;
plot(C, p_40(:,1), '-k'); figure(gcf);
xlabel('Total Time Taken (s)');

```

```

ylabel('linear momentum(m)');
legend('1.381 m/s (40rpm)', 'Location', 'northeast');
grid on

figure(17);
hold on;
plot(C,p_44(:,1), '-k');figure(gcf);
xlabel('Total Time Taken (s)');
ylabel('linear momentum(m)');
legend('1.5942 m/s (44rpm)', 'Location', 'northeast');
grid on

figure(18);
hold on;
plot(C,p_48(:,1), '-k');figure(gcf);
xlabel('Total Time Taken (s)');
ylabel('linear momentum(m)');
legend('1.8072 m/s (48rpm)', 'Location', 'northeast');
grid on

figure(19);
hold on;
plot(C,p(:,1), '-k');figure(gcf);
xlabel('Total Time Taken (s)');
ylabel('linear momentum(m)');
legend('1.5942 m/s (44rpm)', 'Location', 'northeast');
grid on

figure(20);
hold on;
plot(C,p_40(:,1), '-r');figure(gcf);
plot(C,p_44(:,1), '-g');figure(gcf);
plot(C,p_48(:,1), '-b');figure(gcf);
plot(C,p(:,1), '-k');figure(gcf);
xlabel('Total Time Taken (s)');
ylabel('linear momentum(m)');
legend('1.381 m/s (70.2g)', '1.5942 m/s (70.2g)', '1.8074 m/s (70.2g)', '1.5942 m/s (32.2g)', 'Location', 'northeast');
grid on

figure(21);
hold on;
plot(C,KE_40(:,1), '-k');figure(gcf);
xlabel('Total Time Taken (s)');
ylabel('Kinetic Energy(kg m^2/s^2)');
legend('1.381 m/s (40rpm)', 'Location', 'northeast');
grid on

figure(22);
hold on;
plot(C,KE_44(:,1), '-k');figure(gcf);
xlabel('Total Time Taken (s)');
ylabel('Kinetic Energy(kg m^2/s^2)');

```

```

legend('1.5942 m/s (44rpm)', 'Location', 'northeast');
grid on

figure(23);
hold on;
plot(C, KE_48(:,1), '-k'); figure(gcf);
xlabel('Total Time Taken (s)');
ylabel('Kinetic Energy(kg m^2/s^2)');
legend('1.8074 m/s (48rpm)', 'Location', 'northeast');
grid on

figure(24);
hold on;
plot(C, KE(:,1), '-k'); figure(gcf);
xlabel('Total Time Taken (s)');
ylabel('Kinetic Energy(kg m^2/s^2)');
legend('1.5942 m/s (44rpm)', 'Location', 'northeast');
grid on

figure(25);
hold on;
plot(C, KE_40(:,1), '-r'); figure(gcf);
plot(C, KE_44(:,1), '-g'); figure(gcf);
plot(C, KE_48(:,1), '-b'); figure(gcf);
plot(C, KE(:,1), '-k'); figure(gcf);
xlabel('Total Time Taken (s)');
ylabel('Kinetic Energy(kg m^2/s^2)');
legend('1.381 m/s (70.2g)', '1.5942 m/s (70.2g)', '1.8074 m/s (70.2g)', '1.5942 m/s (32.2g)', 'Location', 'northeast');
grid on

B = [0:0.1003:40]';
figure(26);
hold on;
plot(B, pwr_40(:,1), 'k'); figure(gcf);
plot(B, rms_40, 'r', 'linewidth', 8); figure(gcf);
xlabel('Total Time Taken (s)');
ylabel('Power (Watts)');
legend('1.381 m/s (40rpm)', 'RMS Power = 50.58 x 10^-6W', 'Location', 'northeast');
grid on

figure(27);
hold on;
plot(B, pwr_44(:,1), 'k'); figure(gcf);
plot(B, rms_44, 'r', 'linewidth', 8); figure(gcf);
xlabel('Total Time Taken (s)');
ylabel('Power (Watts)');
legend('1.5942 m/s (44rpm)', 'RMS Power = 88.02 x 10^-6W', 'Location', 'northeast');
grid on

figure(28);

```

```

hold on;
plot(B,pwr_48(:,1),'k');figure(gcf);
plot(B,rms_48,'r','linewidth',8);figure(gcf);
xlabel('Total Time Taken (s)');
ylabel('Power (Watts)');
legend('1.8074 m/s (48rpm)','RMS Power = 327.45 x 10^-6W','Location','northeast');
grid on

figure(29);
hold on;
plot(B,pwr(:,1),'k');figure(gcf);
plot(B,rms,'r','linewidth',8);figure(gcf);
xlabel('Total Time Taken (s)');
ylabel('Power (Watts)');
legend('1.5942 m/s (44rpm)','RMS Power = 42.68 x 10^-6W','Location','northeast');
grid on

figure(30);
hold on;
plot(1.381,rms_40,'+r');figure(gcf);
plot(1.5942,rms_44,'*g');figure(gcf);
plot(1.8074,rms_48,'xb');figure(gcf);
plot(1.5942,rms,'ok');figure(gcf);
xlabel('Incoming Wind Speed(m/s)');
ylabel('Power (Watts)');
legend('70.2g @ 40rpm','70.2g @ 44rpm','70.2g @ 48rpm','32.2g @ 44rpm','Location','northeast');
grid on

figure(31);
hold on;
plot(1.381,2*rms_40,'+r');figure(gcf);
plot(1.5942,2*rms_44,'*g');figure(gcf);
plot(1.8074,2*rms_48,'xb');figure(gcf);
plot(1.5942,2*rms,'ok');figure(gcf);
xlabel('Incoming Wind Speed(m/s)');
ylabel(' Total Power (Watts)');
legend('70.2g @ 40rpm','70.2g @ 44rpm','70.2g @ 48rpm','32.2g @ 44rpm','Location','northeast');
grid on

z=[1.381 rms_40;1.5942 rms_44;1.8074 rms_48];
figure(32);
hold on;
plot(z(:,1),z(:,2),'+r');figure(gcf);
plot(1.5942,rms,'ok');figure(gcf);
xlabel('Incoming Wind Speed(m/s)');
ylabel('Power (Watts)');
legend('70.2g @ different wind speed','32.2g @ 44rpm','Location','northeast');
grid on

```

```
z_1=z(:,2)*2;
figure(33);
hold on;
plot(z(:,1),z_1(:,1),'+r');figure(gcf);
plot(1.5942,rms,'ok');figure(gcf);
xlabel('Incoming Wind Speed(m/s)');
ylabel('Power (Watts)');
legend('70.2g @ different wind speed','32.2g @
44rpm','Location','northeast');
grid on
```